THE UNIVERSITY *of* EDINBURGH

Quantifying the impact of on-road transport on fine particulate matter over Delhi megacity

Caterina Mogno

Doctor of Philosophy

THE UNIVERSITY OF EDINBURGH

2022

Copyright Notice

This thesis formatting has been produced using the LaTex template *University of Edinburgh: The Latex Template for Formatting a PhD Thesis* developed by George Taylor and Mathew Topper and available under GNU General Public License v3.

Declaration

I declare that this thesis has been composed solely by myself, and that it contains only my work except where otherwise specified, or where the work is explicitly indicated to have formed a jointly-authored publication. This work, either in whole or in part, has not been submitted for any other degree or professional qualification.

Caterina Mogno

August 2022

Abstract

Outdoor air pollution is an increasing public health burden. Fine particulate matter ($PM_{2.5}$) is a pollutant of major concern for human health, and it also affects the climate and ecosystems. Understanding and quantifying emission sources and their impact on particulate air pollution is critical for improving global health and for informing climate action. Poor air quality across the globe disproportionately affects middle- and lower-income countries. Delhi, the capital of India, is one of the most populated and polluted megacities in the world, where in 2017 almost 12,000 premature deaths were attributed to outdoor air pollution.

My thesis aims to advance our understanding of outdoor air pollution in Delhi megacity, with a focus on the impact of on-road transport emissions on surface levels of $PM_{2.5}$ and its implications for air quality policymaking. To do this, I use a combination of a state of the art regional atmospheric chemistry transport model, recently developed local emissions inventories, and sensitivity analysis techniques.

In the first research chapter I use the WRF-Chem atmospheric chemical transport model to understand the regional influence on air quality over Delhi. As part of this work, I characterise seasonal anthropogenic, pyrogenic, and biogenic influences on fine particulate matter and one of its main constituents, organic aerosol (OA), over the Indo-Gangetic Plain (IGP). My results show that anthropogenic emissions influence the magnitude and distribution of $PM_{2.5}$ and OA throughout the year, especially over cities including Delhi, while pyrogenic emissions from crop residues burning result in localized contributions over the central and upper parts of IGP in all non-monsoonal seasons, with the highest impact during the post-monsoon season that correspond to the post-harvest season in

the agricultural calendar. Biogenic emissions play an important role in the magnitude and distribution of $PM_{2.5}$ and OA during the monsoon season, particularly over the lower IGP. In all seasons mean values of $PM_{2.5}$ still exceed the recommended levels, indicating that air pollution is a year-round problem.

In the second research chapter I develop the WRF-Chem model used in my first chapter to include local emission inventories, in order to quantify the contribution of the on-road transport sector to surface $PM_{2.5}$ over Delhi during the highly polluted post-monsoon season. This contribution is compared to the contributions of other local (within Delhi) and regional (within the National Capital Region, NCR) anthropogenic sectors. My results show that emissions from the local transport sector contribute typically less than 10% to daily mean $PM_{2.5}$ values over Delhi, rising to 17% when regional transport sources are included. The contribution from the local transport sector is largest (18%) during the evening traffic peak. The total transport impact is dominated by contributions from two- and three-wheelers (50%) and heavy-duty vehicles (30%). The largest individual contributions to daily mean $PM_{2.5}$ values are found to be from regional power and industry (14%) and domestic (11%) sectors.

In the third research chapter I drive the WRF-Chem model with future transport emissions scenarios to investigate the potential impact of electric and clean-fuel vehicles on surface $PM_{2.5}$ and ozone (O_3) over Delhi for two contrasting seasons, pre-monsoon and post-monsoon. My results show that the conversion of diesel vehicles to compressed natural gas (CNG) brings a greater reduction in $PM_{2.5}$ concentrations than the full electrification of two- and three-wheelers. However, the maximum reduction of daily mean $PM_{2.5}$ concentrations for all scenarios is within 5% compared to baseline values for both seasons. Electrification of two- and three-wheelers increases average 8-hour daily

maximum (MDA8) ozone (1.3-3.5% in pre-monsoon 5-13% in post-monsoon) compared to baseline values. On the other hand, conversion of all diesel vehicles to CNG reduces MDA8 O_3 in both seasons (by 2.3-5.3% in pre-monsoon and by 1-1.5% in post-monsoon) compared to baseline values.

In conclusion, the findings of my thesis highlight different factors that can be relevant for designing effective policies to meet $PM_{2.5}$ air quality standards over Delhi megacity, with a focus on mitigating the impact from the on-road transport sector. First, air quality over Delhi is strongly influenced by regional and seasonal pollution sources from the IGP. As such, effective mitigation of $PM_{2.5}$ pollution over Delhi will require a range of regional and state-level policies. In particular, cooperative mitigation strategies between the Delhi megacity and the broader NCR is needed if $PM_{2.5}$ pollution is to be reduced. Second, two-and three-wheelers and heavy-duty vehicles dominate on-road transport impact on $PM_{2.5}$, thus emissions reductions from these vehicles should be given priority, both within Delhi and in the NCR. Third, cleaner mobility plans of electrification of two- and three-wheelers should be accompanied by diesel vehicles conversion to compressed natural gas, to limit ozone pollution increase and further reduce $PM_{2.5}$ concentrations. This also highlights the importance of coordinated control of $PM_{2.5}$ and other pollutants such as O_3 when considering emission control strategies for transport over Delhi.

Lay Summary

Outdoor air pollution is a global public health emergency and has been recently defined as a “pandemic in slow motion”. Middle- and lower-income countries are affected disproportionately by poor-air quality. Delhi, the capital of India, is one of the most populated and polluted megacities in the world, with estimated 12,000 premature deaths were attributed to outdoor air pollution. My thesis aims to advance our understanding of outdoor air pollution in Delhi megacity. I focus on the impact of emissions from on-road transport on fine particulate matter ($PM_{2.5}$), a pollutant of major concern for human health. To do this, I use air quality modelling and local emissions datasets.

In Chapter 2 I use the WRF-Chem atmospheric chemical transport model to understand the regional influence on air quality over Delhi. I characterise the influence of seasonal emissions from human sources, fires and natural sources on fine particulate matter and one of its main constituents, organic aerosol (OA), over the Indo-Gangetic Plain, where Delhi is located. In Chapter 3, I use the WRF-Chem model together with local emissions data to quantify the contribution of on-road transport to $PM_{2.5}$ in Delhi during the highly polluted post-monsoon season. The on-road transport contribution is compared to the contributions from other local and regional human emissions sources. In Chapter 4 I use the WRF-Chem model together with future transport emissions scenarios over Delhi to investigate the impact of electric and clean-fuel vehicles on surface $PM_{2.5}$ and ozone (O_3), another pollutant o concern for human health.

The results of my thesis highlight three factors that can be relevant for designing policies to effectively reduce $PM_{2.5}$ in Delhi, with a focus on mitigating the contribution from the on-road transport sector. First, air pollution over Delhi is strongly influenced by regional and seasonal pollution sources from the Indo-Gangetic Plain. Thus, effective mitigation of $PM_{2.5}$ pollution over Delhi will require a range of regional and state-level policies. Second, two-and three-wheelers and heavy-duty vehicles are the main contributor of on-road transport $PM_{2.5}$ pollution, thus emissions reductions from these vehicles should be given priority, both within Delhi and the regional area. Third, future electrification of 2- and 3- wheelers vehicles should be accompanied by conversion of diesel heavy duty vehicles to clean-fuel vehicles (such as compressed natural gas,CNG) to limit ozone pollution increase and further reduce $PM_{2.5}$ concentrations. This highlights also the importance of multi-pollutant control when considering strategies for emissions reduction from vehicles over Delhi.

Acknowledgements

Looking back at the long roller-coaster journey of my PhD there are so many people I am grateful to.

I want first to thank the Ford Motor Company University Research Program for the generous scholarship which supported me and my research. Thanks also to Sandy, Wei and James from Ford for all the stimulating discussions on my thesis work during these years.

My gratitude goes to my first supervisor Paul Palmer for his continuous guidance and for helping me to stay on track during my PhD. He encouraged me and believed in me all the times I wasn't. I am also thankful to my second supervisor Tim Wallington, for his support and feedback throughout my PhD, and especially for his and Ali warm welcome I received during my stay in Ann Arbor. I won't easily forget all the lovely Saturday mornings spent at Zingerman's in front of an hot breakfast in the freezing Michigan winter. Thanks also to Allison Steiner, who openly welcomed me in her research group during my stay at the University of Michigan in Ann Arbor. This visiting term has been one of the best experiences during my PhD. Thanks to all the group members, in particular to Tamanna and Yingxiao, for their kindness and for the lovely time spent together.

My PhD journey would not have been the same without all the people and friends I met in Crew building and in the School of GeoSciences. In particular, thanks to Chiara, my partner in crime in Crew for all these years, and Margherita. Thank you for being my closest friends and my Italian family in Edinburgh. Thanks to all the Palmer Group members for the nice research and social time spent together, in particular thanks to Maggie, for her mentoring and friendship. I want to thank also all the great flatmates

I had the opportunity to know and spend memorable time with during my PhD: Josh, Sara, Bianca, James, Anjali. In particular, thanks to Bianca and James, it has been a gift to meet you and to share a place I could call Home. Thanks also to all my dearest friends, here in the UK and back in Italy, our friendship is precious. Being always there for each other helped me a lot in the journey of my PhD. Thanks to all my (big!) family, which has always supported me in my decisions and always believed in me. This gives me the strength to go on my way in the world. Finally, thanks to Federica, who, from near or far, is always with me and has supported me all along this journey and beyond.

Contents

Figures and Tables

Figures

Tables

Chapter 1

Introduction

1.1 Motivation and scientific questions

Air pollution is a global public health emergency and has been recently defined as a "pandemic in slow motion" (National Geographic, 2021). Outdoor air pollution is estimated to be the sixth leading risk factor for human mortality, contributing to 11.65% of deaths globally every year (Ritchie and Roser, 2021). The Global Burden of Disease study (GBD) estimates that 4.5 million premature deaths worldwide were due to outdoor air pollution in 2019 (Murray et al., 2020). The air pollution death toll estimate could be even higher, with recent study estimating that 8.7 million deaths globally in 2018 were due to the air pollution caused by burning fossil fuels, almost one-fifth of all deaths globally (Vohra et al., 2021). As a comparison, at the time I am writing this introduction (June 2022) COVID-19 pandemic has on average caused $\sim$ 2.5 million deaths worldwide per year since the start of the pandemic (Johns Hopkins University, 2022).

The pollutant that is responsible for most deaths linked to outdoor air pollution is particulate matter with diameter less than 2.5 microns ($PM_{2.5}$). The size of particulate matter and their composition is linked to their potential for causing human health problems (EPA, 2018). Main chemical components of $PM_{2.5}$ are dust, sulfate (SO_4^{2-}) nitrate (NO_3^-) and ammonium (NH_4^+), black carbon (BC) and Organic Aerosol (OA). Each component is associated with different toxicity and effects on human health (Masselot et al., 2021; Xue et al., 2021). $PM_{2.5}$ is small enough to penetrate into lung tissue and even enter in the

bloodstream, causing cardiovascular and respiratory diseases that may lead to stroke, cancer and premature death affecting both adults and children (WHO, 2021). Based on current scientific evidence, surface pollutants of concern other than $PM_{2.5}$ are nitrogen dioxides (NO_x), sulfur dioxide (SO_2) and ozone (O_3) (WHO, 2021).

Exposure to outdoor air pollution is an environmental health problem affecting people worldwide, where more than 99% of the world population live in places where air pollution is higher than recommended guidelines from WHO. However, people living in low- and middle-income countries suffer almost the totality of the burden of outdoor air pollution: 91% of premature deaths attributable to outdoor air pollution occur in these countries (WHO, 2021).

Most populated cities and megacities (metropolitan areas with populations over 10 million) present a major challenge for global outdoor air pollution. This is because outdoor air pollution in the world's most populous cities is both more severe and it affects a considerable proportion of the global population. Indeed, urban population growth together with (often) unsustainable urban development practices, drove increase in transportation, energy and industrial activities, thus leading to increasing levels of air pollution to which urban dwellers are exposed (Molina, 2021). In 2018, more than half of global population lived in urban settlements, and this is projected to reach almost 70% by 2050, with nearly 90% of the increase concentrated in Asia and Africa (UN DESA, 2019a). Pollutant emissions of on-road transport are of particular concern for their impact on air quality and human health, since dense road traffic activity is located in and around urban environments, and urban dwellers live, commute and work in proximity to traffic (Colvile et al., 2001). Some megacities experience episodic extreme air pollution, while for other, extreme levels of air pollution are chronic, especially in China and India (Marlier et al., 2016). In particular, 13 of the 20 most polluted cities in the world are in India according to the WHO (WHO, 2018).

Given the population increase in urban areas, it is thus fundamental to better understand the sources, trends and impacts of outdoor air pollution over cities. This can help to inform policy makers and relevant stakeholders on suitable and effective practices to transition to sustainable cities where clean air is available to everyone. My thesis aims to advance our understanding of outdoor air pollution in Delhi megacity, the capital of India, with a focus on the impact of on-road transport emissions on surface levels of $PM_{2.5}$ and its implications for air quality policymaking.

The megacity of Delhi, located in the northern part of India in the Indo-Gangetic Plain (IGP), is one of the most populated and polluted cities in the world (WHO, 2018). Almost 28 million people live in Delhi today, and between 2018 and 2030, the population of Delhi is projected to increase by more than 10 million inhabitants and overtake Tokyo as the world's largest city in the world by 2030 (UN DESA, 2019b). Delhi experiences continuously severe levels of air pollution, with seasonal and annual $PM_{2.5}$ concentration levels far beyond WHO's latest air quality guidelines levels (5 $\mu g\ m^{-3}$) (WHO, 2021) and Indian National Standards (40 $\mu g\ m^{-3}$). In 2017, in Delhi the annual average population-weighted mean of $PM_{2.5}$ reached 209 $\mu g\ m^{-3}$, and almost 12,000 premature deaths were attributable to outdoor air pollution that year (Balakrishnan et al., 2019). A pollution exposure assessment in the city, found that the levels of $PM_{2.5}$ pollution to which on-road commuters were exposed was at least 1.5 times compared to the average exposure concentrations in Delhi (Apte et al., 2011). Challenges to mitigate such extreme levels of air pollution arise from the complexity of air pollution over Delhi, which is shaped by concurrent local sources and regional sources in the IGP, and by the large scale monsoon system, which brings strong seasonal variations in the meteorological condition over the region. In addition, there is increasing evidence that if strategies focus exclusively on mitigating $PM_{2.5}$ concentrations, elevated levels of surface ozone (O_3) could become more of a significant health concern, because of the non-linear chemistry involved in ozone formation (Ojha et al., 2022).

In this context, my thesis first tries to better characterise and understand the regional and seasonal context of $PM_{2.5}$ over the IGP where Delhi is located. The main research question addressed in Chapter 2 is the following:

1. What are the seasonal drivers of $PM_{2.5}$ in the Indo-Gangetic Plain?

(i) What are the seasonal variations of total $PM_{2.5}$ over the IGP?

(ii) What are the seasonal variations of $PM_{2.5}$ components over the IGP, in particular organic aerosol (OA)?

(iii) What is the sensitivity of $PM_{2.5}$ and OA to anthropogenic, pyrogenic and biogenic seasonal emissions?

After the regional context is set, I move to the local context of Delhi, and focus on the impact of the transport sector in one of the most polluted seasons for the city, which has been identified as the post-monsoon in Chapter 2. Chapter 3 thus addresses the following research question:

2. What is the role of the on-road transport sector on $PM_{2.5}$ over Delhi during the post-monsoon season?

(i) What is the impact of on-road transport sector on average $PM_{2.5}$ over Delhi compared to other main local and regional anthropogenic sources?

(ii) How does the impact in i) changes when considering the diurnal variation of $PM_{2.5}$ over Delhi?

(iii) What is the contribution of each on-road transport subsector to the total on-road transport impact on $PM_{2.5}$?

(iv) Which is the impact of $PM_{2.5}$ mitigation strategies on ozone levels?

As Chapter 3 investigated the current impact of the transport sector on $PM_{2.5}$, the final research chapter looks to estimate the transport impact in the future, both for $PM_{2.5}$ an O_3. Chapter 4 thus addresses the following research questions:

3. Which will be the impact of electric and clean-fuel vehicles on future air quality over Delhi?

(i) How will surface $PM_{2.5}$ and O_3 change over Delhi under future transport emission scenarios?

(ii) How will these changes differ in contrasting (pre-monsoon and post-monsoon) seasons?

To investigate these questions and their implications for air-quality policy-making, I use a combination of a state of the art regional atmospheric chemistry transport model, recently developed local emissions inventories, and sensitivity analysis techniques.

The remainder of this chapter, provides a brief introduction to tropospheric chemistry and air pollutants (Sec. 1.2), with a focus on particulate matter (Sec. 1.3). The chapter continues with an overview of emissions from the on-road transport sector with a focus on India (Sec. 1.4), air quality modelling (Sec. 1.5) and a brief introduction of air pollution over Delhi megacity (Sec. 1.6). The final section describes the thesis layout (Sec. 1.7).

1.2 Tropospheric chemistry and air pollution

The branch of atmospheric chemistry that deals with air pollution mainly focuses on understanding, monitoring and forecasting, surface air pollutants related to human exposure. Thus, mainly the factors and processes that form pollutants in the lower part of the atmosphere, the troposphere are investigated. The troposphere extends up to 10-15km from Earth's surface, and contains 85% of all atmospheric mass, as well as being the recevoir for all the chemical species emitted from the surface. (Seinfeld and Pandis, 2016). The term "air pollutant" refers to a range of diverse atmospheric species which can have harmful effects effect for human health and the environment. Detrimental effects on human health range from acute respiratory inflammation, to chronic respiratory

and cardiovascular diseases and cancer. (Vallero, 2014). Understanding tropospheric chemistry is thus key in quantifying and monitoring the levels of air pollutants to which humans and the environment are exposed. Here follows a brief description of tropospheric constituents and processes that are relevant to atmospheric air pollution.

1.2.1 Oxidation in the troposphere

The atmosphere is a complex dynamical system, with a myriad of gaseous and particulate species continuously exchanged and produced from vegetation, ocean, land and human activities, transformed, and eventually removed from the atmosphere. Processes involving atmospheric gas and particle species span a wide range of spatial and temporal scales, from seconds and metres to million of years and thousands of km. Spatial scales relevant to urban and regional air pollution range from 100m - 1000 km, while temporal scales range from hours to days (Seinfeld and Pandis, 2016).

During the time spent in the atmosphere, almost all gas and aerosols species will be involved in physio-chemical reactions, transforming them to another physical (gas, liquid or solid) and/or chemical (different species) state.

Solar radiation plays an important role in the reactions taking place in the atmosphere, especially enabling reactions of non-radical species. The ensemble of chemical reactions in the atmosphere enabled by sunlight is called *atmospheric photochemistry*. Specifically, when a chemical compound is broken down by sunlight the reaction is called *photolysis*.

The main atmospheric process in which chemical species are involved is “oxidation”. Oxidation is the process that removes electrons from a compound through a chemical reaction. When oxidation occurs, the compound increase its oxidation state. Many trace gases are removed from the atmosphere through oxidation reactions. The most abundant oxidants on Earth’s atmosphere are O_2 and O_3 (Jacob, 1999).

Radicals are chemical species with an unfilled electron orbital. Radical species are highly reactive, because through reactions they can fill up the unpaired electron orbitals and lower their internal energy. Conversely, a non radical species is a molecule that has all its electrons paired up, and thus they are less reactive. (Jacob, 1999)

In the 1970s it was discovered that the hydroxyl radical (OH) is also a fundamental oxidant in the troposphere (Levy, 1971). Because of its role in reducing the lifetime of many pollutants, it is sometimes called “the detergent of the atmosphere” (Riedel and Lassey, 2008).

Production of OH is enabled by sunlight ($h\nu$) in the presence of O_3 and water vapour (H_2O). First, photolysis of ozone forms $O(^1D)$ (electronically excited O atoms) by absorption of a photon. Second, O(1D) reacts with H_2O to produce two OH radicals (Levy, 1971):

$$O_3 + h\nu \longrightarrow O_2 + O(^1D) \tag{1.1}$$

$$O(^1D) + H_2O \longrightarrow OH + OH \tag{1.2}$$

OH concentrations show strong diurnal and seasonal cycles. OH concentrations also tend to decrease with increasing altitude (due to decreasing humidity), because of its dependence on sunlight and water vapour respectively. Because of its high reactivity, OH has a very short lifetime ($\sim 1s$) and its concentrations are usually low. OH concentrations are estimated to be 1.1-1.2 $\sim 10^{-6}$ molecules cm^3 (Li et al., 2018; Rigby et al., 2017). Thus, OH is also very difficult to measure, leading to high uncertainties in the estimations of its budget and therefore there are large uncertainties in its atmospheric concentrations (Heard and Pilling, 2003).

1.2.2 Gaseous pollutants

Gaseous pollutants that affect human health and the environment are trace gases, i.e. gases that are present in small amounts in the atmosphere. Trace gases constitute just $<$0.1 % of all atmospheric mass. Usually, concentrations of gases in the atmosphere are expressed in terms of *mixing ratio*. The mixing ratio C_x of a species X is defined as the number of moles of X for moles of air. it is given in units of mol/mol (moles per mole) or v/v (volume of gas per volume of air), since the volume of a gas in proportional to the number of gas molecules. Mixing ratios of trace gases, are mainly expressed in units of *parts per million by volume (ppm)* (ppm= 1x10^{-6} mol/mol),*parts per billion by volume (ppm)* (ppb=1x10^{-9} mol/mol), and *parts per trillion by volume (ppm)* (ppt = 1x10^{-12} mol/mol). These are the units that are typically reported by air pollution surface measurements networks. Mixing ratios can be converted to μg m^{-3} through the ideal gas law.

The most important ambient (outdoor) gaseous air pollutants are carbon monoxide (CO), sulphur dioxide (SO_2), nitrogen oxides (NO_x), volatile organic compounds (VOCs), and ozone (O_3). All these pollutants are associated with negative health impacts when commonly emitted from anthropogenic activities in and around human settlements. These pollutants are also “criteria pollutants”, i.e. their concentrations are monitored and benchmarked against national and/or international air quality standards to determine whether a city, region or nation is meeting safe concentrations for humans health.

CO Carbon monoxide is a major sink for OH, thus playing an important role in tropospheric chemistry (Jacob, 1999). Main sources of CO are incomplete combustion (fossil fuel burning, biomass burning, wildfires), and almost all the CO present in today troposphere is of anthropogenic origin (Jacob, 1999). The main sink of CO is oxidation

by OH. Because of OH its dependence, seasonal variability in CO is due mainly to the role of sunlight in OH production following Equation 1.1. This results in an estimated lifetime which varies between of 30-90 days (Novelli et al., 1992), with longer lifetime during winter and lower during summer.

Concentrations of CO can vary from around 50 ppb in rural areas to over 300 ppb in urban areas, and reach peaks beyond 1000 ppb at hot spots of CO, such as forest fires (Hornbrook et al., 2011; Palmer et al., 2013). The current WHO guidelines for CO are set to 7 $\mu g\ m^{-3}$ 24-hour mean (WHO, 2021).

SO$_2$ Sulfur dioxide is a gas of both anthropogenic and biogenic sources. Anthropogenic sources originates from fossil-fuel burning, such as in coal power-plants, and industrial processes, while natural emissions of SO_2 are almost entirely produced by volcanic activities (Smith et al., 2001). Beyond being toxic for humans, it is a major contributor to acid rain, through subsequent oxidation that forms sulfuric acid in the atmosphere that are then deposited by rain, snow, fog (Bricker and Rice, 1993). SO_2 has also implications in the formation of sulfate secondary aerosols (Section 1.3.2) The lifetime of SO_2 is around 1 week against OH oxidation (Brasseur and Jacob, 2017). The current WHO guidelines for SO_2 are set to 40 $\mu g\ m^{-3}$ 24-hour mean (WHO, 2021).

NOx Nitrogen oxides radicals (NO_x = NO + NO_2) are emitted in the troposphere from anthropogenic sources through by fossil fuel combustion, and from natural sources from wildfires, lightning and microbial processes in the soil. Combustion is by far the major source of NO_x in the troposphere (Lee et al., 1997; Logan, 1983). During daytime a fast cycling (timescale of $\sim$ a minute) between NO and NO_2 take place in the troposphere (Jacob, 1999):

$$\mathrm{NO} + \mathrm{O_3} \longrightarrow \mathrm{NO_2} + \mathrm{O_2} \tag{1.3}$$

$$NO_2 + h\nu \xrightarrow{O_2} NO + O_3 \tag{1.4}$$

This is a *null cycle*, since it has no effect on atmospheric composition. Because of the short time of the cycling between NO and NO_2, it is more appropriate to consider them together in the NO_x family, although NOx is mainly emitted in the form of NO. During nighttime only reaction 1.3 in the cycle takes place because of the absence of sunlight, and NO_x is present only as NO_2. The principal sink of NO_x is oxidation against nitric acid (HNO_3), both at daytime and nighttime resulting in a lifetime of tropospheric NO_x of up to 1 day. HNO_3 is then removed from the atmosphere through wet deposition given its high solubility in a time scale of few days, and thus cannot be considered as a recevoir species that then recycle NO_x in the atmosphere through subsequent reactions (Jacob, 1999). Because of short lifetime of NO_x and fast removal of nitric acid, NO_x distribution across the globe shows strong gradients between combustion sources and remote regions (Brasseur and Jacob, 2017). The current WHO guidelines for NO_2 are set to 10 $\mu g\ m^{-3}$ annual mean and 25 $\mu g\ m^{-3}$ 24-hour mean (WHO, 2021).

VOCs Volatile organic compounds are a group of species mainly found in the form of hydrocarbons (C_xH_y), excluding of methane (CH_4). Atmospheric oxidation of VOCs leads to a chain of oxygenated VOCs and production of secondary particulate matter (see Section 1.3.2) that eventually ends with the highest oxidation state in CO or CO_2. VOCs are short-lived against oxidation (typically hours to few days), with OH being the main sinks for most VOCs. VOCs chemistry is responsible for much for the complexity of the chemistry of the troposphere (Brasseur and Jacob, 2017). Natural sources are the dominant source of VOCs on a global scale (90% of all VOCs emitted) with isoprene the most abundant. However their spatial distribution is heterogeneous when considering geographical location. Natural emissions of VOCs are found mainly in the tropical regions, while anthropogenic emissions of VOCs occur mainly in densely

populated, industrialised and urbanised regions where natural emissions are relatively low. Thus anthopogenic VOCs can have significant impacts on urban and regional air quality chemistry despite small emissions on the global scale (Prather et al., 2001). However, emissions from urban vegetation can also have a non-negligible impact on urban air quality (Chameides et al., 1988). Many VOCs are also emitted by common household and self-care products (McDonald et al., 2018; Rösch et al., 2014; Wallace et al., 1987), thus mainly affecting indoor air quality. Guidelines levels for VOCs are mainly set for indoor environments (Public Heath England , 2019), and for selected VOCs mainly from solvent uses in industrial manifacturing (Dobson, 1999) and common consumer and household products (Steinemann, 2015).

O$_3$ About 90% of atmospheric ozone is in the stratosphere between 20-30km above the surface, and it is important as natural filter for damaging UV light radiation (Seinfeld and Pandis, 2016). However the remaining ozone that is found in the troposphere is harmful to human health as well damages crop yields (McKee, 1993).

Tropospheric ozone is not emitted directly into the troposphere, but is produced by oxidation of CO and VOCs by HO$_x$ radicals (HO$_x$ =OH+ HO$_2$) in the presence of NOx. The main source of ozone in the troposphere is given by a sequence of reactions. In the simple case of CO: (Brasseur and Jacob, 2017):

$$\mathrm{CO} + \mathrm{OH} \xrightarrow{\mathrm{O_2}} \mathrm{CO_2} + \mathrm{HO_2} \tag{1.5}$$

$$\mathrm{HO_2} + \mathrm{NO} \longrightarrow \mathrm{OH} + \mathrm{NO_2} \tag{1.6}$$

$$\mathrm{NO_2} + \mathrm{h}\nu \xrightarrow{\mathrm{O_2}} \mathrm{NO} + \mathrm{O_3} \tag{1.7}$$

$$\text{Net} \quad \mathrm{CO} + 2\,\mathrm{O_2} \longrightarrow \mathrm{CO_2} + \mathrm{O_3} \tag{1.8}$$

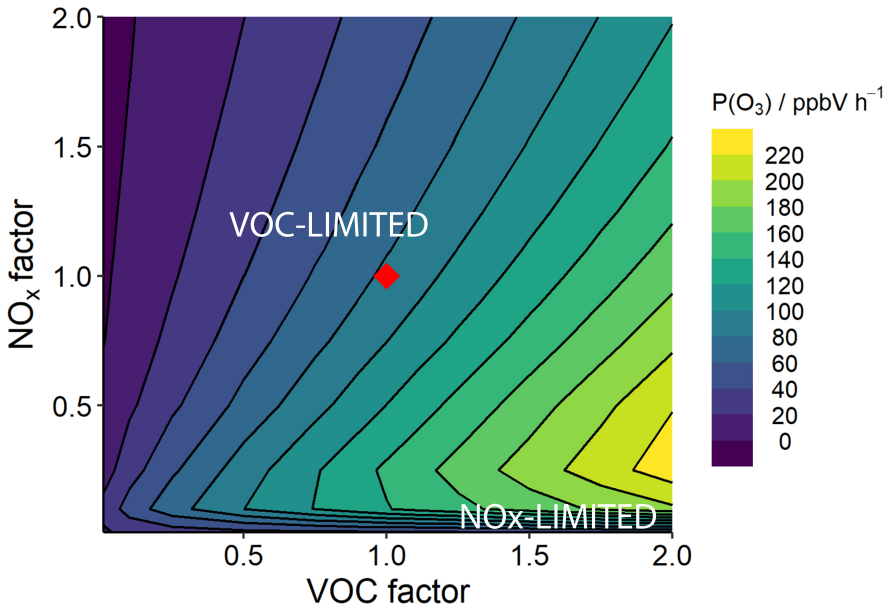

Figure 1.1: Ozone isopleth diagram showing the dependence of mean ozone production $P(O_3)$ on NO_x and VOCs concentrations from a box model simulation for the city of Delhi. VOC- and NO_x limited regimes are shown. The red diamond at point (1,1) represents modelled at observed VOC and NO_x concentrations in Delhi, supporting the assignment of Delhi being, on average, in a VOC-sensitive photochemical regime. The factor shown on both axis is a scaling factor for VOC and NO_x concentrations relative to the observed VOC-NO_x concentrations in Delhi (red diamond). Modified and adapted from Nelson et al. (2021).

For VOCs, the chain of reaction is similar, but with organic peroxy radical RO_2 reacting with NO to form NO_2, which then undergoes photolysis. In both processes, NO_x and with HO_x are catalysts for the oxidation of CO and VOCs by O_2. An additional minor source of O_3 is provided through transport of ozone from the stratosphere. Thus the rate of ozone production is strongly dependent on HOx, NOx and VOCs supply in a non-linear way, mainly controlled by cycling of HO_x in competition with HO_x removal (Brasseur and Jacob, 2017). This results in two main ozone production regimes. A *NO_x-limited regime*, when ozone production rate increase with NO_x concentrations but does not depends on concentrations of VOCs and CO. The NO_x-limited regime is typical of location downwind of urban and suburban areas. A *VOC_x- limited regime*, occurs when ozone production rate increase inversely with NO_x concentrations and linearly

with VOCs and CO concentrations. The VOC-limited regime is typical of polluted urban environments (Brasseur and Jacob, 2017). Figure 1.1 shows the calculation of a simple chemical model for ozone isopleths production (i.e. lines with constant mixing ratio) and its dependence on NO_x and VOCs concentrations for the city of Delhi, highlighting non -linearity in the range of transition production states between the NO_x- and VOC- limited regimes.

The major sink for tropospheric ozone is the photochemical loss in the presence of water vapour and reactions with HO_x radicals (Seinfeld and Pandis, 2016) with an additional sink from deposition to the surface. Lifetime of ozone ranges from a few days close to the surface to months in the upper troposphere.

The current WHO guidelines for O_3 are set to 100 $\mu g\ m^{-3}$, 8-hour daily maximum average $\mu g\ m^{-3}$ and 60 $\mu g\ m^{-3}$ 8-hour mean for peak season. WHO defines the peak season as the average of daily maximum 8-hour mean O_3 concentration in the six consecutive months with the highest six-month running average O_3 concentration. (WHO, 2021).

1.3 Particulate matter

Aerosols particles are usually defined as a complex mixture of solid particles and liquid droplets found in the air (EPA, 2018). In the air quality community, particulate matter PM refers in general to the solid particles phase. Unit of measure for PM is usually micrograms per cubic metre $[\mu g\ m^{-3}]$ (Brasseur and Jacob, 2017). The current WHO guidelines for $PM_{2.5}$ (PM with diameter $\leq$ 2.5 μm) are set to 5 $\mu g\ m^{-3}$ annual mean and to 15 $\mu g\ m^{-3}$ 24-hour mean. For PM_{10} (PM with diameter $\leq$ 10 μm), it is 15 $\mu g\ m^{-3}$ annual mean and 45 $\mu g\ m^{-3}$ 24-hour mean (WHO, 2021). Here follows a brief description of sources and sinks of PM, their composition and the role of meteorology in shaping PM concentrations.

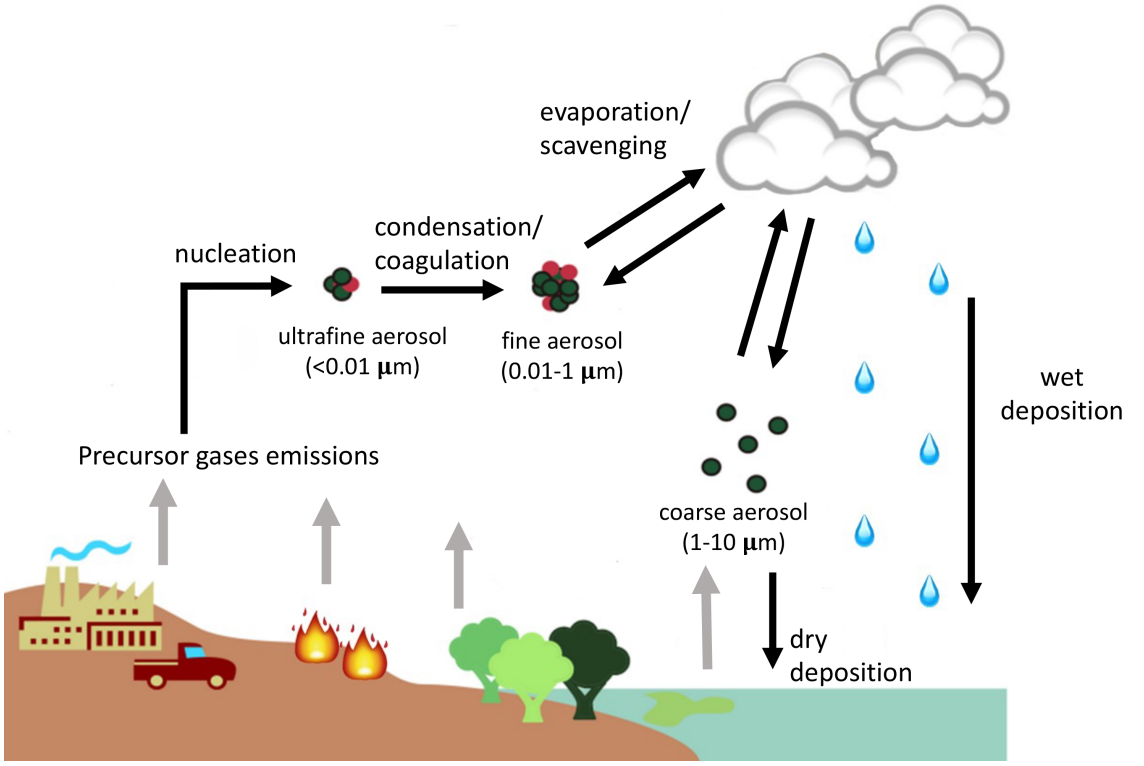

Figure 1.2: Schematic representation of the processes governing PM life cycle. Modified and adapted from Riipinen et al. (2011).

1.3.1 Sources and sinks

PM is introduced in the atmosphere both as direct emissions from sources (primary PM) or form in the atmosphere as a result of complex physio-chemical reactions (secondary PM) (Figure 1.2).

A first distinction in PM is done according on the particles size. PM_{10} refers to PM particles with diameter $\leq$ 10 µm in diameter, $PM_{2.5}$ those with diameter $\leq$ 2.5 µm, also called *fine particulate matter*. Sources of primary PM_{10} and $PM_{2.5}$ include natural sources such as such as dust, seaspray, volcanic activity, wildfires, as well as human (anthropogenic) activities, such as combustion of fuels, agricultural activities, construc-

tion dust, industrial processes (Figure 1.2). Primary natural PM are mainly found in the *coarse mode*, which consist of PM with a radius 1-10 μm, thus contributing more to PM_{10}, while anthropogenic emissions from combustion processes (soot) usually are found in the *fine mode*, with radius ≤ 1 μm, and they contribute more to $PM_{2.5}$ mass.

Secondary PM are mainly found as $PM_{2.5}$, and form from precursors gases through gas-to-particle transformation processes, as shown in Figure 1.2 (Brasseur and Jacob, 2017; Jacob, 1999). They are almost exclusively found in the fine mode. Gas molecules have usually a size between 10^{-4} - 10^{-3} of a μm. When gas molecules cluster together (*nucleation*), they form particles with a radius between 10^{-3} - 10^{-2} of a μm, called *ultrafine aerosols*. Ultrafine aerosols then grow either through more gas molecules collected on their surface and converted to particles (*condensation*) or through random collisions with other particles (*coagulation*). Growth beyond 1 μm is slower because both condensation and coagulation rates are reduced by larger particle size. Thus particles formed through condensation and coagulation tends then to accumulate in the 0.01 - 1 μm size range, which takes then the name of *accumulation mode* (Jacob, 1999).

Once in the air, both $PM_{2.5}$ and PM_{10} has an average residence time in the lower troposphere (atmospheric lifetime) of around 1-2 weeks, before being removed from the atmosphere to the ground (Figure 1.2). PM are removed effectively by *dry deposition* and *wet deposition* processes. Through dry deposition, PM is directly deposited to the Earth's surface. Through wet deposition, PM is deposited in an aqueous form through precipitation processes, such as rain, snow or fog. Dry and wet deposition also apply to gaseous species, and this is important when considering removal of precursors gases of secondary $PM_{2.5}$. Dry deposition is most effective closer to the ground and for PM_{10}. Wet deposition is most predominant at altitudes above 100m from the surface, and is the main removal process for $PM_{2.5}$ in the ultrafine and accumulation mode, which are removed mainly by scavenging by cloud droplets followed by rainout (Brasseur and Jacob, 2017; Seinfeld and Pandis, 2016).

1.3.2 Composition

$PM_{2.5}$ chemical composition is classified based on dominant aerosol types found in the $PM_{2.5}$. Primary components of $PM_{2.5}$ usually consist in dust from natural mechanical removal of soil, sea salt from marine spray, black carbon (BC) and *primary organic aerosol* (POA) which originate by incomplete combustion both from natural (e.g. wildfires) and anthropogenic (fossil fuel burning) processes. Organic aerosol (OA) refers to particulate matter composed of organic compounds. OA is mainly composed of organic carbon OC, a typical complex mixture of several organic compounds (Seinfeld and Pandis, 2016).

An important secondary component of $PM_{2.5}$ is *secondary organic aerosol* (SOA). SOA formation is enabled through processes that change the *volatility* of OA, with lower volatility *volatility* favouring SOA formation. Volatility describes the tendency of a substance to evaporate. For practical reasons, volatility of a compound is usually expressed in term of its saturation mass concentration C^0, in units of μg m^{-3}. The saturation concentration is obtained from the saturation vapour pressure via the ideal gas law (Seinfeld and Pandis, 2016). The most important atmospheric mechanism of SOA formation is the oxidation of gas-phase volatile organic compounds (VOCs), that creates products with lower volatility that then can condense into the particle phase forming SOA (Jimenez et al., 2009). Oxidation process has been introduced in Section intro:oxidation. POA also can dilute and evaporate forming vapours, which can react and recondense to SOA (Robinson et al., 2007). Precursor VOCs that lead to SOA formation are mainly found in the form of hydrocarbons. All VOCs species, with saturation concentration C^* higher than $10^6\ ug\ m^{-3}$ are well known SOA precursors. However, recent studies have pointed out that semivolatile organic compounds (SVOCs) and intermediate volatile organic compounds (IVOCs) (volatility range $10 - 10^6\ ug\ m^{-3}$) can also contribute to SOA formation (Hodzic et al., 2010; Kroll and Seinfeld, 2008; Robinson et al., 2007). Oxidation can be initiated by different chemical species in the atmosphere, such as OH and

ozone (introduced in Section 1.2.2) and nitrate radical (NO_3) (Kroll and Seinfeld, 2008; Seinfeld and Pandis, 2016). Oxidation of gas-phase VOCs have shown also an important dependence on nitrogen oxides (NO_x) concentrations. Indeed NO_x levels influence the relative proportion of OH, NO_3, and O_3, and the peroxy radicals RO_2 fate, by controlling the branching of subsequent reactions, i.e. the number and type of active intermediates which are created in the reaction chain (Ng et al., 2007; Presto et al., 2005; Zhang et al., 2006a). Processes that lead to the formation of SOA are still not completely explained and understood, and despite significant advances in understanding SOA properties and formation mechanisms have occurred over the past decade, understanding SOA remains an important challenge for atmospheric science (Fuzzi et al., 2015).

Other significant secondary component are inorganic secondary aerosols, mainly sulfate (SO_4^{2-}) nitrate (NO_3^-) and ammonium (NH_4^+). Typically, sulfate and nitrate are coupled with ammonium, so that one talks about the sulfate-nitrate-ammonium aerosol (SNA) (Brasseur and Jacob, 2017). SNA forms through oxidation of precursors gases SO_2, NO_x and NH_3. NH_3 is emitted by agricultural activities, especially through the use of fertilisers.

Overall, the composition of $PM_{2.5}$ can vary greatly from one location to another across the globe, reflecting the peculiarity due to the geographical and physio-chemical environment and type and location of emissions sources (Figure 1.3).

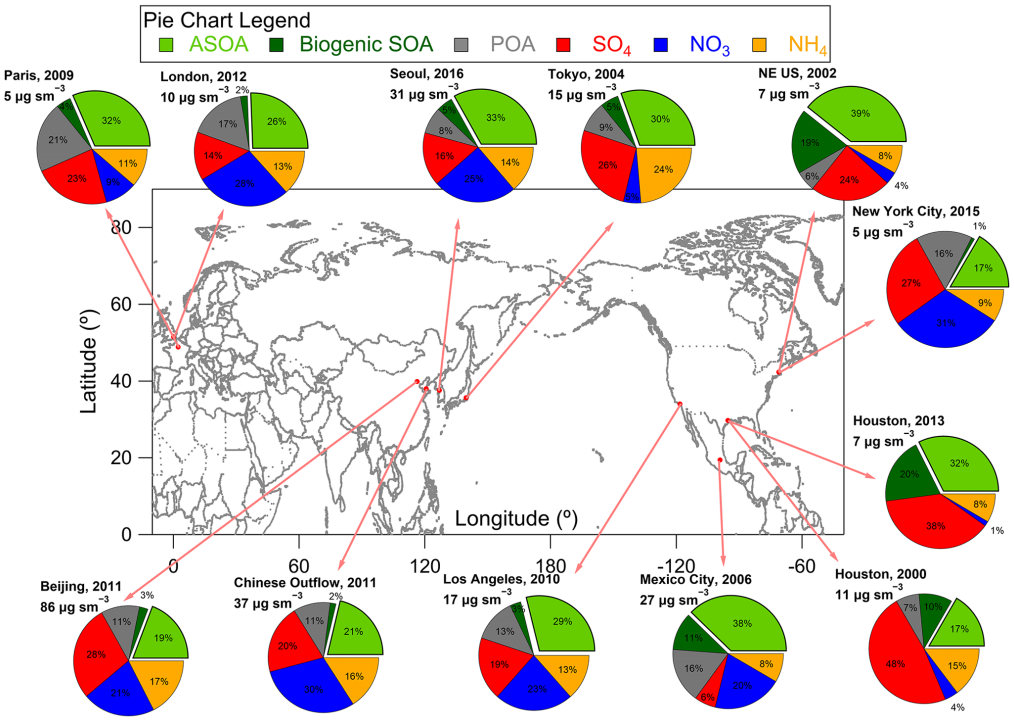

Figure 1.3: PM_1 composition (non-refractory only, i.e. excluding BC) measured in urban and urban outflow regions (units of $\mu g m^{-3}$) at standard temperature (273 K) and pressure (1013 hPa). ASOA= secondary organic aerosol from anthropogenic sources; Biogenic SOA= secondary organic aerosol from biogenic sources; POA= primary organic aerosol; SO_4 = sulfate; NO_3 = nitrate; NH_4 = ammonium. Adapted from Nault et al. (2021)

1.3.3 Role of meteorology

Meteorology can affect concentrations of $PM_{2.5}$ and PM_{10} as well of gaseous pollutants, and thus influencing the air we breathe. The fundamental meteorological variables that affect the movements of air pollutants in the air are wind speed and direction the planetary boundary layer (PBL) height. The PBL is the layer of the atmosphere that interacts with the Earth surface on a timescale of a day or less. Both wind and PBL affect turbulent air mixing, such that more turbulence promotes faster and more efficient pollution mixing and dispersion.

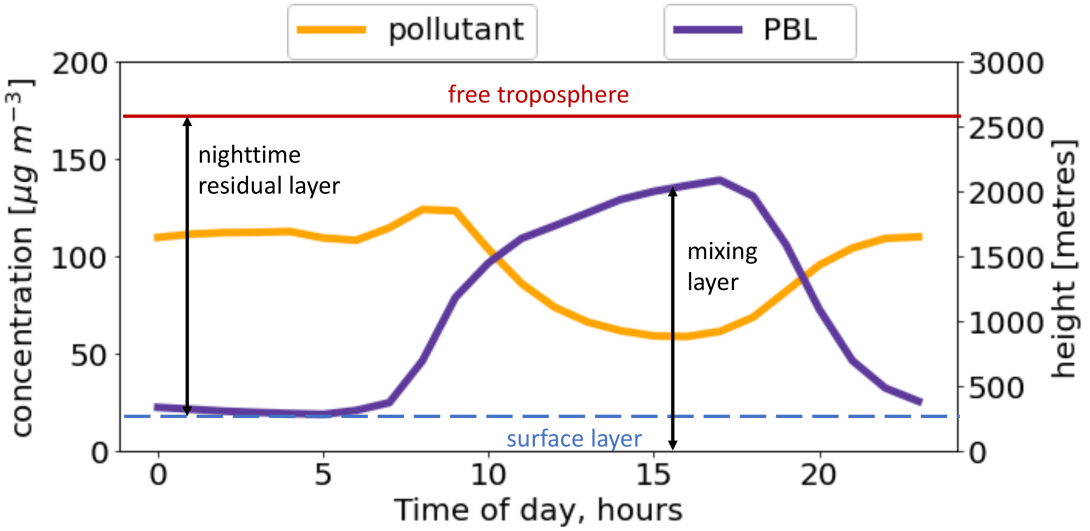

Figure 1.4: Diurnal evolution of the planetary boundary layer (PBL) and implications for surface pollutants concentrations.

The stronger the wind speed and the more constant the wind direction, the more the pollutants are effectively dispersed in the air, leading locally to lower $PM_{2.5}$, PM_{10} and other gaseous pollutants concentrations. $PM_{2.5}$ and PM_{10} and can be transported by the wind for very long distances from where they were emitted or formed to other location at downwind distances (Figure 1.2), and this is called long-range transport. Pollution can be transported to neighboring regions, to across borders and even across continents. An example of long-range transport of pollutants is the travel of large plumes of dust from the Sahara desert to Southern Europe and to Trans Atlantic regions (Sakhamuri and Cummings, 2019; Wang et al., 2020b). Ambient $PM_{2.5}$ and PM_{10} concentrations in urban settlements are usually determined by a combination of local emissions and long-range transport, while in rural or remote regions are mainly determined by long-range transport, since local emissions are often small (Moran et al., 2014).

PBL diurnal dynamics have an important impact in determining the daily cycle of air pollutant concentrations at the surface of Earth (Figure 1.4). As discussed above, mixing of pollutant in the PBL is caused by turbulence. Turbulence can be *mechanical turbulence*, generated by the friction of winds with rough surfaces, or *buoyant turbulence*, driven by

buoyancy (the ability of objects to float in water or air). Figure 1.4 shows how the PBL structure evolves over land. The evolution of PBL is mainly driven by surface heating and cooling across the day, with solar heating promoting vertical mixing of pollutants within the PBL. During the night hours, cooling of surface reduces the PBL to a shallow surface of around 10-100m of height. At night the PBL layer is maintained stable and well-mixed thanks to mechanical turbulence. Above that, there is a stable residual layer. From sunrise onward, the surface heats up and destroys the stability of the residual layers from above, creating an unstable mixed layer above the surface layer. The mixed layer grows in the morning hours with the sun radiation that intensifies and reaches the maximum height in the middle of the day (1-3km). After sunset, the cooling of surface shrinks the mixed layer and the nighttime conditions return again (Brasseur and Jacob, 2017). Driven by the PBL diurnal dynamics, air pollutant emissions during the night remains trapped in the shallow surface layer, resulting in higher concentrations. As the mixed layer starts to grows at morning, it helps to dilute pollutants from the surface, leading to a decrease in pollutant concentrations (Figure 1.4).

1.4 Emissions from the transport sector

Emissions from the transport sectors impact the climate by direct emissions of GHG, and air quality, by direct emissions of harmful pollutants and precursors gases that contribute the formation of secondary pollutants. The transport sector as a whole, including road, rail, shipping and aviation transport, is a significant emitter of GHG and harmful pollutants. It is estimated that in 2019 the transport sector produced 8.7 $GtCO_2eq$ (carbon dioxide equivalent) of direct GHG emissions, approximately 23% of total energy-related CO_2 emissions. Emissions from transport in middle income countries, such as India, have increased more rapidly than North America and Europe, a trend that is likely to continue in coming decades (IPCC, Chapter 10 - Transport, 2022). Despite the emer-

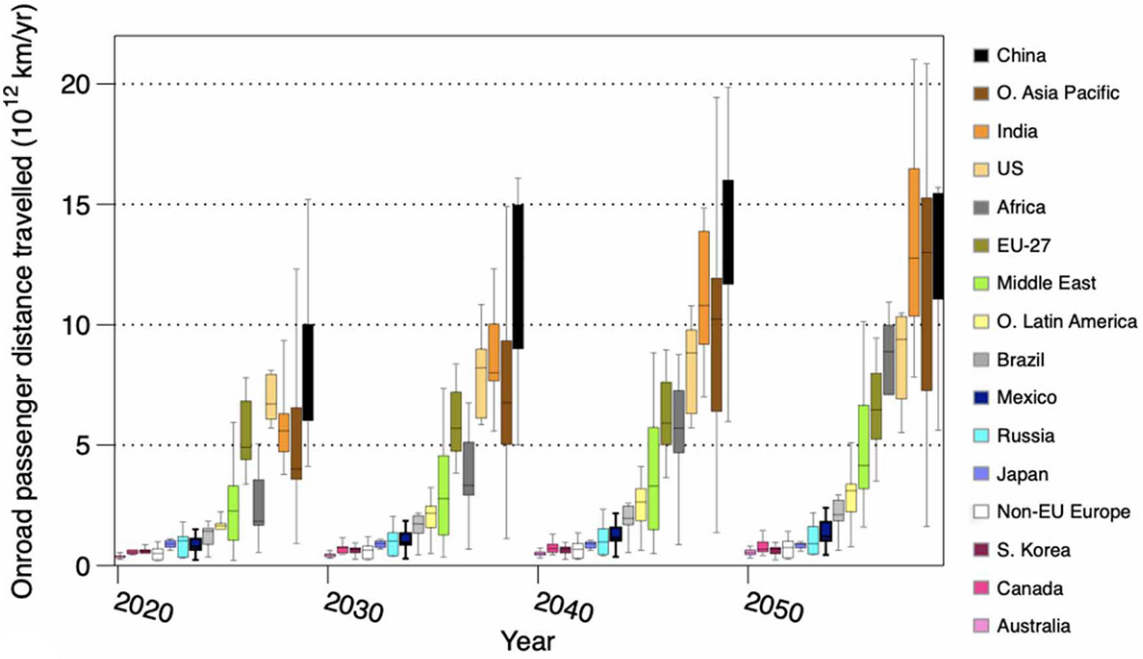

Figure 1.5: Projections of annual on-road passenger distance travelled, 2020–2050, based on transport systems models that contribute to the International Transport Energy Modeling (iTEM) intercomparison exercise (`https://transportenergy.org/`). The box plots show the interquartile ranges between the first and third quartile. The whiskers are drawn to the smallest/largest non-outlier. Modified and adapted from Yeh et al. (2022).

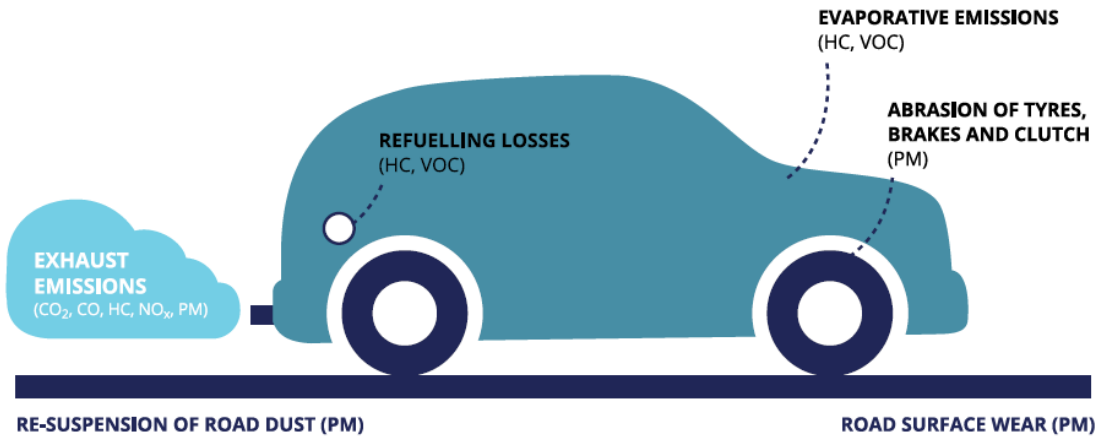

Figure 1.6: Schematic representation of emissions from on road vehicles. Adapted from European Environmental Agency (2016).

gence of electric mobility, reducing global transport emissions is a challenge since the continuing growth in passenger and freight activity, especially in lower and middle income countries (IEA, 2021; Lamb et al., 2021). Figure 1.5 shows future projections for travel demand across the world.

Road transport is the major source of emissions from transport, accounting for 70% of total GHG emissions from the whole transport sector (IPCC, Chapter 10 - Transport, 2022). Emissions of road transport are also the most of concern for their impact on air quality and human health (Colvile et al., 2001). Dense road traffic activity is located in and around urban environments, which are home today to around half of global population, a trend that is expected to increase in the coming decades (UN, DESA, 2018).

1.4.1 Road transport emissions

Emissions from road transport are directly emitted from the tailpipes of cars, trucks and other on-road vehicles (exhaust emissions), brake and tyres wear (non-exhaust emissions), re-entrained from materials found on the roadway (fugitive dust), and created by secondary formation from precursor emissions (Hodan and Barnard, 2004) (Figure 1.6).

Exhaust emissions are mainly the product of incomplete internal-combustion engines of the vehicle. Main pollutants emitted are gaseous pollutants: NO_x, CO, CO_2, and VOCs and SO_2, but also account for emissions of POA and BC (soot). However, exhaust-emissions of pollutants can vary considerably between engines (and thus fuel used), and are dependent on many other factors like ignition timing, speed, and fuel/air ratio (Abdel-Rahman, 1998) and driving behaviour (Suarez et al., 2022). Despite average lower CO_2 emissions through better mileage efficiency, diesel vehicles tends to emit more air pollutants than gasoline vehicles, especially NO_x, POA and BC (Abdel-Rahman, 1998; Jacobson, 2010). Diesel fuel has been shown to produce more SOA than gasoline. This has been linked to the different volatility distribution of the hydrocarbons mixture for diesel and gasoline fuels. Gasoline hydrocarbons fall mostly within the VOCs range, which corresponds to saturation mass concentration higher than $10^6\ ug\ m^{-3}$ as described previously in Section 1.3.2. On the other hand, diesel hydrocarbons are mostly in the IVOCs range (volatility range $10 - 10^6\ ug\ m^{-3}$) and only 30% of diesel fuel hydrocarbons are in the VOCs range, leading to a higher SOA formation for diesel compared to gasoline (Gentner et al., 2012; Gordon et al., 2014).

Historically, stringent emission regulations have driven the reduction of exhaust-emissions from vehicles. In the US, landmark Clean Air Act in 1970 established the legal authority for the Environmental Protection Agency to regulate pollutant emissions from transportation. Adopting increasingly stringent standards, sparked technology development and implementation from the automotive industry, such as the catalytic converter, fuel injection, on-board diagnostics, and currently, electric vehicles. Europe as well started to regulating vehicle emissions in the second half of the last century, with the introduction of a standard framework in the early 90's . The standards are defined in a series of regulations with progressive increasingly stringent standards. The stages are referred to as EURO I, EURO II, EURO III, EURO IV, E EURO V and finally EURO VI which is currently adopted. These Standards regulates emission of the major gaseous and

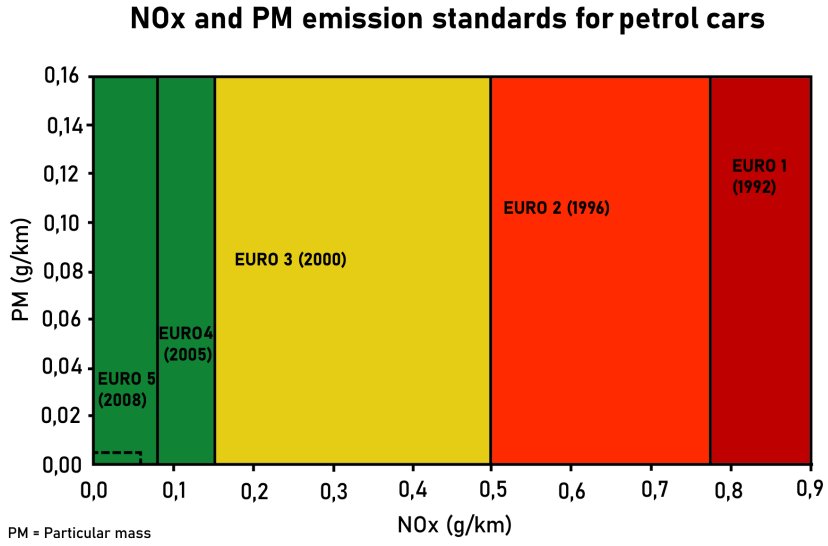

(a)

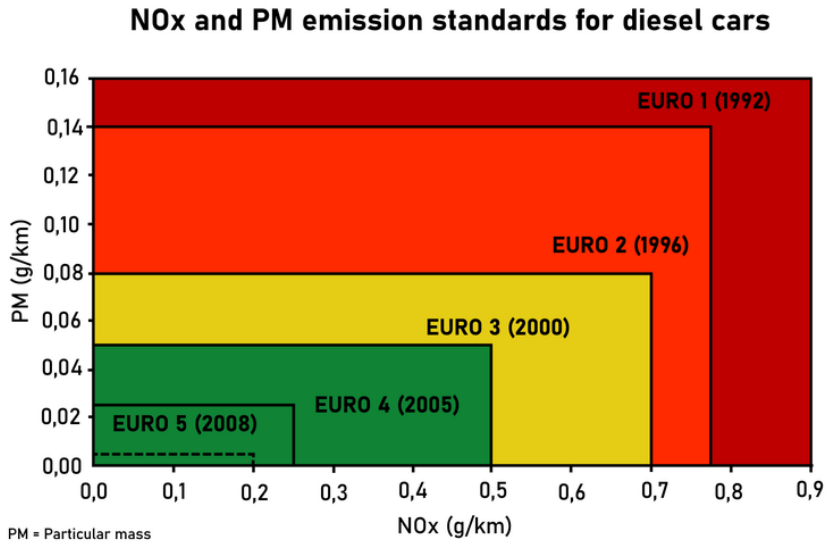

(b)

Figure 1.7: Progression of European emission standards for gasoline cars (a) and diesel cars (b) for Nox and PM. PM here refers to PM_{10}. Source: Wikimedia Commons, by Rfeba - Own work, CC0, `https://commons.wikimedia.org/w/index.php?curid=113499715`)

particulate pollutants described in Section 1.2.2, namely NOx, VOCs, CO, and PM, and compliance to the standards is done through a lab-based test. For each vehicle type, different standards apply. Figure 1.7 shows the EURO standard progression for petrol and diesel cars for NOx and PM pollutants (Hooftman et al., 2018). These regulations has made possible in western countries to witness in the last decades decreasing trends in total exhaust-emissions from road vehicles, despite the increase in total kilometres driven (Frey, 2018). For example, in Europe between 1990 and 2016, emissions of NO_x from road transport shrinked by 41%, those of CO and VOCs by 85 %, SOx by 63 %, and emissions of $PM_{2.5}$ had decreased by 40 % from 2000 levels (EEA, 2018). With the EU banning on the sale of new petrol and diesel cars from 2035, and the increasing popularity of electric vehicles, emissions from transport have the potential to be further reduced (Weiss and Scherer, 2023). However, there is increasing evidence that emissions performance of vehicle during lab-base test for approval is not representative of real driving conditions, leading to an underestimation of true emissions of vehicles on the road. Indeed, real emissions are dependent on driver behaviour, vehicle age, and many other factors that are not taken into account during the lab-based approval test. The European Commission has introduced a new measurement requirement with portable emissions measurement system (PEMS), which can test emissions in real driving conditions to try to reduce this gap (Hooftman et al., 2018).

In contrast to the situation regarding exhaust emissions, no policies are in place to reduce tyre wear emissions or resuspension, and usually countries do not report these emissions, but they can be important especially for their contribution to PM_{10} (Denier van der Gon et al., 2013) . Indeed, non-exhaust particles are mainly emitted through mechanical processes and thus tends to be coarse and contributes mainly to the mass of PM_{10}. However, tyre and brake abrasion can emit also particles $\leq$ 1 µm, contributing to the $PM_{2.5}$ mass fraction (Gietl et al., 2010).

Transport emissions can be quantified through mainly two different approaches, “top-down” and “bottom-up” to generate an emissions inventory. These inventories can be also used in air quality models, to estimate the impact of these emissions on a different range of pollutants. To estimate road transport emissions with a top-down approach, total pollutant activities for the area of interest need to be estimated (e.g. national/regional petrol sales for road transport). This quantity is then related to the air pollutant emissions by emissions factors, usually expressed as grams of pollutant per liter of fuel. Emissions factors can be obtained by laboratory measurements of representative sample of vehicles. Then the total pollutants amount is disaggregated spatially to obtain local emissions, by scaling the emissions proportionally to other variables which are assumed to correlate geographically to transport polluting activity, e.g. population density, or road lengths per unit area (Colvile et al., 2001).

The bottom-up approach starts by estimating local geographical resolved data through direct data collection (e.g.traffic flow at lengths of different road types). Direct measurements of all traffic sources are not possible, and thus these need to be estimated through emissions factors. (Colvile et al., 2001). All the individual contribution are then sum up for the area of interest to obtain the total emissions for the areas as:

$$E = \sum_i A_i \times EF_i$$

where A_i is the activity (in this case km travelled) and EF_i is the emission factor (g/km) for the vehicle source i.

Invariably, the top-down and bottom-up methods give different total emissions estimates, as each is affected by different error sources. Significant systematic errors can be given by the estimation of emission factors and fleet composition, especially when considering road transport emissions with high temporal resolution which depend strongly on the daytime, weekday and road category (Kühlwein and Friedrich, 2000). To reduce uncertainty,

more spatially and temporally resolved traffic volume data are required. The application of new technologies, especially remote sensing of traffic emissions, are showing to be promising in improving the estimates of real time traffic emissions (Dallmann, 2018; Mukherjee et al., 2021).

1.4.2 Indian road transport

India has seen a rapid population growth and economic liberalisation in the last few decades. Today, India is home to 1.38 billion people, which is almost 20% of the total global population, and it is estimated to be the fifth largest economy in the world by gross domestic product (World Bank, 2022). The increase in urbanisation and volume of economic activities resulted in an increase in mobility for transportation goods and services and for personal mobility. The number of on-road vehicles in India has grown steadily, with the number of motor vehicles increasing from 19 million in 1990 to over 48 million in 2000 (+155%), and they are expected to reach 200 million by 2030 (Kumar et al., 2022; Singh et al., 2008).

In India the most popular type of motor vehicle is the two wheelers, representing 75-80% of all vehicles sales in India, followed by 4 wheelers for passenger cars (12-15%), and three wheelers and commercial vehicles (5% each) (MoRTH, 2021). Two wheelers are popular because of their affordability and because, together with 3 wheelers, they are an efficient means of transport for daily commuting and for commercial purposes, especially in urbanised areas. Main mega cities of India (Delhi, Kolkata, Mumbai, Bangalore, Chennai, Hyderabad) have seen a shift since the end of the last century from the share from public transport to private transport (Jalihal et al., 2005). Typically, public passenger and cargo vehicles are fueled by diesel, while private two wheelers, cars and light motor vehicles (passenger) are fuelled by petrol. Diesel consumption constitutes around 80% of

total fuel consumption, primarily due to the high volume of freight and passenger traffic, and diesel fueled passenger and freight vehicles are the biggest contributors to the total emissions from the transport sector (Guttikunda and Mohan, 2014; Ramachandra et al., 2009; Singh et al., 2008).

In particular in Delhi, two- and three-wheelers such as auto-rickshaws and motorized two-wheelers represented almost 65% of the total number of registered motor vehicles in Delhi in 2019 (MoRTH, 2021). Passenger cars accounted for 30% of the total number of registered motor vehicles in Delhi in 2019 (MoRTH, 2021). Freight vehicles (light-duty and heavy-duty vehicles) are a smaller fraction of the total number of registered motor vehicles, but share a high fraction of the total on-road transport sector emissions because they generally travel further each day into and within the city (Goel and Guttikunda, 2015; Jain et al., 2016; Malik et al., 2019). The on-road transport fleet in Delhi has grown from 7.5 million vehicles in 2012 to 11.4 million in 2019, the highest number of registered vehicles of any state in India (Goel and Guttikunda, 2015; MoRTH, 2021). Passenger cars and freight activity in Delhi is forecasted to more than double from 2020 to 2050 (He et al., 2021).

Growing number of vehicles in Delhi and in all India meant also a proportionate increase in pollutant emissions from the transport sector, and their growing contribution to poor air quality especially in cities. Increase in emissions has been due to an increase both in the number of motor vehicles on the road and the distance these vehicles travel (Ramachandra et al., 2009). The on-road transport sector is a major contributor to the total emissions of NO_x (50%) and VOCs (30%) in India (Li et al., 2017), with different vehicles type contributing differently to key pollutants (Guttikunda and Mohan, 2014). Increasing air pollution over India from O_3 and secondary particulate matter (Gani et al.,

2019; Kunchala et al., 2022), for which NO_x and VOCs act as precursors, makes on-road transport a key source to tackle. The Indian government has in the past few decades promoted measures to curb the impact of the growing on-road transport sector on air pollution.

1.4.3 Indian transport regulations

The main mitigation measure for air pollution from road transport adopted by the Indian government is the imposition of stringent emission regulations on all new vehicles nationwide, from Bharat Stage III (corresponding to EURO III European vehicle emission standards) nationwide in 2010 to Bharat Stage VI (corresponding to EURO VI European vehicle emission standards) in 2020 (Hakkim et al., 2022).

Since the beginning of the 2000s, the city of Delhi has in addition been converting public transport vehicles, including buses, three-wheelers and taxis, to operate on compressed natural gas (CNG) following a Supreme Court judgment in 1998 (Kathuria, 2004). Older vehicles are also being phased out Delhi. Other cities are following this trend as well as have experimented with substituting diesel vehicles with CNG (Hakkim et al., 2022). Recent measures to control traffic emissions in the Indian capital also include the introduction of a alternating “odd–even” licence plate pilot policy for passenger cars during the winter and the pre-monsoon seasons. However, the odd–even strategy only marginally reduced the $PM_{2.5}$ concentrations in Delhi (Chowdhury et al., 2017; Kumar et al., 2017; Sharma et al., 2017b). Despite these interventions, air pollution levels in Indian cities, in particular Delhi, remain hazardous to human health. Thus there is the need for a more systemic analysis of the traffic contribution to Indian cities pollution aiming at assessing and improving current intervention strategies.

These intervention strategies could also take advantage of emerging transport technologies. Indeed, with the emergence in the global market of electric vehicles and their increasing affordability, also India is investing in promoting EVs adoption. In 2015 India launched the Faster Adoption and Manufacture of (Hybrid and) Electric Vehicles (FAME) scheme which began in 2015, and now in its second stage. Through the FAME scheme for example, electric two- and three-wheelers are eligible for subsidy support (MHI, 2022). Thus, electric two-wheelers and three-wheelers are driving the first wave of EVs adoption in India. On the other hand, the shift to EVs for passenger cars and freight vehicles is not currently affordable (Kumar and Chakrabarty, 2020). In the case of heavy duty vehicles, there are no yet available EVs technologies and infrastructure (Cunanan et al., 2021). Alternative fuels such as compressed natural gas (CNG) can be promoted as an interim more sustainable solution for these vehicles. In addition, in 2017 India joined the EV30@30 campaign, under the Electric Vehicle Initiatives (EVI) of the Clean Energy Ministerial, aims for EVs to account for 30% of new vehicle sales by 2030 (CEM, 2017). In the coming decades, it will be key for India and Indian cities to manage to balance the increasing transport demand in their growing economy and overall air quality.

1.5 Air quality modelling

Air quality models are a simplified representation of the complex system of the atmosphere based on our knowledge of atmospheric processes (Brasseur and Jacob, 2017). Starting from the current knowledge of the physics and the chemistry of atmospheric processes, their formulation into equations is coded into pieces of software that can simulate the behaviour of the atmosphere. Air quality models can be used for different purposes. They can complement the observations of a monitoring network, which is usually spatially limited, and provide continuous spatial coverage for air pollutants. They can be used to improve the understanding of the sources and processes that determine

air quality; to forecast air quality, to inform policy-makers and citizens about hazardous conditions in advance; to support policy-makers in designing air quality management plans for mitigating air pollution, by predict the air quality as a result of changes in emissions for different scenarios on the relevant scale. (Daly and Zannetti, 2007; Gulia et al., 2015; Pisoni et al., 2019; Shrivastava et al., 2011). Here follows an overview of types of air quality models, and a more detailed description of the model used in this thesis work, WRF-Chem.

1.5.1 Types of air quality models

There are different air quality models types, depending on the particular application. A first distinction of air quality models can be done between *mathematical models* and *statistical models*. Mathematical models explicitly simulate the behaviour of pollutant species on the basis of the mathematical equations that represent physical, chemical and dynamical processes in the atmosphere. They are complex and their numerical implementation normally requires high performance computing to run them. Statistical models are based on empirical relationships between variables that are are established from a large number of previous observations. Statistical models are simpler than mathematical models, but cannot be extrapolated beyond the range of validity given by the data used in their derivation. Thus they are mainly used to explore the relationships between input and output variables and not usually suitable for exploring different air quality scenarios as they have a limited predictive ability, contrary to mathematical models (Brasseur and Jacob, 2017; Srinivas and Sarin, 2014).

Two types of mathematical models are *Eulerian Models* and *Lagrangian Models*. Eulerian models describe and solve the mathematical equations of the evolution of chemical concentrations in a geographically fixed frame of reference. The area of interest (domain) is divided in fixed 3-D grid cells and the model solves equations to produce solutions on a fixed grid of points representing the model domain. Lagrangian models use a frame

of reference that moves with the atmospheric flow, i.e. calculates wind trajectories and the transportation of air parcels along these trajectories. Eulerian models are generally preferred in 3-D models because it guarantees a well-defined concentration field over the whole domain, while Lagrangian models are better suited for tracking the transport of pollution plumes, and for describing the source influence function contributing to observations made at a particular location(Brasseur and Jacob, 2017). Types of Eulerian models are Chemical Transport Models (CTMs), while types of Lagriangian models are dispersion models (e.g. Gaussian Plume model).

Mathematical models can be *global models*, which simulate the atmosphere at a global scale, while *regional models* can simulate the atmosphere features at a higher resolution over a reduced geographic region. Because they cover a limited area, regional models need input data for their *boundary* and *initial conditions*, which are generated from global models. Initial conditions (ICs) describe the initial state of the atmosphere which is provided at the start of the run. Initial conditions include meteorological variables (like wind, temperatures, pressure, and moisture) and chemical variables (e.g. pollutants concentrations). It is a common practice to discard the initial part of the simulation, which amount of time depends on the application, before studying the air quality model outputs in order to minimize the influence of the initial conditions. This practice is called model *spinup*. Boundary conditions (BCs), in contrast, are meteorological and chemical fields that are provided throughout the simulations, and constraint the model solution and fields to prescribed values of atmospheric variables. The process of using BCs and ICs for a regional model generated from a global model is a form of *nesting*. More generally, the terms nesting refers to the process of inserting a higher resolution domain (child or nested domain) into a coarser domain (parent or outer domain), referred to as the "mother" or "outer" domain. Two basic strategies exist: 1-way or 2-way nesting. In the one-way nesting, meteorological and chemical calculations are first performed for the

parent domain, and the results are used as BCs and ICs for the nested domain. In Two-way nesting the interaction between the parent and the nested domain is reciprocal and simultaneous, because not only does the parent provides BCs for the nest (as in 1-way nesting), but feedback from the nest to the parent also exists (Lozej and Bornstein, 1999).

A further distinction for atmospheric chemistry models is if they are operating *online* and *offline*. Models that do not generate their own meteorological environment and instead use 3-D time-dependent data generated by an external meteorological model are called “offline” models. Meteorological fields (temperature, wind speed and direction, humidity and so on) are provided by pre-calculated meteorological data (reanalysis data). CTMs are usually offline models.

Models that instead integrate the parent meteorological model so that meteorological equations and the continuity equations for chemical species are solved together are called online. Online models have the advantage that they fully couple chemical transport with dynamics and able to explore interactions between meteorology and chemistry, such as meteorology-aerosols feedback. They avoid the need for high-resolution meteorological archives, but they are far more complex to operate, and interpret and require more computation time than offline models. (Brasseur and Jacob, 2017).

Regardless of type of mathematical model, the part of the model that deals with calculating the production and loss (continuity equation) of chemical species considered for each time step is called *chemical scheme or chemical mechanism* (Brasseur and Jacob, 2017). The chemical scheme used in a model can vary in complexity, in terms of number of species and number and types of processes included. Since the chemistry of the atmosphere is complex, all the reactions for individual species cannot be represented

and resolved, and thus it is common practice in chemical mechanism to lump together species by common traits and reactions. The chemical mechanism to be used in simulation needs to be chosen on the type of scientific questions and processes that are to be investigated.

CTMs need large amount of external input data for reproducing the atmosphere: meteorological data, emissions of pollutants, and data about the characteristics of the surface and terrain (LULC, Land Use and Land Cover). Emissions of chemical species to use are usually provided by inventories, pre-calculated emission fields by type of source. The main types of sources are anthropogenic, biogenic or pyrogenic (biomass burning). To compile these inventories, either a top-down or bottom-up approach is used. Emission fluxes can be compiled with different spatial and temporal resolutions depending on the requirements of the model and of the study. For some species (e.g. NO from traffic exhaust) the diurnal variation of emissions is significant, and should be taken into account in the emissions field, while for others with long term variability (e.g. CO_2) a high temporal resolution is not usually needed.

Despite the improvements of atmospheric models in the last decades, no model is perfect in its predictions: there always be uncertainty about the understanding of how physics and chemistry of the atmosphere actually works (i.e. not all processes are well represented by model equations), errors in the code of the software and introduced by methods to solve the equations, errors in the data that are fed into the model as input, and by the intrinsic chaotic nature of the atmosphere. This results in a non-perfect simulation of the state of the atmosphere and air pollutants (Brasseur and Jacob, 2017). For air quality models to be useful to they need to reproduce the atmosphere with a degree of confidence that is required for the particular application. This is why it is important to evaluate the model performance with independent observations (satellite data, ground-based monitoring stations, output from other independent models). Evaluating a model

for an application means to broadly assess the model results, by looking at metrics to quantify the differences between model predictions and observations, in order to find model strenghts and limitations and determine if it is suitable for the questions under investigation (Brasseur and Jacob, 2017).

1.5.2 WRF-Chem model: introduction

WRF-Chem is the Weather Research and Forecasting (WRF) model coupled with Chemistry (Chem). WRF-Chem is a state-of-the-art online Eulerian chemistry transport model that simulates the emission, transport, mixing, and chemical transformation of trace gases and aerosols simultaneously with the meteorology. WRF-Chem is a fully compressible model, i.e. it allows for significant changes in fluid density, and non-hydrostatic model, i.e. it calculates the full vertical momentum equation (Skamarock et al., 2008). Being an online model, chemical continuity equations and meteorological equations are solved together in WRF-Chem, as discussed in the previous paragraph.

The model is used for investigation of regional air quality, field program analysis, and interactions between meteorology and chemistry. (Grell et al., 2005; Powers et al., 2017). The WRF-Chem model is flexible across spatial scales, serving applications from hundreds of metres to study urban air quality to hundreds of kilometres, to study regional air quality.The development of WRF-Chem is a collaborative effort among international modeling community, with NOAA/ESRL scientists leaders and continuing caretakers of the code (NOAA, 2020). It has been widely tested and used for investigating air pollution of cities and megacities around the world (Im and Kanakidou, 2012; Kuik et al., 2016; Li et al., 2011; Reátegui-Romero et al., 2018; Tie et al., 2013). In particular, its suitability has been tested and used for air quality studies over India (Conibear et al., 2018; Govardhan et al., 2015; Kumar et al., 2014,1; Michael et al., 2014; Ojha et al., 2020) and also for studies focussing on Delhi (Beig et al., 2013; Gupta and Mohan, 2013,1; Jena et al., 2021; Mohan and Bhati, 2011; Sharma and Khare, 2017). WRF-Chem

allows users to choose among different parametrisation schemes for various physical processes (turbulence exchange, atmospheric radiation, cumulus cloud precipitation, cloud microphysics, and land surface type), and chemical processes (e.g. gas-phase chemistry, aerosol chemistry, emissions). Thus resulting in a flexible tool to be set-up ad-hoc for the specific application. Separate modules and tools in WRF-Chem are used to prepare LULC and meteorological input data (WPS, WRF Pre-Processing System). Meteorological input data are needed in WRF-Chem as initial and boundary conditions, because it is a regional model, but, as an online model, WRF-Chem generates its own meteorological fields at each time step (Section 1.5.1). Chemical initial and boundary conditions and emissions within the domain for anthropogenic,pyrogenic and biogenic sources are also prepareed using separate modules (ACOM-NCAR, 2020). In the next section, we describe the specific set-up chosen in this thesis for addressing the scientific question outlined in Section 1.1.

1.5.3 WRF-Chem model set-up

Across all research chapters 2, 3 and 4, we use a common WRF-Chem set-up for the meteorological and chemical parametrisations, initial and boundary conditions, terrain data (LULC), and biogenic and fire emissions. However, in each chapter the choice of the anthropogenic emissions, model domain(s), period of simulations experiments differ. These WRF-Chem set-up aspects are chosen differently to better suit the research question addressed in each research chapter. The combination of parametrisations we choose are based on the work of Conibear et al. who tested and used this combination in WRF-Chem for air quality applications over India (Conibear et al., 2018).

Version and domain settings We use v.3.9.1.1 of WRF-Chem. The vertical resolution is of 33 vertical levels that span from the surface to 50 hPa ($\simeq$19 km). As mentioned, horizontal resolution and period of simulation differ among the research chapters according to the research questions being addressed.

In Chapter 2, which focus on understanding seasonal factors influencing $PM_2.5$ at a regional scale over the Indo-Gangetic Plain (IGP), the WRF-Chem domain covers the entire IGP at horizontal resolution of 20km, as shown in Figure 1.8. We run the model for four distinct months each one representative of one different Indian season: 18th April to 16th May 2017 (pre-monsoon), 3rd to 31st July 2017 (monsoon), 18th October to 16th November 2017 (post-monsoon) and 8th January to 5th February 2018 (winter). More information on Indian seasons and their characteristics will be discussed in Sec 1.6.

In Chapters 3 and 4, where the focus is on $PM_{2.5}$ at a city-level scale over Delhi, we use a nested domains set-up (Section 1.5.1). The parent domain encompasses north India at 12 km horizontal resolution, while the nested domain covers Delhi and the broader National Capital Region (NCR) at 4 km horizontal resolution, as shown in Figure 1.9. In Chapter 3 we focus on the impact of the transport sector during the post-monsoon season, so we run the model for a short representative period in this season (6-16 October 2019). In Chapter 4 we explore the impact of future transport emissions, and to account their impact in different chemical environments, we run the model for a representative period of two contrasting seasons, 1-30 April 2019 for pre-monsoon and 1-31 October 2019 for post-monsoon. More details on the period of simulation and simulation experiments will be given in each research chapter.

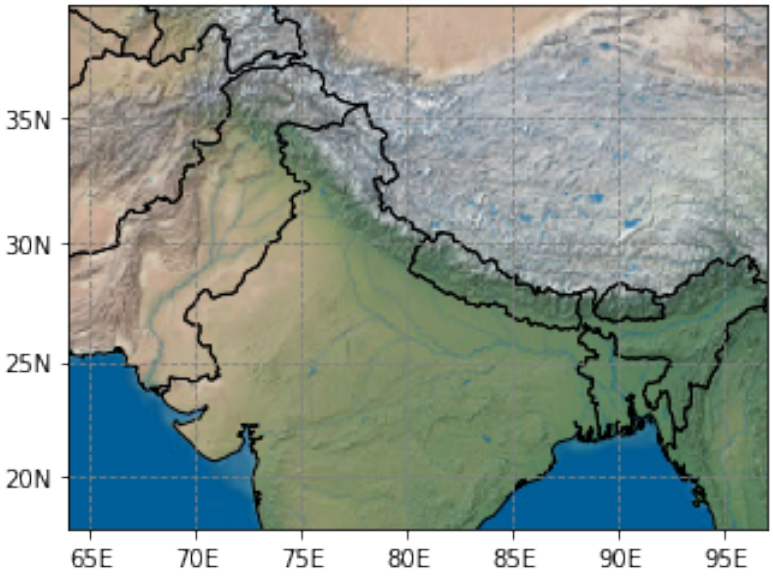

Figure 1.8: WRF-Chem model domain used in research Chapter 2 (17°–40° N and 64°–97° E) at 20km horizontal resolution.

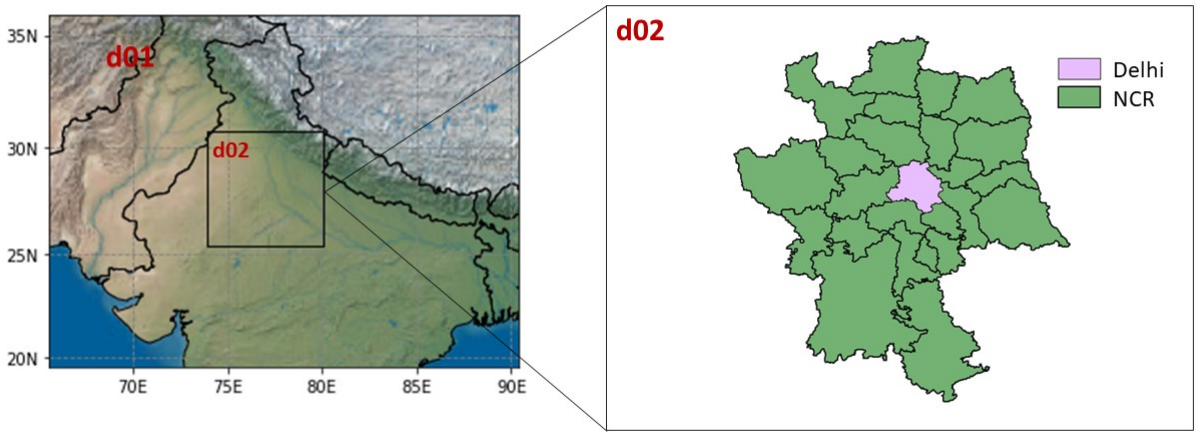

Figure 1.9: WRF-Chem model domains used in this study: d01 refers to parent domain described with a 12 km horizontal resolution (19°–36° N, 65°–90° E), and d02 refers to the nested domain (25–31° N and 74–80° E), described with a 4 km resolution, that covers Delhi (in pink) and the broader National Capital Region (NCR, in green).

Meteorological Parametrisations For meteorological processes, Morrison double- moment scheme scheme describes cloud microphysics Morrison et al. (2005), the Mellor-Yamada Nakanishi and Niino 2.5 (MYNN2) Nakanishi and Niino (2006) the planet boundary layer and the Grell 3D scheme is used for cumulus parametrization Grell and Dévényi (2002). The Rapid Radiative Transfer Model (RRTM) parametrise both short and long wave radiation Iacono et al. (2008). Land surface is parametrised by the Noah Land Surface Model Ek et al. (2003) coupled with a urban canopy model Kusaka and Kimura (2004).

Chemical Parametrisations To describe gas-phase chemistry we use the Model for OZone And Related chemical Tracers, version 4 (MOZART-4) chemical mechanism (Emmons et al., 2010). The standard MOZART-4 mechanism includes 85 gas-phase species, 39 photolysis and 157 gas-phase reactions and 12 bulk aerososls. The version we use, includes also the extended treatment of some volatile organic compound (VOC) chemistry, in particular monoterpenes and aromatics, and uses and updated isoprene oxidation scheme (Knote et al., 2014). Photolysis rates are calculated by the Fast Tropospheric Ultraviolet–Visible (FTUV) module (Tie et al., 2003). We use the Model for Simulating Aerosol Interactions and Chemistry (MOSAIC) to simulate aerosols chemistry (Zaveri et al., 2008), including aqueous-phase chemistry (Knote et al., 2014). MOSAIC describes aerosols using four sectional discrete size bins: 0.039—0.156μm, 0.156—0.625μm, 0.625—2.5μm, 2.5–10μm. The first three of these bins represent $PM_{2.5}$, while the largest one describes coarse particulate matter ($PM_{2.5-10}$). MOSAIC is coupled with the bulk aerosols species of MOZART, as well as accounts for aerosol feedbacks on photolysis.

Secondary Organic Aerosol scheme Since changes in OA volatility is key for the formation of SOA 1.3.2, we take advantage of the Volatility Basis Set (VBS) model to describe SOA in WRF-Chem (Ahmadov et al., 2012; Knote et al., 2015; Lane et al., 2008b). The VBS helps to describe succinctly the evolving volatility of OA through oxidative chemistry in the atmosphere (Chuang and Donahue, 2016; Donahue et al., 2006,1). The VBS has been used successfully in a range of modelling studies (Ahmadov et al., 2012; Bergström et al., 2012; Lane et al., 2008b; Zhang et al., 2013; Zhao et al., 2016). For each of the four aerosol size bins in MOSAIC, the 1-D VBS implementation considers five volatility bins for semi-volatile organic compounds (SVOCs), described by effective saturation concentrations C* of 10^{-4}, 1, 10, 100 and 10^3 μg m^{-3} at 298 K. The $log_{10}C^* = -4$ volatility corresponds to an inert compound, and serves computationally as a loss of particle phase organics to avoid unrealistic volatile mixtures due to continuously aging of gas-phase SVOCs. Lumped anthropogenic, pyrogenic, and biogenic gas-phase aerosol precursors undergo continuous gas-phase oxidation and partition between the gas and aerosol phase using pseudo-ideal partitioning theory (Pankow, 1994). For SOA formation, partitioning between the gas and aerosol phase depends on total organic aerosol load and temperature. At thermodynamic equilibrium, for species i with saturation mass concentration C_i^*, the fraction of the total OA amount present in the aerosol phase, $X_{p,i}$, is given by Seinfeld and Pandis (2016):

$$X_{p,i} = (1 + \frac{C_i^*}{C_{OA}})^{-1} \qquad C_{OA} = \sum_i C_i X_{p,i} \tag{1.9}$$

Note that at $C_i^* = C_{OA}$ then $X_{p,i} = 1/2$, so half of the species is in the gas phase and the other half in the particulate phase, giving the equipartition point. Also the total amount of C_{OA} has an important role in the partitioning. Indeed, changing the total organic mass C_{OA} translates in a shift in the partitioning. Thus gas-particle partitioning near the sources is very different from the one in the remote atmosphere. If C_{OA} is present in

only small quantities, only the less volatile compound will partition in the aerosol phase, while the rest of the compounds in the gas phase can undergo gas-phase oxidation steps. On the contrary, if the starting levels of C_{OA} are high, almost all the semivolatile oxidation products partition in the particle phase as soon as they are formed, removing them from the possibility to subsequently undergo further gas-phase oxidation Seinfeld and Pandis (2016). SOA yields are also dependent on NO_x levels, so SOA yields is calculated differently for low and high NO_x conditions, through a branching ratio (Lane et al., 2008a). The WRF-Chem model option we chose include also the SOA formation from glyoxal (Knote et al., 2014). Loss of SVOCs is from washout via convective and grid scale precipitation. Our chosen implementation of VBS only accounts for SVOCs, and assumes that POA is inert so that it contributes only to the aerosol mass. We do not include direct emissions of SVOCs or intermediate VOCs (IVOCs). This is a limitation of our current implementation given evidence that SVOC and IVOC vapours creates a considerable amount of regional SOA, and that POA emissions are semivolatile and undergo oxidation and should be also considered in describing SOA production (Robinson et al., 2007). To describe POA using the VBS approach we would require information about the volatility distribution of POA, but conventional inventories typically consider POA as non-volatile.The 1-D version of the VBS model is unable to describe some aspects of SOA formation, including fragmentation and the increase in OA oxidation state, which are better described by the 2-D version of the model that tracks the oxygen-to-carbon ratio (O:C) in addition to organic mass (Donahue et al., 2012). Previous studies have shown that the 2-D VBS model improves model-measurement agreement in SOA (e.g., Zhao et al. (2016)) but has a significant associated computational burden when used in 3-D chemistry transport models. Further details of this VBS implementation in WRF-Chem are described in (Knote et al., 2015) and references therein.

Input data and emissions For input data in the model, initial conditions and lateral boundary conditions, and for nudging (Newtonian relaxation), we use meteorological reanalyses from NCEP FNL Operational Model Global Tropospheric Analyses Data (National Centers for Environmental Prediction, National Weather Service, NOAA, U.S. Department of Commerce, 2015) at a spatial resolution of $0.25^\circ \times 0.25^\circ$ and at a temporal resolution of six hours. We use the nudging approach at all levels to prevent our calculations from deviating too far from observed meteorology. Chemical initial conditions and lateral boundary conditions for each month are provided by six-hourly Community Atmosphere Model with chemistry (CAM-Chem) global model data (Buchholz et al., 2019). The description of terrain data for the domain (land use and soil categories) we use MODIS IGPB 21-category data at 30 arc-seconds resolution ($\sim$ 1 km) (Friedl et al., 2010). To define our For pyrogenic emissions, hourly biomass burning emissions are taken from the Fire Inventory from NCAR (FINNv1.5) (Wiedinmyer et al., 2011). The FINNv1.5 inventory includes global estimates of trace gas and particle emissions from open burning of biomass, which includes wildfire, agricultural fires, and prescribed burning. Biogenic emissions are calculated online using the Model of Emissions of Gases and Aerosol from Nature (MEGANv2.1), Guenther et al. (2006)). Anthropogenic emissions are taken from different databases. In Chapter 2, we use monthly anthropogenic emissions from Emission Database for Global Atmospheric Research with Task Force on Hemispheric Transport of Air Pollution (EDGAR-HTAP v2.2) for year 2010 (Janssens-Maenhout et al., 2015) as provided by the WRF-Chem community, which provides the total anthropogenic emissions and includes a NMVOC speciation according to the gas and aerosol chemistry scheme we use in this thesis (MOZART-MOSAIC). In Chapter 3 and 4, for the parent domain, we use the newly released EDGARv5.0 monthly anthropogenic emission inventory for 2015 at $0.1^\circ \times 0.1^\circ$ resolution ($\sim$11 km) (Crippa et al., 2019a,1,1). For the nested domain which covers Delhi and the neighborhood NAtional Capital Region (NCR) we use the local anthropogenic emission inventory from Energy

and Resource Institute and The Automotive Research Association of India (TERI/ARAI) that covers the NCR region (TERI & ARAI, 2018) at 4km resolution for the year 2016. Details and discussion on the TERI/ARAI inventory will be provided in Chapter 3. Table 1.1 summarised the set-up of the WRF-Chem model used in this thesis.

Observations for model evaluation For each research chapter, we evaluate the model performance for selected pollutants against observations from ground-based monitoring stations, satellite observations, and pollutants observations from previous literature. In Chapter 2, which investigates regional and seasonal air pollution over the IGP, we evaluate seasonal values of the model with ground-based observations for main gas pollutants and particulate matter from governamental monitoring stations across the IGP, aerosol optical depth (AOD) satellite observations, and organic aerosols data from previous literature. For chapter 3 and 4, which deal with air pollution at the urban scale of Delhi, we evaluate the WRF-Chem model with ground-based observations from Indian governamental data, for $PM_{2.5}$ in Chapter 3 and for $PM_{2.5}$ and O_3 in Chapter 4. In these two chapters, we also evaluate $PM_{2.5}$ composition (Section 1.3.2) with values from previous literature. Observations used are described in the "Data and Methods" section, while the evaluation is presented in "Results" section in each chapter.

Version and domain settings	**Value**
Version	v.3.9.1.1
Vertical resolution	33 layers, up to 50 hPa
Domain	Chapter 2: Figure 1.8 Chapter 3 and 4: Figure 1.9
Period simulated	Chapter 2: 18/04-16/05 2017 (pre-monsoon), 3-31/07 2017 (monsoon), 18/10-16/11 2017 (post-monsoon), 08/01-05/02 2018 (winter) Chapter 3: 6-16/10 2019 (post-monsoon) Chapter 4: 1-30/04 2019 (pre-monsoon), 1-31/10 (post-monsoon)
Process	**Parametrisation**
Cloud microphysics	Morrison double-moment scheme
Planetary boundary layer	Mellor-Yamada Nakanishi and Niino 2.5 (MYNN2)
Convection	Grell 3D scheme
Short and long wave radiation	The Rapid Radiative Transfer Model (RRTM)
Land surface	Noah Land Surface Model coupled with a urban canopy model
Gas-phase chemistry	Model for OZone And Related chemical Tracers (MOZART)
Photolysis	Fast Tropospheric Ultraviolet–Visible module (FTUV)
Aerosol-phase chemistry	Model for Simulating Aerosol Interactions and Chemistry (MOSAIC)
Secondary Organic Aerosols	1-D Volatility Basis Set (1D-VBS)
Input data	**Dataset**
Meteorological Initial and Boundary Conditions	NCEP FNL Operational Model Global Tropospheric Analyses
Chemical Initial and Boundary Conditions	CAM-CHEM global model
Land use and soil categories	MODIS IGPB 21-category
Fire emissions	Fire Inventory from NCAR (FINNv1.5)
Biogenic emissions	Model of Emissions of Gases and Aerosol from Nature (MEGANv2.1) - Calculated online
Anthropogenic emissions	Chapter 2: EDGAR-HTAPv2.2 Chapter 3 and 4: EDGARv5.0 (parent domain), TERI/ARAI (nested domain)

Table 1.1: WRF-Chem set-up used in the research chapters of the thesis (Chapter 2, 3, 4). Unless specified, settings are common to all research chapters.

Preparatory work Although used by a wide range of users the WRF-Chem model is not easy to operate. It has several components that need to be operated in sequence, and each set-up (choice of meteorological and chemical parametrisation, model domain, input data etc.) is unique for the specific application for which is used. There are best practices to run the model, but then a consistent amount of time need to be spent to make the model work smoothly and consistently for the application chosen. For the work in this thesis, several time has been spent to install, make compatible with the IT infrastructure used, configure and test the WRF-chem model. Although not presented here, this preparatory work has been fundamental to be able to fully operate the WRF-Chem model to conduct the research presented in the research chapters.

1.6 Air pollution over Delhi megacity

As introduced in Section 1.2 and 1.3, there are many factors that can influence air pollutant concentrations. The reality of Delhi air pollution is particularly complex, because it is due to the concurrence of many of these different factors: geographical location and meteorological conditions, local and regional sources and trans-boundary air pollution. Here, we give a general overview of these factors, from the regional to the city scale, and how they are linked to pollutants levels in the Indian capital.

1.6.1 Regional context: the Indo-Gangetic Plain

The city of Delhi, officially the National Capital Territory of Delhi (NCT), is located in the Indo-Gangetic Plain (IGP) at 28.5° N latitude and 77° E longitude and 216 m above mean sea level. Delhi is surrounded by hills and the Himalayas in the North and East, central hot plains in the South and the Thar Desert in the West (Figure 1.10).

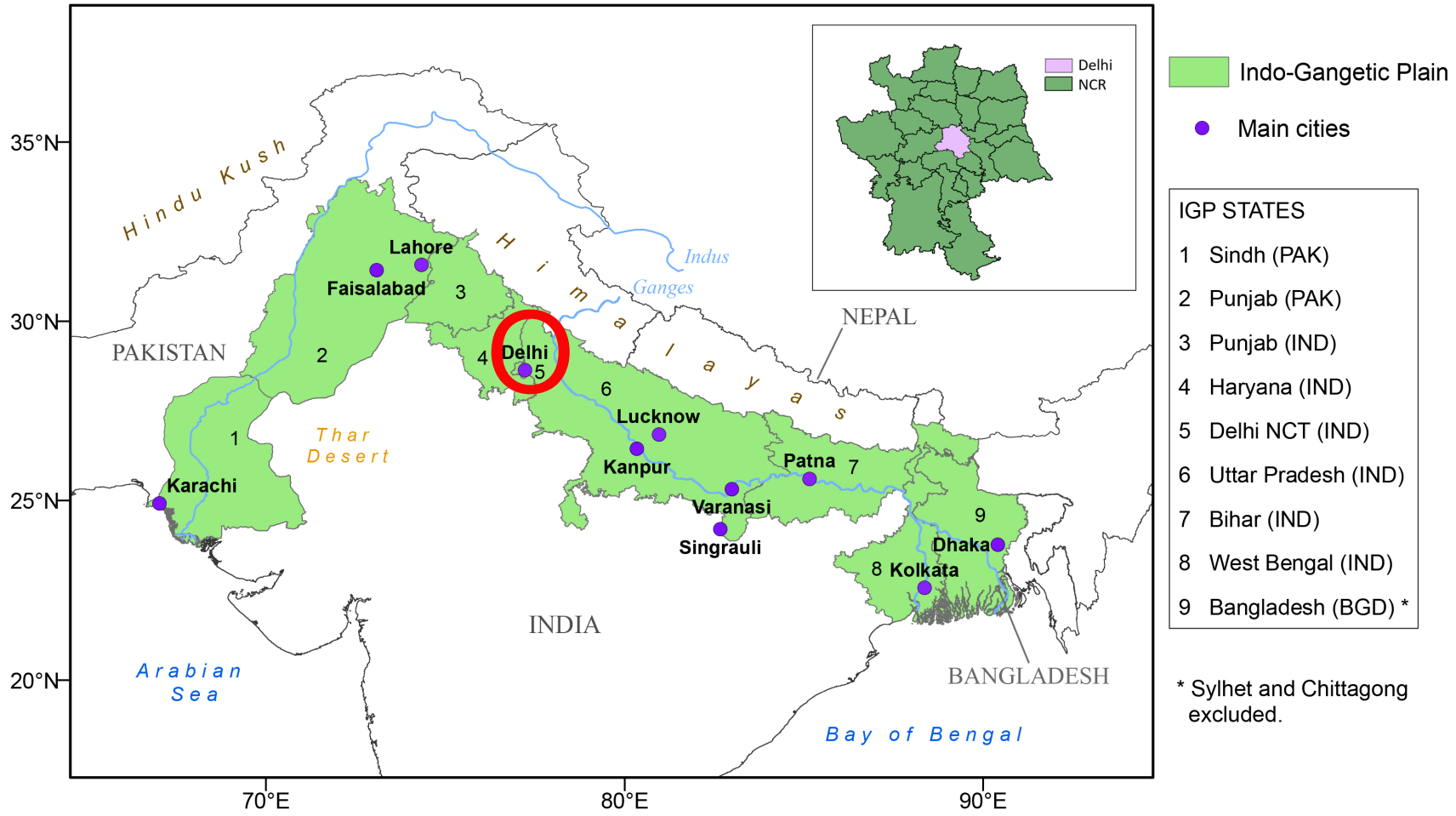

Figure 1.10: Geographical and administrative features of the Indo-Gangetic Plain (IGP), including Pakistan, India, and Bangladesh. Numbers denote individual IGP states and purple dots denote the main cities. Delhi city is circled in red. Inset shows Delhi and broader National Capital Region (NCR) map.

The IGP including parts of Pakistan, India and Bangladesh (Figure 1.10), is one of the most populous and polluted areas in the world. It is home to $\sim$ 700 million people (9% of the global population Bangladesh Bureau of Statistics (2011); Indian National Commission on Population (2020); Pakistan Bureau of Statistics (2017)) and to the associated sources of anthropogenic air pollution, which are distributed proportionally to population, with hotspots over cities of various sizes from megacities of more than 10 million people, e.g. Karachi, Lahore, Delhi, Kolkata, and Dhaka, to smaller cities of a few million inhabitants, e.g. Faisalabad, Patna, Kanpur, Lucknow, and Varanasi (UN DESA, 2019a).

The importance of the IGP lies in the fertility of its soils formed from alluvium that is deposited across the Indus and Ganges basins by the Indus and Ganges rivers. These rivers originate in the Himalaya mountains and the Tibetan Plateau. The Indus and Ganges basins benefit also from precipitation from the seasonal monsoon. A monsoon system is a seasonal change in the direction of the prevailing winds of a region and in the associated amount of rainfall. The Indian monsoon, brings prevailing winds from the northeast during cooler months of the year, and reverses winds direction to blow from southwest during the warmest months, bringing large amounts of rainfall during June and July (Gadgil et al., 2003). The monsoon timing thus defines the main seasons over the IGP (India Meteorological Department, 2020): the pre-monsoon season runs from March to May, the monsoon season is from June to September, the post-monsoon season is from October to December, and winter occurs in January and February. The Indian states across the IGP (e.g. Punjab, Haryana, and Uttar Pradesh) represent the vast majority of nationwide wheat and rice production. Rice and wheat are planted in May and November and harvested in October-November and April-May respectively, following the rice–wheat cropping cycle. The IGP is also an important producer of sugarcane, cultivated mainly in the Indus Valley in Pakistan and in the Indian state of Uttar-Pradesh. The two main seasons for planting are in September-October and February-March,

followed by harvesting during the winter and pre-monsoon months, respectively. Crop residues left from harvesting, e.g. husk, bran, straw, are generally burned in open fires. Traditionally, these residues were ploughed back into the soil to maintain fertility and stability, but the sheer scale of current production precludes these practices in time for a second growing season (Ahmed et al., 2015; Chauhan et al., 2012). Open burning of these residues across the IGP, particularly during the post-monsoon season, is a large source of gaseous and particulate pollution that has implications for regional air quality and human health (Jethva et al., 2019; Sembhi et al., 2020; Vadrevu et al., 2011). Residential biofuel combustion also plays an important role for air quality (Agarwala and Chandel, 2020; Conibear et al., 2020).

The high population density and intense human activity over the IGP result in anthropogenic emissions being a major source of regional surface air pollution (Begum et al., 2013; Guttikunda and Jawahar, 2014; Shahid et al., 2015; Venkataraman et al., 2018). Residential energy consumption represents a major contribution to anthropogenic emissions with a large fraction of the rural and urban population using solid fuel for cooking (Conibear et al., 2018). Emissions from land transportation, particularly in cities, also represents a significant contribution to anthropogenic emissions, as highlighted in Section 1.4.2. (Begum et al., 2013; Guttikunda et al., 2014; Mallik and Lal, 2014). Intense agriculture over the IGP is associated with large emissions of ammonia, an aerosol precursor, from urea fertilizer application, as well as from post-harvest burning as described above (Kuttippurath et al., 2020; Wang et al., 2020c). Vegetation cover over the IGP consists mainly of croplands (Gumma et al., 2019; Stibig et al., 2007), which have lower isoprene emissions than trees (Hardacre et al., 2013). Consequently, biogenic emissions over the IGP are lower compared to other parts of South Asia (Guenther et al., 2006; Stavrakou et al., 2014).

Regional dispersion of air pollution over the IGP is dominated on a seasonal timescale by the monsoon system, influenced by the high mountain ranges of Hindu Kush and Himalayas that lie to the northwest to northeast of the IGP. Agricultural planting and harvesting (and associated burning) are determined by the timing of the monsoon when the majority of the annual rainfall falls. The post-monsoon rice harvesting season corresponds to post-monsoon stable conditions that favour air stagnation. Lower speed wind from west/northwest air flow, lower boundary layer depth, cooler temperatures, high relative humidity favours the transport of pollutants towards east from upwind regions (Cusworth et al., 2018; Nair et al., 2007; Singh and Kaskaoutis, 2014). Stagnating atmospheric conditions characterise also the winter season. In contrast, higher wind speeds from east, start in pre-monsoon and peak in the monsoon season, where the monsoon enables ventilation and rainwash of pollutants in the air and increase in PBL heigh, bringing lower pollution concentration in these two seasons (Bisht et al., 2015; Guttikunda and Gurjar, 2012). Thus, observed variations across the IGP of $PM_{2.5}$ reflect large-scale variations in meteorology and the seasonal variations in anthropogenic, biogenic, and pyrogenic emissions (Jethva et al., 2005; Lelieveld et al., 2018; Schnell et al., 2018). These regional conditions adds on top of local factors that shape air quality in Delhi.

1.6.2 Local air pollution in Delhi

As introduced in the previous section, Delhi is located in the middle of the IGP (Figure 1.10). Delhi climate is classified as sub-tropical, with large seasonal variations in temperatures and precipitation shaped by the Indian monsoon (India Meteorological Department, 2020; Peel et al., 2007). Figure 1.11 shows the monthly average temperature and rainfall in Delhi. The yearly season distribution for Delhi includes warm and low rainfall

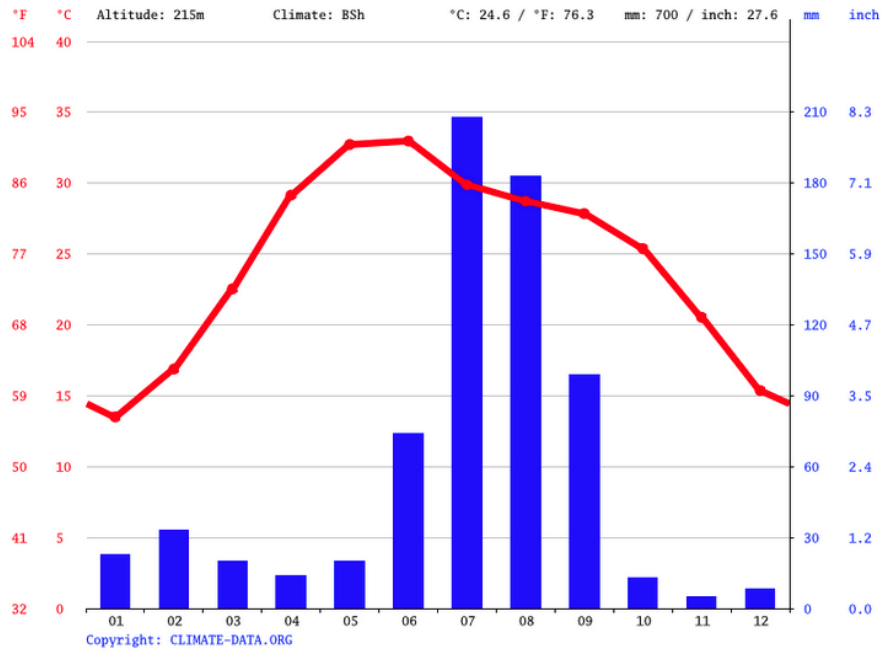

Figure 1.11: Monthly temperature and rainfall over Delhi based on 1991 - 2021 ECMWF data. Source and copyright: climate-data.org.

spring (February and March) hot and almost dry summer, also known as pre-monsoon season (April to June), the heavy rainy monsoon season (July to September), warm and dry autumn, also known as post-monsoon season (October and November), and cold and low rainfall winter (December and January).

Since the 1950s, Delhi has been experiencing phenomenal growth of population, expanding from being Delhi NCT, to National Capital Region (NCR) (NCRPB, National Capital Region Planning Board, 2022). Delhi NCR includes the entire NCT of Delhi and several surrounding districts, and the states of Haryana, Uttar Pradesh and Rajasthan (Figure 1.10), covering a total area of $\sim$ 54,000 km^2 (Ministry of Urban Development, Government of India, 2015). In 2011, the population of NCR Delhi was estimated at $\sim$46 million people, with $\sim$17 million residing within the NCT (Ministry of Statistics, Government of India, 2017). In 2019 Delhi NCT population counted 28 million people within its 11 districts. Figure 1.12 shows the spatial distribution of population in Delhi for 2019 in each city district, which are shown in Figure 1.13.

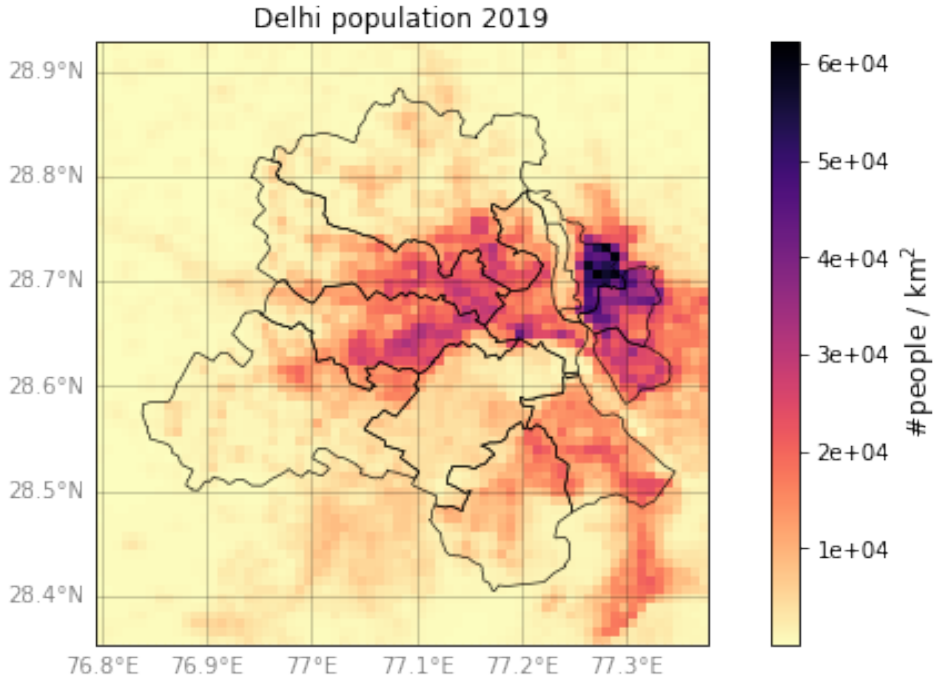

Figure 1.12: Delhi population density in 2019 at 1kmx1km. Population data from Tatem (2017).

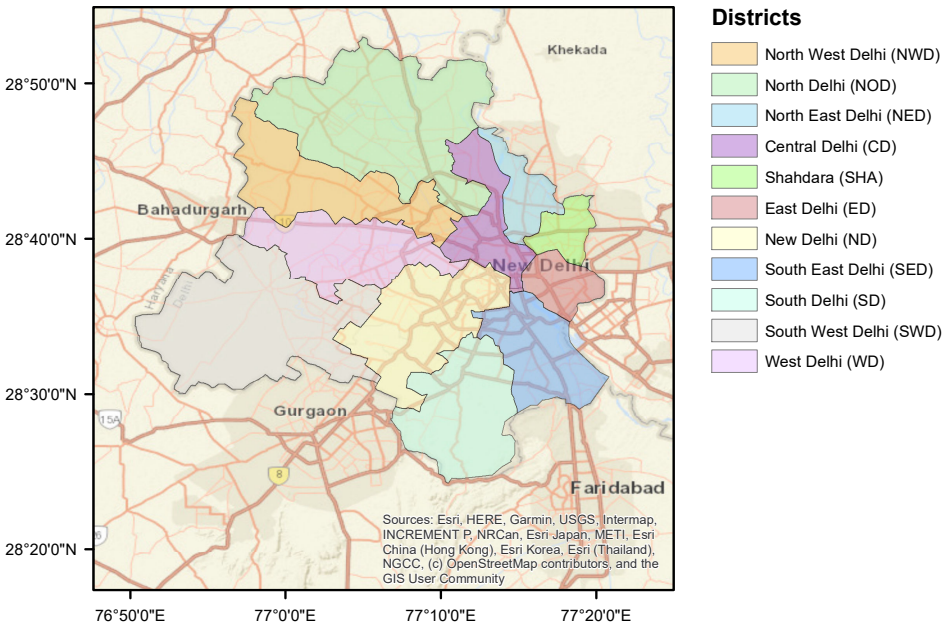

Figure 1.13: Map of the 11 Delhi districts (Government of Delhi NCT, 2022), and road network across the city.

Delhi is projected to continue growing and become the most populous city in the world around 2028 surpassing Tokyo, with 37 million only in the NCT of Delhi (UN, DESA, 2018) The rapid population growth of Delhi and its surroundings, led to a fast urbanisation, infrastructural development and thus to an increasing demand in energy from domestic, transport, and industrial sectors (Government of NCT of Delhi, 2012; NASA EO, 2018; USGS, 2016). This in turns resulted in an increase in local sources of air pollution.

Despite almost constant emissions rates within the city throughout the year, concentrations of $PM_{2.5}$ can be $40-80\%$ higher in the winter and $10-60\%$ lower in summer when compared to the year annual average (Guttikunda and Gurjar, 2012). Mean concentrations of $PM_{2.5}$ during post-monsoon season and winter are around 290 $\mu g\ m^{-3}$ with peaks at the end of October/beginning November that can reach peaks of $\sim$ 450 $\mu g\, m^{-3}$ (Chowdhury et al., 2019), corresponding exactly with the open biomass burning season in the IGP and post-monsoon stagnating conditions, as discussed in the previous section 1.6.1. On the other hand, pre-monsoon wheat harvest residues burning have a lower impact on Delhi air pollution, because of the seasonal reversal of winds (southwesterly direction) and relative increase of the boundary layer depth (Liu et al., 2018; Nair et al., 2007) anticipating the full onset of the monsoon . Indeed, average values remains around $\sim$ 120 $\mu g\ m^{-3}$ (Chowdhury et al., 2019). It is estimated that biomass burning from regional crop residues and residential activities accounts for $\sim 40\%$ of black carbon (constituent of $PM_{2.5}$) over Delhi during autumn-winter and $\sim 20\%$ during spring-summer seasons (Bikkina et al., 2019). However, it is difficult to keep track or detect small fires, especially via satellite measurements (Randerson et al., 2012). Transnational transport of soil dust and smoke can further increase PM_{10} loadings in Delhi region. Dust transport from Central Pakistan (northwest) and arid terrains of Iran and Afghanistan (west) can contribute to high PM_{10} levels through dust transport (Bisht et al., 2015). Moreover,

southwest air masses from Arabian Sea carries both dust and marine aerosols, contributing mainly to moderate $PM_{2.5}$ concentrations in Delhi. However, the major areas that contribute to highest $PM_{2.5}$ LRT are Indian regions in the northwest IGP (Bisht et al., 2015).

Source apportionment studies in the city indicate biomass burning, coal combustion, vehicle emissions and road dust as predominant sources that contribute to $PM_{2.5}$ over Delhi. Chowdhury et al. (2007) quantified that fossil fuels (coal, diesel and gasoline) contribute 25-33 % and biomass burning 7-20% of $PM_{2.5}$ mass loading. Pant et al. (2015) identified wood burning (23%), road dust (14%), traffic (19%) and other organic matter emission sources (33%) as major $PM_{2.5}$ contributors with relatively higher biomass combustion contributions during winter and road dust especially during summer. Sharma and Dikshit (2016) estimates as major $PM_{2.5}$ sources biomass burning, (12-26%), vehicles (9-25%), road dust (4-28%), coal and fly ash (5-26%) with high variability between winter and summer.

Besides the seasonal variations, $PM_{2.5}$ mass concentrations also exhibit a pronounced diurnal variability, linked the role that the planetary boundary layer has on shaping surface pollutants concentrations, as shown in Figure 1.4 and discussed in Section 1.3.3. The PBL dynamics is combined with local human activities during day and night in Delhi. Higher concentrations in the early morning and evening are consistent with the morning and evening rush-hour traffic pattern and residential heating use in winter. Only during monsoon season this pattern is smoothed significantly (Bisht et al., 2015; Guttikunda and Gurjar, 2012; Tiwari et al., 2013).

1.7 Thesis outline

The overarching goal of my thesis is to advance our understanding of outdoor air pollution in Delhi megacity, which complexity and challenges for mitigation have been outlined in Section 1.6. In particular, this thesis focus on the quantification of the impact of on-road transport emissions (Section 1.4) on surface levels of $PM_{2.5}$ and its implications for air quality policy-making in Delhi. To do this, I combine a state of the art regional atmospheric chemistry transport model, WRF-Chem with recently developed local emissions inventories (Section 1.5.3). The specific goals of my thesis, as outlined in Sec. 1.1, are addressed in the following three research chapters. I present each research chapter in the format of a research paper, with an introduction relevant for the chapter, methods, results, discussion and conclusions. Finally, in Chapter 5 I summarise together the key findings of the three research chapters, with a critical discussion of the methods and results of this thesis and an outlook to future research work.

Chapter 2

Seasonal drivers of particulate matter over the Indo-Gangetic Plain

Author contributions declaration

This chapter and the relative appendix have been adapted from a published paper in *Atmospheric Chemistry and Physics* (DOI: `https://doi.org/10.5194/acp-21-10881-2021`). I conceived the study and the methodology together with my supervisor Paul Palmer. I performed all the simulations and the analysis. Christoph Knote provided advice for the set-up the model. Fey Yao provided the aerosol optical depth (AOD) observations to be compared with the model AOD. I interpreted the results with helpful discussion provided by Paul Palmer, Christoph Knote, and Tim Wallington. I wrote the article with contributions and editing from Paul Palmer. All the co-authors provided comments on subsequent manuscript revisions. There were additional amendments made at the suggestion of two anonymous reviewers and the editor.

2.1 Introduction

As discussed in the introduction in Section 1.6, the Indo-Gangetic Plain (Figure 1.10) is one of the most populous and polluted areas in the world. It has been estimated that there would be a potential gain in life expectancy in the IGP of approximately 4-6 years if levels of $PM_{2.5}$ were reduced to standards set by the World Health Organisation (Greenstone et al., 2020; WHO, 2018). The unique geography of the IGP and broader scale meteorological drivers, coupled with the regional diversity of seasonal pollutant emission sources (Section 1.6.1) makes this region one of the most challenging places to study the controls of its air pollution and the consequent impact on human health.

In this chapter, we use the WRF-Chem regional atmospheric chemistry model to describe the seasonal patterns of surface $PM_{2.5}$ and one of its main component, organic aerosol (Section 1.3.2) and to help disentangle the role of anthropogenic, pyrogenic and biogenic emissions on their surface patterns across the IGP.

A growing body of regional models have been used to study the relationship between emissions, meteorology, and $PM_{2.5}$ over India (Bran and Srivastava, 2017; Kulkarni et al., 2020; Kumar et al., 2015b; Ojha et al., 2020), and to estimate the health impacts of outdoor exposure to $PM_{2.5}$ (Conibear et al., 2018; David et al., 2019; Ghude et al., 2016). Many studies have focused on post-monsoon biomass burning episodes and on air pollution during the winter season over the upper-central Indian part of the IGP (Guttikunda and Gurjar, 2012; Jethva et al., 2018; Krishna et al., 2019; Kumar et al., 2015a; Mhawish et al., 2020; Pant et al., 2015; Ram et al., 2012; Singh et al., 2018). But of course the IGP also includes parts of Pakistan and Bangladesh that remain poorly studied even though they are connected via atmospheric advection. With only a few exceptions, these studies have focused on total $PM_{2.5}$ although there is evidence that single aerosol components play a major role in $PM_{2.5}$ composition over the IGP (Gani et al. (2019) and Singh et al. (2018) and references therein). Measurements have shown

that organic aerosol, originating from anthropogenic, pyrogenic, and biogenic emissions, constitute a significant fraction (20-35%) of $PM_{2.5}$ across the IGP especially during post-monsoon and winter seasons (Alam et al., 2014; Behera and Sharma, 2015; Rajput et al., 2014; Ram et al., 2008; Sharma et al., 2016).

Specifically, we use the WRF-Chem model to characterise the seasonal and spatial distributions and composition of $PM_{2.5}$ and OA in light of synoptic meteorology and emission drivers over the IGP. For the purpose of reporting the results, we divide the IGP in three sub-regions, including relevant parts of Pakistan and Bangladesh, as follows: the upper IGP that includes the Pakistani states of Sindh and Punjab and the Indian Punjab; the middle IGP that includes the Indian states of Haryana, Delhi NCT, and Uttar Pradesh; and the lower IGP that include the Indian state of Bihar and West Bengal and Bangladesh, excluding the states of Chittagong and Sylhet (Figure 1.10).

In section 2.2, we summarise the WRF-Chem set-up and input emissions used in this chapter and introduce the approach used to quantify the sensitivity of $PM_{2.5}$ constituent distributions to changes in anthropogenic, pyrogenic and biogenic emissions and to seasonal changes in the atmospheric environment. n section 2.3, we first present the results of the model evaluation with observations, we describe model results for the seasonal meteorology over the IGP, the seasonal distributions and composition of $PM_{2.5}$ and OA and their sensitivity to different emissions sources, and finally the seasonal distribution of SOA volatility. We present conclusions in section 2.4.

2.2 Data and Methods

2.2.1 Model set-up and emissions

The WRF-Chem set-up used in this research chapter has been introduced and described in Section 1.5.3 and summarised in Table 1.1. We summarise here the key elements in the set-up that characterise this research chapter focused on the regional drivers of $PM_{2.5}$. Our study domain encompasses the IGP at a horizontal spatial resolution of 20 km (Figure 1.8). For computational expediency we have chosen a representative period of one month for each distinct season over the IGP for the year 2017/2018 (Table 1.1). In WRF-Chem, we use a 1-D Volatility Basis Set VBS model to describe the evolution of OA and its influence on $PM_{2.5}$ (Section 1.5.3).

We use anthropogenic emissions from EDGAR-HTAP v2.2 for year 2010 (Janssens-Maenhout et al., 2015), which consider only monthly variations in emissions based on monthly profiles, specified for each country and for each sector. Using an anthropogenic emission inventory for 2010 to describe atmospheric chemistry during 2017-2018 will inevitably introduce some biases in our model $PM_{2.5}$ estimates, particularly because our study domain includes regions with rapidly growing emissions. From 2010 to 2017, India has seen reductions in BC, OC, CO and NMVOC emissions from the residential sector owing to policies that have enabled a switch to cleaner residential fuels and energy sources. However India's growing economy had led to a rapid increase of NO_x and SO_2 emissions from the industrial sector($\sim +12\%$,$\sim +10\%$) and energy sector ($\sim +20\%$, $\sim +26\%$), and an increase in NO_x and NMVOC from on-road transportation ($\sim +50\%$, $\sim +27\%$). An increase in intensive agricultural practices over the Indian IGP has increased ammonia emissions NH_3 ($\sim +15\%$) (McDuffie et al., 2020). Inaccurancies in PM precursor gaseous emissions will impact our ability to describe air pollution for our study year, in particular for individual components of secondary inorganic aerosols

(nitrate, sulfate and ammonium) and SOA. It remains difficult to disentangle the impact of using outdated emission estimates from other sources of model error, e.g., meteorology, chemistry, land-cover, and model resolution. For pyrogenic emissions, hourly biomass burning emissions are taken from the Fire Inventory from NCAR (FINNv1.5) inventory for year 2017/2018 (Wiedinmyer et al., 2011). Pyrogenic emissions are apportioned between FINN and EDGAR-HTAP inventories. The FINNv1.5 inventory includes global estimates of trace gas and particle emissions from open burning of biomass, which includes wildfire, agricultural fires, and prescribed burning (Wiedinmyer et al., 2011). EDGAR-HTAPv2.2 is focused on anthropogenic emissions but excludes large-scale biomass burning (e.g. forest fires, peat fires), agricultural waste or field burning. Within its residential sector, emissions include small-scale combustion, including heating, lighting, cooking and solid waste disposal or incineration (Janssens-Maenhout et al., 2015). Biogenic emissions are calculated online using the Model of Emissions of Gases and Aerosol from Nature (MEGANv2.1, Guenther et al. (2006)).

Figure 2.1 shows the seasonal distributions of total anthropogenic, pyrogenic, and biogenic (predominately isoprene) emissions over the IGP. Total anthropogenic emissions have been calculated by summing the mass contribution from all the chemical species (gas and particle) specified in the inventory once preprocessed onto the model domain using the WRF-Chem tools for the community ACOM-NCAR (2020). We converted gas emissions to mass units using the appropriate molar mass for each species. The same approach has been used to calculate fire emissions, while isoprene emissions are calculated online by MEGAN in the WRF-Chem model and then converted to mass units. Anthropogenic emissions generally dominate in all seasons (Figure 2.1a,d,g,j) with daily values ranging from 10^1 to 10^2g m^{-2} day^{-1}. The two largest localised regions of anthropogenic emissions are Delhi and Kolkata with emissions $>$100 g m^{-2} day^{-1}, followed by smaller indian cities, e.g. Patna, Varanasi, Kanpur and Lucknow (Figure 1.10). Just south of the border of Uttar-Pradesh, the Madhya Pradesh district of Singrauli hosts several

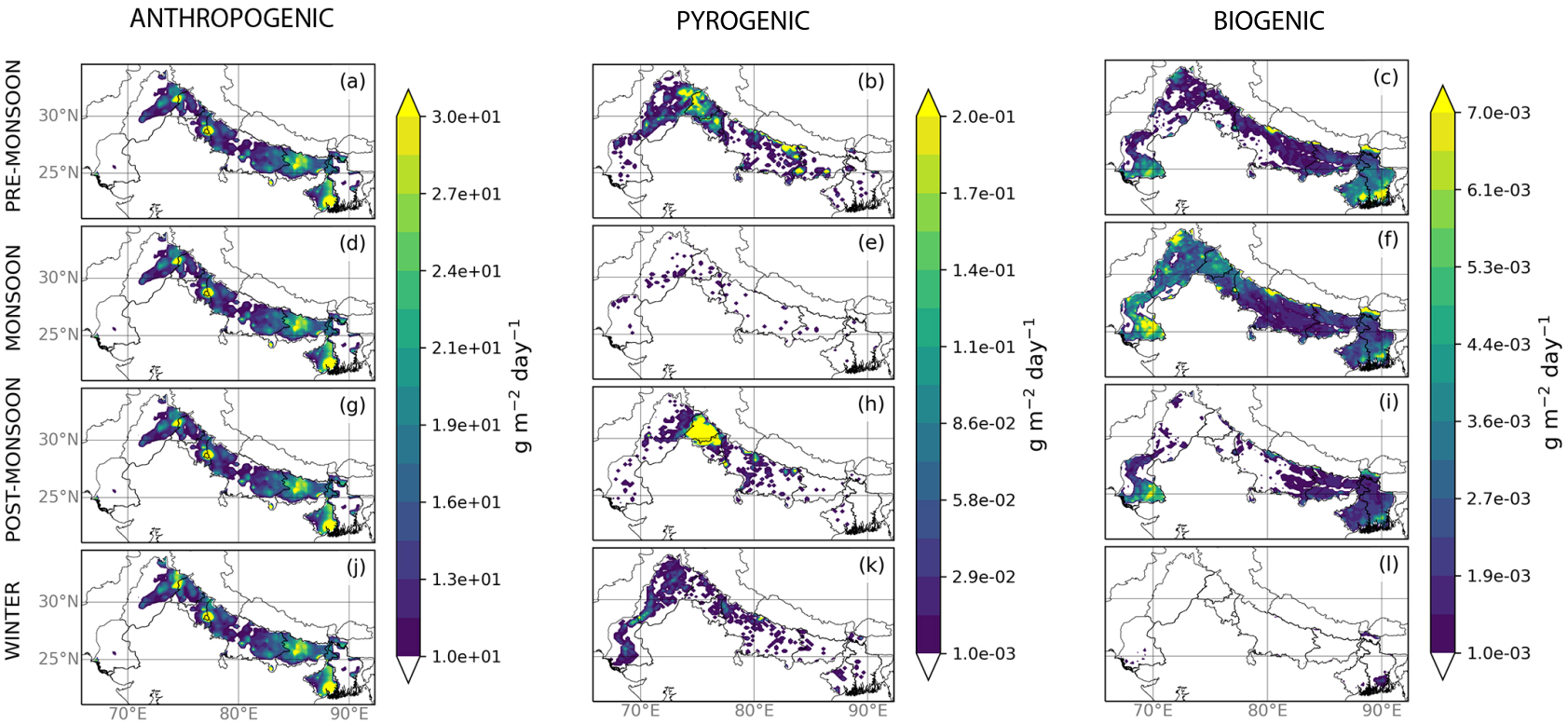

Figure 2.1: Seasonal mean daily emissions over the IGP (g m^{-2} day^{-1}) of anthropogenic (range: 0-177 g m^{-2} day^{-1}), biomass burning (range: 0-1.28 g m^{-2} day^{-1}), and biogenic from isoprene (range: 0-0.02 g m^{-2} day^{-1}) emissions. Anthropogenic emissions from EDGAR-HTAP and fire emissions from FINN. Biogenic emissions are calculated online in WRF-Chem using MEGAN. To determine total anthropogenic and pyrogenic emissions we sum across all emitted species, respectively, while for biogenic emissions we consider only isoprene. Modeled time periods: pre-monsoon season: 18th April to 16th May 2017; monsoon season: 3rd to 31st July 2017; post monsoon season: 18th October to 16th November 2017; winter season: 8th January to 5th February 2018.

large power plants. The Pakistani and Bangladeshi parts of the IGP generally have the lowest anthropogenic emissions, with the exception of Karachi in south Pakistan, the north Pakistani Punjab (the most populated part of Pakistan where Lahore and Faisalabad are located), and Dhaka in Bangladesh. Emissions from Karachi and Dhaka have lower per capita emissions than Indian cities of comparable size.

Fires have a strong seasonal cycle, peaking during pre-monsoon and post-monsoon seasons (Figure 2.1b,h), with emissions $\sim 10^{-1}$g m^{-2} day^{-1} mainly due to agricultural stubble burning. The post-monsoon harvesting season includes fire emissions rates that are three times higher compared to the pre-monsoon season ($\sim$ 0.3 g m^{-2} day^{-1} and $\sim$ 0.9 g m^{-2} day^{-1}, respectively). Post-monsoon fires are almost exclusively located in the Indian Punjab, with the largest values at the border with Haryana state. Pre-monsoon fires are located around the border of Pakistani and Indian Punjab and upper Haryana. There are also some isolated fires in the eastern part of the IGP. During winter (Figure 2.1k), low fire activity is present in the Indus valley in Pakistan and mainly over Uttar-Pradesh from post-harvesting of sugarcane crop.

Biogenic emissions peak during pre-monsoon and monsoon seasons (Figure 2.1c,f), with values of 2×10^{-3}g m^{-2} day^{-1} and 1.5×10^{-2}g m^{-2} day^{-1}, respectively over the lower and upper IGP. The largest values are over Sindh in Pakistan, West Bengal, and Bangladesh. Land cover over the IGP is dominated by croplands, but state of Sindh includes coastal mangrove plantations, inlands riverine forests, irrigated plantations, and rangelands (Ministry of Environment Government of Pakistan, 2009). Moreover, West Bengal and Bangladesh emissions are mostly confined close to the coast, where forest land is present (Reddy et al., 2016). During these two seasons there are also isoprene emissions over Uttar Pradesh from forests in Pilibhit and Kheri, and from northeast Pakistan.

Season	Base run	Sensitivity run
pre-monsoon	18th April - 16th May 2017	1-7 May 2017
monsoon	3-31 July 2017	10-17 July 2017
post-monsoon	18th October - 16th November 2017	1-7 November 2017
winter	08th January - 5th February 2018	23-31 January 2018

Table 2.1: Summary of baseline and sensitivity simulations performed in this research chapter.

2.2.2 Determining the Sensitivity of $PM_{2.5}$ and OA to Changes in Precursor Emissions

We use a perturbative approach to determine the importance of different source sectors on $PM_{2.5}$ and OA, which takes into account the non-linear chemical environment. Alternatively, setting a particular emission source to zero would result in a significant non-linear response that is unique to the source, consequently precluding any meaningful comparison of the importance of a particular source to $PM_{2.5}$ and OA.

First, we run a base run for each season. We then, for each season, systematically perturb one emission source by +5% over the study domain for one week of each season, keeping the other sources the same as the base run. Table 2.1 summarises the simulations performed. Finally, we calculate the sensitivity S_{ij} of species concentration to the changes in a given source of emissions as:

$$S_{ij} = \frac{\Delta C_{ij}}{\Delta E} = \frac{\Delta C_{ij}}{E^p_{tot} - E^b_{tot}} = \frac{\sum_t (C^p_{ij,t} - C^b_{ij,t})}{\sum_{ij,t,s} (E^p_{ij,t,s} - E^b_{ij,t,s})}, \tag{2.1}$$

where ΔC_{ij} represents the concentration change of our target species ($PM_{2.5}$ and OA in this study) at grid point ij in response to an emission change ΔE summed over the IGP for a particular source. We perturb directly anthropogenic and fire emissions rates. Biogenic emissions are calculated online by scaling normalized emission rates by factors that describes changes in, for example, temperature, photosynthetic active radiation, leaf

area index (LAI) (Guenther et al., 2006). We modify the WRF-Chem code to increment only isoprene emissions because our calculations suggest they account for almost all of biogenic emissions over the IGP, in agreement with other studies (Singh et al., 2011; Surl et al., 2018). ΔC_{ij} is calculated by summing over time the difference in concentrations at each grid cell ij of the perturbed run p $C^{p}_{ij,t}$ and the base run b $C^{b}_{ij,t}$. The change in concentration in each grid cell is therefore scaled by the same ΔE, allowing to consider local and non-local emission influences equally and to avoid singularities in grid cells where there is no net emission change. We use this scaling because it allows us to compare the sensitivity of atmospheric concentrations to different sources types. ΔE is calculated as the difference of total emissions within the IGP domain between the perturbed model run and the base model run for a given source type.

Total emissions across the IGP for the perturbed run E^{p}_{tot} and for the base run E^{b}_{tot} are calculated by summing emissions from all species for the length of the simulation and for all grid cells across the IGP. In more detail, emissions at each grid point ij for species s between two consecutive model outputs at t and $t+1$ is calculated (for both the perturbed and base runs) by $E_{ij,t,s} = \varepsilon_{ij,t,s}\Delta t A_{ij}$. $\varepsilon_{ij,t,s}$ denotes the emission rate of species s at location ij and output time t, A_{ij} denotes the area of grid point ij, which in our calculations is constant at 400 km^2, and Δt corresponds to an interval of model output which in our calculation is 3 hours. To take into account the different spatial variability of emissions from different sources (Figure 2.1), we scale ΔE with the total number of grid cells within the IGP for which the emission difference is $>$0.001 g m^{-2} day^{-1}, corresponding approximately to cumulative emissions > 2.8 Mg for each grid cell in one week. This threshold corresponds to a lower limit for significant emissions rate across the area considered (Figure 2.1). We also neglect values of S_{ij} for which the change in the pollutant concentration C_{ij} $<$5% of mean pollutant seasonal concentration over the IGP (4 μg m^{-3} and 1 μg m^{-3} for $PM_{2.5}$ and total OA, respectively). Using this additional threshold allows us to isolate significant changes in concentrations due

to direct changes in emissions, and remove smaller values due to model non-linearity. We report the sensitivity parameter S_{ij} with units of μg m^{-3} Gg^{-1}. In a policy-making context, our sensitivity parameter provides information about how to control atmospheric concentrations by changing different emission sources in order to obtain the highest air quality benefits from certain emission reductions.

2.2.3 Observations for model evaluation

As introduced in Section 1.5.3, in this Chapter we evaluate the WRF-Chem model performance against ground-based observations of main gaseous pollutants and $PM_{2.5}$ and PM_{10}, OA values literature, and aerosol optical depth (AOD) from satellite observation.

Ground-based measurements We use in situ measurements corresponding of our simulated time periods (Section 2.2.1) of $PM_{2.5}$, PM_{10}, CO, NO_2, O_3, and SO_2 from the Indian Central Pollution Control Board (CPCB, 2021) and $PM_{2.5}$ data collected atop the US Embassy in Pakistan and Bangladesh (US Embassy, 2020). Data from Pakistan are only available from 2019 so we use 2019 data for the monsoon and post-monsoon seasons and data from 2020 for the winter and pre-monsoon seasons. We accessed these data from the OpenAQ Platform (OpenAQ, 2020).

We apply a cleaning procedure of data for each pollutant. The cleaning procedure followed five sequential steps: 1) Exclude non valid, negative and zero values. Negative values have been removed as representing suspicious values, rather than being indicative of possible low concentrations that hover around zero, which are unlikely to occur in a highly polluted environment such as Delhi; 2) exclude hourly data with $z_{score} \geq 3$ respect to daily mean; 3) exclude days with fewer than 12 hourly measurements per day; 4) exclude stations with less then 15 days measurements per simulated season; and 5) exclude all stations but one if there are multiple stations in the same model grid-cell

(for statistical independence in the comparison). From this cleaning procedure we get 31 independent stations (Table A.1, Figure A.1), with a total number of measurements (all seasons): 63 for CO, 54 for SO_2, 61 for NO_2, 50 for O_3, 84 for $PM_{2.5}$, 20 for PM_{10}. For particulate matter, we compare the dry mass of $PM_{2.5}$ and PM_{10}.

Organic Aerosols Given the lack of continuous measurements of OA and its components POA and SOA over the IGP, we compare our model OA with measurements available from the literature which report seasonal values available for years other than the one under study: Delhi, 2013-2016 (Jain et al., 2020), Kanpur 2008-2009 (Ram et al., 2012), Kharagpur 2009-2010 (Srinivas and Sarin, 2014), Kolkata 2006 (Chatterjee et al., 2012) and Lahore 2007 (Stone et al., 2010). Location of measurement sites is shown in Figure A.1 OA are converted from organic aerosol mass to organic carbon mass assuming OA/OC ratios 1.4 for POA and 2.0 for SOA to take into account the different oxidation level between POA and SOA,following Knote et al. (2015). However, these values have been derived from ambient studies in urban environments in the American continent, and may not be fully representative of the highly polluted Indian chemical environment, and do not take into account further aging of POA, which may lead to an underestimation of the POA and SOA to OC ratios (Robinson et al., 2007).

Total AOD column We also evaluate the model using satellite observations of aerosol optical depth (AOD) from the NASA Moderate Resolution Imaging Spectroradiometer (MODIS) instrument aboard the Terra and Aqua satellites. Aerosol Optical Depth (AOD) is derived through optical properties of aerosol. Aerosol particles interfere with the propagation of radiation through the absorption and scattering of light. This interference can be expressed through an *extinction coefficient* β_{ext} , which is the sum of a scattering coefficient β_{scat} and an absorbing coefficient β_{abs}, which are defined based on the probability that a photon colliding with the particle is absorbed or scattered. Scattering depends on the particle geometry, while absorption depends on its the chemical properties. The

optical path is defined as the physical path of light scaled by the extinction coefficient β_{ext} (Seinfeld and Pandis, 2016). The aerosol optical depth, for a given radiation wavelength, is defined as the optical path for the sun radiation propagating vertically from the top of the atmosphere to the surface of the Earth. MODIS have a local equatorial overpass time of 1030 (Terra) and 1330 (Aqua). AODs are retrieved at 550 nm, corresponding to particle sizes of 0.1–2μm and comparable to the $PM_{2.5}$ size range. In particular, we use the MODIS Collection 6.1 Level 2 combined Dark Target and Deep Blue AOD product available on a 10 km spatial resolution (Levy et al., 2013). We re-grid the 10 km Terra and Aqua MODIS AOD data to the coarse WRF-Chem 20 km$\times$20 km model grid.

2.3 Results

2.3.1 Model Evaluation

Gaseous pollutants and PM To compare the model against ground-based observations, we sample the model at the location of each monitoring station. In practice, we identify the model gridcell closest to the measurement location (nearest-neighbours method). For each measuring station, we calculate seasonal mean of pollutants that we compare with corresponding modelled seasonal mean. We evaluate the model performance for the seasonal mean values only because in this chapter we are interested in the seasonal variation of pollutants over the IGP, contrary to what is investigated in Chapter 3 and Chapter 4, where higher temporal and spatial resolution of pollutants is taken into account. The seasonal mean is calculated for the representative time period for each season used in this study (Table 2.1). The resulting comparison is shown in Figure 2.2. We evaluate the model using five metrics: the Mean Bias (MB), Root Mean Square Error (RMSE), Normalised Mean Bias (NMB), Mean Normalised Absolute Error (MNAE), and Pearson correlation coefficient (r), calculated using seasonal average

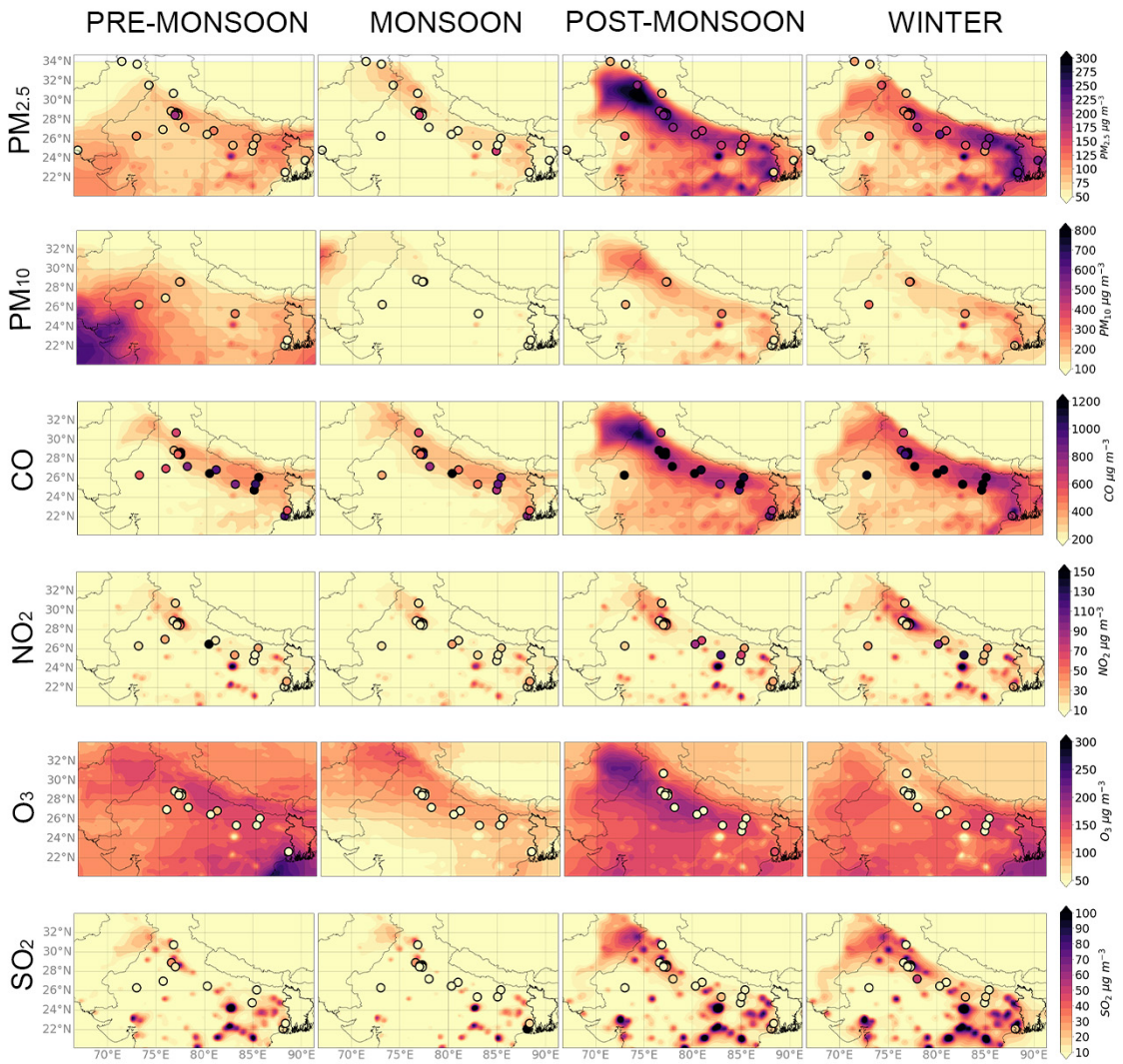

Figure 2.2: Seasonal mean spatial distributions of main pollutants for model and observations (dots) Season periods are defined as in Table 1.1. Modeled time periods: pre-monsoon season: 18th April to 16th May 2017; monsoon season: 3rd to 31st July 2017; post monsoon season: 18th October to 16th November 2017; winter season: 8th January to 5th February 2018.

model-observation pairs,reported in Figure 2.2. These metrics are widely used for air quality model evaluation (Brasseur and Jacob, 2017; Conibear et al., 2018; Kumar et al., 2012b; Zhang et al., 2006b). Table 2.2 summarises the seasonal evaluation of the model with the metrics described.

pollutant	season	NMB	NMAE	MB [$\mu g\ m^{-3}$]	RMSE [$\mu g\ m^{-3}$]	r
$PM_{2.5}$	pre-monsoon	0.12	0.31	10	34	0.62
	monsoon	0.41	0.65	19	36	0.09
	post-monsoon	0.19	0.28	33	62	0.84
	winter	0.004	0.28	0.7	53	0.69
PM_{10}	pre-monsoon	0.15	0.59	32	133	0.11
	monsoon	-0.21	0.28	-25	46	0.69
	post-monsoon	-0.14	0.36	-41	122	0.66
	winter	-0.25	0.43	-64	131	-0.85
CO	pre-monsoon.	-0.64	0.64	-643	825	0.44
	monsoon	-0.55	0.55	-428	567	0.12
	post-monsoon	-0.65	0.65	-1439	2272	0.29
	winter	-0.52	0.61	-703	1163	-0.20
NO_2	pre-monsoon	0.14	0.95	6	57	0.27
	monsoon	0.46	1.00	11	32	0.08
	post-monsoon	0.65	1.44	36	97	0.15
	winter	0.31	0.98	17	66	0.30
O_3	pre-monsoon	1.59	1.67	75	91	-0.52
	monsoon	2.92	2.92	64	66	-0.12
	post-monsoon	2.96	2.98	98	113	-0.75
	winter	2.87	2.92	71	87	-0.55
SO_2	pre-monsoon	0.25	0.85	3	13	0.04
	monsoon	0.27	1.38	4	34	-0.18
	post-monsoon	2.36	2.44	33	49	0.51
	winter	1.85	2.15	27	43	0.04

Table 2.2: Statistical evaluation of model performance with ground based measurements for main PM and main gas pollutants. Season periods are defined as in Table 1.1. Metrics are calculated using seasonal average model-observation pairs,reported in Figure 2.2.

On average, the model tends to overestimate surface $PM_{2.5}$ concentrations in all season ($0.004 <$NMB$<$0.4) especially during monsoon season (NMB=0.4) where it is overestimated almost at each monitoring station (Figure 2.2) across the IGP. During post-monsoon and winter, the model has a better performance, with NMB < 0.2, although during postmonsoon the model tends to highly overestimate $PM_{2.5}$ concentrations in the lower IGP (Figure 2.2). The model has skill in reproducing observed seasonal variations across the IGP in all seasons as shown in Figure 2.2 ($r > 0.62$) with the exception of the monsoon season ($r = 0.09$). Poorer model performance during the monsoon

period may be due to a number of compounding factors. In particular, it is challenging to reproduce observed atmospheric water vapour and precipitation over the Bay of Bengal, western coasts of India and the Himalayan foothills during summer months. Uncertainties in the representation of topography, insufficient mixing in the boundary layer, errors in moisture advection and simulation of surface moisture availability, soil temperature and an excessive water vapour flux from the ocean all contribute to model error (Kumar et al., 2012a). Previous studies have shown that monsoonal rainfall is not well described by regional models such as MM5 or WRF (Rakesh et al., 2009; Ratnam and Kumar, 2005). When we compare our WRF model simulation with MERRA-2 reanalysed meteorology (Gelaro et al., 2017) we find that precipitation rates have a negative model bias of $\simeq$80% over the IGP, similarly to what Conibear et al. (2018) obtained with a similar model set-up. For PM_{10}, the model tends to underestimate the observation in all seasons (NMB up to -0.25) except in premonsoon season (NMB=0.15) and has poorer skill in reproducing observed PM_{10} variations compared to $PM_{2.5}$ ($r \leq 0.69$), especially during winter and pre-monsoon season, even because of the low number of monitoring station with available measurements (Figure 2.2). We generally find poorer model agreement with gas-phase pollutants, including a positive model bias and comparatively poor correlations with observations of NO_2, SO_2 O_3 and negative bias for CO across the whole IGP (Table 2.2, Figure 2.2). We attribute this to multiple sources of uncertainties. Given the coarse spatial and temporal resolution our model (20 km$\times$20 km spatial, 3 hour temporal), we expect our model not to be able to capture variations in pollutants at a higher spatial and temporal resolution, thus struggling to reproduce observations at the CPCB network sites, often being located near to roadsides or in dense urban areas. This phenomenon preferentially affects reactive trace gases that react on timescales with advection across individual model grid cells. Previous studies have reported similar model limitations (Balasubramanian et al., 2020; Fountoukis et al., 2013; Kuik et al., 2016; Paolella et al., 2018; Sirithian and Thepanondh, 2016; Tan et al., 2015). Data for Pakistan are not

available for our modelling study period (2017/2018) so we instead use data from 2019 for the monsoon and post-monsoon seasons and data from 2020 for the winter and pre-monsoon seasons, which represents an additional source of error. Previous studies show that regional modelling over south Asia tends to overestimate satellite column observations of NO_2 by 10–50% over the Indo-Gangetic Plain, the bias peaking as high at 90% during winter months (Kumar et al., 2012b), and up to +131% when compared to ground-based observations over densely populated urban regions (Karambelas et al., 2018). These differences have been attributed mainly to errors in NO_x emission inventories over densely populated areas, uncertainties in seasonal variations of emissions, absence of diurnal and vertical profiles of anthropogenic emissions(Karambelas et al., 2018; Kumar et al., 2012b), and underestimation of precipitation rate that will reduce the loss of soluble trace gases Kumar et al. (2012a). Similarly, previous regional model studies of IGP region have tended to over-predict concentrations of SO_2, with NMB$>$3.5 (Conibear et al., 2018; Kota et al., 2018). We attribute our positive model bias of SO_2 (Table 2.2) to using an outdated emission inventory that does not take into account the beginning of a shift from coal to gas-based power plants (Sharma and Khare, 2017). Urbanisation has been shown to affect the diurnal spatial distribution of surface ozone (Li et al. (2014) and references therein), and also the magnitude and location of anthropogenic emissions of NO_x and VOCs that subsequently affect surface ozone photochemistry (Ghude et al., 2013; Zhang et al., 2004). Finally, some fraction of the overestimation of surface ozone is linked to our use of the MOZART chemical mechanism that has been previously reported to have a positive model bias over south Asia compared to other mechanisms (Sharma et al., 2017a). Collectively, these model limitations associated with describing reactive trace gases will impact our ability to model particulate matter, especially secondary components over urban areas across the IGP.

Organic Aerosol As for gaseous and PM pollutants, to compare the model with the observation, we sample the model at the time and location of each measurement station. Table 2.3 shows the comparison of modeled OC with measurements studies. For OA, the model reproduces the order-of-magnitude seasonal trends. However, complex meteorology and interannual variability are a key factor in determining air pollution levels, and this might drive the uncertainties in our comparison. Additional measurements are needed to robustly assess model performance.

AOD We calculate the 550 nm AOD using WRF-Chem values at 300 nm and 1000 nm by interpolation using the Ångström power law following Kumar et al. (2014). We sample the model at the local overpass time of Terra (1030) and Aqua (1330) where there exists at least one best-quality AOD retrieval. We then mean model and MODIS AOD values over time to generate seasonal statistics across the IGP. Table 2.4 reports the main statistical metrics for AOD evaluation together with the range of observed and modeled AOD.

Table 2.4 shows that WRF-Chem AOD agree with spatial distributions of MODIS AODs with r typically > 0.5 with the exception of the monsoon season (r=0.35). Poor model skill during the monsoon season may reflect difficulties in retrieving AOD during extensive seasonal cloud coverage. In addition, the model has specific difficulties in reproducing atmospheric aerosol abundances during monsoon season, as highlighted earlier in this section, that could affect the simulated total AOD column. The model tends to overestimate MODIS AOD during pre-monsoon (NMB=0.33, 0.26 for Terra and Aqua satellites) and slightly underestimate AOD in the other seasons (NMB ranges from -0.06 to -0.19).

number ID	location	period	species	OC obs [$\mu g\ m^{-3}$]	OC model [$\mu g\ m^{-3}$]	reference
1	Delhi	Jan-Feb 13-16	$PM_{2.5}$	23.6 $\pm$ 12.9	23.4	Jain et al. (2020)
		Mar-May 13-16		9.82 $\pm$ 4.16	13.3	
		Jun-Set 13-16		6.77 $\pm$2.63	12.1	
		Oct-Dec 13-16		25.2 $\pm$14.7	38.6	
1	Delhi	Jan-Feb 13-16	PM_{10}	30.1$\pm$12.1	23.5	Jain et al. (2020)
		Mar-May 13-16		23.4 $\pm$ 10.7	13.4	
		Jun-Set 13-16		15.9 $\pm$9.7	12.3	
		Oct-Dec 13-16		39.4 $\pm$15.6	38.7	
2	Kanpur	Oct-Nov 08	PM_{10}	53.3 $\pm$21.2	37.2	Ram et al. (2012)
		Dec 08 - Feb 09		29 $\pm$ 14.5	21.9	
		Mar-Apr 09		23.1 $\pm$ 11.5	12.3	
3	Kharagpur	Nov 09 - Mar 10	$PM_{2.5}$	30.7$\pm$ 12.1	42.0	Srinivas and Sarin (2014)
4	Kolkata	Jan-06	$PM_{2.5}$	18.5$\pm$2.0	67.2	Chatterjee et al. (2012)
		Apr-May 06		15.5$\pm$ 3.6	7.8	
		Jul-06		5$\pm$1	14.3	
		Oct-Nov 06		11.5$\pm$5.0	57.4.	
5	4*Lahore	Jan-07	$PM_{2.5}$	76.5	34.0	Stone et al. (2010)
		Apr-May-07		43.5	20.0	
		Jul-07		31.5	18.2	
		Oct-Nov 07		111.2	61.0	

Table 2.3: Comparison of modeled OC with measurements studies in the literature.Model values refers to the mean over the corresponding season of observations.

satellite	season	MB	NMB	NMAE	RMSE	r	range obs	range model
Terra	pre-monsoon	0.33	0.53	0.56	0.44.	0.53	0.06 - 1.78	0.10 - 2.29
	monsoon	0.04	0.05	0.45	0.52	0.35	0.00 - 3.42	0.10 - 3.78
	post-monsoon	-0.05	-0.06	0.25	0.25	0.76	0.07 - 3.50	0.12 - 1.71
	winter	-0.11	-0.19	0.30	0.21	0.64	0.05 - 1.74	0.11 - 1.16
Aqua	pre-monsoon	0.27	0.44	0.49	0.40	0.52	0.07 - 3.50	0.08 - 2.82
	monsoon	-0.18	-0.19	0.43	0.53.	0.35	0.04 - 2.53	0.11 - 3.17
	post-monsoon	-0.05	-0.06	0.25	0.23	0.74	0.06 - 2.23	0.12 - 1.47
	winter	-0.08	-0.14	0.33	0.22	0.47	0.09 - 1.17	0.08 - 1.2

Table 2.4: Seasonal comparison of modeled total AOD column and satellite AOD observations for the Terra and Aqua instruments over the IGP for the simulated period 2017/2018

.

2.3.2 Seasonal Meteorological Drivers

Figure 2.3 shows model seasonal mean values for planetary boundary layer height (PBLH, m), surface relative humidity (RH, %), surface temperature (°C), mean daily rainfall (mm day^{-1}), and 10 m wind (m s^{-1}) over the IGP. Given that PBLH and RH show a diurnal cycle with high variance we report nighttime and daytime values for these variables across the IGP.

During the pre-monsoon season, mean surface temperatures are higher than 30°C. Mean PBLH ranges from 1000 m up to 4500 m at daytime, with the highest values are over Pakistan and central IGP, and is almost an order of magnitude smaller during nighttime (120 m up to 400 m). Seasonal mean winds are typically 3 m s^{-1}, southward from the northern mountain chain of Hindu Kush and the Himalayas, and stronger northward from the coast, allowing pollutants to be advected mainly in the inland. Air is much more humid over the lowest part of the IGP (>60%). Rainfall follows similar patterns of RH, limited to Bangladesh with values below $\sim$3 mm day^{-1}.

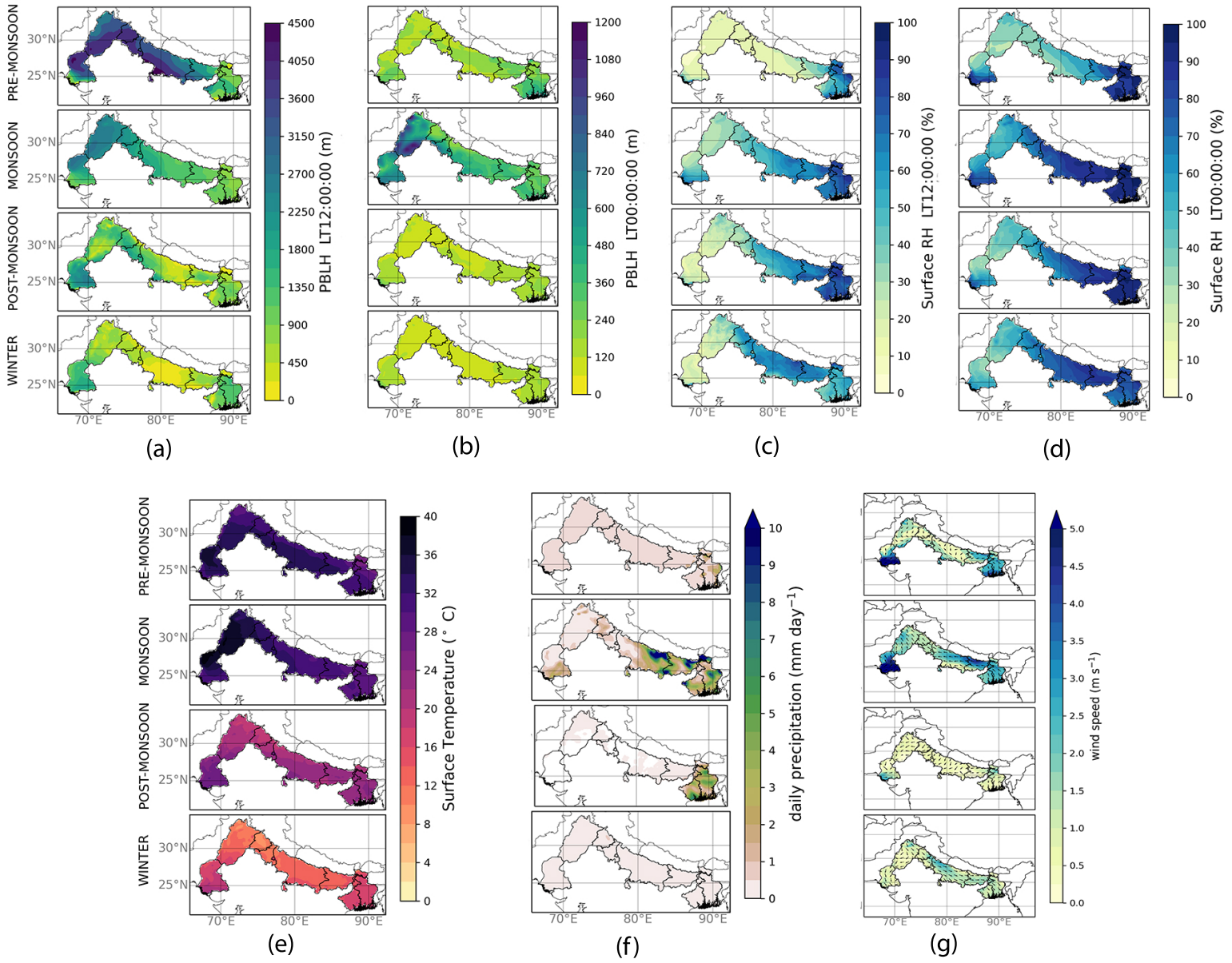

Figure 2.3: Seasonal mean WRF-Chem meteorological fields: (a) daytime planetary boundary layer height (m); (b) nighttime planetary boundary layer height (m); (c) daytime surface relative humidity (%); (d) nighttime surface relative humidity (%); (e) surface temperature at 2 m (°C; (f) daily precipitation rate (mm day^{-1})); and (g) wind speed (m s^{-1}) and direction at 10 m. Modeled time periods: pre-monsoon season: 18th April to 16th May 2017; monsoon season: 3rd to 31st July 2017; post monsoon season: 18th October to 16th November 2017; winter season: 8th January to 5th February 2018.

During the monsoon season, the dominant feature is the monsoon itself. This manifests most obviously in increased rainfall, which increases the washout of hydrophillic pollutants, mainly in the central and lower part of the IGP, with mean daily rainfall values of 3-7 mm day^{-1} with localized regions of rainfall in excess of 15 mm day^{-1}, and wind speeds in excess of 6 m s^{-1} north-northeastward. Values of RH are $>$50% almost everywhere over the IGP, and relatively low values for the PBLH allow a well mixed chemical environment, with smaller day to night variation compared to pre-monsoon (1000-3000 m day, 500-1200 m night). Mean temperatures are similar to those during the pre-monsoon, with the most prominent increase over northern Pakistan (>35 $^{\circ}$C).

The post-monsoon season is characterized by cooler temperatures than the previous two seasons with mean values of $\sim$23°C, much lower values for PBLH (below 2000 m during day and $\sim$200 m during night), and weaker wind speeds (< 1 m s^{-1} with no predominant direction, a combination of factors that results in pollution stagnation. With the exception of Bangladesh and the Indian states that are adjacent to the Bay of Bengal, rainfall is almost absent from the IGP. Nevertheless, air continues to be humid with the distribution and values of RH similar to the monsoon season, with values of up to 80% over the central and lower IGP, environmental conditions that favour water significantly contributing to PM mass without washout from rain.

During winter, mean temperature further drops to $\sim$15°C with cooler temperatures over regions adjacent to the northern mountain chains. PBLH values are at their daily annual minimum ($<\sim$1000 m) and its night values are similar to post-monsoon ($<\sim$200 m). Winds speeds are typically $<$3.5 m s^{-1} with a net west-east gradient from the upper IGP to the lower IGP, which advect pollutants towards Bihar, West Bengal and Bangladesh, and with a north-south gradient over the Indus Basin that advects pollution from northern Pakistan to the coast. Daily rainfall is below 3 mm day^{-1} anywhere across the IGP, but as for post-monsoon, RH remains high over the central and lower IGP (>40% daytime, 70% during nighttime).

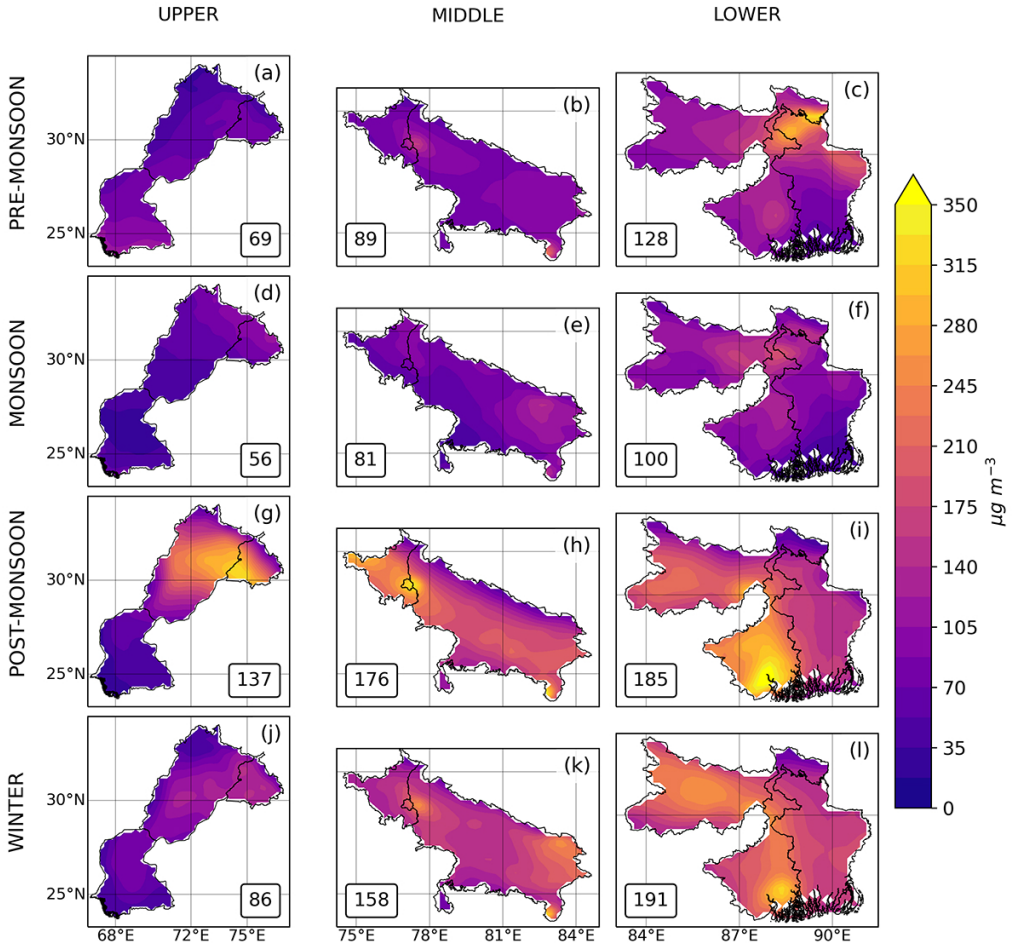

Figure 2.4: Seasonal mean spatial distributions of $PM_{2.5}$ (μg m^{-3}) over the upper, middle and lower IGP. The numbers inset of pre-monsoon (a–c), monsoon (d–f), post-monsoon (g–i), and winter (l–n) seasons denote the regional mean $PM_{2.5}$ value. Modeled time periods: pre-monsoon season: 18th April to 16th May 2017; monsoon season: 3rd to 31st July 2017; post monsoon season: 18th October to 16th November 2017; winter season: 8th January to 5th February 2018.

2.3.3 Seasonal Distributions of Surface $PM_{2.5}$

Figure 2.4 shows seasonal variations of surface $PM_{2.5}$ across the upper, middle, and lower IGP. Generally, we find the highest values of surface $PM_{2.5}$, up to 350 μg m^{-3}, during post-monsoon and winter seasons that are associated with lower PBLH allowing large anthropogenic emissions to accumulate in the boundary layer without ventilation from strong winds. From this section we begin our narrative from the post-monsoon

season and finish with the monsoon season, but retain the figure panels in chronological order for a particular calendar year. Our seasonal distributions of $PM_{2.5}$ are similar to recent studies which are performed over the same region but for different years than the one we investigated (Mhawish et al., 2020; Ojha et al., 2020; Shahid et al., 2015). We report higher $PM_{2.5}$ concentrations especially over the lower IGP compared to these studies, however we acknowledge that interannual variability in meteorology can influence air pollution levels and thus affect our comparison. In addition, our model also takes into account water content in $PM_{2.5}$ mass on top to dry $PM_{2.5}$ mass through aqueous phase chemistry. Our results shows that water content in $PM_{2.5}$ is substantial, especially over the lower IGP where water makes up to 42% of total $PM_{2.5}$ mass (see later in this section). This helps to explain our comparatively high $PM_{2.5}$ estimates.

During the post-monsoon season (Figure 2.4 (g–i)), the mean values of surface $PM_{2.5}$ in the upper, middle, and lower IGP are 137 μg m^{-3}, 176 μg m^{-3}, and 185 μg m^{-3}, respectively. On a local scale, Kolkata and its surroundings in the lower IGP experience the worst air quality with mean $PM_{2.5}$ values in excess of 300 μg m^{-3}, closely followed by Delhi NCT, the border region between Indian and Pakistani Punjab, and Singrauli at the southern border of middle IGP ($\sim$300 μg m^{-3}). The best air quality is found in the Pakistani state of Sindh with $PM_{2.5}$ concentrations below 75 μg m^{-3}. Biomass burning in the Indian Punjab plays a key role in shaping the distribution of $PM_{2.5}$ during this season. Figure 2.5h shows that fire emissions have the largest impact on $PM_{2.5}$ concentrations across the Indian and Pakistani Punjab region, Haryana and Delhi NCT (sensitivities of up to $> 10^3$ μg m^{-3} Gg^{-1}). The impact of post-monsoon biomass burning emissions extends to the central part of the middle IGP over Uttar-Pradesh, where sensitivity of $PM_{2.5}$ to pyrogenic emissions (up to 6×10^2 μg m^{-3} Gg^{-1}) is higher than anthopogenic emissions (up to 4×10^2 μg m^{-3} Gg^{-1}). The sensitivity of $PM_{2.5}$ to changes in biogenic emissions (Figure 2.5i) have non-negligible values ($< 2 \times 10^2$ μg m^{-3} Gg^{-1}) only over part of West Bengal in the lower IGP in this season.

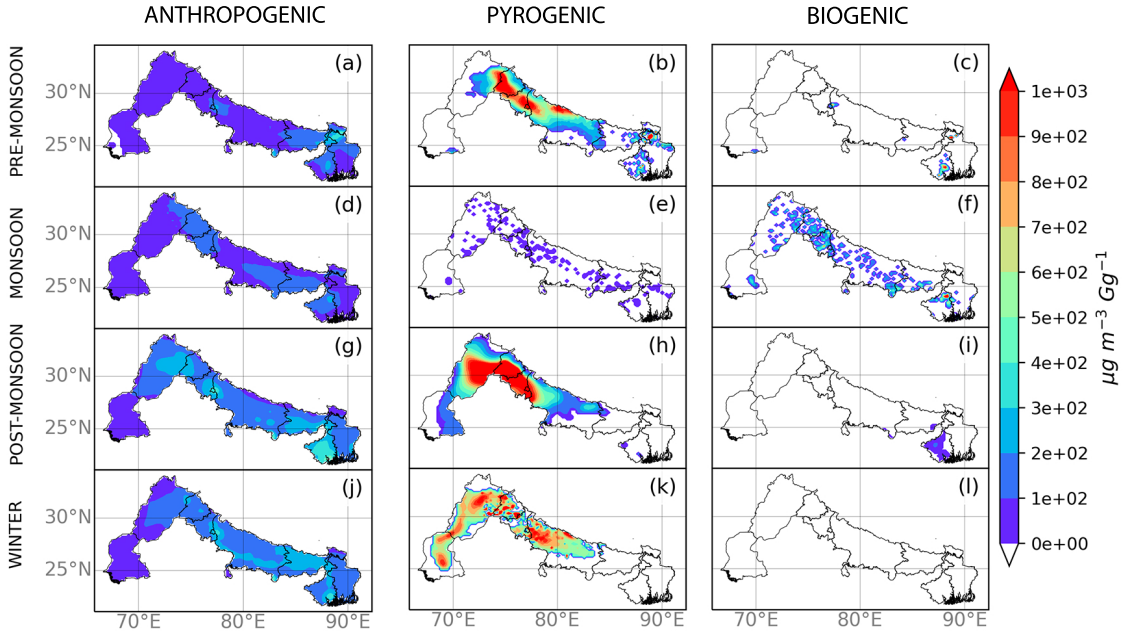

Figure 2.5: Seasonal sensitivity of $PM_{2.5}$ concentrations to changes in (left column) anthropogenic, (middle column) pyrogenic, and (right column) biogenic emissions (μ g $m^{-3}Gg^{-1}$). The calculation is described in Section 2.2.2. Regions marked as white denote where sensitivity corresponds to $PM_{2.5}$ concentrations below the set threshold of 4 μg m^{-3}. Modeled time periods: pre-monsoon season: 18th April to 16th May 2017; monsoon season: 3rd to 31st July 2017; post monsoon season: 18th October to 16th November 2017; winter season: 8th January to 5th February 2018.

During the winter season (Figure 2.4(j–l)), wind patterns advect pollutants from the upper IGP to the lower IGP (Figure 2.3, resulting in west-east gradient in seasonal mean $PM_{2.5}$ concentrations . The mean $PM_{2.5}$ value in the lower IGP is 191 μg m^{-3}, the highest mean seasonal value for the IGP. The highest $PM_{2.5}$ concentrations are reached in Kolkata ($>$300 μg m^{-3}), and in the Bihar state, with a local peak in Patna ($>$220 μg m^{-3}) known as the 'Bihar pollution pool' (Kumar et al., 2018). In the middle IGP, mean $PM_{2.5}$ concentrations are 18 μg m^{-3} lower than post-monsoon levels, with east Delhi and Singauli remaining the largest hotspots of the region ($>$220 μg m^{-3}). The upper IGP experiences the lowest seasonal $PM_{2.5}$ concentration (86 μg m^{-3}), lower than half the value in the lower IGP, with concentrations decreasing from the Punjab to the Sindth coast. Anthropogenic emissions dominate the distribution of $PM_{2.5}$ during

winter over the lower IGP (sensitivity up to 4×10^2 μg m^{-3} Gg^{-1}, Figure 2.5j), with the highest sensitivities over cities Kolkata, Singrauli. The influence of biomass burning is pronounced over the the Indus basin, stretching until Uttar Pradesh (sensitivity up to 10^3 μg m^{-3} Gg^{-1}, Figure 2.5k), while biogenic emissions do not show a significant influence during this season (Figure 2.5l).

During the pre-monsoon season (Figure 2.4 a–c), air quality begins to improve due to higher PBLHs and stronger winds (Figure 2.3) that help to disperse pollutants. Mean $PM_{2.5}$ concentrations are similar over the upper and middle IGP with values lower than 90 μg m^{-3}. Higher concentrations remain in the lower IGP (128 μg m^{-3}) due to the accumulation of pollutants from the winds blowing from the Bay of Bengal to the slopes of the Himalayas over North Bangladesh. High aerosol loading over the lower IGP during the premonsoon season is also influenced by biomass burning from Northeast India and Myanmar-Laos, which are partially included in our model domain. $PM_{2.5}$ values over the upper part of the middle IGP (Figure2.4 b) show some influence from biomass burning (Figure 2.5 b). We find that anthropogenic emissions are most important over the lower IGP and localized region in the central IGP (Figure 2.5 a). $PM_{2.5}$ concentrations in Delhi NCT are jointly influenced by biomass burning and anthropogenic sources. Biogenic sources only have a significant impact over localized regions in the lower and middle IGP (Figure 2.5(c)).

Generally, the onset of the monsoon results in better air quality across the IGP due to higher rainfall rates, which increases wet deposition of aerosols, and higher PBLHs that improve the physical dispersal of surface emissions. Mean values of $PM_{2.5}$ are $\leq$100 μg m^{-3} across the IGP. The largest values of $PM_{2.5}$ are over the lower IGP (up to 170 μg m^{-3}). We find that $PM_{2.5}$ is sensitive to biogenic emissions over localized regions across the IGP, where $PM_{2.5}$ can be more sensitive to changes in biogenic emissions than changes in anthropogenic emissions ($\sim$200-500 μg m^{-3}) and $<$200 μg m^{-3}, respectively). Fires play only a small role in $PM_{2.5}$ during this season.

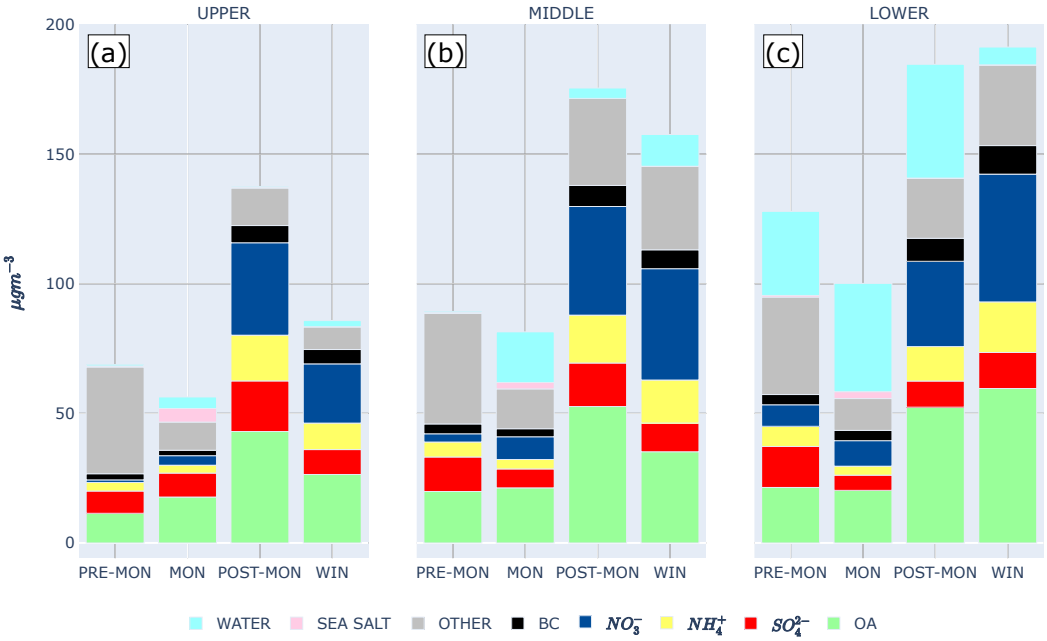

Figure 2.6: Seasonal mean $PM_{2.5}$ composition from the WRF-Chem model across the IGP: (a) upper, (b), middle, and (c) lower IGP. The constituents include sea salt (sum of sodium (Na) and chloride (Cl)), NH_4^+, SO_4^{2-}, NO_3^-, the sum of the remaining inorganic compounds (OTHER), total OA, BC, and liquid water. Modeled time periods: pre-monsoon season: 18th April to 16th May 2017; monsoon season: 3rd to 31st July 2017; post monsoon season: 18th October to 16th November 2017; winter season: 8th January to 5th February 2018.

Surface $PM_{2.5}$ composition

Figure 2.6 shows the modelled composition of $PM_{2.5}$ across the IGP. Generally, we find more variability between seasons than across different parts of the IGP, except for the water contribution to $PM_{2.5}$ mass. The results we report for the chemical composition and seasonal trends of $PM_{2.5}$ are broadly consistent with chemical characterisation studies over the region (Bhowmik et al., 2020; Chowdhury et al., 2007). As discussed in Section 2.3, model limitations in reproducing precursor trace gases will affect our ability to model secondary components of particulate matter.

Inorganic species (secondary inorganic aerosol of sulfate, nitrate and ammonium and other inorganic aerosol) dominate the chemical composition by mass of $PM_{2.5}$, representing between 30–80% of total $PM_{2.5}$ for each season across the IGP (Figure 2.6). The mean seasonal mass of total inorganics across the IGP is 54–70 μg m^{-3} during the pre-monsoon season, 27–35 μg m^{-3} during the monsoon season,79–111 μg m^{-3} during the post-monsoon season, and 51–114 μg m^{-3} during winter. The largest inorganic aerosol values are found during the post-monsoon and winter seasons due to nitrate from fossil fuel combustion and from residential and energy use. We find a similar but relatively muted seasonal variation for black carbon with mass values between 2–11 μg m^{-3}. Sea salt transported from the coasts during the monsoon season adds 3–5 μg m^{-3} (3–9%) to $PM_{2.5}$ across the IGP.

The water contribution to $PM_{2.5}$ is substantial over the lower IGP during pre-monsoon, monsoon, and post-monsoon seasons, with mass contribution of 32–44 μg m^{-3} (25–42%), while during winter it accounts for 6 μg m^{-3} (3.5%). For the middle IGP, water is a non-negligible fraction of $PM_{2.5}$ mainly during monsoon (20 μg m^{-3}, 24%) and winter (12 μg m^{-3}, 8%) seasons, while for the upper IGP the highest values of water mass are found during only the monsoon season (4 μg m^{-3}, 8%). The seasonal variation of water content reflects RH distritbuions, which above values of 60–70% allows PM hydrophilic components (e.g., nitrate, sulfate, sea salt) to uptake water via deliquescence.

The sum of primary and secondary OA contributes by mass between 17% and 31% of $PM_{2.5}$ across the IGP, with contributions from POA and SOA varying with season. During the pre-monsoon season, OA contributes 11–21 μg m^{-3} to $PM_{2.5}$, representing 17–22% of the total mass. A similar mass contribution is found during the monsoon season (18–21 μg m^{-3}) but with higher percentage contribution to $PM_{2.5}$ (20–31%). The percentage mass contribution of OA to $PM_{2.5}$ is similar during the post-monsoon (28–31%, 43–52 μg m^{-3}) and winter (22–31%, 26–60 μg m^{-3}), with higher mass contribution during

post-monsoon for the middle and lower IGP and during the winter season for the lower IGP. Our results for modeled $PM_{2.5}$ composition confirm the significance of OA contribution to fine particulate matter, and we analyse in more detail OA and its components in the next sections.

2.3.4 Seasonal Distribution of Surface OA

Figure 2.7 shows the season mean distributions of total OA with the corresponding POA and SOA distributions shown by Figures 2.8 and 2.9. We generally find that POA dominates seasonal values of total OA across the IGP, with the exception of the post-monsoon season when SOA and POA have comparable values.

During the post-monsoon season (Figure 2.7g-i), the largest OA concentrations are over the upper IGP at the border of Pakistani and Indian Punjab ($>$ 80 μg m^{-3}), where POA values can exceed 50 μg m^{-3}. Although the largest regional mean is found over the lower IGP (52 μg m^{-3}) due to urban anthropogenic emissions in and around Kolkata and Patna where values are $>$70 μg m^{-3}. Over the middle IGP, the mean OA value is similar to the lower IGP (52 μg m^{-3}) but shows a more homogeneous distribution, with the highest OA values found at the borders between upper and lower IGP. Regional mean POA values range 23–29 μg m^{-3} (Figure 2.8g-i), similar to SOA values (20–24 μg m^{-3}, Figure 2.9g-i). POA levels are much higher than SOA over the Punjab states in India and Pakistan and in the Indian lower IGP (40–70 and 30–40 μg m^{-3} for POA and SOA, respectively). Over the middle IGP, SOA is generally higher than POA (29 and 24 μg m^{-3} for SOA and POA, respectively), with highest concentrations of SOA found in the lower Uttar Pradesh (up to 40 μg m^{-3}). Over Bangladesh and the Pakistani state of Sindth POA and SOA have comparable values ($<$35 μg m^{-3}).

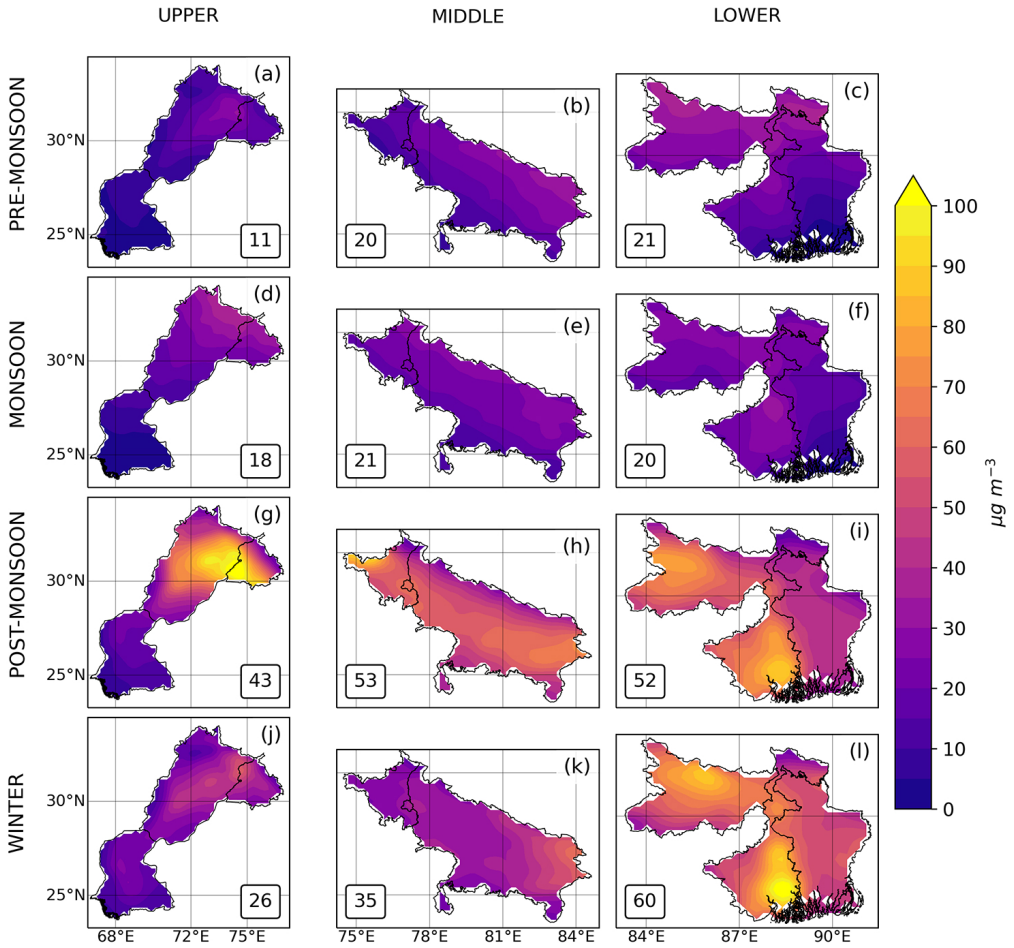

Figure 2.7: Seasonal mean distributions of total OA over the upper, middle and lower IGP. The numbers inset of pre-monsoon (a–c), monsoon (d–f), post-monsoon (g–i), and winter (l–n) seasons denote the regional mean total OA value. Modeled time periods: pre-monsoon season: 18th April to 16th May 2017; monsoon season: 3rd to 31st July 2017; post monsoon season: 18th October to 16th November 2017; winter season: 8th January to 5th February 2018.

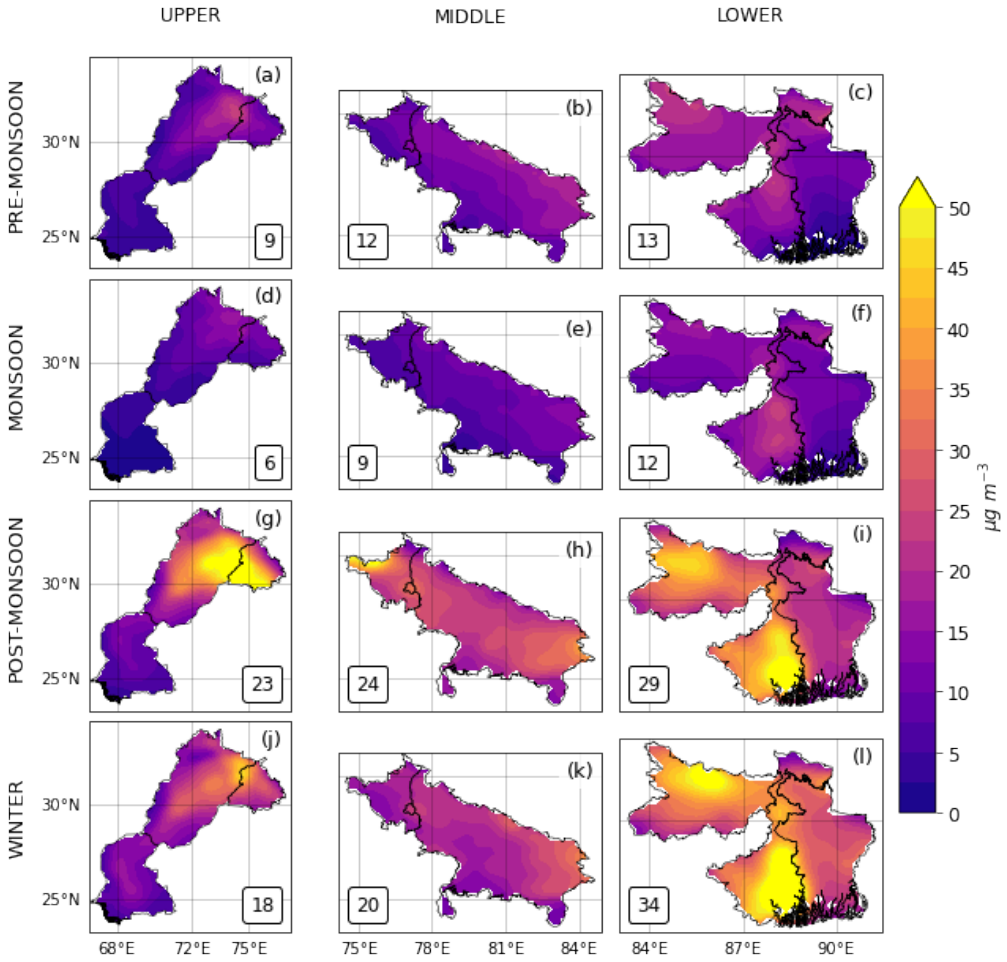

Figure 2.8: Seasonal mean distributions of POA over the upper, middle and lower IGP. The numbers inset of pre-monsoon (a–c), monsoon (d–f), post-monsoon g–i), and winter (j–l) seasons denote the regional mean POA value. Modeled time periods: pre-monsoon season: 18th April to 16th May 2017; monsoon season: 3rd to 31st July 2017; post monsoon season: 18th October to 16th November 2017; winter season: 8th January to 5th February 2018.

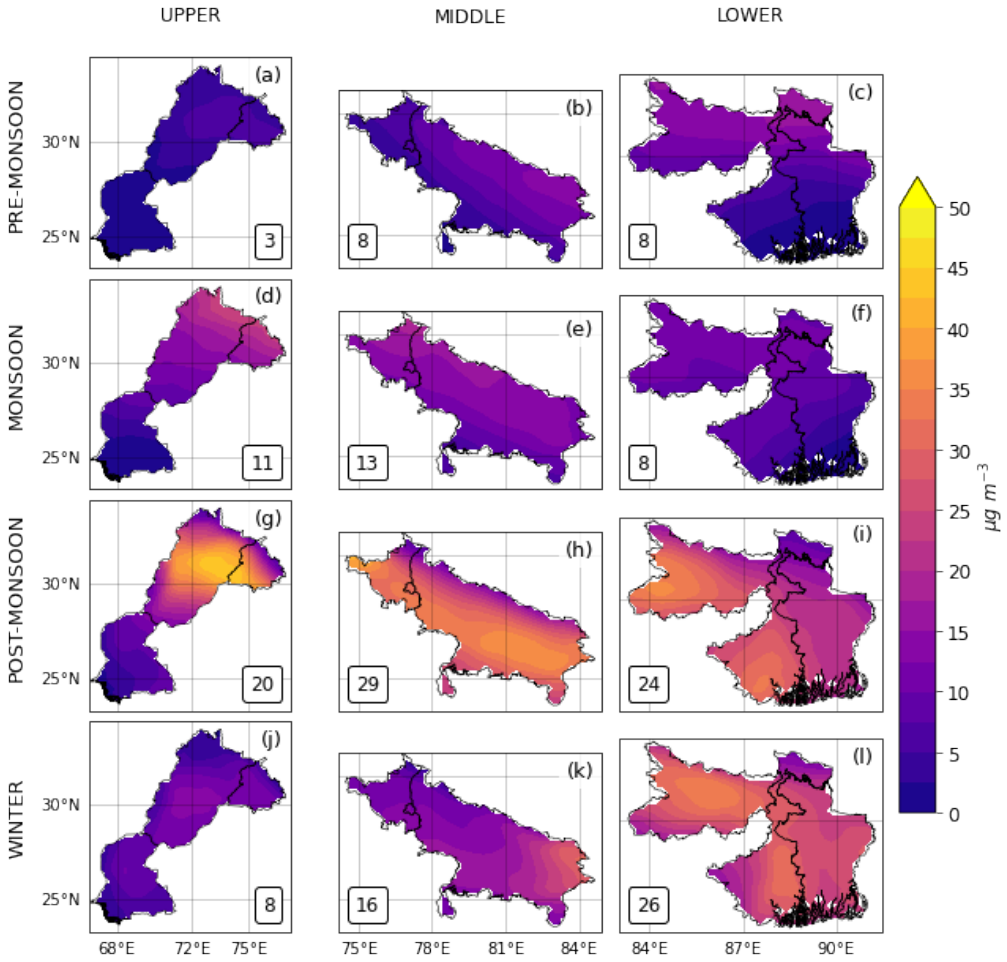

Figure 2.9: Seasonal mean distributions of SOA over the upper, middle and lower IGP. The numbers inset of pre-monsoon (a–c), monsoon (d–f), post-monsoon g–i), and winter (j–l) seasons denote the regional mean SOA value. Modeled time periods: pre-monsoon season: 18th April to 16th May 2017; monsoon season: 3rd to 31st July 2017; post monsoon season: 18th October to 16th November 2017; winter season: 8th January to 5th February 2018.

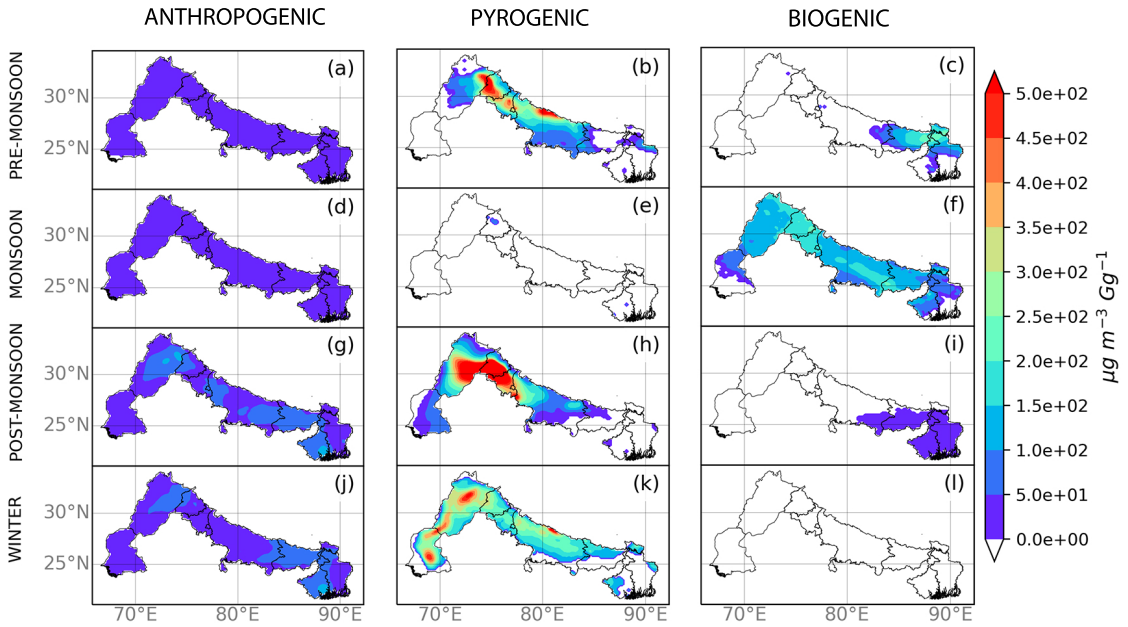

Figure 2.10: Seasonal sensitivity of total OA to changes in (left column) anthropogenic, (middle column) pyrogenic, and (right column) biogenic emissions (μ g m^{-3}Gg^{-1}). The sensitivity calculation is described in Section 2.2.2. Regions marked as white shows where sensitivity corresponds to OA concentrations below the set threshold of 1 μg m^{-3}. Modeled time periods: pre-monsoon season: 18th April to 16th May 2017; monsoon season: 3rd to 31st July 2017; post monsoon season: 18th October to 16th November 2017; winter season: 8th January to 5th February 2018.

Similarly to $PM_{2.5}$, we find that during the post-monsoon season, the OA distribution across the IGP is most sensitive to changes in biomass burning emissions (Figure 2.10g-i), with higher values over the Punjab to Delhi NCT, and part of Uttar Pradesh (up to 10^3 μg m^{-3} where fires are located over Indian Punjab). The sensitivity of OA to changes in biomass burning are localised, with POA most influenced by fires over Punjab and Haryana (Figure 2.11h) and corresponding impact on SOA extending over Pakistani Punjab and towards the middle IGP (Figure 2.12h). Similarly, biogenic emissions play only a localised role in OA and SOA concentrations where biogenic emissions are still significant during this season (Figures 2.10i) and 2.12i).

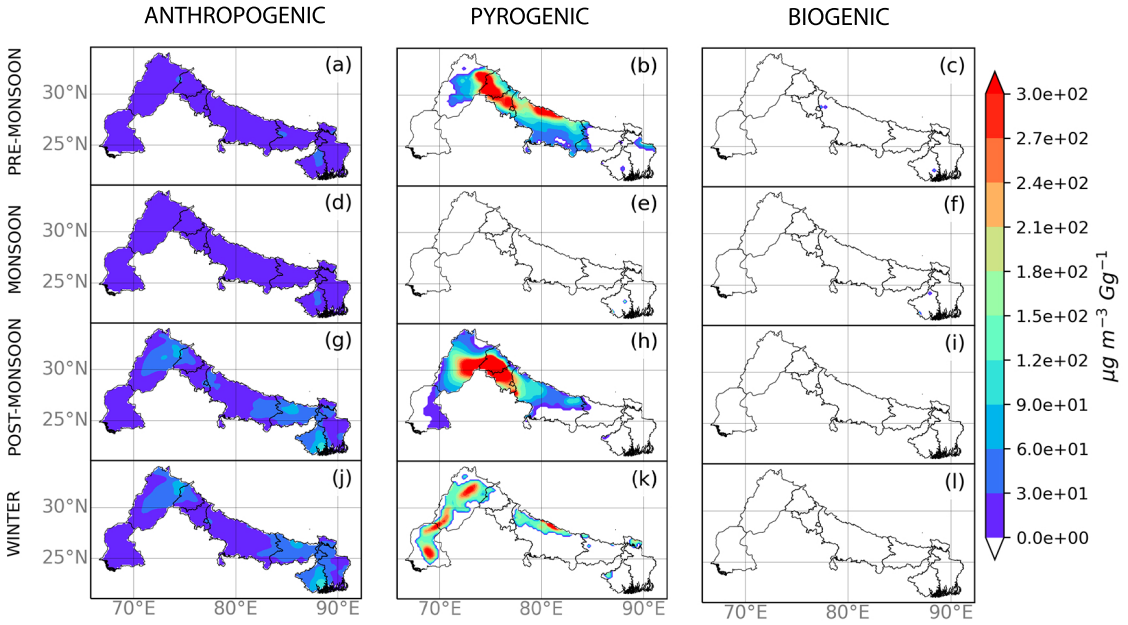

Figure 2.11: Seasonal sensitivity of POA to changes in (left column) anthropogenic, (middle column) pyrogenic, and (right column) biogenic emissions (μ g m^{-3}Gg^{-1}). The sensitivity calculation is described in Section 2.2.2. Regions marked as white shows where sensitivity corresponds to OA concentrations below the set threshold of 1 μg m^{-3}. Model outputs are for the following Modeled time periods: pre-monsoon season: 18th April to 16th May 2017; monsoon season: 3rd to 31st July 2017; post monsoon season: 18th October to 16th November 2017; winter season: 8th January to 5th February 2018.

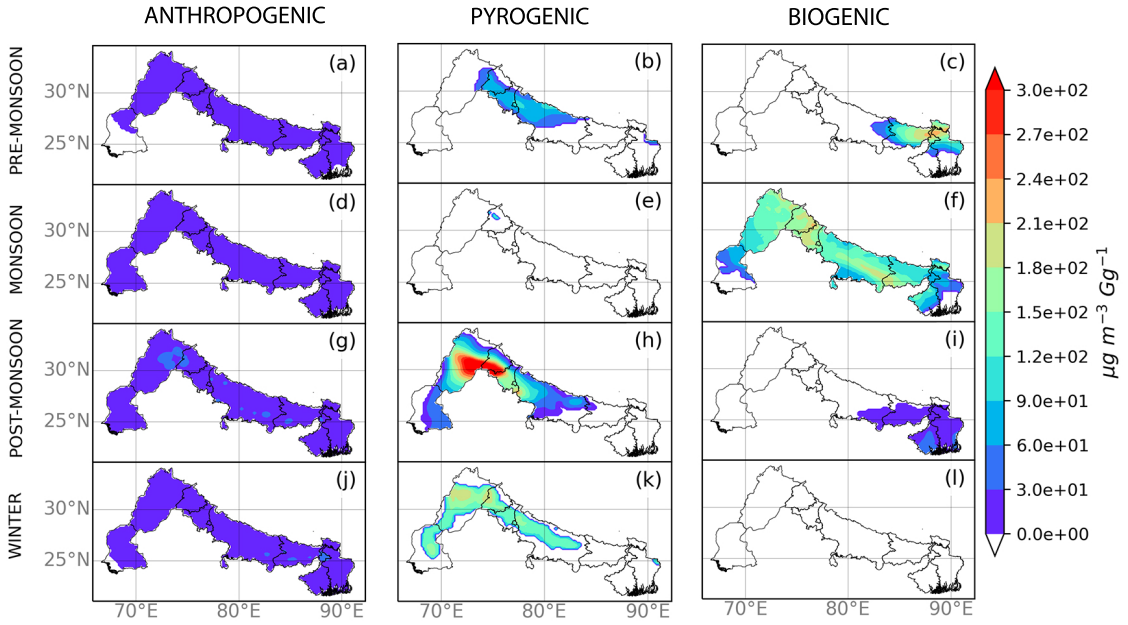

Figure 2.12: Seasonal sensitivity of SOA to changes in (left column) anthropogenic, (middle column) pyrogenic, and (right column) biogenic emissions (μ g m^{-3}Gg^{-1}). The sensitivity calculation is described in Section 2.2.2. Regions marked as white shows where sensitivity corresponds to OA concentrations below the set threshold of 1 μg m^{-3}. Modeled time periods: pre-monsoon season: 18th April to 16th May 2017; monsoon season: 3rd to 31st July 2017; post monsoon season: 18th October to 16th November 2017; winter season: 8th January to 5th February 2018.

OA are most sensitive to anthropogenic emissions over the Indian part of the lower IGP and in the Pakistani Punjab values (between 50-150 μg m^{-3}). We find that OA over the Delhi NCT megacity is as sensitive to these changes unlike other cities mentioned previously, so that Delhi is not one of the main hotspots of OA across IGP during this season (Figure 2.7h) unlike it is for $PM_{2.5}$ (Figure 2.4h). We find that the sensitivity of POA and SOA to changes in anthropogenic emissions are comparable across major cities of the Punjab states (Figures 2.11g, 2.12g).

We find that the largest seasonal mean values of OA are during winter over the lower IGP (60 μg m^{-3}, Figure 2.7j-l) with contributing localised peaks over Kolkata and Patna ($>$80 μg m^{-3}) and at the border between Pakistan and India (ranging 40–70 μg m^{-3}). Seasonal mean values of POA and SOA also peak during winter over the lower IGP (34 μg m^{-3} and 26 μg m^{-3}, respectively.) During winter, the OA distribution is shaped by anthopogenic and pyrogenic emissions (Figure 2.10j-l). POA concentrations show to be sensitive to anthropogenic emissions in a similar way as it is for post-monsoon season (Figure 2.11g,j). SOA is also mostly determined by anthropogenic emissions over the lower IGP (Figure 2.12j). POA and SOA are also sensitive to pyrogenic emissions, but during this season it is limited to fires over the Indus basin in Pakistan and central IGP (Figures 2.11k, 2.12k). We find that biogenic emissions do not significantly influence OA during winter.

During pre-monsoon and monsoon seasons, the OA distributions (Figure 2.7a-f) have similar mean values over the middle and lower IGP (20–21 μg m^{-3}) and lower mean values over the upper IGP (11 and 18 μg m^{-3}, respectively). The highest POA concentrations are found at the border on India and Pakistan and over the lower IGP ($\simeq$30 and 40 μg m^{-3}, respectively). In both seasons, mean SOA concentrations are below 15 μg m^{-3}) across all the IGP. During pre-monsoon and monsoon seasons, OA concentrations are sensitive to anthropogenic emissions across the IGP with similar spatial distributions (Figure 2.10a,d). Pyrogenic emissions influence the OA distribution during

the pre-monsoon season over the central IGP (Figure 2.10b), but OA less sensitive to these emissions compared with the post-monsoon season (Figure 2.10h). During the monsoon season, the influence of fires on OA is negligible across the IGP. The influence of biogenic emissions on OA, determined exclusively in our model via SOA, is limited to the lower IGP during the pre-monsoon season. During the monsoon season, these emissions have a widespread impact on OA (Figure 2.10f) with seasonal mean peak sensitivity of up to 2.3×10^2 μg m^{-3} Gg^{-1}.

We found that $PM_{2.5}$ and OA are more sensitive to changes in biogenic emissions than changes in anthropogenic emissions during the monsoon period. This might be linked to the role that anthropogenic emissions can play in the production of biogenic SOA. Previous studies have shown that anthropogenic emissions can enhance biogenic SOA production, with NO_x concentrations playing a strong role in enhancing SOA formation from gas-phase organic carbon emitted by vegetation (isoprene, and terpenes) due to substantial increase in oxidants (OH and ozone) promoted by NOx emissions within the urban environment (Spracklen et al., 2011; Shilling et al., 2013; Shrivastava et al., 2019; Xu et al., 2020). We might observe this phenomenon only during monsoon because is the only season where biogenic emissions occur across all the IGP (Figure 2.1). A disadvantage of our using a single-variable perturbative method is that we can only consider the impacts of one controlling factor in the production of OA. A study that considers the interactions between controlling factors is outside the scope of this study.

2.3.5 Seasonal Distribution of SOA Volatility

We use aerosol volatility to describe how SOA is partitioned between the gas and particle phase to understand when it contributes to $PM_{2.5}$ mass loading. The importance of volatility for SOA formation has been described in Section 1.3.2. Figure 2.13 shows the seasonal mean volatility distributions for SOA across the IGP simulated using the 1-D VBS model in WRF-Chem (Section 1.5.3). Seasonal and regional variations reflect

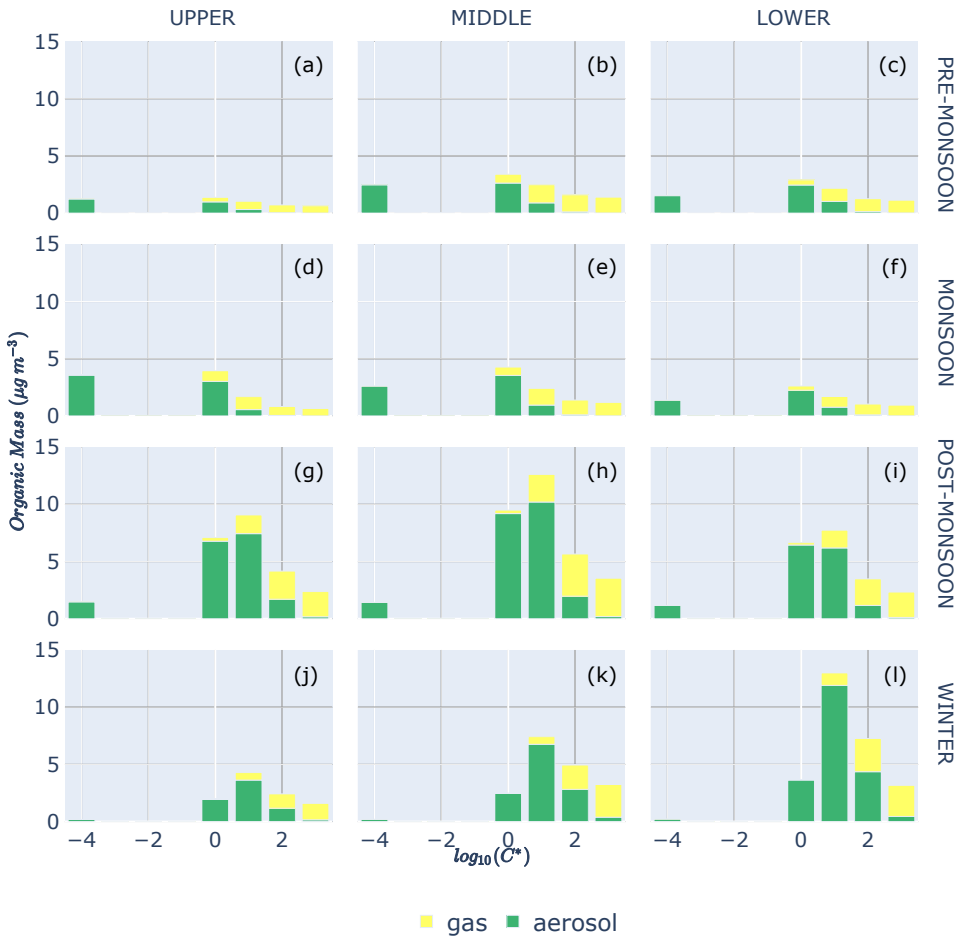

Figure 2.13: Seasonal mean volatility distribution of SOA over the upper, middle, and lower IGP as calculated within the WRF-Chem 1-D VBS scheme for (a–c) pre-monsoon, (d–f) monsoon, (g–i) post-monsoon, and (j–l) winter seasons. Modeled time periods: pre-monsoon season: 18th April to 16th May 2017; monsoon season: 3rd to 31st July 2017; post monsoon season: 18th October to 16th November 2017; winter season: 8th January to 5th February 2018.

changes in the physical and chemical environment in which the SOA is formed. Broadly, we find a gradual increase in the volatility of SOA from the pre-monsoon season to the winter season, mainly reflecting the increase in the mean OA loading (Figure 2.7). Higher OA loading leads to a shift in the gas-particle partitioning towards more volatile

bins, reflected in the seasonal variation in the population of the inert bin (denoted here as $log_{10}C^* = -4$, as described above). The contribution of this inert bin is negligible during winter and peaks during the monsoon season, with intermediate values during the pre-monsoon and post-monsoon transition seasons.

During the post-monsoon season, the particle phase organic mass is present at high volatility bins up to $log_{10}C^* = 2$. The largest particle phase mass loading (10 μg m^{-3}) is found over the middle IGP. The upper and lower IGP show a similar volatility distribution as the middle IGP but with lower mass loadings, with the lower IGP having the lowest mass loadings. The smallest values over the lower IGP reflect the persistence of rainfall over this region (Figure 2.3) that may leads to continued removal of water soluble gas-phase and aerosol-phase organics.

Surface-level atmospheric organic mass becomes even more volatile during the winter season, with particle phase organic matter present in all volatility bins. This can be related to the higher aerosol loading during winter, which induce oxidation products to partition in the particle phase as soon as they are formed, removing them from the possibility to subsequently undergo further gas-phase oxidation, as discussed in Section 1.5.3.

The largest mass loading for SOA are found over the lower IGP (> 10 μg m^{-3}) and decreases westwards towards the upper IGP, reflecting the E-W gradient of the total OA loading (Figure 2.7j–l).

SOA during the pre-monsoon (Figure 2.13 a–c) and monsoon (Figure 2.13 d–f) seasons are characterised by a volatility $\leq log_{10}C^* = 1$, and with aerosol masses lower than 5 μg m^{-3} for each volatility bin in both seasons. The higher volatility bins ($log_{10}C^* = 2$ and $log_{10}C^* = 3$) are occupied exclusively by gas-phase organic compounds. This might be related to water-soluble SVOCs being washed out by monsoonal rainfall. The washout of SVOCs results in gas-aerosol re-partitioning to establish thermodynamic equilibrium,

associated with particle phase organics partitioning to the gas-phase (Section 1.5.3). Aerosols can be removed via wet and dry deposition but previous studies find that most of the loss of SVOCs and SOA mass is lost via the gas phase (Knote et al., 2015). This also helps to explain the low levels of OA during the pre-monsoon and monsoon seasons (Figure 2.7). The OA volatility distribution is similar across the IGP for the pre-monsoon (2.13 a-c) and monsoon season (2.13 d-f), reflecting similar meteorological (Figure 2.3) and emissions drivers (Figure 2.1) in these two seasons.

2.4 Discussion and Conclusions

We used the WRF-Chem regional atmospheric chemistry model to understand the influence of anthropogenic, pyrogenic and biogenic emissions and meteorology on seasonal variations of the magnitude, distribution, and composition of $PM_{2.5}$ and organic aerosol across the Indo-Gangetic Plain (IGP) during 2017/2018.

We find that the model reasonably reproduces concentrations of $PM_{2.5}$ in all seasons (NMB$<$0.2, r$>$0.6) except for the monsoon season (NMB=0.4, r=0.09), a reflection that modelling monsoonal meteorology remains challenging. However, uncertainty in our estimates remains on the individual $PM_{2.5}$ secondary components, given the limitation we found in the modeling to reproduce precursors gases surface concentrations when compared with observations. Availability of additional monitoring stations outside urban areas that are more representative of the spatial scales associated with model grid cells would help to evaluate model error, as well as use of finer-resolution and up to date inventories for precursors gases over the rapidly changing region of IGP.

We find that the IGP experiences the highest seasonal mean levels of $PM_{2.5}$ during the post-monsoon (October—December, 166 $\mu g\ m^{-3}$) and winter (January—February, 145 $\mu g\ m^{-3}$) seasons with an heterogeneous distribution, in agreement with previous studies. The magnitude and distribution of anthropogenic emissions across the IGP

are approximately constant throughout the year. During the post-monsoon season, agricultural burning emissions of post-harvest residues influence $PM_{2.5}$ mostly over the upper and middle IGP, particularly affecting the Indian and Pakistani Punjab region. These additional emissions are exacerbated by stagnating meteorological conditions that reduce dispersion of surface air pollution. During the winter season, ongoing anthropogenic emissions, wind patterns, and a seasonally shallow boundary layer result in a gradient in air quality from the upper to lower IGP, with the highest $PM_{2.5}$ values (in excess of 250 $\mu g\ m^{-3}$) over Kolkata and the state of Bihar. During the pre-monsoon (March–May) and monsoon (June–September) seasons wet scavenging of hydrophilic gas-phase aerosol precursors and aerosols, and more rigorous vertical mixing, reduces levels of $PM_{2.5}$ (95-79 $\mu g\ m^{-3}$ respectively).Generally, we find that $PM_{2.5}$ composition has a stronger seasonal variation than a geographical variation within each season. Total inorganic species dominate $PM_{2.5}$ composition (30-80%), with water uptake contributing substantially to the $PM_{2.5}$ mass especially over the lower IGP (up to 40%).

We find that OA represents a significant contribution to $PM_{2.5}$ throughout the year. On an annual mean basis, OA represents 17–30% of $PM_{2.5}$, with higher contributions during post-monsoon and winter seasons. Typically, POA contributes more to the OA loading than SOA in all seasons across the IGP. Anthropogenic and pyrogenic sources impact POA and SOA with similar patterns of $PM_{2.5}$ across the IGP during all seasons. Biogenic sources have a significant impact on SOA distribution across the IGP during the monsoon season but are limited to the lower IGP during the pre- and post- monsoon seasons. We find that the volatility distribution of SOA is driven mainly by the mean total OA loading and the washout of aerosols and gas-phase aerosol precursors that result in SOA being less volatile during the pre-monsoon and monsoon season than during the post-monsoon and winter seasons.

Mitigating levels of $PM_{2.5}$ over the IGP will require a range of regional and state-level policies that address the influences of intra- and inter- state anthropogenic, pyrogenic, and biogenic emissions. The relative influence of these emissions on $PM_{2.5}$ and the broader photochemical environment will likely change in the context of a warmer climate, e.g. biogenic emissions will increase as they are temperature dependent. It is therefore imperative that future studies should also consider sub-regional and city spatial scales, where individual sectors will be more important, and where there is the highest population density that will suffer from poor air quality.

Chapter 3

Road transport impact on $PM_{2.5}$ pollution in Delhi during the post-monsoon season

Author contributions declaration

This chapter and the relative appendix have been adapted from a paper published in *Atmospheric Environment: X* (DOI: `https://doi.org/10.1016/j.aeaoa.2022.100200`). I conceived the study and the methodology together with my supervisor Paul Palmer and contribution from Ying Chen and Oliver Wild. I performed all the simulations and the analysis. Margaret Marvin contributed to adapt the EDGAR v5 inventory for use in WRF-Chem. Sumit Sharma provided the TERI/ARAI emissions inventory and support on its use. I wrote the article with contributions and editing from Paul Palmer. All the co-authors provided comments on subsequent manuscript revisions.

3.1 Introduction

As introduced in Section 1.6 and seen in Chapter 2, Delhi is one of the most density populated megacities in the world and suffers from some of the most unhealthy air on Earth with particulate matter ($PM_{2.5}$, particles with aerodynamic diameters $\leq$ 2.5μm) pollution often exceeding average 24h mean World Health Organisation (WHO) Global Air Quality Guidelines of 15 $\mu g\, m^{-3}$ and the Indian National Ambient Air Quality Standard (NAAQS) of 60 $\mu g\ m^{-3}$ (CPCB, 2020; WHO, 2021). In 2019, elevated ambient PM pollution was responsible for an estimated 16,600 deaths in Delhi (Pandey et al., 2021). Mitigating this human health crisis in Delhi is challenging, with PM pollution levels driven by seasonal local and regional emissions and seasonal meteorology, exacerbated by the geography of the Indo-Gangetic Plain as introduced in 1.6.1 and analysed more in depth in Chapter 2. In this Chapter, we use the WRF-Chem model to explore in detail the anthropogenic factors determining air pollution during the post-monsoon season in Delhi when $PM_{2.5}$ is particularly high (Section 2.3.3). As seen in Chapter 2, during the post-monsoon season, Delhi air quality is worsened by seasonal biomass burning from post-harvest crop in the neighbouring states of Haryana and Punjab. Deteriorating air quality due to crop residue burning has been a major focus for mitigation strategies but these emissions occur when there are already hazardous background levels of $PM_{2.5}$ (Bikkina et al., 2019; Kulkarni et al., 2020; Liu et al., 2018; Ojha et al., 2020). Thus there is the need to investigate more *in situ* control of anthropogenic emissions. In this chapter we focus in particular on on-road transport emissions, which is one of the main targets of emission control strategies for Delhi (Section 1.4.2). As discussed in Section 1.6.2, the main sources of air pollution in Delhi are local anthropogenic sources from within the megacity Delhi and from nearby states within the National Capital Region (NCR). This highlights the need for a coordinated emissions reduction strategy to mitigate Delhi $PM_{2.5}$ pollution. The local on-road transport sector is a substantial source of $PM_{2.5}$ pollution in

Delhi (Section 1.6.2). Source apportionment studies based on $PM_{2.5}$ measurements at sites in Delhi found that vehicular emissions contribute seasonally between 17-30% for $PM_{2.5}$ pollution, with the highest share during the post-monsoon and winter seasons (Jain et al., 2020; TERI & ARAI, 2018).

We have seen in Section 1.4.2 that on-road transportation fleet in India and Delhi has been is dominated by two- and three-wheelers, which are used for personal and commercial transportation, followed by passenger cars, and that freight vehicles (light-duty and heavy-duty vehicles) are a small fraction of vehicles in the fleet, but account for a high share of emissions, since they travel further and longer within the city. The continuous growth of the on-road transport fleet and activity in India and Delhi has forced the Indian government to promote measures to curb emissions from the transport sector in the past few decades (Section 1.4.3), but air quality levels in Delhi continue to remain unsafe for human health.

In addition, recent studies have shown that if mitigation strategies focus exclusively on minimising $PM_{2.5}$ concentrations, elevated levels of surface ozone could become more of a significant health concern (Ojha et al., 2022; Chen et al., 2021; Nelson et al., 2021; Tiwari et al., 2015). Because ozone forms through non-linear pathways from its precursors in the troposphere (Section 1.2.2), reductions in some ozone precursors emissions which are also precursors for $PM_{2.5}$, may reduce $PM_{2.5}$ concentrations but enhance O_3 pollution. In particular, reductions in NOx emissions, emitted mainly from the transport sector, may lead to large increases in ozone concentrations in a VOC-limited regime such as in Delhi if VOC emissions are not sufficiently reduced (1.2.2).

Thus there is an urgent need to better understand the traffic contribution to Delhi's pollution, and assessing current and possible future intervention strategies for $PM_{2.5}$ with a systemic approach.

In this Chapter we use the WRF-Chem regional atmospheric chemistry transport model to investigate the contributions from on-road transport sectors and fleet segments (two- and three-wheelers, cars and light duty vehicles, heavy duty vehicles and resuspended road dust) to surface $PM_{2.5}$ levels over Delhi during the post-monsoon season. We drive WRF-Chem with local-scale emissions inventories at a spatial resolution of 4 km, and through a series of sensitivity studies we investigate the contribution to $PM_{2.5}$ of on-road transport and its subsectors compared to other anthropogenic sectors. We consider contributions from local (within Delhi) and regional (within the NCR) anthropogenic sectors and how they impact the 24-h mean and diurnal cycle of $PM_{2.5}$. We also assess with a simple model the health impacts of possible interventions aiming to reduce $PM_{2.5}$ exposure by taking into account also changes in O_3 exposure.

In the next section we describe the data and methods, including a summary of the WRF-Chem model set-up, emission inventories, methods we use to explore individual section contributions to surface $PM_{2.5}$. The results are presented in section 3, and conclusions are discussed in section 4.

3.2 Data and Methods

3.2.1 Model setup and emissions

The WRF-Chem set-up used in this Chapter has been introduced and described in Section 1.5.3. We summarise here the key elements in the set-up that characterise this research chapter focused on the impact of the transport sector during the post-monsoon season. WRF-Chem set-up for the work in this chapter has two one-way nested domains. The parent domain encompasses north India at 12 km horizontal resolution, while the nested domain covers the entire NCR at 4 km horizontal resolution (Figure 1.9). We run simulations for the post-monsoon season from 6th October to 16th October

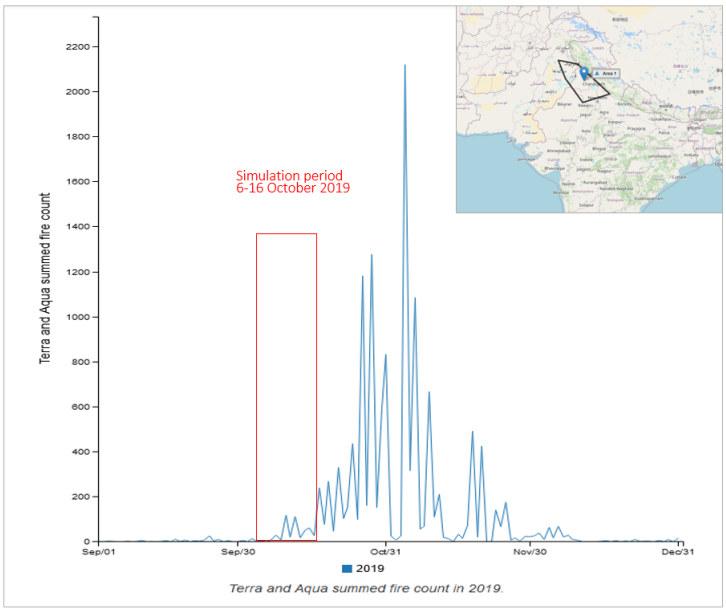

Figure 3.1: Fire counts from MODIS Terra and Aqua satellite instruments during post-monsoon 2019 over north-west India. The data have been visualised using the Global Fire Emissions Database (GFED) online analysis tool at `http://www.globalfiredata.org/analysis.html` The red rectangle encloses the time-window chosen for the post-monsoon simulations (1-16 October 2019).

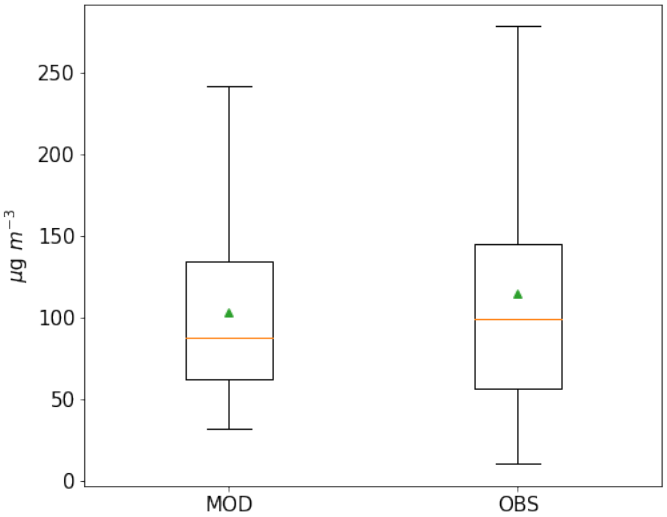

Figure 3.2: Comparison of the hourly frequency distributions of observed (OBS, 1-31 October 2019) and simulated (MOD, 6-16 October 2019) $PM_{2.5}$ over Delhi. In the boxplots, the median is the orange line, the mean the green triangle. Observations: mean 114 $\mu g\ m^{-3}$, median 99 $\mu g\ m^{-3}$. Model: mean 103 $\mu g\ m^{-3}$, median 88 $\mu g\ m^{-3}$. In the observed data, the day of Diwali Festival (27 October 2019) was removed, as episodic event driving short-term severe $PM_{2.5}$ levels ($>$500 $\mu g\ m^{-3}$).

2019 (Table 1.1). Each simulation has a spin-up period of 5 days (1-5 October 2019) to minimize the influence from the established initial conditions at the start of the model run. This period in October is chosen to minimize the the imapct resulting from biomass burning emissions, which peak later in October and November 2019 (Figure 3.1), and this allows us to focus on anthropogenic emissions while maintaining the post-monsoon meteorological and chemical characteristics and a manageable computational burden for the simulations. We further check that the 10 days considered are representative of a longer post-monsoon period by comparing the hourly frequency distribution of modelled $PM_{2.5}$ between 6-16 October over Delhi with hourly distribution of observations at the sites shown in Figure B.1 listed in Table B.1 for the whole month of October (Figure 3.2). The frequency distributions of modelled $PM_{2.5}$ are similar to the observations. Even if high concentration spikes are not fully captured by the model, the difference in the mean $PM_{2.5}$ concentrations is 10% (observations 114 $\mu g\ m^{-3}$, model 103 $\mu g\ m^{-3}$) and in the median concentrations is 11% (observations 99 $\mu g\ m^{-3}$, model 88 $\mu g\ m^{-3}$), making the selected period acceptable as representative for a longer post-monsoon period (Figure 3.2).

In addition, we modified the code to increase the minimum value of the vertical turbulent diffusion coefficient within the planetary boundary layer (PBL), following (Du et al., 2020) who previously identified that this modification was key in successfully reducing model bias for diurnal variations of urban $PM_{2.5}$, particularly during nighttime. Through sensitivity runs, we found that a lower limit for the PBL vertical turbulent diffusion coefficient of 5 $m^2\ s^{-1}$ led to the best comparison with ground-based observations over Delhi (Figure 3.3). This is the same value found by Du et al. (2020) for cities in eastern China. Additional information on our model set up can be found in Mogno et al. (2021). This modification has not been implemented for the set-up of the WRF-Chem model used

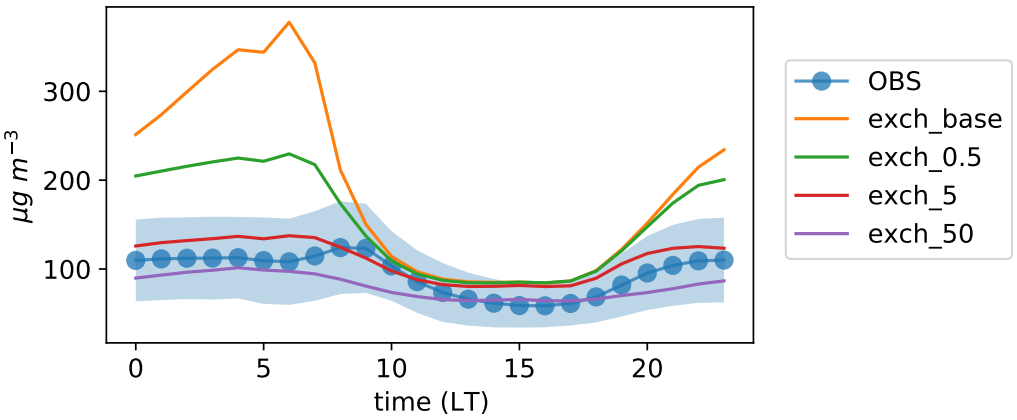

Figure 3.3: Sensitivity of modeled average surface $PM_{2.5}$ over Delhi to different values of the PBL lower vertical turbulent diffusion coefficient (exch_min, $[m^2 s^{-1}]$), after implementing code modification as in (Du et al., 2020). The values tested are exch_min= 0.1 (exch_min_base, the default in WRF-Chem), 0.5, 5, 50. The blue line represents the average $PM_{2.5}$ over Delhi observed during the simulation period (see section 3.3.1). As in (Du et al., 2020) we found that the value of exch_min=5 is a good fit that maintains lower bias without deteriorating the correlation with observations (as for exch_min= 50). Modeled time period: from 6th October to 16th October 2019.

in Chapter 2, because in Chapter 2 the analysis was focusing on a temporal scale of seasonal values, and not on the scale of the diurnal cycle of pollutants. Thus this kind of modification wasn't needed, and even if implemented, the improvements brought would likely not to be as relevant after doing a seasonal mean.

We use here different anthropogenic emissions compared to Chapter 2, as outlined in the Introduction (Section 1.5.3). For the parent domain (d01), we use the recently released EDGARv5.0 anthropogenic emission inventory for 2015 at $0.1^\circ \times 0.1^\circ$ resolution ($\sim$11 km) (Crippa et al., 2019a,1,1). As for EDGAR-HTAPv.2.2 used in Chapter 2, we use only monthly variations in the emissions based on monthly profiles, specified for each country and for each sector in EDGARv5.0. For the nested domain (d02) we use the anthropogenic emission inventory from Energy and Resource Institute and The Automotive Research Association of India (TERI/ARAI) that covers the NCR region (TERI & ARAI, 2018); more details are provided below. Emissions for the fraction of the nested

grid that lies outside the NCR are described by the EDGARv5.0 inventory. For both inventories, we map the original speciated non-methane volatile organic compounds (NMVOC) emissions to the MOZART chemical mechanism used by WRF-Chem. Details of this mapping for the EDGARv5.0 inventory are summarised in Mogno and Marvin (2022) and details of the mapping for the TERI/ARAI inventory are described in Table B.2.

3.2.2 TERI/ARAI anthropogenic emission inventory for the NCR

The TERI/ARAI anthropogenic emission inventory (TERI & ARAI, 2018) describes emissions of nitrogen oxides (NOx = NO + NO_2), sulfur dioxide (SO_2), carbon monoxide (CO), particulate matter (PM_{10}), and NMVOCs for all the main anthropogenic sectors and subsectors for the NCR at a spatial resolution of 4×4 km for 2016. The sectors include transport, domestic (use of biomass fuel, kerosene and LPG for cooking and heating), power, industry, and other (including refuse burning, crematoria, landfill fires, incinerators, refinery, airport, restaurant, construction). The inventory also includes factors that describe seasonal (monthly) and diurnal (hourly) emission variations, developed with activity data surveys for different sectors. Figure 3.4 shows sector and on-road transport subsector contributions to key pollutant emissions in the NCR and Delhi. Figure 3.4c shows the corresponding annual mean distribution for on-road transport, domestic, and industry, power and other sectors.

The on-road transport sector of the TERI/ARAI inventory includes emissions for eight vehicles types: 1) two wheelers, 2) three wheelers, 3) passenger cars, 4) multi utility vehicles, 5) buses, 6) light duty vehicles, 7) heavy duty vehicles, and 8) tractors. The inventory also includes PM emission estimates from road dust resuspension due to vehicles. Figure 3.4b shows the contribution from individual on-road transport subsectors to total emissions by pollutant species within the NCR and Delhi. Emissions from different vehicle types are assumed to have the same spatial distribution at 4 km and to follow the

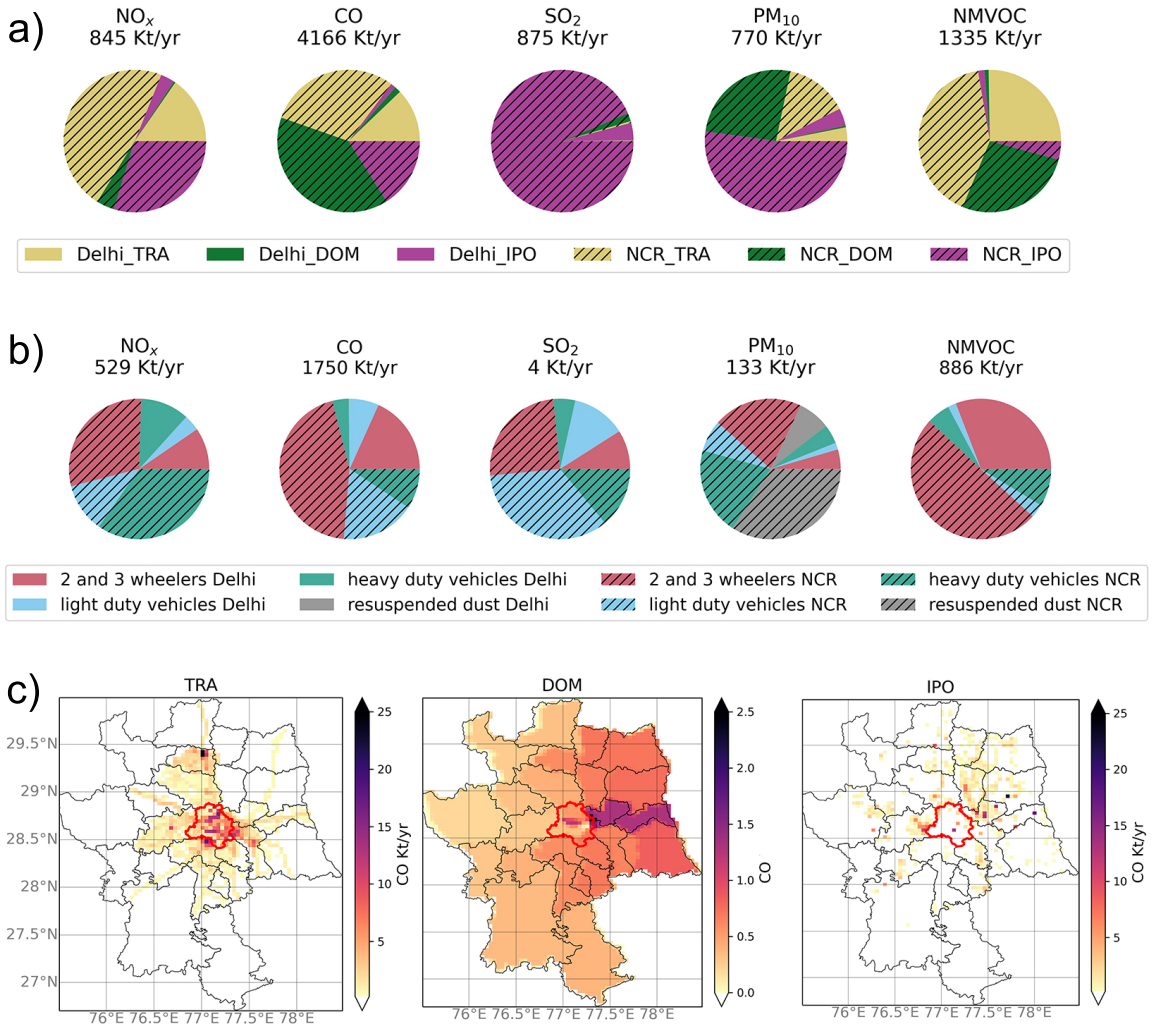

Figure 3.4: Annual sector contributions and distributions of the TERI/ARAI anthropogenic emissions inventory for the regional NCR (areas outlined in black) and Delhi (central area outlined in red). Panel a) shows sector contributions to total annual emissions of nitrogen oxides (NOx), sulfur dioxide (SO_2), carbon monoxide (CO), particulate matter (PM), and non methane volatile organic compounds (NMVOCs). Sectors include on-road transport (TRA), domestic (DOM), industry power and others (IPO). Emissions within Delhi only and within the broader NCR but excluding Delhi are denoted by Delhi and NCR respectively, determined by using relevant administrative boundaries. Panel b) is the same as Panel a) but for on-road transport subsectors. Panel c) shows the spatial distribution of CO emissions from the TRA, DOM and IPO sectors (TERI & ARAI, 2018).

same diurnal cycle. The seasonal change in road dust re-suspension was customized for local conditions using the information from sampling silt loading on the roads, and the weight of vehicular fleet (taken from traffic counts). On-road transport sector emissions in Delhi and the NCR have been estimated using a bottom-up approach, through activity data estimated from primary traffic count surveys in Delhi and surroundings. The inventory takes into account high-emitting vehicles, which are not taken into account in the development of standard emissions factors for representative vehicles in the fleet (TERI & ARAI, 2018).

3.2.3 Observations for model evaluation

The model ability to reproduce observed surface $PM_{2.5}$ over Delhi is evaluated using ground based observations. As for Chapter 2, we use the Central Pollution Control Board (CPCB) hourly observations of $PM_{2.5}$, here downloaded for the period 6–16 October 2019 over Delhi. Data that have negative values, outliers, and stations with poor temporal coverage have been discarded following the same cleaning procedure used in Section 2.2.3. The resulting 34 selected stations in Delhi are shown in Figure B.1, and listed in Table B.1.

3.2.4 Emission reduction impact (ERI) method

We use the emission reduction impact (ERI) method to quantify the role of the on-road transport sector and its subsectors compared to other main sectors on surface $PM_{2.5}$ over Delhi. The ERI method determines the role of a given source to air pollution levels by taking the difference of two air quality model simulations performed with the full emission source (control) and a reduced emission source (perturbed). This method is also referred to as the brute-force method, or a one at time sensitivity analysis (Clappier et al., 2017; Thunis et al., 2019). The ERI method has been widely used for air quality management

studies (Conibear et al., 2018; Huang et al., 2018; Huszar et al., 2016; TERI & ARAI, 2018), and it is usually preferred to other methods for its suitability to support air quality interventions planning (Thunis et al., 2019). Care is taken to ensure the perturbation is sufficiently small that the resulting change in the non-linear chemistry is approximately linear. Formally, the impact of an emission source s on a receptor pollutant P is given by:

$$I^{P}_{s,\alpha} = \frac{P_{s,\alpha} - P}{\alpha} = \frac{\Delta P_{s,\alpha}}{\alpha}, \tag{3.1}$$

where the P is the pollutant from the control model and $P_{s,\alpha}$ is the modeled pollutant from the perturbed model for which the source s reduced by percentage α. Where α=100% the source is completely switched off (zero-out approach). In relative values $I^{P}_{[s,\alpha]\%}$ (percentage of the baseline P concentration), the impacts are expressed by dividing $I^{P}_{s,\alpha}$ by the baseline concentration P.

To reduce the computational burden of the ERI method, we group together the main anthropogenic emissions sectors by source type: on-road transport, TRA (linear sources), domestic, DOM (area sources) and industry, power and others, IPO (point sources). For the TRA sector, we also group the emissions in four subcategories that reflect the Indian emissions regulation categories for vehicles (Bansal and Bandivadekar, 2013): light commercial vehicles (TRL), heavy duty vehicles (TRH), two- and three-wheelers (TRW). We also consider resuspended dust (DST). For each source we consider both emissions within Delhi only and emissions from NCR (excluding Delhi). Table 3.1 summarises the anthropogenic sources parameters used for the ERI application.

The key assumption associated with using the ERI method is that emission sources are changed by an amount that maintains linearity between emissions and concentration changes, as mentioned above. Here, we perform a series of simulations, each for the period 6-16 October 2019 (10 days), to establish the threshold value of α_t beyond which the perturbed chemical regime is inconsistent with the control calculation. In practice, this

TERI/ARAI sectors	ID
industry + power + others	IPO
domestic	DOM
on-road transport	TRA
bus + trucks+ heavy duty vehicles	TRH
light duty vehicles + multi utility vehicles +passenger cars	TRL
2wheelers+ 3wheelers	TRW
resuspended dust	DST

Table 3.1: Groupings of anthropogenic emissions used in the ERI study. For each parameter we consider both emissions within Delhi only (Delhi_) and within the National Capital Region only, excluding Delhi (NCR_).

means identifying the value of α for which 1) there remains a linear relationship between a change in emissions and $PM_{2.5}$ concentrations and 2) the interaction terms associated with perturbed multiple related parameters are negligible. The second criterion ensures that the individual impacts are additive, i.e., the sum of the impacts are equal to the impact of the sum where $\alpha \leq \alpha_t$.

This impact method approach has similarities with the perturbation method used in Chapter 2 (Section 2.2.2). Both these methods are of the class of brute-force method, or a one at time sensitivity analysis (Clappier et al., 2017; Thunis et al., 2019) and quantify changes in pollutant concentrations due to changes in emissions. However, there are differences in their formulation and aims. The perturbation method used in Chapter 2 and defined in Equation 2.1, produces a sensitivity index which express how much a pollutant concentrations varies due explicit changes in the quantity of direct emissions E, and has units of a pollutant concentration over emissions total mass. In addition, also the spatial dimension is considered (index i,j) and sensitivity spatial maps can be produced. The ERI method described here and defined by Equation 3.1 also consider changes in pollutant concentrations due to changes in emissions, but this is done implicitly through the scaling factor α, and thus has units of concentration. In addition, here we do not consider spatial

variability of the impact I. The impact method gives a more direct measure of the total contribution of an emissions source to a pollutant compared to the sensitivity index used in Chapter 2. Thus, it is more suitable when analysing the impact of potential mitigation strategies, as we do in this Chapter.

3.3 Results

3.3.1 Model Evaluation

For the scope of this Chapter, to evaluate our model performance in describing surface observations of $PM_{2.5}$ over Delhi we restrict ourselves to the evaluation of the diurnal cycle. We consider the city scale mean diurnal cycle value for $PM_{2.5}$ i.e. the mean of $PM_{2.5}$ obtained from averaging observations at the 34 sites described in Section 3.2.3. We match model gridcells to observation sites using nearest neighbour approach as we did in Chapter 2. Figure 3.5 shows the mean observed and modelled diurnal cycle of $PM_{2.5}$ obtained averaging the observations across the 34 stations and corresponding matching 34 gridcells. Table 3.2 summarises statistics separately for daytime (8:00-20:00 LT) and nighttime (21:00-07:00 LT). Modeled $PM_{2.5}$ has a positive mean bias lower at daytime (MB=0.13) than nighttime (MB=0.16), although there is a better overlap in the standard deviation across the observations at sites and the model during nighttime than during daytime. The model does not capture the observed morning peak at 0800–0900 local time, possibly due to an inaccurate simulation of the timing between morning emissions peak and the PBL increase. However the broader observed pattern during daytime is well reproduced by the model (r=0.87), while it has more difficulties to reproduce patterns at nighttime (r=0.55). On a city-scale resolution as opposed to street level resolution, we argue this is acceptable performance.

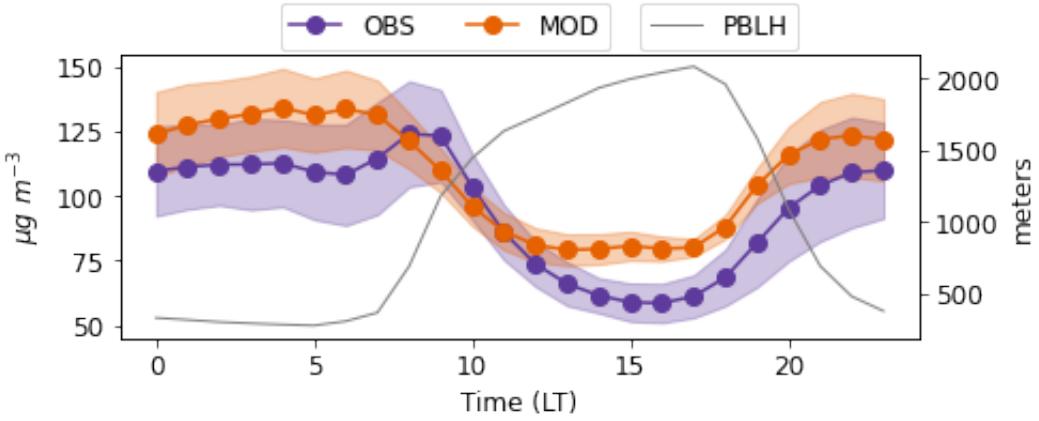

Figure 3.5: Model evaluation of $PM_{2.5}$ over Delhi using ground-based observations during 6-16 October 2019. The plot shows the city-scale mean comparison of model and observed average diurnal cycle of $PM_{2.5}$, obtained averaging $PM_{2.5}$ observations across the 34 monitoring stations (section 3.2.3). The diurnal cycle is shown as function of local time (LT). Shaded envelopes denote the standard deviation of the spatial variation of $PM_{2.5}$ across the 34 stations at each hour of observation. The grey line is the model boundary layer height (PBLH). Modeled time period: from 6th October to 16th October 2019.

	NMB	NMAE	MB [ug/m3]	RMSE [ug/m3]	r
DAY TIME (8:00-20:00 LT)	0.13	0.18	10.69	16.08	0.87
NIGHT TIME (21:00-07:00 LT)	0.16	0.16	17.91	18.30	0.55

Table 3.2: Model evaluation statistics for average diurnal cycle $PM_{2.5}$ shown in Figure 3.5, divided between for day time (08:00-20:00 LT) and night time (21:00-07:00 LT). Statistics are the same used in Chapter 2 evaluation: normalised mean bias (NMB), mean bias (MB), root mean square error (RMSE), and Pearson correlation coefficient (r).

Other sources of error may also be responsible for the overestimation of individual $PM_{2.5}$ components. The inorganic fraction (sulfate, nitrate, ammonium) of model $PM_{2.5}$ represents $\sim$37% of the total $PM_{2.5}$ mass (Figure 3.6),the organic fraction (primary and secondary organic aerosols) represents $\sim$22%, and black carbon represents $\sim$6%. Previous measurement studies over Delhi have reported an inorganic fraction of 23–27%, an organic fraction (OA, usually calculated at 1.4 times organic carbon, OC) of 20–32%, and an elemental carbon fraction (equivalent to our model black carbon) of 5–15%

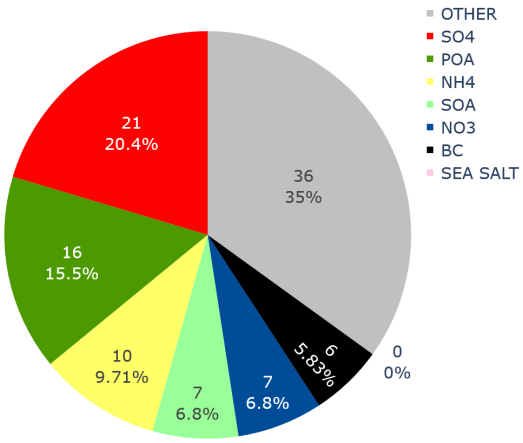

Figure 3.6: Post-monsoon average modeled $PM_{2.5}$ composition across Delhi. OTHER = dust,SO_4 = sulfate, NO_3 = nitrate, NH_4 = ammonium, POA = primary organic aerosols, SOA = secondary organic aerosols, BC = black carbon, SEA SALT = sodium chloride. Numbers refers to mass concentrations ($\mu g\ m^{-3}$). Modeled time period: from 6th October to 16th October 2019.

(Bawase et al., 2021; Dumka et al., 2017; Jain et al., 2020). These observed values are broadly consistent with our model values except for the inorganic fraction for which the model has a bias of 10%. As we did in Section 2.3.1 when comparing OA concentrations with previous studies, we acknowledge that comparing the composition of our 10 day period in year 2019 to studies covering different period and years is a limitation, since we cannot take into account interannual variability of the chemical and meteorological environment. However, regardless of the period under investigation, studies have found that the WRF-Chem model tends to overestimate the SO_2 precursor over the Indian region (Conibear et al., 2018; Kota et al., 2018), a result that we found as well in the previous Chapter (Section 2.3.1). This could lead to overestimating the impact of the IPO sector on $PM_{2.5}$ through overestimation of the sulfate component, since industry and power sectors are main emitter of SO_2 in the NCR (Figure 3.4).

sector	emissions scaling							
TRA_Delhi	2	1.75	1.5	1.25	0.75	0.5	0.25	0
DOM_Delhi	2	1.75	1.5	1.25	0.75	0.5	0.25	0
IPO_Delhi	2	1.75	1.5	1.25	0.75	0.5	0.25	0
TRA-_NCR	2	1.75	1.5	1.25	0.75	0.5	0.25	0
DOM_NCR	2	1.75	1.5	1.25	0.75	0.5	0.25	0
IPO_NCR	2	1.75	1.5	1.25	0.75	0.5	0.25	0
TRL_Delhi	2	1.75	1.5	1.25	0.75	0.5	0.25	0
TRH_Delhi	2	1.75	1.5	1.25	0.75	0.5	0.25	0
TRW_Delhi	2	1.75	1.5	1.25	0.75	0.5	0.25	0
DST_Delhi	2	1.75	1.5	1.25	0.75	0.5	0.25	0
TRL_NCR	2	1.75	1.5	1.25	0.75	0.5	0.25	0
TRH_NCR	2	1.75	1.5	1.25	0.75	0.5	0.25	0
TRW_NCR	2	1.75	1.5	1.25	0.75	0.5	0.25	0
DST_NCR	2	1.75	1.5	1.25	0.75	0.5	0.25	0

Table 3.3: Sensitivity runs performed for the ERI range of applicability. Each sector emissions has been scaled one at the time from complete removal (emissions scaling =0) to doubling (emission scaling =2) with a 0.25 scaling increment. Each sensitivity simulation has been performed for the whole period of the baseline run, from 6th to 16th October 2019.

3.3.2 Emission reduction impact (ERI) range of applicability

To establish the range of applicability of the emissions reduction impact method in our study, we consider the response of emissions changes from each source in Table 3.1 to the 24-h average $PM_{2.5}$ (WHO metric) and the hourly value of $PM_{2.5}$ over Delhi for the whole period of the simulation (6-16 October 2019). We consider symmetrical emission decreases and increases in the scaling range from 0% to 200% from the baseline, with a 25% increment. Table 3.3 summarises all the sensitivity runs performed.

Figure 3.7a shows a near-linear relationship between changes for emissions from individual sectors and 24-h mean $PM_{2.5}$ over Delhi over our range of considered perturbations. This is true also for each of the individual on-road transport subsectors (Figure 3.7b). Simultaneous changes in emissions from all the main sectors results in interactions between pollutants that cannot be captured when considering one source at

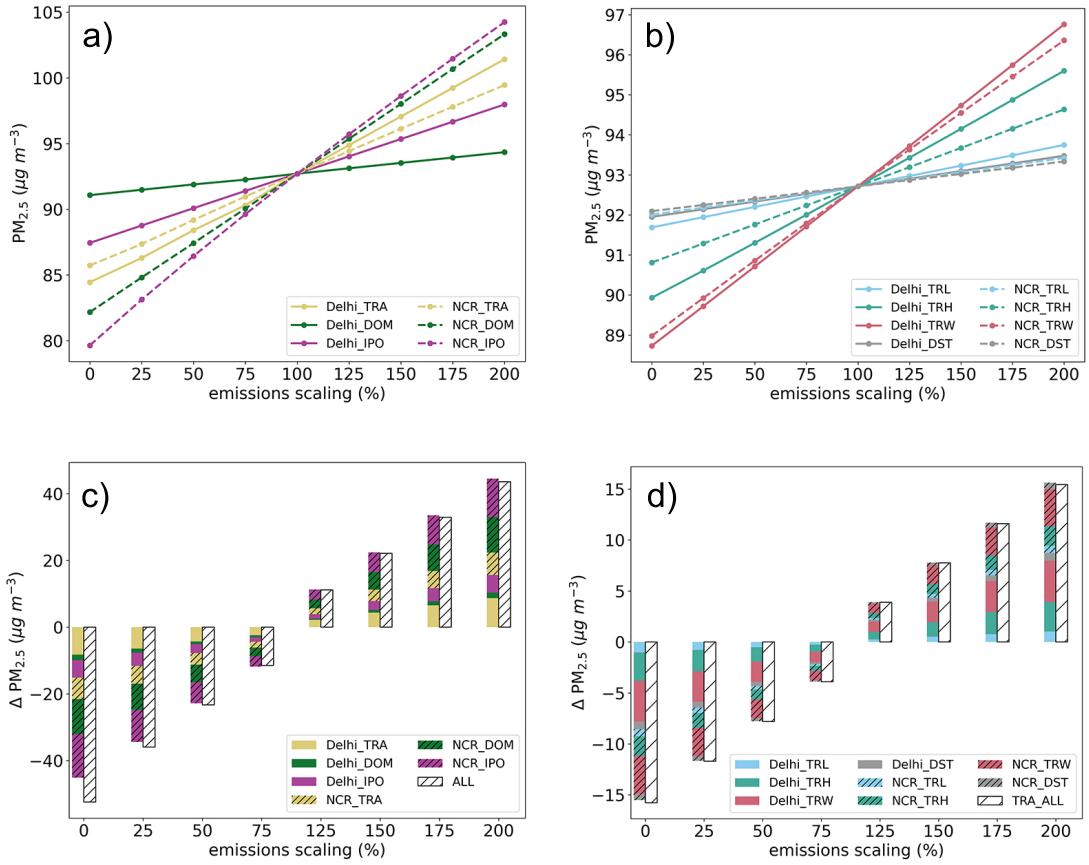

Figure 3.7: Linearity test for average 24-h $PM_{2.5}$ response over Delhi due to fractional emission changes from different sectors. Panel a): response to change in emissions from individual main sectors (DOM, TRA,IPO) within Delhi (Delhi_) and the surrounding region (NCR_). Panel b): same as panel a) but for the on-road transport subsectors. Sector names are defined in Table 3.1. Panel c): comparison between the response obtained by summing the responses of individual change in emissions from the main sectors and the response obtained by changing emissions from the main sectors all simultaneously. 'ALL' refers to the simultaneous change of emissions for all the sectors together. Panel d): same as panel c) but for the on-road transport subsectors. Modeled time period: from 6th October to 16th October 2019.

the time. These interactions account for an additional impact that increases with larger emission changes (Figure 3.7c). We find this nonlinearity result in additional reductions of up to 16% in $PM_{2.5}$ when all the sectors are turned off but only a reduction of 2% when all sector emissions are doubled (200%). Moderate changes in emissions ($<$25%) result in non-linearities of $<$5% in $PM_{2.5}$. Non-linearities are smaller when considering the on-road transport subsectors, where they account for $\pm$5% additional impact in $PM_{2.5}$

over the whole range of emissions changes (Figure 3.7d), likely because of their total smaller magnitude. We found similar results for hourly values of $PM_{2.5}$ over Delhi, which show an almost linear relation to changes in emissions over the range of $\pm$75% (Figure 3.8,3.9, 3.10, 3.11). The sign and magnitude of non-linear terms vary across the range of emission changes, especially when considering the symmetric reduction/increase in emissions, suggesting that different chemical regimes may be reached. Based on our analysis, we establish an upper limit for linearity as α_t=75% within which non-linearities account for maximum $\sim \pm$5% on top of the total impact on $PM_{2.5}$ given by summing the individual sectors impacts. This magnitude of non-linear impact is small in the context of other uncertainties associated with air quality modelling, and still provides practical information for policy makers. Other studies have also identified linearity in the response of surface $PM_{2.5}$ to changes in main sector emissions (Chen et al., 2020; Conibear et al., 2021; Thunis et al., 2015). Non-linearities are expected to be more important in particular for the formation of secondary pollutants at higher spatial and temporal resolution (e.g. local pollution episodes) (Thunis et al., 2015). The contribution from all anthropogenic sectors considered in this study, including any non-linear terms, accounts for $\sim$60% of the 24-h average $PM_{2.5}$ mass over Delhi. This suggests there is a large contribution originating outside of Delhi and the broader NCR region. To check this pollution contribution, we perform a simulation for which the boundary conditions for the nested domain (Figure 1.9) are switched off. We acknowledge that we should be careful in performing such large perturbation, because of potential large non-linear impacts. However in this case we are doing a simple sanity check rather than an in depth analysis as done for the impacts of anthropogenic sectors. When switched off, we find that the boundary conditions account for $\sim$40% of changes in the 24-h average $PM_{2.5}$, ignoring the additional non-linear impacts. This highlights that long range advection of pollutants makes a substantial contribution to surface $PM_{2.5}$ in Delhi in the post-monsoon season even before the full onset of the agricultural biomass burning.

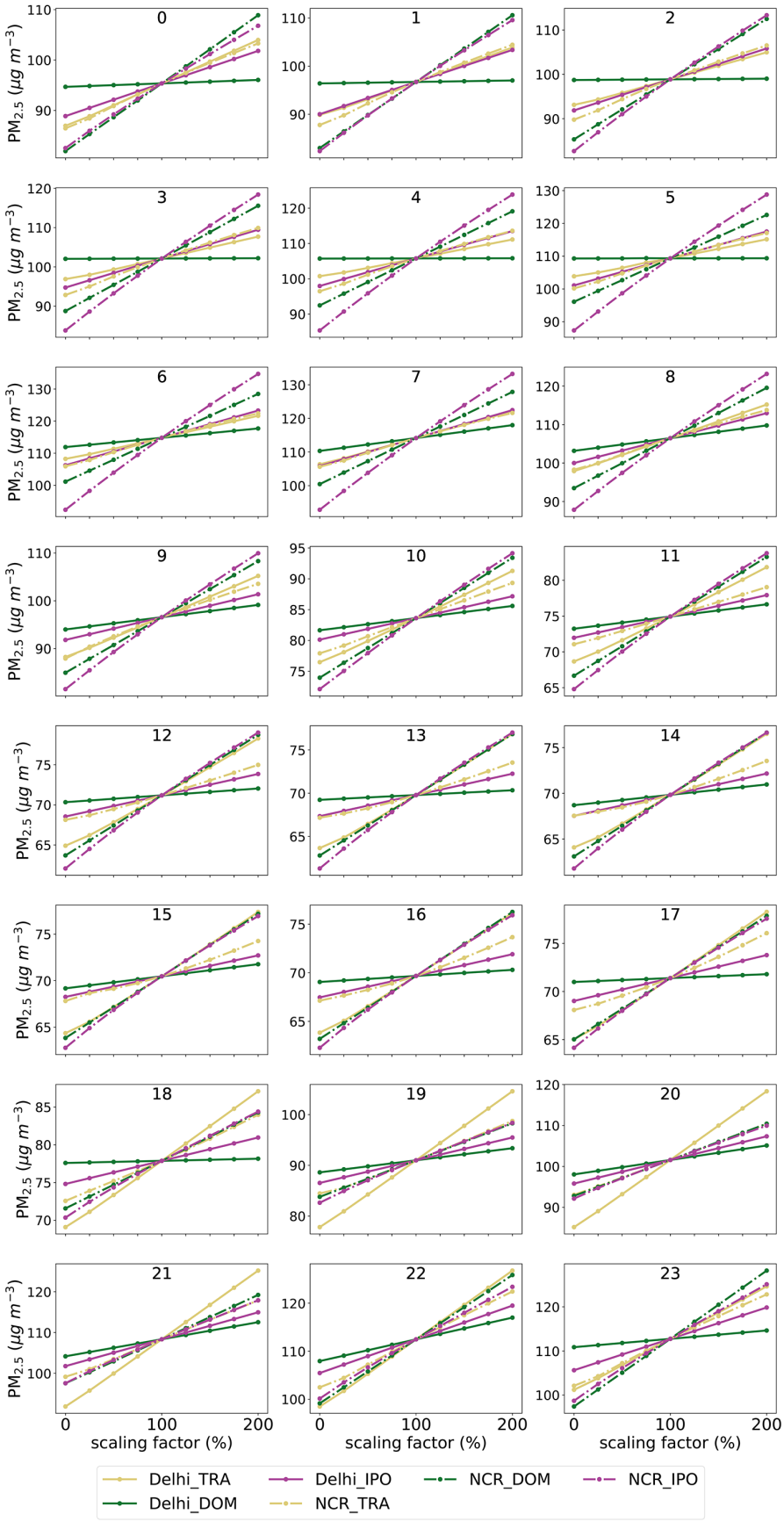

Figure 3.8: Linearity test for $PM_{2.5}$ hourly response over Delhi due to fractional emission changes from individual main sectors (DOM, TRA,IPO) within Delhi (Delhi_) and the surrounding region (NCR_). Hourly values ranges from 00:00 to 23:00 local time. Modeled time period: from 6th October to 16th October 2019.

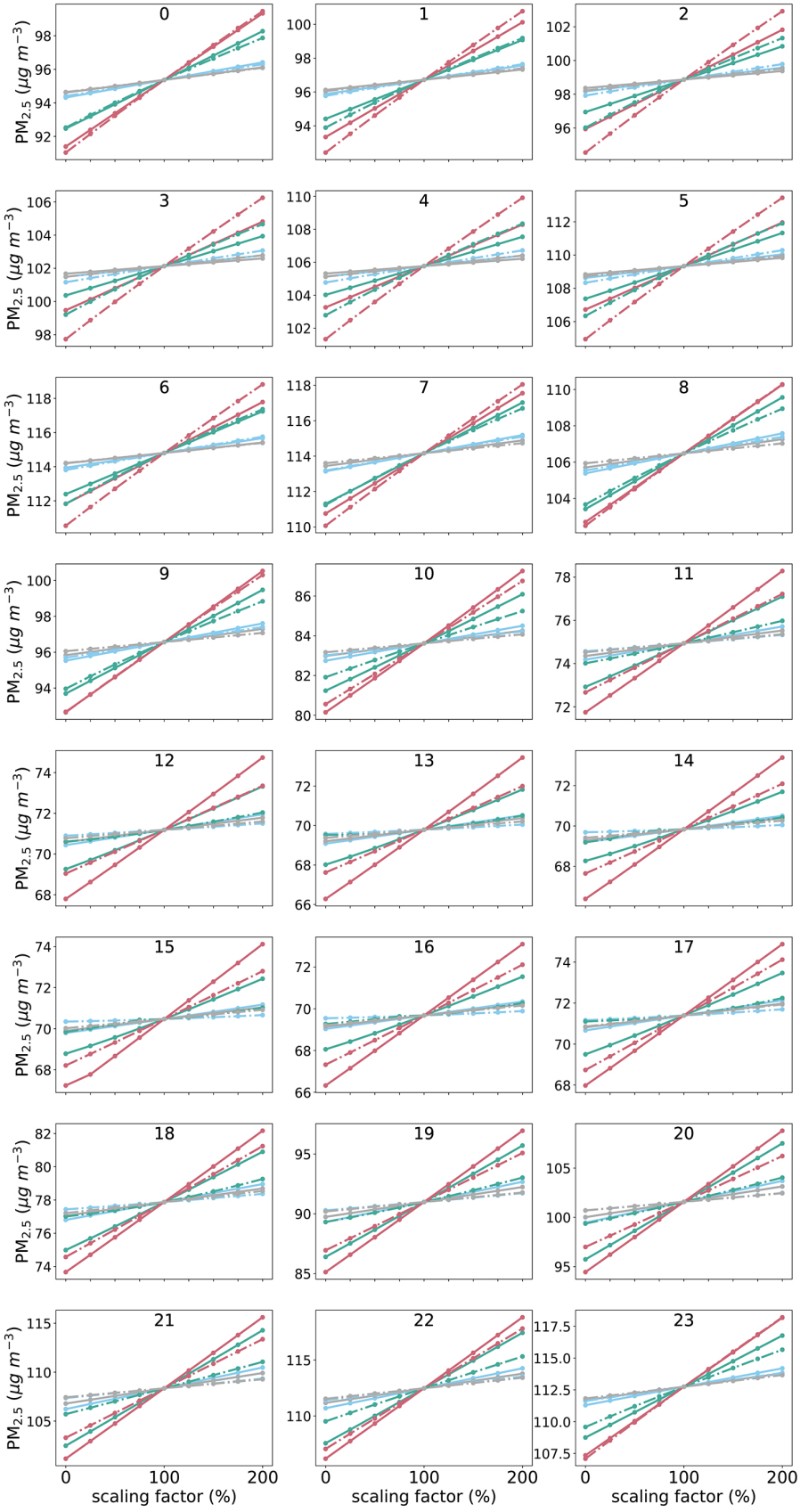

Figure 3.9: Linearity test for $PM_{2.5}$ hourly response over Delhi due to fractional emission changes from individual transport subsectors (TRW, TRL,TRH, DST) within Delhi (Delhi_) and the surrounding region (NCR_). Hourly values ranges from 00:00 to 23:00 local time. Modeled time period: from 6th October to 16th October 2019.

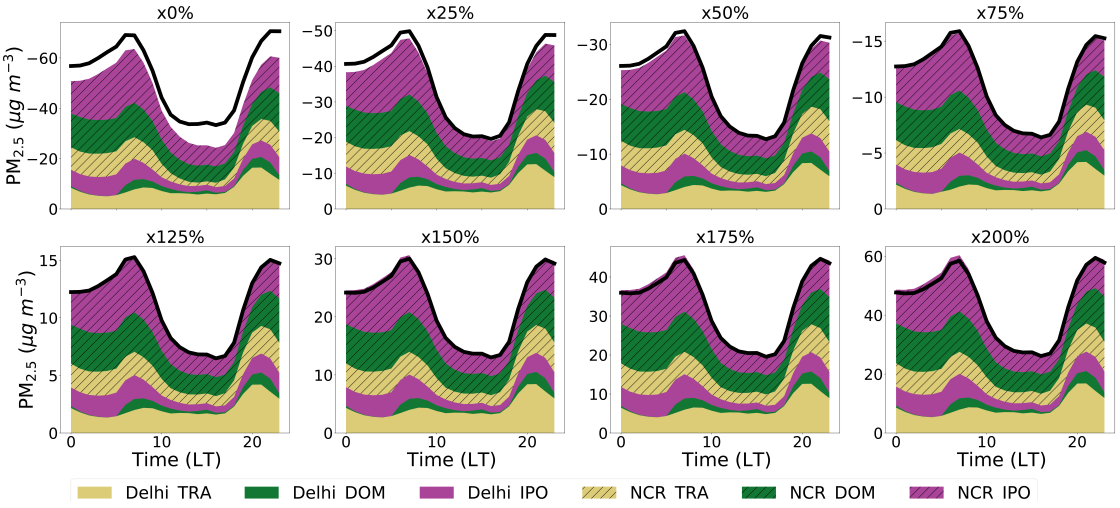

Figure 3.10: Linearity test for $PM_{2.5}$ hourly response over Delhi to changes in emissions from different sectors. Comparison between the response obtained by summing the responses of individual change in emissions from main sectors (DOM, TRA,IPO) within Delhi (Delhi_) and the surrounding region (NCR_), and the response obtained by changing emissions from the all the main sectors simultaneously (black line). Hourly values ranges from 00:00 to 23:00 local time. Modeled time period: from 6th October to 16th October 2019.

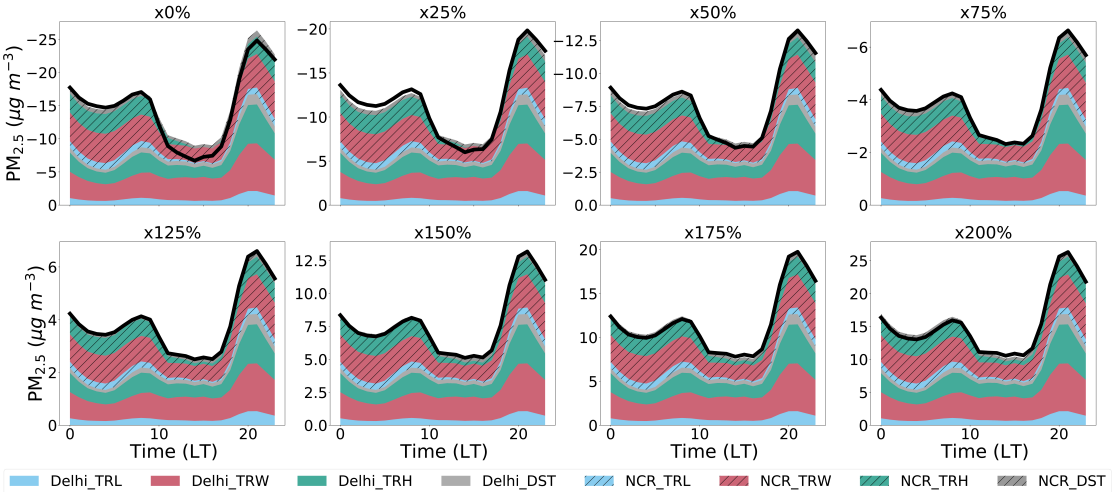

Figure 3.11: Linearity test for $PM_{2.5}$ hourly response over Delhi to changes in emissions from different sectors. Comparison between the response obtained by summing the responses of individual change in emissions from transport subsectors (TRW, TRL,TRH, DST) within Delhi (Delhi_) and the surrounding region (NCR_), and the response obtained by changing emissions from the all the transport subsectors simultaneously (black line). Hourly values ranges from 00:00 to 23:00 local time. Modeled time period: from 6th October to 16th October 2019.

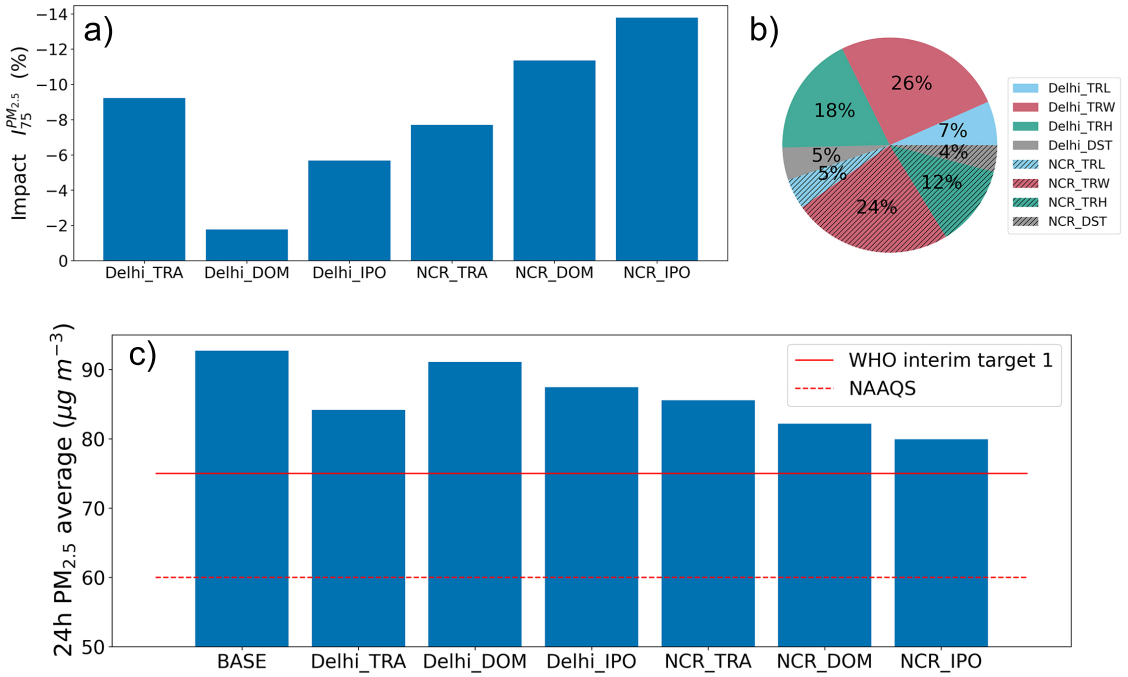

Figure 3.12: Impacts of anthropogenic sectors on 24-h mean $PM_{2.5}$ over Delhi. Panel a) Impacts of the main anthropogenic sectors. Panel b) Share of subsectors to the total on-road transport impact (Delhi_TRA+NCR_TRA). Panel c) Potential mitigation of $PM_{2.5}$ levels in Delhi for individual sector impacts, compared to the WHO interim target 1 and the Indian National Ambient Air Quality Standard (NAAQS). Modeled time period: from 6th October to 16th October 2019.

3.3.3 Impacts on 24-h average $PM_{2.5}$

Figure 3.12a shows the relative impact of each anthropogenic sector on the 24-h average $PM_{2.5}$ over Delhi, calculated from equation 3.1 with α=75%. We find that NCR anthropogenic sources from industries and power (NCR_IPO) and domestic (NCR_DOM) have the highest impact on Delhi $PM_{2.5}$, with potential reductions from baseline $PM_{2.5}$ concentrations of 14% and 11%, respectively. The same two sectors (Delhi_IPO and Delhi_DOM) within Delhi have the lowest impacts, with potential reductions of $<$6%. This contrast between the local and regional sources is broadly consistent with the emission distribution from the domestic (DOM) and the industry and power (IPO) sectors. Almost all power plants, industries, and other point sources are located outside Delhi

and they account for most of the IPO sector emissions. As shown in Figure 3.4c, the rate of emissions from the domestic sector is similar inside and outside Delhi. However, because the area outside Delhi is much larger, domestic sector emissions from outside Delhi make a much larger contribution to regional emission totals (see Figure 3.4a).

As seen in Figure 3.12a, the on-road transport sector within Delhi (Delhi_TRA) has the highest impact on $PM_{2.5}$ among the local sources, with a potential reduction up to 9.2%, which is almost a third higher than the local industry and power sector and almost five times the local domestic sector. The impact from the local on-road transport sector is slightly higher than for regional sources (NCR_TRA, up to 7.7%). While emissions from local on-road transport represent almost half of emissions from regional on-road transport, traffic in Delhi remains the main hotspot for on-road transport emissions in the region, with spatially homogeneous distribution and with higher emissions rates (Figure 3.4a and 3.4c), which might help explain its higher impact on Delhi $PM_{2.5}$. Two- and three-wheelers from local and regional traffic account for almost 50% of the impact of the on-road transport sector on $PM_{2.5}$, with an approximately equal contribution of local (Delhi_TRW) and regional (NCR_TRW) two- and three-wheelers (Figure 3.12 b). Local heavy duty vehicle traffic (Delhi_TRH) accounts for an additional 18% of the total on-road transport impact, followed by 12% from regional heavy duty vehicle traffic (NCR_TRH). Traffic from passenger and light duty vehicles (TRL) and resuspended dust (DST) have a relatively small impact on Delhi $PM_{2.5}$, each accounting for around 10% of the total traffic impact, equally split between local and regional sources. In summary, we find that two- and three-wheelers and heavy duty vehicles collectively account for almost 80% of the total traffic impact. This is consistent with these subsectors accounting for 50% of PM and SO_2, for more than 80% of NO_x emisssions, and for more than 90% of NMVOCs emissions from total on-road transport sector (Figure 3.4b).

In terms of absolute $PM_{2.5}$ concentrations, we find that no one sector alone is impactful enough that its removal would improve air quality to meet the WHO interim target 1 (Figure 3.12c). If the emissions from local on-road transport were eliminated completely, $PM_{2.5}$ in Delhi would be reduced to 84 $\mu g\ m^{-3}$ from a baseline concentration of 93 $\mu g m^{-3}$. If we then also removed the impact from regional on-road transport, the level of $PM_{2.5}$ in Delhi would decline to 77 $\mu g\ m^{-3}$, still above the Indian NAAQS (60 $\mu g\ m^{-3}$) and the WHO interim target 1 (75 $\mu g m^{-3}$) (WHO, 2021). We find that only a multi-sectoral, multi-scale approach targeting regional and local emissions is sufficient to reduce mean Delhi $PM_{2.5}$ values to target values. For example, if we consider the linear regime and the impacts in Figure 3.7a for each sector, reducing regional domestic emissions by 75%, regional industry and power by 50% and local traffic by 50% would achieve the WHO interim target 1. If also local and regional on-road transport emissions were reduced by 75%, mean Delhi $PM_{2.5}$ would reach the Indian NAAQS threshold.

3.3.4 Impacts on $PM_{2.5}$ diurnal cycle

The diurnal cycle of $PM_{2.5}$ is determined by the diurnal cycle of emissions, pollutant transport, boundary layer dynamics, and atmospheric chemistry. Figure 3.13 shows the percentage impact of local sectors (panel a) and regional sectors (panel b) on the mean diurnal cycle of $PM_{2.5}$ over Delhi, determined from equation 3.1 with α=75%.

Nighttime concentrations (00:00-06:00 local time) are impacted most strongly by regional sources, with contributions of $\sim$15–25% from industry and power, $\sim$15% from the domestic sector, and $\sim$10% from on-road transport. Contributions from local emission sectors are below 10%, with the largest impacts from industry and power followed by the on-road transport sector. The contribution from local domestic emissions is negligible, reflecting the large reduction of emissions from this sector during nighttime. Continuous emissions from the energy and industry sector combined with the shallow nighttime boundary layer results in the contribution from this sector peaking during the nighttime.

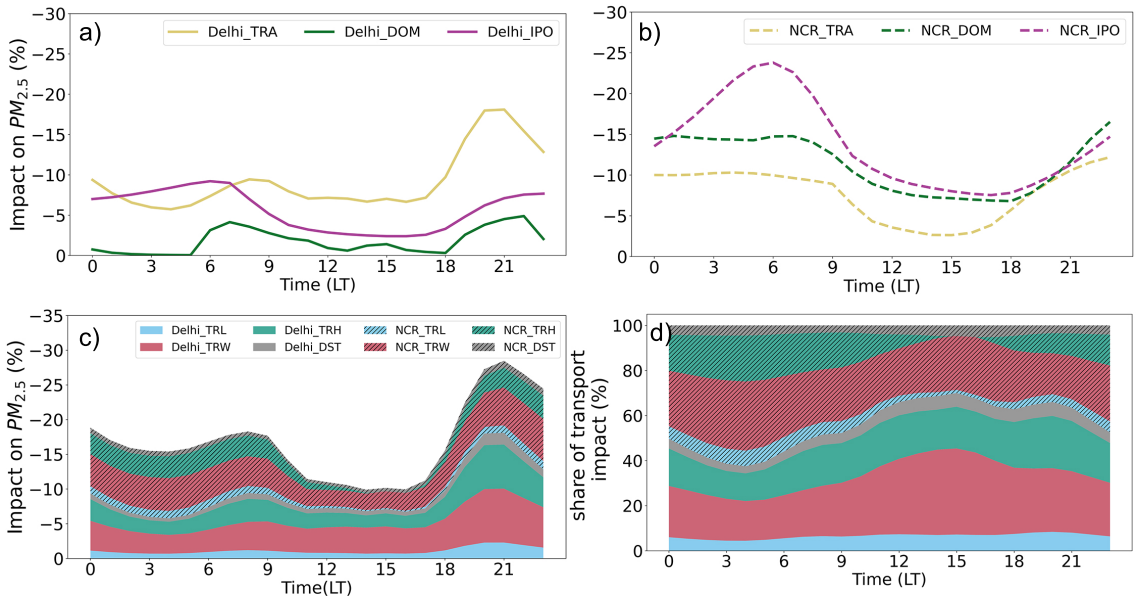

Figure 3.13: Impacts of local (a), regional (b) anthropogenic sectors on the diurnal cycle of average $PM_{2.5}$ over Delhi. Panel (c) shows the impacts of on-road transport subsectors. Panel (d) shows the relative share for total on-road transport impact (Delhi_TRA+NCR_TRA). Modeled time period: from 6th October to 16th October 2019.

Concentrations of $PM_{2.5}$ during daytime hours (06:00-18:00) are still mainly impacted by non-local sources from the industry, power, and domestic sectors although their contributions almost halve (reaching below 10%) towards late afternoon when the boundary layer continues to expand and mixing is over longer vertical scales. The contribution from local on-road transport increases to $\sim$10% during peak traffic activity at 08:00 and then plateaus around 7% between 11:00–17:00. The contribution from non-local on-road transport decreases during daytime, reaching an impact of $<$5%, comparable to local industry and power sector. The contribution from the local domestic sector increases during the daytime to $<$5%. Local on-road transport makes the highest anthropogenic contribution to $PM_{2.5}$ during evening hours (18:00–00:00), reaching up to 18% at around 20:00. This is due to the evening traffic peak combined with the collapse of the boundary layer. Regional sources progressively contribute more to $PM_{2.5}$ during the evening, peaking during nighttime hours.

The impact of local on-road transport on $PM_{2.5}$ reflects typical diurnal patterns of on-road transport emissions, with morning and evening peaks. The contribution to $PM_{2.5}$ from regional on-road transport emissions shows a similar trend to local emissions but smoothed reflecting the influence of PBL mixing and atmospheric advection timescales. Consequently, the nighttime peak contribution from the regional on-road transport sector impacts the morning peak of Delhi $PM_{2.5}$, and the absence of nighttime regional on-road transport, amplified by the deeper boundary layer, results in a drop in the contribution for this sector to $PM_{2.5}$ later in the day. Overall, the sum of the local and regional on-road transport sectors contribute up to 20% to $PM_{2.5}$ during nighttime hours, $\sim$12% during the central hours of the day, and peaking at almost 30% during the evening traffic peak (Figure 3.13c). Two- and three-wheelers and heavy duty vehicles dominate the impact of the on-road transport sector on the diurnal cycle of $PM_{2.5}$, accounting for 60% to 70% of the total impact at any hour of the day (Figure 3.13). Local two- and three-wheelers (30-40%) and local heavy duty vehicles (15-23%) have the highest share of the total on-road transport contribution during the central hours of the day and during the evening. Regional two- and three-wheelers (up to 30%) and regional heavy duty vehicles (up to 20%) dominate during the nighttime hours (Figure 3.13c, 3.13d). We find minimal contributions from passenger cars and light commercial vehicles and from resuspended road dust, each accounting for $<$10% at any time during the day for the local and regional fleets.

3.3.5 Simple model for $PM_{2.5}$ and O_3 health impact estimate

As noted the introduction, if mitigation strategies focus only on minimising $PM_{2.5}$ exposure, elevated levels of surface ozone (O_3) could become more of a significant health concern. For example, reducing nitrogen oxide emissions from the on-road transport sector could result in an increase in surface ozone. We build a linear model to investigate which sectors would be best to target to minimise the total health impacts in terms

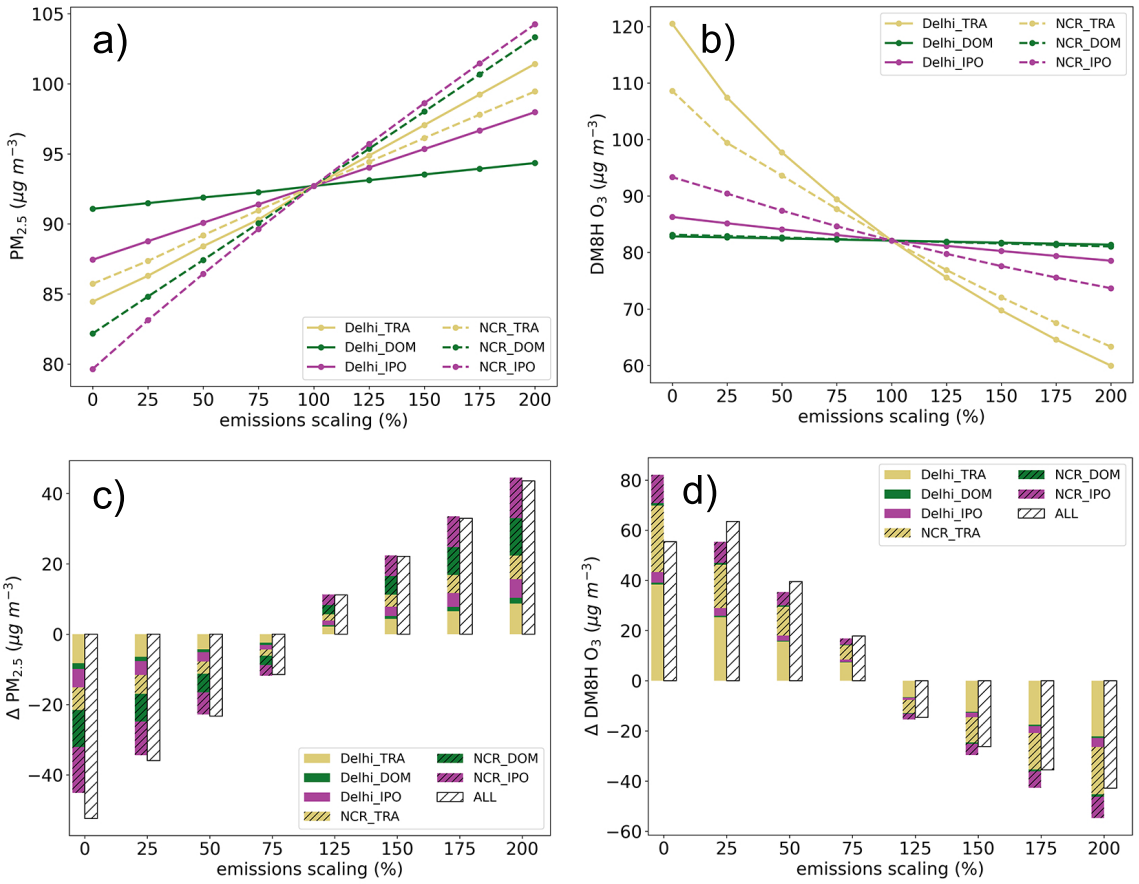

Figure 3.14: Linearity analysis for test for $PM_{2.5}$ and O_3 metrics. The $PM_{2.5}$ plots are the same as in Figure 3.7, but are reported again here for clarity. Modeled time period: from 6th October to 16th October 2019.

sector	24-h $PM_{2.5}$	MDA8 O_3
Delhi_DOM	1.65	-0.73
Delhi_IPO	5.27	-3.84
Delhi_TRA	8.75	-27.91
NCR_DOM	10.60	-1.06
NCR_IPO	12.17	-9.81
NCR_TRA	6.93	-21.57

Table 3.4: Rates of change in average 24-h $PM_{2.5}$ and in MDA8 O_3 for each main sector ($[\mu g m^{-3}]$). These value are interpolated from Figure 3.14 in the linearity range of scaling factors $\pm$ 50% (i.e. [0.5, 1.5]).

of mortality when considering both $PM_{2.5}$ and O_3 . We restrict to these two pollutants because they are the most important outdoor air pollutants related to mortality currently

recognised, consistently with the methodology adopted in the Global Burden of Diseases Study (Cohen et al., 2017; Pandey et al., 2021) and the EPA analysis of the clean air act (Agency, 2011). Ozone is associated with respiratory impacts independent of $PM_{2.5}$ exposure, so we can sum their mortality effects (Jerrett et al., 2009).

We build the model starting from our linearity analysis in Section 3.3.2, which we extend also to O_3, for the metric of daily maximum 8-hour concentration (MDA8). As for average daily $PM_{2.5}$, we found that also changes of MDA8 O_3 over Delhi is almost linear with changes in emissions for up to $\pm$ 50% (Figure 3.14), scaling factors of emissions between $[0.5, 1.5]$). However, contrary to $PM_{2.5}$, decreases in emissions increase ozone concentrations, and thus lead to negative health impacts from ozone (Figure 3.14 b,d). Reducing on road transport emissions leads the increase in surface ozone concentrations compared to reduction of emissions from other sectors, which brings similar (but smaller) increases in surface ozone.

From the linearity assumption, we can write the changes in 24-h $PM_{2.5}$ and MDA8 O_3 from baseline values due to reduction of emissions for the anthropogenic sectors as:

$$\begin{cases} \Delta PM_{2.5} = \sum_{i=1}^{n} m_i \cdot (S_i - 1) \\ \Delta O_3 = \sum_{i=1}^{n} l_i \cdot (S_i - 1) \end{cases} \tag{3.2}$$

with n=6, the total number of the sectors considered in Table 3.4. For each sector i, m_i and l_i are the rate of change for average 24-h $PM_{2.5}$ and in MDA8 O_3 respectively, obtained from linear interpolation of data in Figure 3.14, and reported in Table 3.4. S_i is the scaling factor applied in reduction/increase of emissions for each sector within the linearity range for the reduction of emissions $[0.5, 1]$ %. For example, S_{Delhi_TRA} =0.5 means that the emissions from the transport sector within Delhi are scaled by 50% i.e. reduced by half.

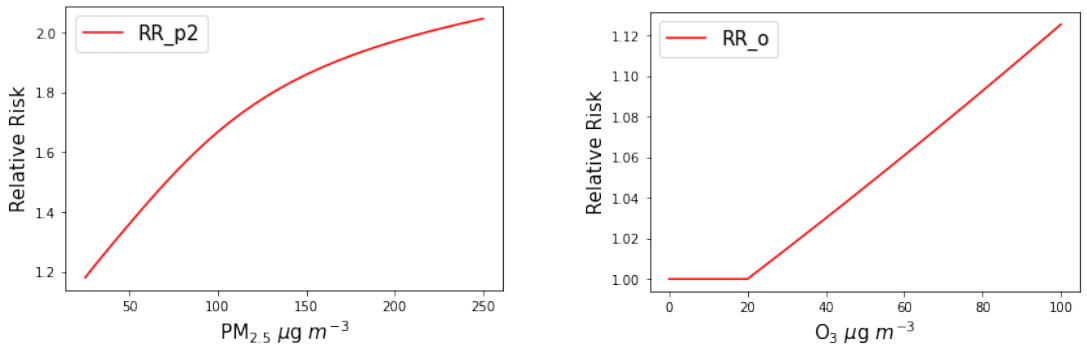

(a) **(b)**

Figure 3.15: Relative risk functions RR_p for $PM_{2.5}$ (a) and RR_o O_3 used in Equation 3.3. The mathematical expression of the two functions is the same used in Wang et al. (2020a).

Mortality due to disease j from air pollution exposure at concentration (C) is commonly given by:

$$M_j(C) = p \cdot I_j \cdot (1 - \frac{1}{RR_j(C)}) \tag{3.3}$$

where p is population exposed, I_j is the baseline adjusted mortality rate for disease j, and $RR_j(C)$ the relative risk function calculated at concentration C (Apte et al., 2015; Wang et al., 2020a). For simplicity in the calculation, the health impact is restricted to mortality due to chronic obstructive pulmonary disease (j=COPD). In addition for simplicity, we consider homogeneous density of population within Delhi, all the population equally exposed, and relative risk equal among age groups, so p to be treated as a constant and so we have just one mathematical formulation of the $RR_j(C)$.

Equation 3.3 is normally used to quantify mortality for long term exposure to air pollutants. Even if our study focuses on the post-monsoon season, our estimate can be used as a proxy of long term $PM_{2.5}$ decrease and ozone increase arising when cutting emissions. Indeed, other studies have pointed out that emissions reduction aiming solely at reducing $PM_{2.5}$ levels, especially significant reduction of NO_x from on-road transport,

can lead to an increase of ozone pollution also during pre-monsoon (Chen et al., 2020), winter (Tiwari et al., 2018) and summer (Chen et al., 2021). For the COPD RR functions for $PM_{2.5}$ and O_3, RR_p and RR_o respectively, we used the mathematical expressions in Wang et al. (2020a), which are based on the Global Exposure Mortality Model (GEMM) for $PM_{2.5}$ and the Global Burden of Disease (GBD) for O_3. The two RR functions used are shown in Figure 3.15. The difference in mortality due to exposure to concentration C and C_1 is:

$$\Delta M = M(C) - M(C_1) \tag{3.4}$$

The effective emission reduction strategy would be given by the set of S_i that maximise the avoided mortality due the combined exposure to $PM_{2.5}$ and O_3:

$$max_{S_i \in [0.5,1]} \{ \Delta M = \Delta M_{PM_{2.5}} + \Delta M_{O_3} \} \tag{3.5}$$

Explicitly, using Equation 3.3 and Equation 3.4:

$$\begin{aligned} max_{S_i \in [0.5,1]} \{ \Delta M = p \cdot I_{COPD} \big(& \frac{1}{RR_p(PM_{2.5}^{base} + \Delta PM_{2.5})} - \frac{1}{RR_p(PM_{2.5}^{base})} \\ & + \frac{1}{RR_o(O_3^{base} + \Delta O_3)} - \frac{1}{RR_o(O_3^{base})} \\ & = \frac{1}{RR_p(PM_{2.5}^{base} + \sum_{i=1}^{n} m_i \cdot (S_i - 1))} - \frac{1}{RR_p(PM_{2.5}^{base})} \\ & + \frac{1}{RR_o(O_3^{base} + \sum_{i=1}^{n} l_i \cdot (S_i - 1))} - \frac{1}{RR_o(O_3^{base})} \\ \big) \} & \end{aligned} \tag{3.6}$$

To solve this equation and find the maximum, we use a Python library (SciPy optimize), which provides solvers for minimizing (or maximizing) non-linear functions subject to constraints. By solving this equation, we found that the optimal combination of emission reduction is:

$$S^* = \{S_{Delhi\_DOM} = 0.5, S_{Delhi\_IPO} = 0.5, S_{Delhi\_TRA} = 1, S_{NCR\_DOM} = 0.5,$$

$$S_{NCR\_IPO} = 0.5, S_{NCR\_TRA} = 1\}. \tag{3.7}$$

This is a unique solution (there are no other local maxima). The solution highlights that to reduce mortality for COPD, emissions to be prioritised for reduction are from the industries and power (IPO) and the domestic (DOM), over the transport sector (TRA), both within Delhi and from the broader NCR. This is because for when reducing transport emissions, the adverse health impact arising from an increase in ozone are higher than the benefit of reducing $PM_{2.5}$, while for the IPO and DOM sectors the positive impact of $PM_{2.5}$ is greater than the negative of O_3. This is because in our calculation we assume that on-road transport emissions are reduced uniformally, i.e., all pollutants are reduced by the same amount. Thus it might explain why we find that health impact resulting from the increase in ozone are higher than the benefit of reducing $PM_{2.5}$ for the transport sector, but it might not be the case if individual pollutant are reduced differently (e.g. by reducing VOCs more than NOx from transport). We highlight that the solution values are those values at the boundary conditions, i.e. either S=0.5 (reduction by 50%) or S=1 (emissions not changed). The range [0.5,1] has been chosen for ensuring the linearity in emission changes. We obtain values at the boundaries when solving the equation because of the combination of the linearity assumption for the variation in concentrations and the fact that the RR functions are monotonic. Other assumptions on the RR functions could lead to a different solution.

For a population of 31 million in Delhi (DESA, 2018))and a baseline adjusted mortality for COPD 54 deaths every 100000 inhabitants (Chowdhury and Dey, 2016)) the solution above would avoid $\sim$15 premature deaths for the period considered of the first two weeks of October 2019, which is a decrease of 4% from the baseline mortality for COPD due to $PM_{2.5}$ and ozone exposure combined for the same period. This value is obtained by doing a daily pro-rata scaling of the total avoided mortality obtained starting from Equation 3.3, which is usually used for exposure to yearly concentrations.

This is a simple estimates, with uncertainties due to different factors: modeled concentrations, linearity assumption, assumptions on the distribution and age of the population exposed, and considering COPD as the only disease. Also we note that while reduced NOx emissions are projected to lead to increased ozone levels in VOC-limited urban areas, the rural areas are NOx limited and likely to experience ozone decreases and that such benefits are not captured in our first-order analysis. However, our simple calculation illustrates the expected responses despite the uncertainties, and it highlights the importance of weighting the health benefit of reducing $PM_{2.5}$ with the drawbacks of ozone increase. This is important in particular in VOC-limited urban environments such as Delhi, where reduction of emissions, especially from transport sector, could increase the adverse health impact from increased ozone levels.

3.4 Discussion and Conclusions

We studied the contribution of the on-road transport sector to surface $PM_{2.5}$ over Delhi during the post-monsoon season using the WRF-Chem model. By using the WRF-Chem model we were able to find that the response between changes in emissions from different emissions sectors and $PM_{2.5}$ concentrations is linear at the city level scale during post-monsoon. We defined the range of validity of the linear response, which holds for reduction in emissions within 75%. We calculated the impacts of the transport

sector and its subsectors compared to other local (within Delhi) and regional (within NCR) sources on both mean 24-h and diurnal cycle of $PM_{2.5}$ in Delhi, and quantified mitigation strategies to achieve $PM_{2.5}$ air quality standards in the city during the post-monsoon season. Although a posteriori the response of $PM_{2.5}$ to emissions changes has proven to be linear, our results cannot be captured solely by the analysis of the emissions inventory, highlighting the added value of using a chemical transport model for emission reduction and mitigation studies.

We found that local on-road transport sectors contribute less than 10% to 24-h mean $PM_{2.5}$ values over Delhi during the post-monsoon season, and if we add the regional contribution, the total impact of the on-road transport sector increases to 17%. The highest impact from individual regional sectors is from power and industry (14%) and domestic (11%), while the local power and industry and domestic sectors have minimal impact (6% each). This is consistent with previous studies that showed that on a city-scale regional sources from the NCR can have a significant impact on annual mean $PM_{2.5}$ values over Delhi (Amann et al., 2017) and during the pre-monsoon season (Chen et al., 2020). Long range advection of pollutants from outside the NCR also contributes substantially to $PM_{2.5}$ over Delhi for the period considered in our simulations ($\sim$40%), which is comparable to the $\sim$30% annual average long range advection contribution found by Amann et al. (2017). Within the on-road transport sector, we found that two- and three-wheelers dominate the on-road transport contribution to ambient $PM_{2.5}$ in Delhi, with around 50% share of the total on-road transport impact for the joint regional and local fleet. Heavy duty vehicles contribute 18% for the local and 12% for the regional fleet. Light commercial vehicles, including passenger cars and light duty vehicles, and resuspended dust from on-road transport individually contribute about 10% of the total impact.

We showed that targeting emissions reductions from only the on-road transport sector would fail to bring $PM_{2.5}$ down to meet relevant ambient air quality standards (namely WHO interim target 1 or Indian NAAQS). Similar results are found for all the other individual sectors we studied. Only regional cooperation with stringent emissions reductions (50-75%) of the NCR industrial and energy and domestic sectors, jointly with the on-road transport sector (local and regional) has the potential to meet ambient air quality standards. The recent order from the Commission for Air Quality management (CAQM) to phase out of coal from across Delhi and the NCR from January 2023 is a significant step in this direction (CAQM, 2022).

When considering the impact of each sector on the average diurnal cycle of $PM_{2.5}$ over Delhi, we found that the industry and power sectors from NCR dominated nighttime and almost all daytime concentrations (10-25% day/night), with significant contributions from the NCR domestic sector (7-15% day/night). The local on-road transport sectors have the highest absolute impact (18%) during the evening traffic peak (18:00-21:00). If the contribution from the regional on-road transport sector is also included the total impact from the traffic sector reaches almost 30%.

We found that within the on-road transport sector, two- and three-wheelers dominate the on-road transport contribution to daily mean $PM_{2.5}$ values, followed by heavy duty vehicles. Two- and three-wheelers and heavy duty vehicles combined account for 60-70% of the total on-road transport impact on $PM_{2.5}$ throughout the day, with local two- and three- wheelers accounting between 30-40% of the total on-road transport hourly impact on $PM_{2.5}$ during daytime hours. These findings suggest that prioritising reduction of emissions from two- and three-wheelers (e.g., converting to electric vehicles), and heavy duty vehicles (e.g., converting to cleaner fuel such as compressed natural gas), could be an efficient way to reduce the impact of the on-road transport sector on $PM_{2.5}$, particularly during the evening traffic peak. Our results also help to explain why the even-odd pilot mitigation strategies have yet to deliver the expected benefit on surface air

quality. We find that the targeted on-road transport subsector of passenger cars play only a minor role in on-road transport sector emissions during the post-monsoon season (and this will likely hold true for other seasons). Our findings can therefore help inform the development of more effective mitigation strategies for $PM_{2.5}$ over Delhi during the post-monsoon season.

However, if mitigation strategies focus exclusively on minimising $PM_{2.5}$ exposure, it could lead to elevated levels of surface ozone (O_3), especially in VOC-limited cities such as Delhi. We also found that reduction in emissions from the transport sector lead the increase in surface ozone concentrations. Decreasing emissions from other sectors led to similar (but smaller) increases in surface ozone. We built a simplified linear model to find the optimal emission reduction strategy to minimise health impacts when considering both $PM_{2.5}$ and O_3. We found that, during the post-monsoon season, emission reductions from domestic and industry and power sectors should be prioritised over reducing emissions from the on-road transport sectors, if all pollutants are to be reduced by the same amount. Although our estimate is a simple calculation, it highlights the importance of the coordinated control of $PM_{2.5}$ and ozone. This is important in particular in VOC-limited urban environments such as Delhi.

Results are reported for city-scale mean, so they might not be representative of the sub-city scale, where the different source attribution and thus potential impact reductions may be different. Indeed, socio-economical factors also play an important role in determining high air pollution inequalities within the city (Fecht et al., 2015; Lane et al., 2022; Nguyen and Marshall, 2018). In addition, mean values tend to drive the responsibility towards regional action that might be less effective in solving the pollution issue in different parts of the city (Thunis et al., 2021).

Future work is thus needed to characterise $PM_{2.5}$ at finer spatial and temporal scales over Delhi to establish which local controls can be effective at reducing pollution levels. In addition, sensitivity studies within the city will need to consider the location-dependent photochemical environment that will also help determine how the balance of emission changes will influence surface ozone production, to inform effective and impactful emissions control strategies that maximise health benefits for Delhi residents.

Chapter 4

Impact of electric and clean-fuel vehicles on future $PM_{2.5}$ and O_3 pollution over Delhi

4.1 Introduction

In the previous Chapter we have seen that, as part of a multi-sector and multi-scale approach, there is the need to considerably reduce emissions (>50%) from the transport sector to improve air quality over Delhi during high polluted seasons.

The emergence of new transport technologies, such as electric vehicles (EVs), offers an opportunity to scale systemic emission control interventions. The transition to EVs is expected both to contribute toward the net-zero climate targets and improve air quality especially in cities, where traffic is more pronounced. Recent studies showed that vehicle fleet electrification can reduce direct pollutant emissions from the transport sector of main gaseous pollutants (Section 1.2.2), such as CO, NO_x, VOCs, and can have positive impact on fine particulate matter ($PM_{2.5}$) pollution over Europe (Gómez Vilchez et al., 2019; Soret et al., 2014; Xu et al., 2020), the US (Babaee et al., 2014; EPRI, 2007; Pan et al., 2019), and China (Horton et al., 2021; Li et al., 2019; Liang et al., 2019). India, is

also expected to benefit from the introduction of EVs. Large scale vehicle electrification over India between 2020-2040 could reduce direct emissions of hazardous pollutants and $PM_{2.5}$ concentrations (Hakkim et al., 2022; He et al., 2021) and lead to net air quality and health benefits (Sen et al., 2021a,2).

As seen in Section 1.4.3, the Indian government is already promoting the shift to electric mobility, through a series of pledges and interventions, such as incentives and subsidies for electric two- and three-wheelers EVs in the country and the ambitious goal to reach 30% of EVs in all new vehicle sales by 2030 (EV30@30 campaign). For vehicles for which electrification is not yet possible nor affordable, such as heavy duty vehicles (HDV) or cars, alternative fuels already popular in India such as compressed natural gas (CNG) can be promoted as an interim solution.

However, the impact on air quality from the adoption of EVs can vary substantially between regions depending on existing transportation fleet, proximity to power generation, and the region's chemical regime (Requia et al., 2018; Schnell et al., 2019). For urban environments, which are VOC-limited like Delhi (Section 1.2.2), we have seen that reduction in transport emissions could lead to adverse increase in O_3 and potentially hinder the health benefit from $PM2.5$ reduction (Chapter 3). In particular, reduction in NO_x emissions without enough reduction in VOCs emissions could lead to significant O_3 increase under a continued VOC-limited regime in Delhi (Chen et al., 2021; Nelson et al., 2021). Consideration of the specific chemical environment at the city level scale is thus needed to carefully assess the effects of large scale introduction of EVs and clean-fuel vehicles on air quality. However, the impact of future vehicle electrification strategies remain understudied for Indian cities.

In this chapter we use the WRF-Chem model to investigate how $PM_{2.5}$ and O_3 surface concentration in Delhi would be impacted by large-scale introduction of EVs and cleaner fuels adoption in two contrasting season, pre-monsoon and post-monsoon. We drive WRF-Chem with four possible transport emissions scenarios for year 2030, which include detailed projections for each pollutant and vehicle type. We then assess the impacts of each scenario on concentration of $PM_{2.5}$ and O_3 over Delhi and its district (Figure 1.13). In the next section we describe the data and methods used, which include a summary of the WRF-Chem model set-up and projections of future transport emissions used. We present our results in section 4.3. Section 4.4 presents the final discussion and conclusions.

4.2 Data and Methods

4.2.1 Model setup and emissions

The baseline WRF-Chem set-up and emissions used in this Chapter is the same one used in the previous Chapter 3 (Section 3.2.1) at the exception of the simulation period. We run a baseline simulation for a representative period of the pre-monsoon season from 1st April to 30th of April 2019, and of the post-monsoon season from 1st October to 31st October 2019. Each of the two simulations include 3 days spin-up to minimize the influence of the initial conditions at the start of the model run.

To assess the impact of future transport emissions over Delhi, 4 different future scenarios are considered for year 2030, representing short to medium term traffic emissions interventions. We use the future transport emissions scenarios developed in Hakkim et al. (2022) for India for 2030. Projections are developed for major air pollutants and speci-

Scenario	Description
BAU	Business as Usual scenario. Road transport emissions projected of under a SSP-5.
S1	All 2W and 3W are converted to electric vehicles for all fuel types.
S2	3W, 4W and HDV vehicles fueled by diesel are converted to CNG.
S3	S1+S2 scenario combined.

Table 4.1: Summary of future transport emissions scenarios from transport in India for 2030 developed in (Hakkim et al., 2022) and used in this study.

ated NMVOCs by vehicle type, which are based on the new Road Transport emission inventory for India (RTEII) (Hakkim et al., 2021). The projections cover India at 10km resolution. The four emissions scenarios are summarised in Table 4.1, and described below:

- **BAU: Business as Usual scenario.** This scenario represents the projected road transport emissions for the year 2030 under a Shared Socioeconomic Pathways (SSPs) projection 5 (SSP-5), which seems to best capture current trends in the Indian transport sector (Kriegler et al., 2017). The SSP-5 is usually referred to the ‘’Fossil-Fueled Development” scenario. It describes a world scenario of high fossil fuel use, resource intensive development and high consumption patterns, resulting in up to tripling the global energy demand and greenhouse gas emissions over the course of the century (Kriegler et al., 2017). In the BAU scenario, no EVs are introduced in the fleet.
- **S1: All 2W and 3W are converted to electric vehicles for all fuel types.** Especially in urbanised areas of India, 2W and 3W area popular means of transport, because of their fuel efficiency and their important role for private, commercial and commuting transportation needs. The 2W and 3W fleets have expanded rapidly, and they are forecasted to grow further with government subsidies under the FAME initiative.

This scenario aims to represent the impact of large scale adoption of electric vehicles for the popular segment in India of 2W and 3W. This scenario is relevant for urban environment such as Delhi where exposure to road emissions is the highest and where 2W and 3W are widespread.

- **S2: 3W, 4W and HDV vehicles fueled by diesel are converted to CNG.** The shift to EVs for passenger cars and HDV are still not affordable or, in the case of HDV, there are no yet available EVs technologies and infrastructure. Alternative fuels such CNG can be an interim more sustainable solution for these segments compared to diesel fuel, while maintaining the current vehicle fleet through retrofitting and using the existing refuelling infrastructure. This scenario aims to represent the impact of interim strategies in the short and medium term promoting a shift from diesel to more sustainable fuel such as the already popular CNG in India.
- **S3: S1 and S2 combined**. This scenario considers the combination of the intervention for electrification of all 2W and 3W and the substitution of diesel 4W and HDV vehicles with CNG, of hence aiming to represent the maximum impact from transport emissions reduction policy short to medium term interventions.

Table 4.2 summarises the simulation performed in this research chapter. We assume that electric vehicle are fully electric, and we assume that all other sectors emissions remain at the same level of the baseline scenario, in order to isolate the effect of emissions projections for the traffic sector. In particular, for the energy sector, recent studies have shown that the marginal increase in energy demand to charge 2W and 3W EVs is estimated to be less than 5% in 2030 in India (Barbar et al., 2021). Thus it is not a drastic assumption to neglect the contribution of increase in power generation emissions as byproduct of vehicle electrification. We also assume no seasonal variations in transport emissions, so that emissions from the transport sector are the same for each scenario for the pre- and post-monsoon seasons. Only the diurnal cycle of transport emissions, which is assumed the same for the two seasons, is included as we did for the set-up in

Run	Description
BASE	Baseline run. premonsoon: 1-30 April 2019; post-monsoon: 1-31 October 2019
BAU	transport emissions scenario Business as Usual. Run for the same period of baseline run for pre- and post-monsoon.
S1	transport emissions scenario with electric 2W and 3W . Run for the same period of baseline run for pre- and post-monsoon.
S2	Transport emissions scenario with diesel vehciles converted to CNG. Run for the same period of baseline run for pre- and post-monsoon.
S3	Transport emissions scenario combination of S1+S2. Run for the same period of baseline run for pre- and post-monsoon.

Table 4.2: Summary table of the baseline and future scenarios simulations performed.

Chapter 3. Table For building the gridded projected emissions scenarios for Delhi, we obtain scaling factors for the Delhi area only for each emissions scenario from Hakkim et al. (2022). Scaling factors for each of the four future scenarios over Delhi are obtained for each individual pollutant species, fuel and vehicle type. We then apply these scaling factors to project our base TERI/ARAI emissions (Chapter 3), for each transport future scenario.

Figure 4.1 report the resulting scaled transport emissions integrated over Delhi for each scenario. Further details on the projections can be found in (Hakkim et al., 2022). For NOx emissions, there is a $\sim$30% reduction in the BAU scenario compared to the BASE scenario. The future stringent emissions regulations are projected to overcompensate for the increase in travel demand and activity, as it happened in Europe and in the US (Section 1.4). Electrification of 2W and 3W (S1) lead to a further 8% decrease in NOx emissions from transport, while the conversion of vehicles to CNG (S2) drives an increase in NOx compared to the BAU scenario (+$\sim$20%). This is because NOx emissions from certain vehicle types increase when converted to CNG. The S3 scenario brings a NOx reduction compared to the S2, accounting for the reduction in emissions from 2W and 3W electrification. All future scenarios compared to the BASE lead to a

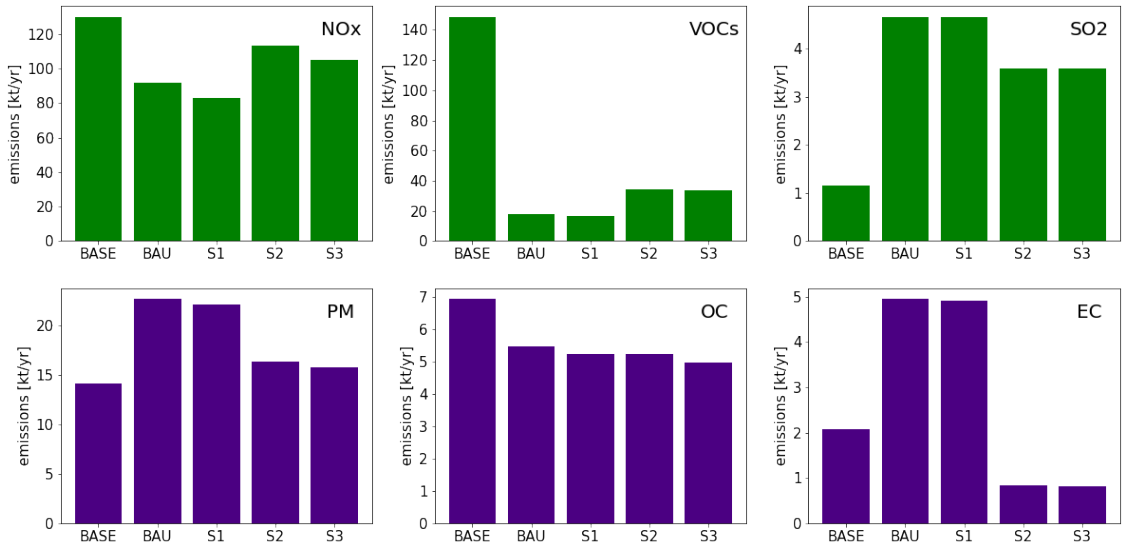

Figure 4.1: Yearly transport emissions in Delhi for main pollutants for each future transport emission scenario in Table 4.1. The BASE scenario refers to transport emissions from the baseline run (TERI/ARAI emissions, 2016). Gaseous pollutants are colored in green, while aerosols pollutants are colored in purple.

decrease of VOCs (>∼80%), lead mainly by stringent regulations for VOCs emissions in the BAU scenario. As for NOx, conversion to CNG diesel vehicles leads to an increase of VOCs emissions compared to the BAU and S1 scenarios (+50%). Contrary to gaseous pollutants, for direct aerosol emissions, the BAU and S1 shows and increase in PM and EC compared to the BASE scenario (+50% and +120% respectively), while conversion to CNG (S2) drives a net decrease in particulate emissions compared to the BAU (∼30% for PM and ∼80%). This is because diesel heavy duty vehicles and passenger cars account for 60-70% of total fuel consumption and are the main contributor to PM pollutants, so their conversion to cleaner CNG lead to a drastic reduction of direct aerosol emissions Hakkim et al. (2021,2).

4.2.2 Observations for model evaluation

We evaluate the model performance evaluated against ground based observations from the central Central Pollution Control Board (CPCB), as done in Chapter 2 (Section 2.3.1) and Chapter 3 (Section 3.2.3). Hourly observations of $PM_{2.5}$ and O_3 at monitoring stations in Delhi have been downloaded for the full months of April and October 2019 from the CPCB portal (CPCB, 2021). We clean the data following the procedure described in Section 2.3.1. The resulting selected stations are shown in Figure C.1 and their full list and pollutant monitored can be found in Table C.1.

4.3 Results

4.3.1 Model evaluation

For the evaluation of the model performance in simulating $PM_{2.5}$ and O_3, we match model gridcells to observation sites using nearest neighbour approach as we did in Chapter 2 and Chapter 3. Figure 4.2 shows the comparison of modeled surface $PM_{2.5}$ and modeled 8-hour daily maximum O_3 (MDA8 O_3) with observations at monitoring sites for both pre-monsoon and post-monsoon. The WRF-Chem model tends to overestimate $PM_{2.5}$ concentrations over Eastern Delhi districts in both seasons. However, on average the model captures well $PM_{2.5}$ values in both seasons. Averages of the individual station statistics show a positive bias to observations within 10% NMB=0.09 (NMB range across stations from -0.28 to +0.44) for pre-monsoon, and NMB=0.03 (NMB range across stations from -0.22 to +0.25) for post-monsoon. The model is able to capture diurnal patterns of $PM_{2.5}$ at almost all sites in both seasons as shown Figure 4.3 and 4.4 with average r=0.82 across observations sites (range from r=-17 to r=0.98) during pre-monsoon and average across observations sites r=0.93 (range from r=0.29 to r=0.97) for post-monsoon.

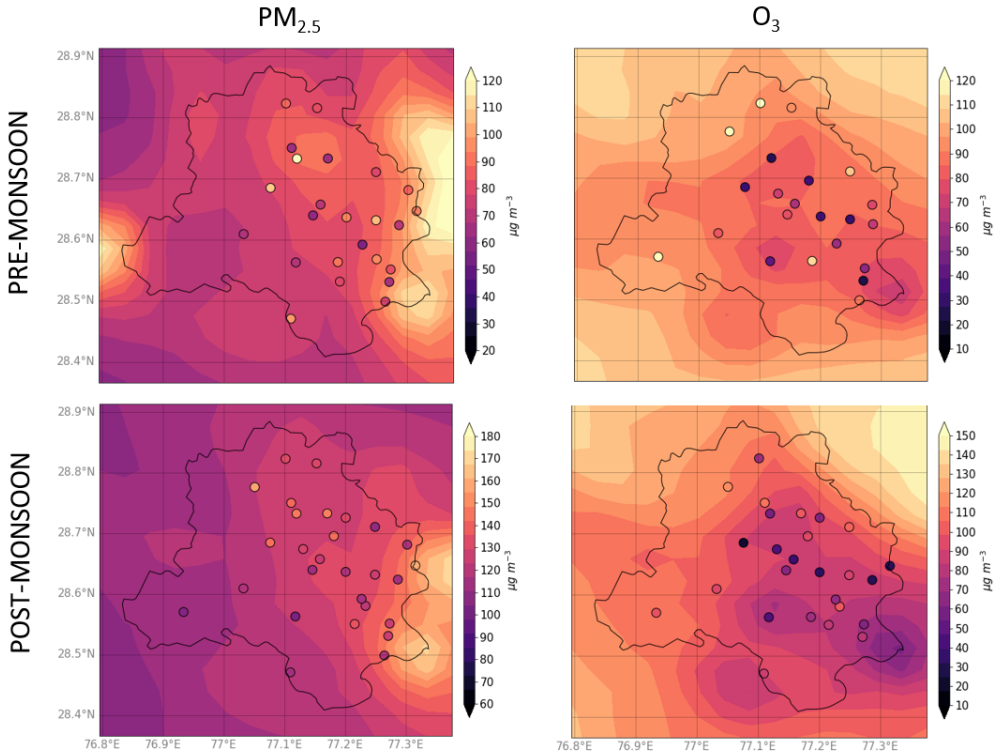

Figure 4.2: Modeled and observed (dots) average surface $PM_{2.5}$ and 8-hour daily maximum O_3 (MDA8 O_3) evaluation for pre- and post-monsoon seasons. Modeled time periods: pre-monsoon 1-30 April 2019, post-monsoon 01-31 October 2019.

For ozone, the model has the tendency to overestimate surface values, with higher bias for MDA8 ozone for pre-monsoon (averages of the individual station statistics NMB=0.31, range from -0.31 to 1.7) than post-monsoon (averages of the individual station statistics NMB=0.17,range from -0.12 to 3). Higher biases are found at stations in the central and east part of Delhi. This might be because these are the most densely populated areas of the city (Figure 1.12), and the model is unable to capture at 4km resolution the emissions sources that determine the chemical environment for local ozone formation, such has high NOx emissions from road-traffic. However, the diurnal cycle of ozone is captured in the majority of stations by the model in both seasons (Figure 4.5 and 4.6) with r=0.92 averaged across observation sites (range from r=0.78 to r=0.96) during pre-monsoon, and r=0.93 averaged across observations sites (range from r=0.56 to r=0.97) for post-monsoon.

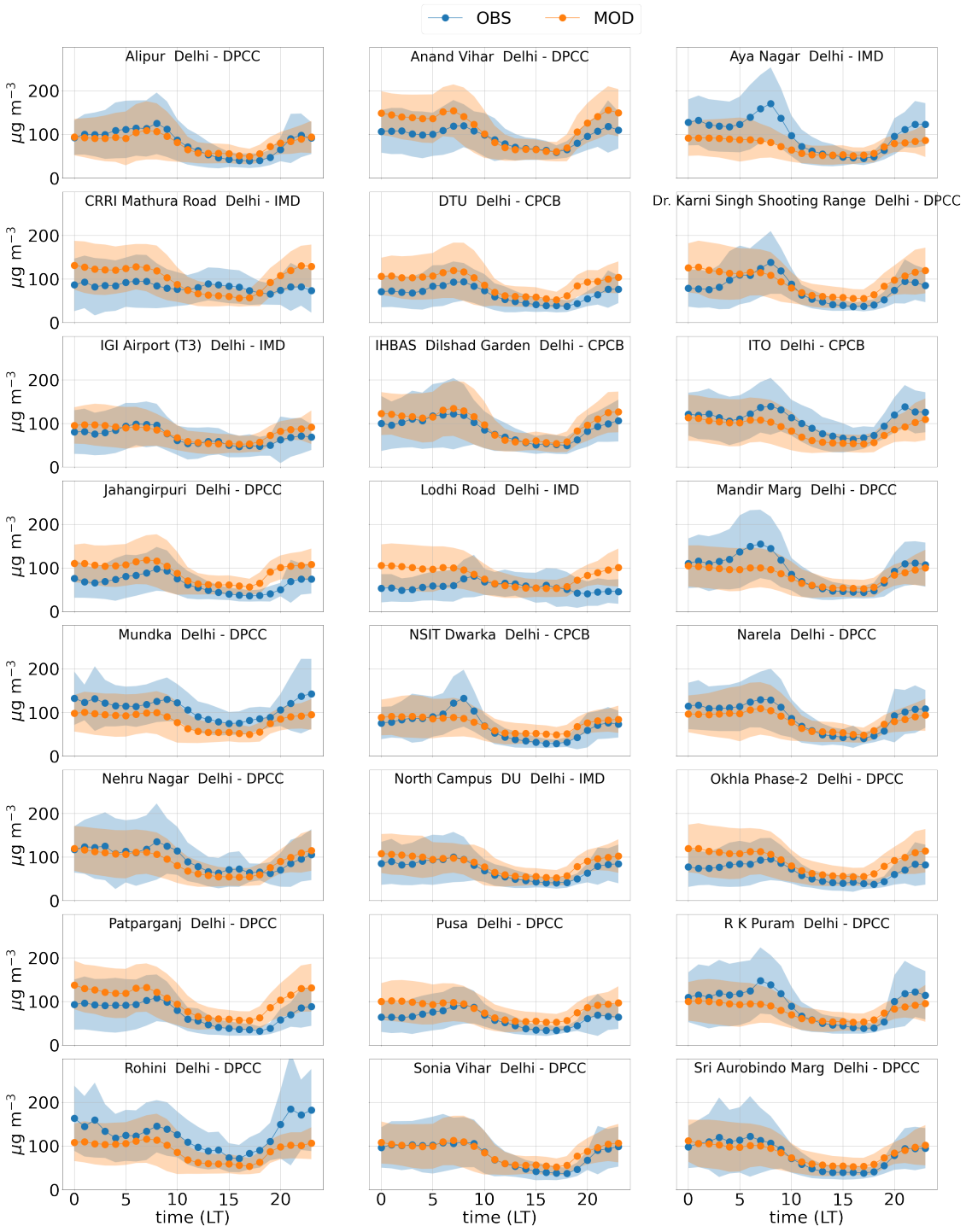

Figure 4.3: Modeled and observed $PM_{2.5}$ average diurnal cycle at selected stations for the pre-monsoon season. The shaded areas represent the standard deviation on the time dimension across stations. Modeled time period: 1-30 April 2019

Figure 4.4: Same as Figure 4.3 but for post-monsoon season. Modeled time period: 01-31 October 2019.

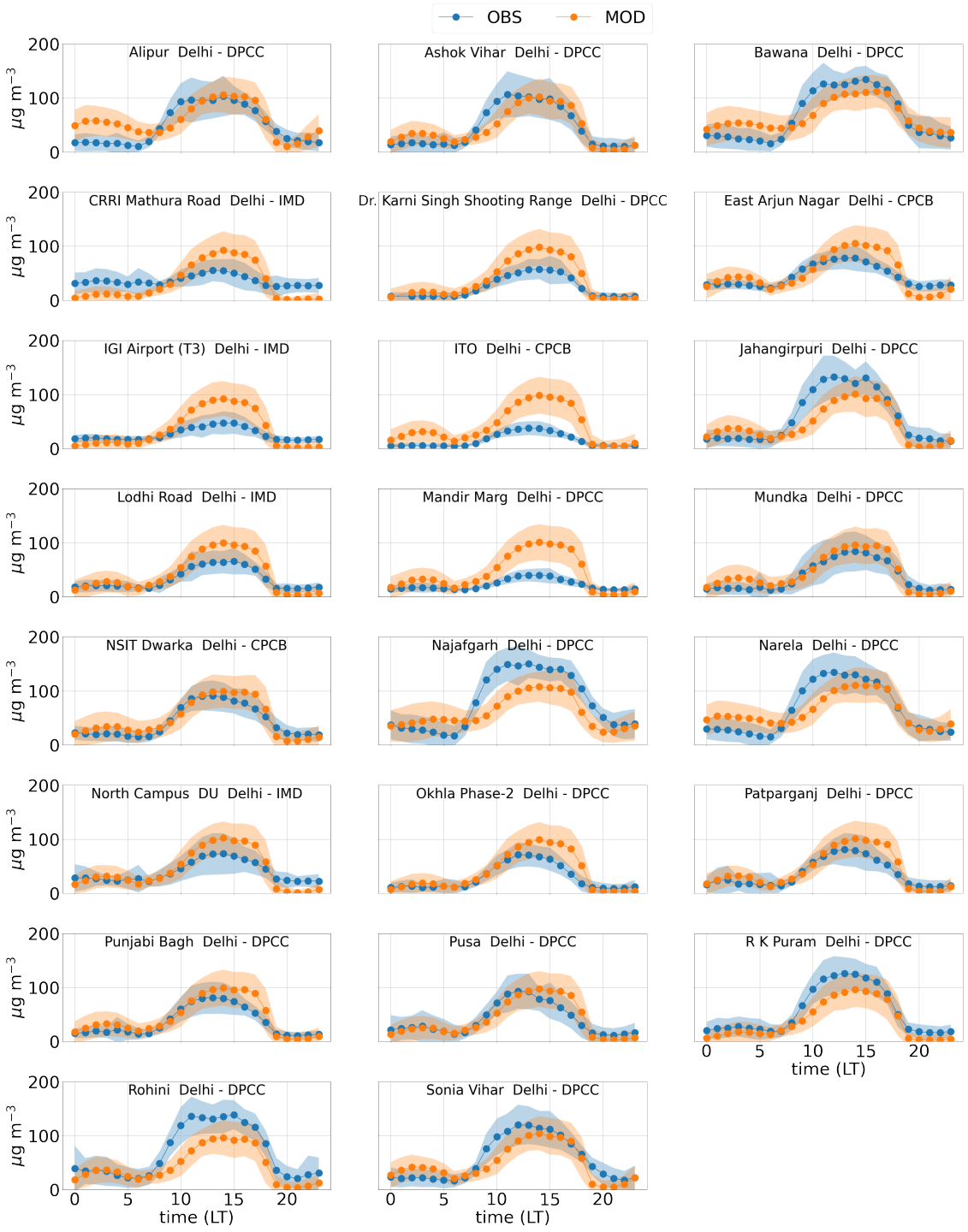

Figure 4.5: Modeled and observed O_3 average diurnal cycle at selected stations for the pre-monsoon season. The shaded areas represent the standard deviation on the time dimension. Modeled time period: 1-30 April 2019.

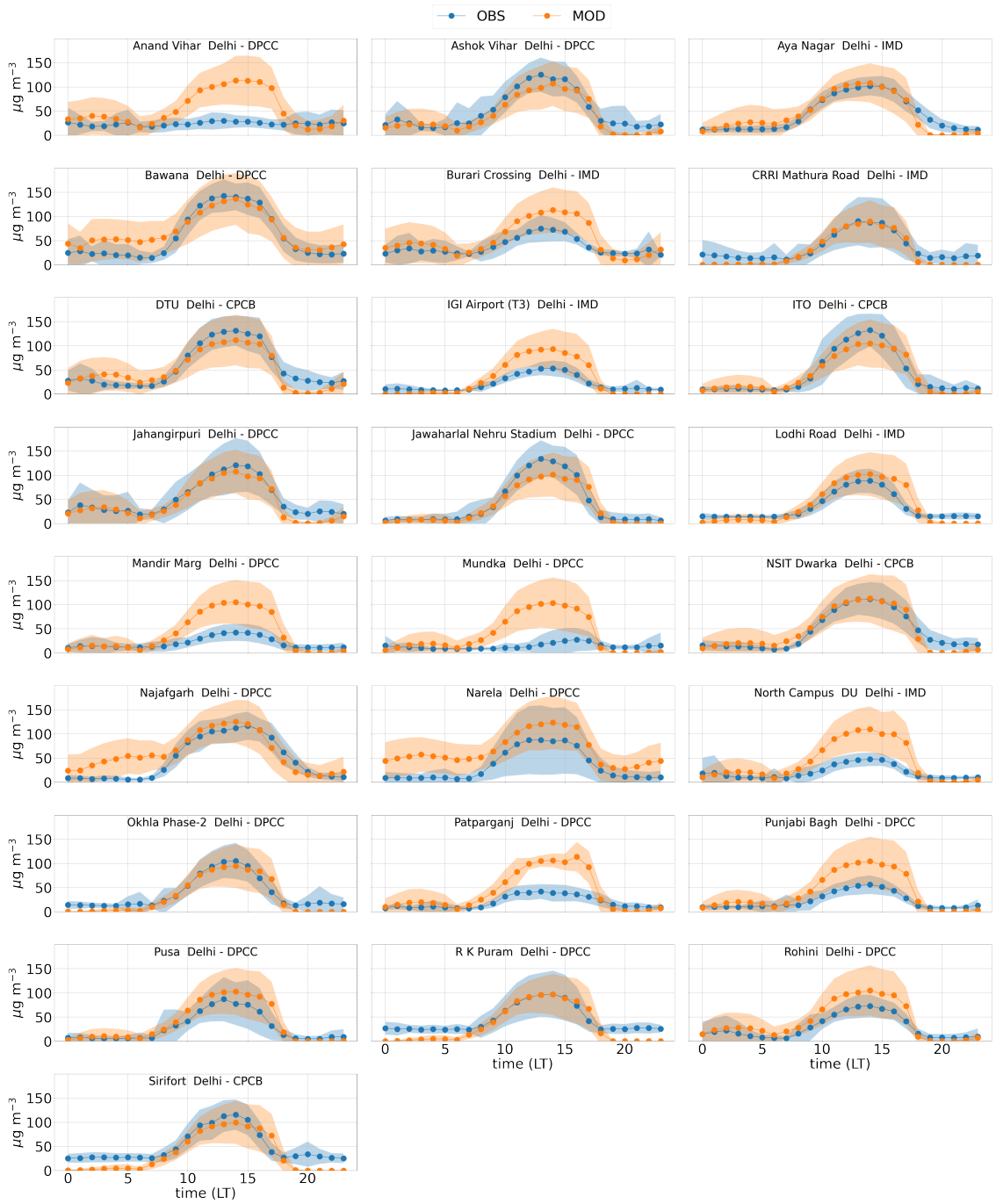

Figure 4.6: Same as Figure 4.5 but for post-monsoon season. Modeled time period: 01-31 October 2019.

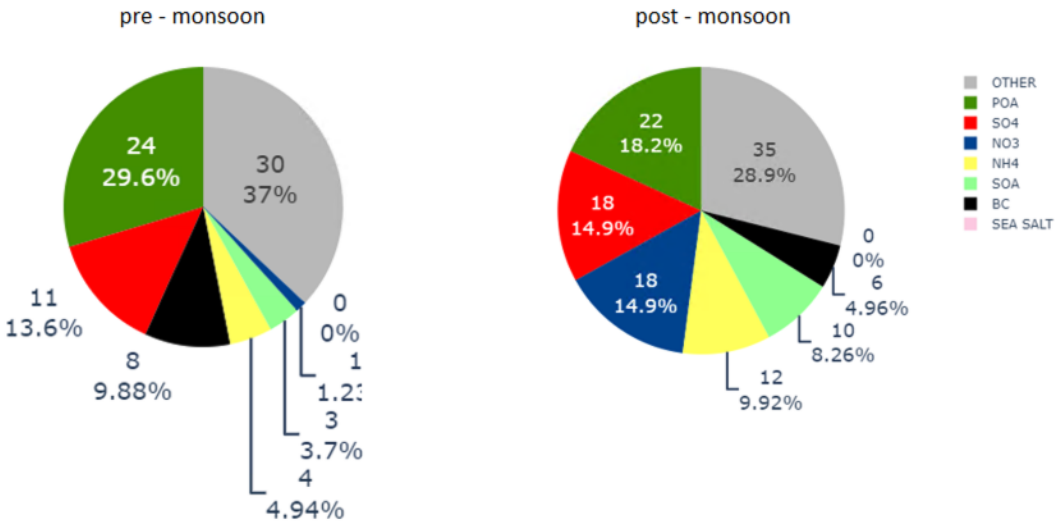

Figure 4.7: Pre-monsoon (left) and post-monsoon (right) average modeled $PM_{2.5}$ composition across Delhi. OTHER = dust,SO_4 = sulfate, NO_3 = nitrate, NH_4 = ammonium, POA = primary organic aerosols, SOA = secondary organic aerosols, BC = black carbon, SEA SALT = sodium chloride. Numbers refers to mass concentrations ($\mu g\ m^{-3}$). Modeled time periods: pre-monsoon 1-30 April 2019, post-monsoon 01-31 October 2019.

For $PM_{2.5}$ composition we evaluate the average composition across entire Delhi, given the lack of extensive observations of $PM_{2.5}$ components across the city. The modeled chemical $PM_{2.5}$ composition for both pre-monsoon and post-monsoon is shown in Figure 4.7. The modeled inorganic fraction (sulfate, nitrate, ammonium) accounts between $\sim$ 20-40% of the total $PM_{2.5}$ mass, while the organic fraction (primary and secondary organic aerosols) for $\sim$ 20-30%, black carbon for $\sim$ 5-10%, with higher values for the post-monsoon season compared to the pre-monsoon season. In particular, the nitrate component may be higher in postmonsoon compared to pre-monsoon period because of higher fossil fuel combustion from residential and energy use. This a result we found in Chapter 2 as well (Figure 2.6). Previous measurement studies of $PM_{2.5}$ composition over Delhi reported the elemental carbon (equivalent to black carbon in models) fraction to be $\sim$ 5-15 %, the total inorganic fraction $\sim$ 20-30%, the organic fraction (OA, usually calculated as 1.4 times organic carbon, OC) between $\sim$ 15-35% (Bawase et al., 2021;

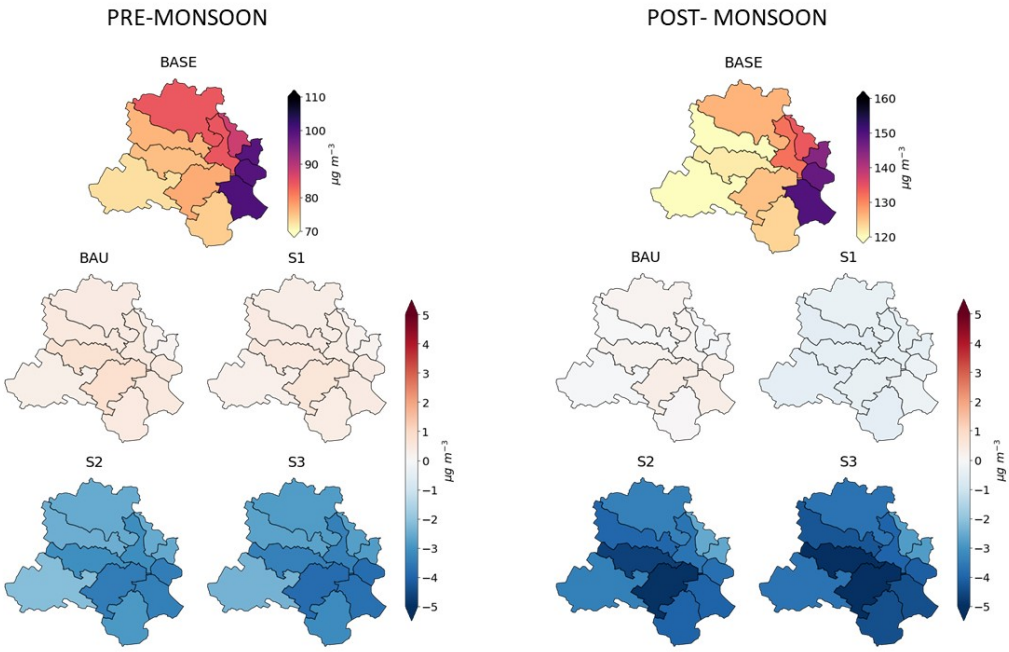

Figure 4.8: Modeled average $PM_{2.5}$ concentrations for the BASE scenario and differences between concentrations obtained with the four future emissions scenarios and BASE scenario for pre-monsoon (left) and post-monsoon (right) seasons. Modeled time periods: pre-monsoon 1-30 April 2019, post-monsoon 01-31 October 2019.

Dumka et al., 2017; Jain et al., 2020). Our modeled $PM_{2.5}$ composition is of the same order of magnitude of these results, although comparing modelled composition to studies covering different period and years doesn't take into account interannual variability of the chemical and meteorological environment, as already highlighted in the Chapter 3 (Section 3.3.1).

4.3.2 $PM_{2.5}$ spatial distribution

Figure 4.8 shows how $PM_{2.5}$ surface concentration change in each Delhi district for each future emission scenario compared to the baseline case. Both during pre-monsoon and post-monsoon the baseline scenario shows a west-east increasing gradient $PM_{2.5}$ over Delhi with differences up to $\sim$ 30 $\mu g\, m^{-3}$ in both seasons, although average values are much lower in pre-monsoon (85 $\mu g\, m^{-3}$) than post-monsoon (131 $\mu g\, m^{-3}$). The highest concentrations are found in the eastern districts of Shahdara (SHA), East Delhi (ED),

South East Delhi (SED) (Figure 1.13) experiencing concentrations of $\sim$ 100 $\mu g\ m^{-3}$ during pre-monsoon and between 145-150 $\mu g\ m^{-3}$ during post-monsoon. The lowest concentrations are found over the districts South West Delhi (SWD), West Delhi (WD), North West Delhi (NWD) (Figure 1.13), between 73-76 $\mu g\ m^{-3}$ in pre-monsoon and between 115-122 $\mu g\ m^{-3}$ in post-monsoon. The remaining districts, Central Delhi (CD), New Delhi (ND), South Delhi (SD), North Delhi (NOD), North East Delhi (NED) (Figure 1.13) have concentrations in the range between 74-88 $\mu g\ m^{-3}$ in pre-monsooon and between 125 and 135 $\mu g\ m^{-3}$ in post-monsoon seasons.

The business as usual scenario (BAU) shows amost no changes to average $PM_{2.5}$ compared to the 2019 baseline scenario for all Delhi district in both seasons, with changes within +0.1-0.8 $\mu g\ m^{-3}$ during pre-monsoon and within $\pm$0.5 $\mu g\ m^{-3}$ during post-monsoon. We find similar results for the full electrification of two- and three-wheelers scenario (S1). For the S1 scenario $PM_{2.5}$ changes will be small and homogeneous across the city districts, but with opposite impact for the two seasons, with an average increase up to 0.6 $\mu g\ m^{-3}$ during pre-monsoon, and an average reduction up to 1 $\mu g\ m^{-3}$ during post-monsoon. This difference between the two seasons are possibly linked to the different meteorological and chemical environment of the two seasons, since transport emission projections are the same for both seasons. However, changes in $PM_{2.5}$ concentrations in S1 remain very small for both seasons (less than 1% change compared to the baseline values), thus it might be difficult to identify a clear driver for this change. The CNG conversion scenario (S2), will bring higher reduction in $PM_{2.5}$ for all districts, although within 5% compared to baseline scenario in both seasons. The reduction is 2.2-3.5 $\mu g\ m^{-3}$ in pre-monsoon, and 2.5-5 $\mu g\ m^{-3}$ in post-monsoon. The highest reduction will be reached over the districts of ND, WD, SED in both seasons (-3.5 $\mu g\ m^{-3}$ in pre-monsoon and -4-5 $\mu g\ m^{-3}$ in post-monsoon). The smallest reductions occur in the NED and SHA districts (-2.1 and 2.4 $\mu g\ m^{-3}$ in pre-monsoon and -2.6 $\mu g\ m^{-3}$ in

post-monsoon). The combination of electrification and CNG conversion (S3), will bring similar improvements to the S2 in both seasons, since the main contributor to reduction is CNG conversion while electrification in S1 shows much more smaller and homogeneous changes across the city.

4.3.3 $PM_{2.5}$ diurnal cycle

Figure 4.9 shows the average change in $PM_{2.5}$ diurnal cycle compared to baseline diurnal cycle for each district. The absolute diurnal cycle concentrations for each scenario is reported in Figure 4.10 averaged over Delhi and in Figure 4.11 for each Delhi district. The average diurnal cycle change for each scenario follows a similar pattern for each district in both seasons. The BAU and S1 scenario have similar average hourly $PM_{2.5}$ concentrations. Compared to the baseline scenario, there is a small increase of $PM_{2.5}$ during the morning traffic peak (08:00-10:00, up to 1.3 $\mu g\ m^{-3}$ in pre-monsoon and 1.6 $\mu g\ m^{-3}$ in post-monsoon). In the central hours of the day (11:00-16:00) there is a small decrease in concentrations (-1 $\mu g\ m^{-3}$) for post-monsoon, while in pre-monsoon the concentrations remain almost unchanged compared to the baseline scenario. However the S1 scenario brings improvements (0.5 $\mu g\ m^{-3}$) during the evening traffic peak (18:00-21:00) compared to the BAU. The CNG conversion scenario (S2) brings consistent reductions of $PM_{2.5}$ for all districts at any hour of the day in both seasons. The highest reduction of $PM_{2.5}$ is observed at the evening traffic peak, with average reduction of -4.6 $\mu g\ m^{-3}$ in pre-monsoon (-6%) and of -6 $\mu g\ m^{-3}$ in post-monsoon (-4.5%), compared to baseline evening traffic peak values. Reduction at central hours of the day (11:00-16:00) are around half those at the evening traffic peak in both seasons (-2.5 $\mu g\ m^{-3}$ in pre-monsoon and -3.4 $\mu g\ m^{-3}$ in post-monsoon). The north-western districts of NOD, NWD, WD also exhibit a reduction of $PM_{2.5}$ during the morning traffic peak during pre-monsoon (-3.5 $\mu g\ m^{-3}$, up to 4.5%) compared to the other districts, where the reduction is not as pronounced. During post-monsoon only the eastern districts of CD, SHA, NED,

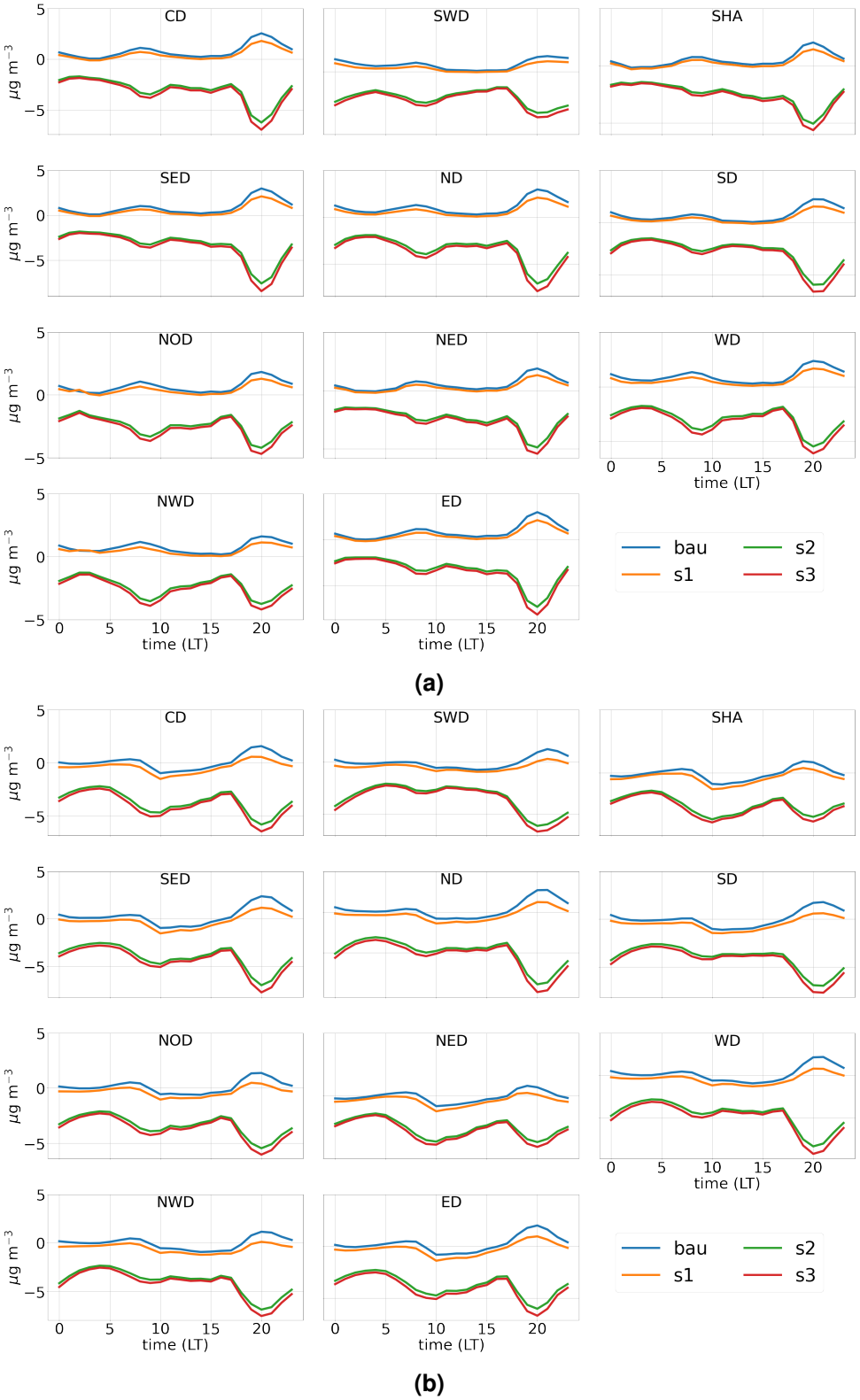

Figure 4.9: Average diurnal differences in $PM_{2.5}$ concentration between future transport emission scenarios and the baseline scenario by district in the pre- (a) and post-monsoon (b) seasons. See Figure 1.13 for a map of the districts. Modeled time periods: pre-monsoon 1-30 April 2019, post-monsoon 01-31 October 2019.

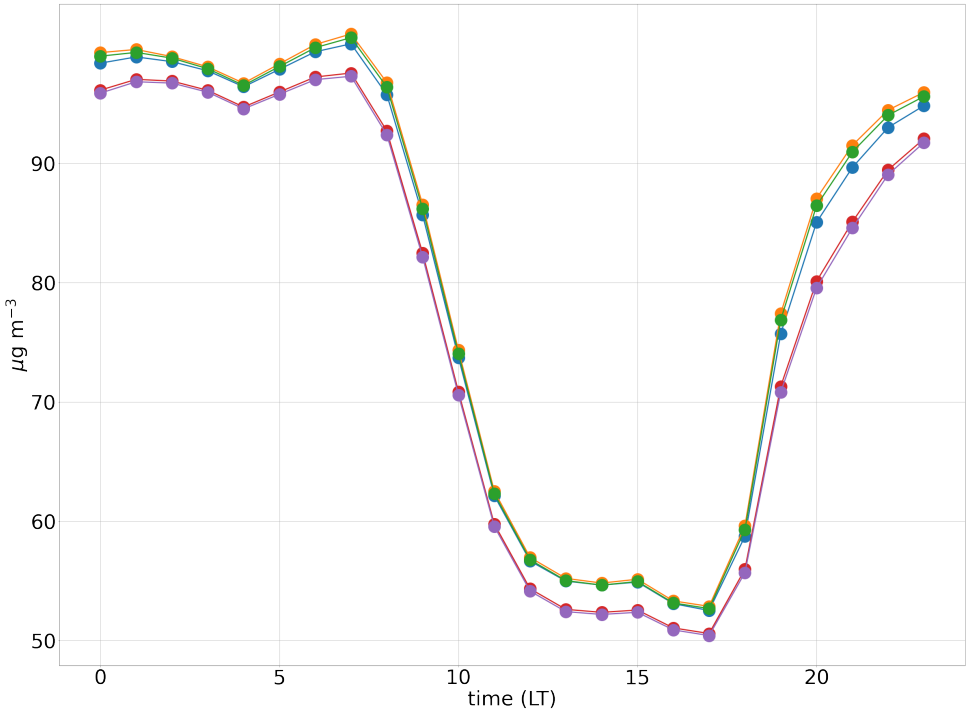

(a)

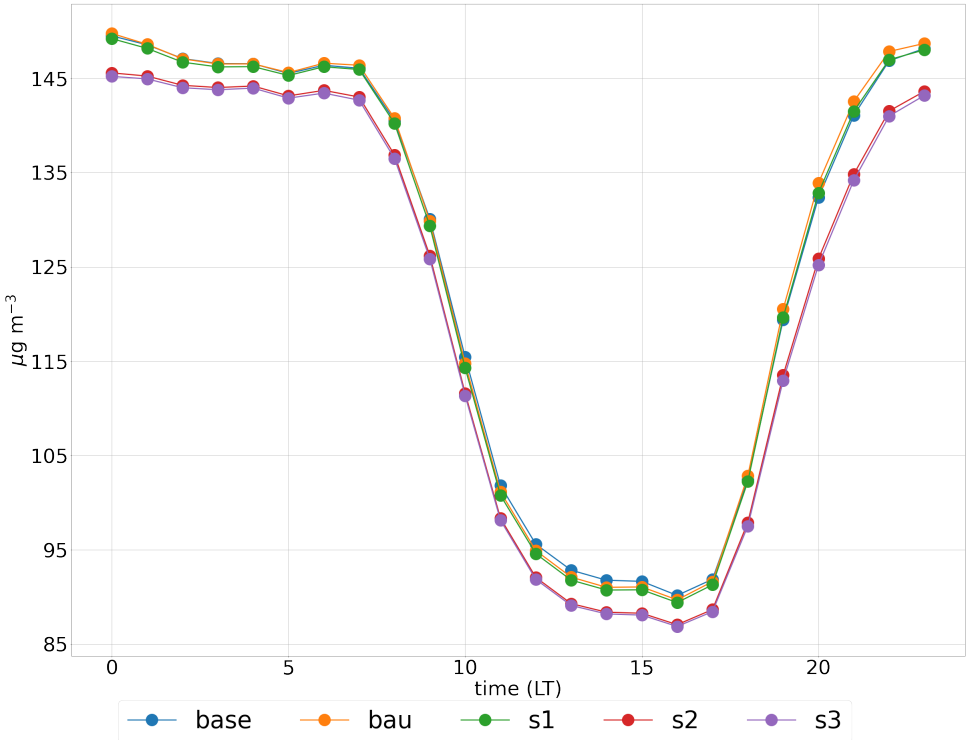

(b)

Figure 4.10: Modeled $PM_{2.5}$ diurnal cycle for the BASE scenario and each future transport emission scenario averaged over Delhi in the pre- (a) and post-monsoon (b) seasons. Modeled time periods: pre-monsoon 1-30 April 2019, post-monsoon 01-31 October 2019.

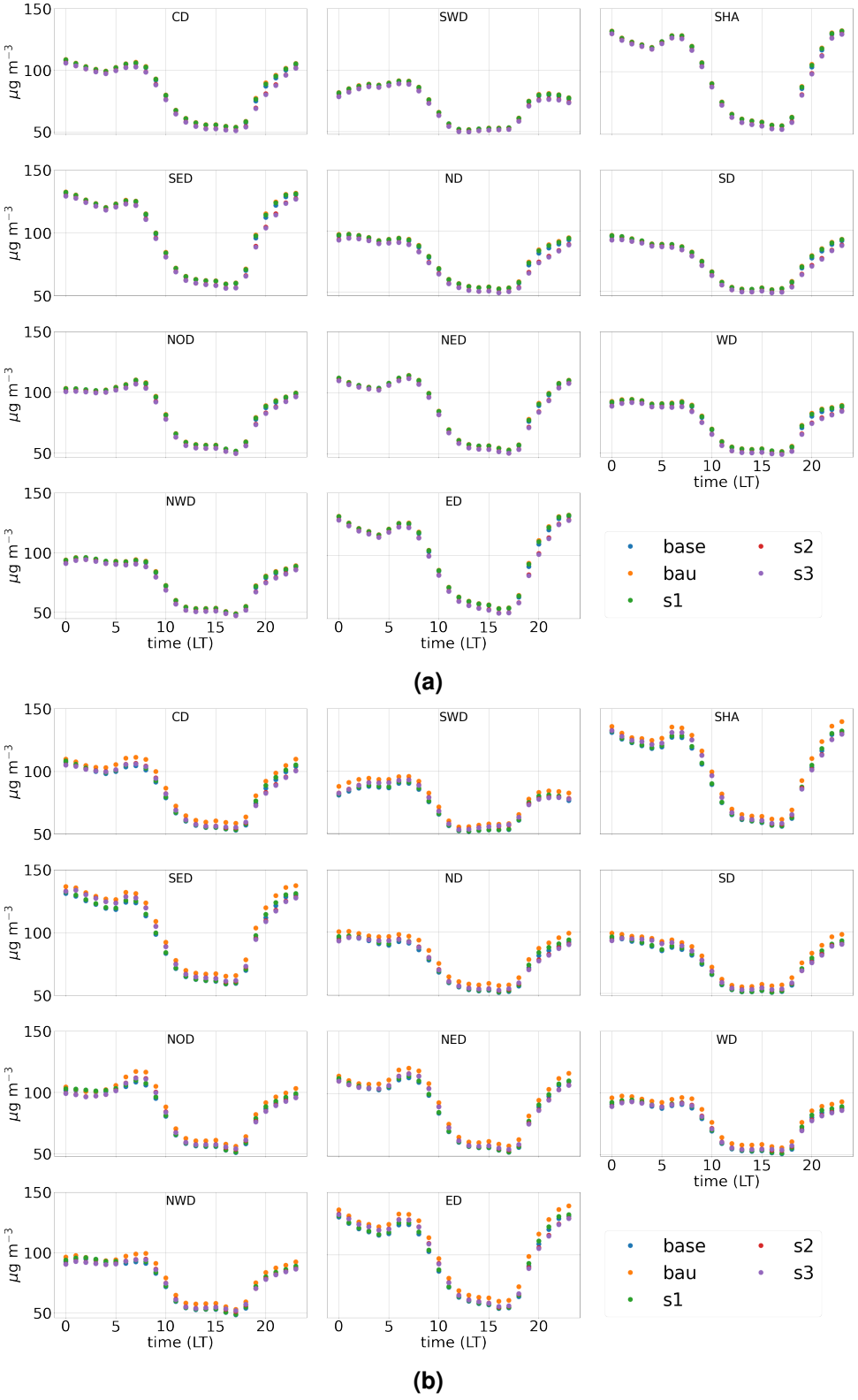

Figure 4.11: Modeled $PM_{2.5}$ average diurnal cycle for the BASE scenario and each future transport emission scenario in each Delhi district for the pre- (a) and post-monsoon (b) seasons. Modeled time periods: pre-monsoon 1-30 April 2019, post-monsoon 01-31 October 2019.

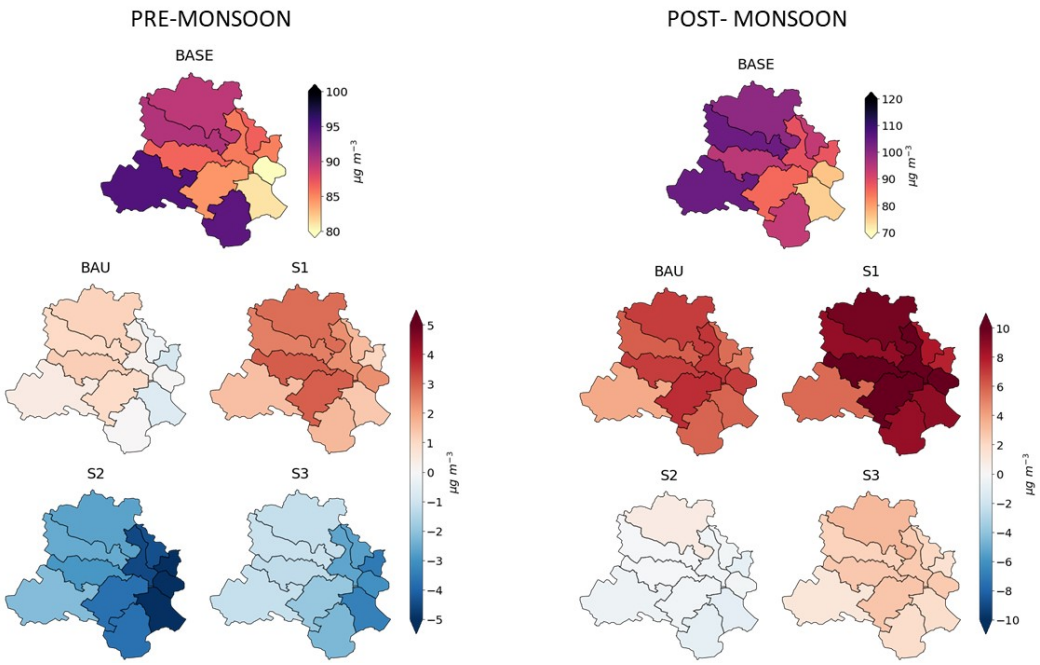

Figure 4.12: Modeled average MDA8 O_3 concentrations for the BASE scenario and differences between concentrations obtained with the four future emissions scenarios and BASE scenario for pre-monsoon (left) and post-monsoon (right) seasons. Modeled time periods: pre-monsoon 1-30 April 2019, post-monsoon 01-31 October 2019.

ED show a reduction of $PM_{2.5}$ during the morning traffic peak (-4 $\mu g\ m^{-3}$, up to 3%). The combined CNG and 2W and 3W electrification scenario (S3), shows almost equal reduction to S2 in average hourly values of $PM_{2.5}$. Compared to S2, S3 shows small additional reduction in evening traffic peak $PM_{2.5}$ concentrations (<1 $\mu g\ m^{-3}$) in both seasons.

4.3.4 O_3 spatial distribution

Figure 4.12 shows how MDA8 O_3 surface concentration changes in each Delhi district for each future emission scenarios compared to the baseline scenario. Average MDA8 ozone concentrations over Delhi are 87 $\mu g\ m^{-3}$ in pre-monsoon and 91 $\mu g\ m^{-3}$ in post-monsoon, with differences across districts of up to 15 $\mu g\ m^{-3}$ for pre-monsoon and 30 $\mu g\ m^{-3}$ for post-monsoon. The highest concentrations are found in the western and south districts of NWD, SWD, and SD with concentrations of 90-95 $\mu g\ m^{-3}$ in pre-

monsoon, and in the western and north NWD, SWD, and NOD with concentrations of 100-105 $\mu g\ m^{-3}$ in post-monsoon. Lowest values are found over the districts of ED, SED in both seasons, with concentrations of around 80 $\mu g\ m^{-3}$ (pre-monsoon) 75 $\mu g\ m^{-3}$ (post-monsoon) . The business as usual scenario (BAU) shows a slightly increase in MDA8 ozone during pre-monsoon (up to 1.2 $\mu g\ m^{-3}$, +1.4%) in all districts except for the eastern districts of NED, SED, SHA, which show a small decrease in ozone (up to -0.9 $\mu g\ m^{-3}$, -1%). For post-monsoon there is a net increase in average MDA8 ozone in all districts, with largest changes in ND, CD, NOD, ED, WD of 6.5-7.5 $\mu g\ m^{-3}$ (+7-9%) compared to baseline scenarios, while the remaining districts will experience increase between 5-6 $\mu g\ m^{-3}$ (+5-6%), and only the SWD district will have increase lower than 4 $\mu g\ m^{-3}$ (+3.6%). The electrification of 2W and 2W (S1) will drive further the increase in MDA8 O_3 with similar patterns to the BAU scenario in both seasons. The increase in pre-monsoon is between 1-3 $\mu g\ m^{-3}$ (+ 1.3-3.5%), while in post-monsoon is much higher, with increases between 6-11 $\mu g\ m^{-3}$ (+ 5-13%). The difference in MDA8 ozone changes for the BAU and S1 scenarios between the two seasons may be linked to differences in the meteorological environment. During the post-monsoon season, the changes in pollutant concentrations may be amplified by meteorological conditions that are less favourable for pollutant dispersion compared to pre-monsoon (Section 2.3.2 and Figure 2.3).

Contrary to BAU and S1, the CNG conversion (S2), will bring reduction of ozone compared to the baseline scenario. Reduction is higher during pre-monsoon season (between 2-5 $\mu g\ m^{-3}$, -2.3-5.3%), with an est-west gradient in the reduction, while during post-monsoon reduction is smaller (up to -1 $\mu g\ m^{-3}$) in every district except from NOD, which experiences a small increase (+0.8 $\mu g\ m^{-3}$). The combination of electrification and CNG

conversion (S3), will bring overall small decrease in ozone during pre-monsoon between 1-3 $\mu g\ m^{-3}$ (1.2-4 %) , with patterns similar to the S2 scenarios. During post-monsoon, the S3 scenario will bring a small increase in MDA8 ozone, with similar patterns of BAU and S1, but lower in magnitude than the S1 (< 3.3 $\mu g\ m^{-3}$, 3.5%).

4.3.5 O_3 diurnal cycle

Figure 4.13 shows the average changes in diurnal cycle of surface ozone compared to baseline diurnal cycle for each district. The absolute diurnal cycle concentrations are reported in Figure 4.14 averaged over Delhi, and in Figure 4.15 for each Delhi district. The impact of the different emissions scenario on ozone diurnal cycle is similar across the districts for both seasons. In all districts, there is a net increase in ozone during the evening traffic peak, greater in magnitude for post-monsoon than pre-monsoon. During post-monsoon the increase is up to 22 $\mu g\ m^{-3}$ for the S1 scenario, followed by the BAU scenario (up to 16 $\mu g\ m^{-3}$) the S3 scenario (up to 5 $\mu g\ m^{-3}$) and the S2 scenario (up to 3 $\mu g\ m^{-3}$). During pre-monsoon these values are almost halved. There is a second highest increase in the ozone during the morning traffic peak in post-monsoon, but almost halved in magnitude compared to the evening traffic peak increase (up to +12 $\mu g\ m^{-3}$ in the S1 scenario). This morning peak increase is almost absent in all districts during pre-monsoon. Although the magnitude of this increase is appreciable, the absolute hourly concentrations of ozone remain below 75 $\mu g\ m^{-3}$ during the evening and below the 100 $\mu g\ m^{-3}$ during the morning peak in both seasons (Figure 4.15). During daytime in pre-monsoon, The S1 scenario brings a small change in ozone of $\pm$ 0.7 $\mu g\ m^{-3}$ over the western and northern districts (NWD, WD, NOD, SWD), while it brings higher reduction over the eastern (ED,SHA), southern (SD, SED) and central districts (ND,CD), with reduction up to -3.5 $\mu g\ m^{-3}$. All the other scenarios on average bring reduction to ozone concentrations compared to baseline values, up to -5 $\mu g\ m^{-3}$ for the BAU to scenario, to -8 $\mu g\ m^{-3}$ for the S3 scenario and to -10 $\mu g\ m^{-3}$ for the S2 scenario, with

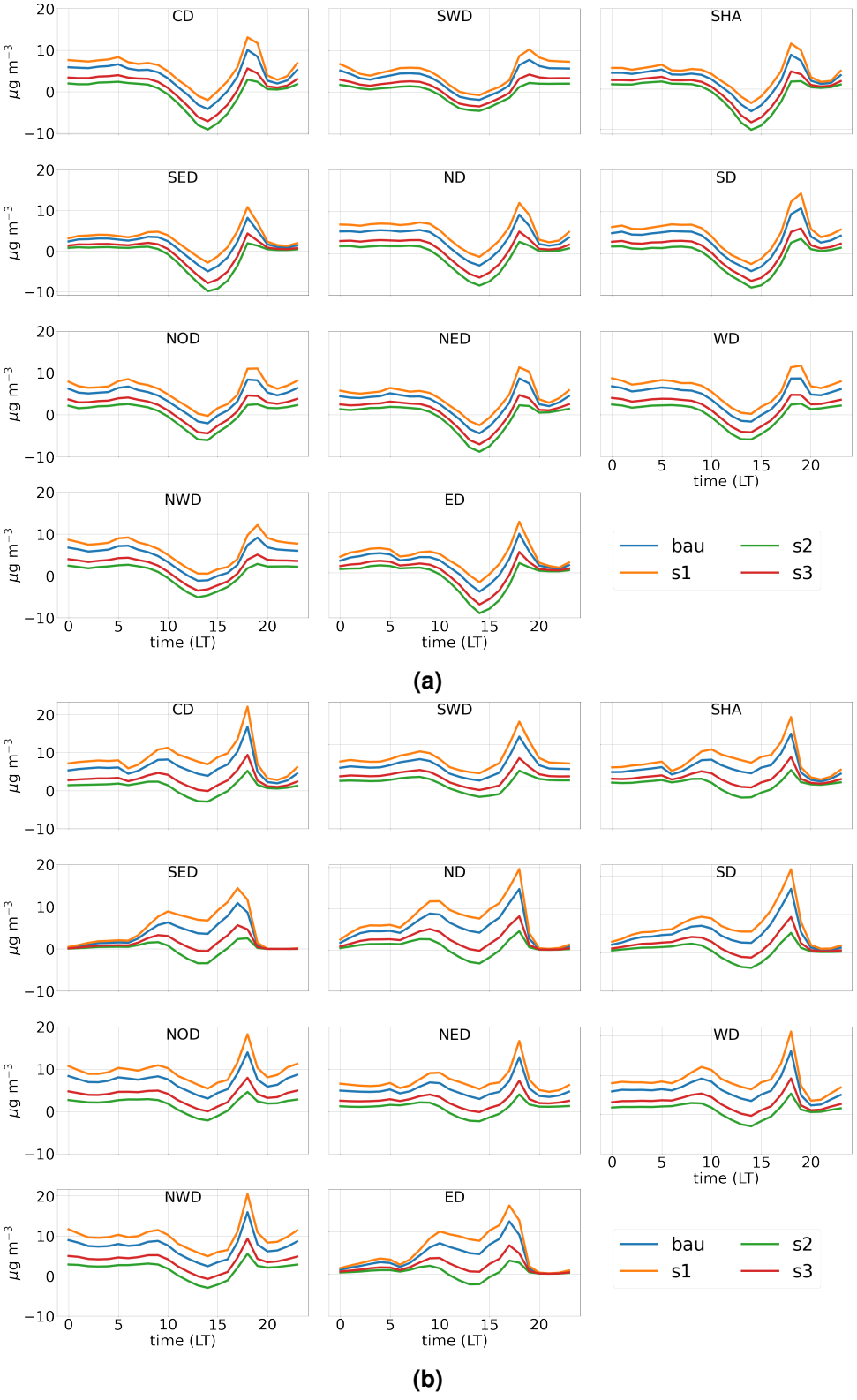

Figure 4.13: Average diurnal differences in O_3 concentration between future transport emission scenarios and the baseline scenario by district in the pre- (a) and post-monsoon (b) seasons. See Figure 1.13 for a map of the districts. Modeled time periods: pre-monsoon 1-30 April 2019, post-monsoon 01-31 October 2019.

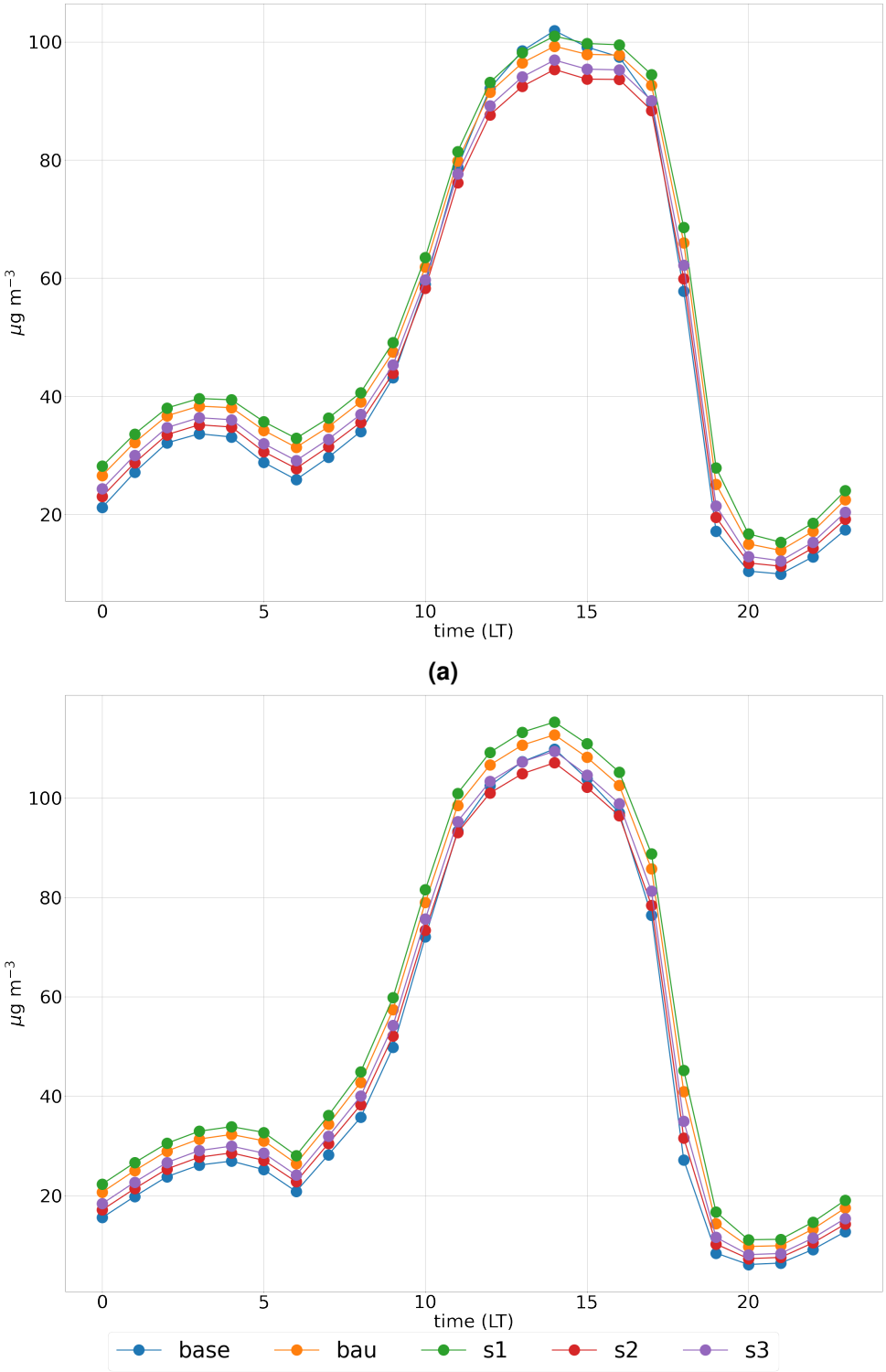

Figure 4.14: Modeled O_3 average diurnal cycle for the BASE scenario and each future transport emission scenario averaged over Delhi district for the pre- (a) and post-monsoon (b) seasons. Modeled time periods: pre-monsoon 1-30 April 2019, post-monsoon 01-31 October 2019.

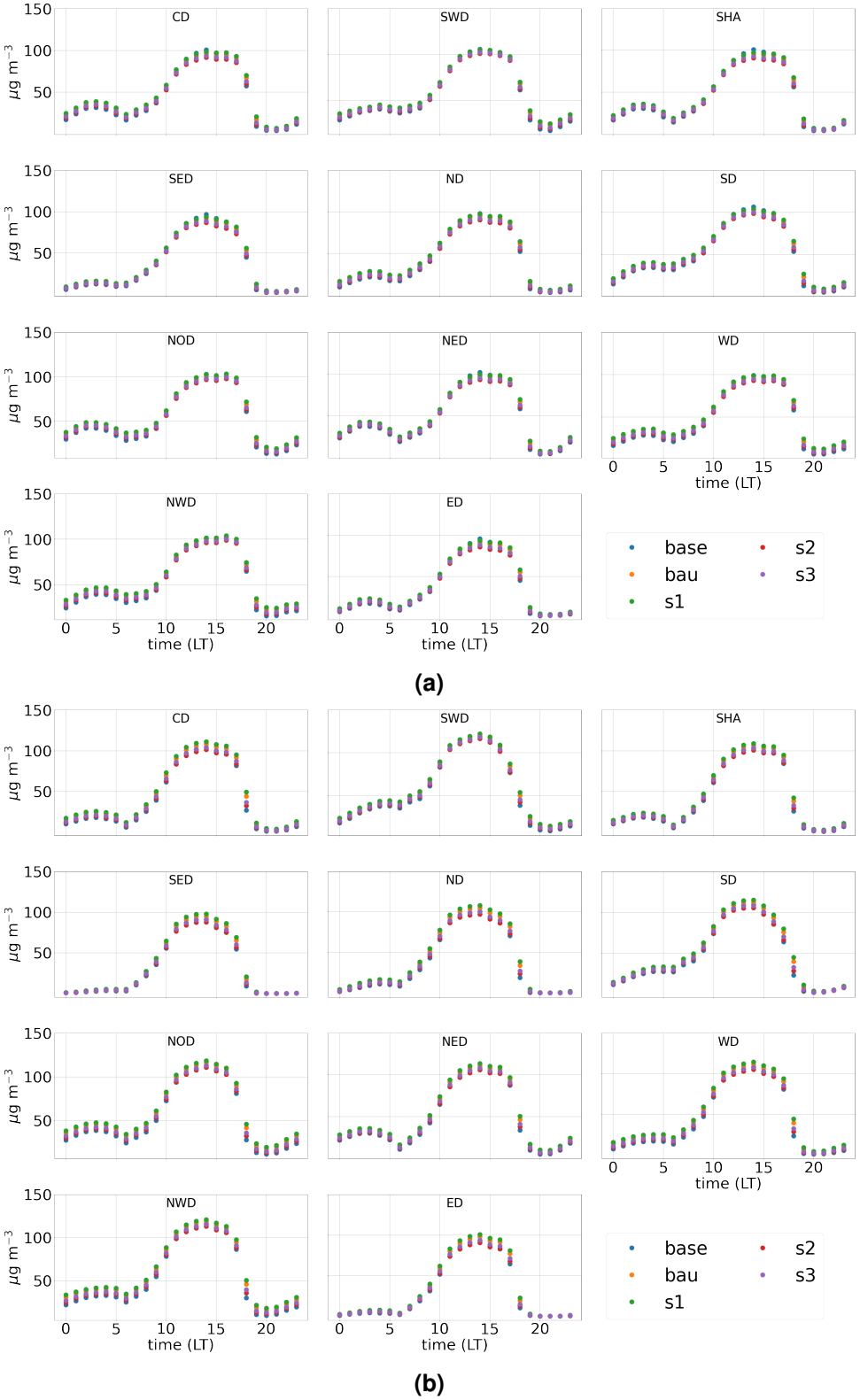

Figure 4.15: Modeled O_3 average diurnal cycle for the BASE scenario and each future transport emission scenario in each Delhi district for the pre- (a) and post-monsoon (b) seasons. Modeled time periods: pre-monsoon 1-30 April 2019, post-monsoon 01-31 October 2019.

central, southern and eastern districts experiences the highest reductions. During post-monsoon, S2 is the only scenario where concentration of ozone decreases for all districts d during the central time of the day compared to baseline scenario. The reduction for S2 during post-monsoon is almost one third of the one observed for pre-monsoon (up to -3.5 $\mu g\ m^{-3}$). For all the other scenarios, the increase is between almost zero (S3) and $\sim$ 8 $\mu g\ m^{-3}$ for S1 scenario. Nighttime values increase up to 5- 10 $\mu g\ m^{-3}$ for almost all districts in both seasons, except for ED, SED during post-monsoon, where nighttime increase is below 3.5 $\mu g\ m^{-3}$.

4.4 Discussion and Conclusions

In this final research Chapter, we investigated the impact of electric and clean-fuel vehicles on surface $PM_{2.5}$ and O_3 pollution over Delhi for two contrasting seasons, pre-monsoon and post-monsoon. We drive the WRF-Chem atmospheric transport model with four transport emissions scenarios for the year 2030: a business as usual scenario (BAU), total electrification of two- and three-wheelers (S1), conversion to compressed natural gas (CNG) of all diesel vehicles (S2), and the combination of the S1 and S2 interventions (S3). Our results show that the conversion of diesel vehicles to CNG brings a greater reduction in $PM_{2.5}$ concentrations (up to 5 $\mu g\ m^{-3}$) than the electrification of two- and three-wheelers (within $\pm$ 1 $\mu g\ m^{-3}$) compared to the 2019 baseline values. The greater reduction in $PM_{2.5}$ from conversion to GNG (S2) compared to 2W and 3W electrification (S1), is possibly driven by the greater reduction in primary emissions of $PM_{2.5}$ and EC for the S2 scenario than the S1 scenario (Figure 4.1). The S3 scenario shows results similar to the S2 scenario. The S2 and S3 scenarios have reductions of average hourly $PM_{2.5}$ especially during the evening traffic peak. However, the maximum reduction of daily average $PM_{2.5}$ concentrations for all scenarios is within 5% for both seasons.

We find that O_3 shows higher relative changes to baseline values due to changes in transport emissions than $PM_{2.5}$. Electrification of two- and three-wheelers increases average 8-hour daily maximum (MDA8) ozone by 1-3 $\mu g\ m^{-3}$ (1.3-3.5%) in the pre-monsoon season, and by 6-11 $\mu g\ m^{-3}$, (5-13%) in the post-monsoon season compared to baseline values. Conversion of all diesel vehicles to CNG (S2) reduces MDA8 O_3 by 2-5 $\mu g\ m^{-3}$, (2.3-5.3%) in the pre-monsoon season and up to -1 $\mu g\ m^{-3}$ for post-monsoon season. In the S3 scenario, the increase in O_3 due to two- and three-wheelers electrification (S1) is contrasted by the decrease due to CNG conversion (S2), resulting in a net small decrease in MDA8 O_3 in pre-monsoon (< 3 $\mu g\ m^{-3}$) and a small increase during post-monsoon (< 4 $\mu g\ m^{-3}$). These results for ozone may be explained by taking into consideration the ozone production regime in Delhi, which is VOC-limited (Figure 1.1), and the changes in transport emissions brought by each future scenario (Figure 4.1). As seen in the Introduction in Section 1.2.2, under a VOC-limited ozone production regime, ozone increases inversely with NOx concentrations, and linearly with VOCs concentrations. Although VOCs emissions are greater in the S2 and S3 scenarios compared to S1 scenario ($\sim$ +15 kt/yr, Figure 4.1), thus theoretically leading to an increase in ozone for S2 and S3, their increase is compensated by a much greater increase in NOx emissions. NOx emissions under the S2 and S3 scenario increase compared to the S1 scenario ($\sim$ +30 kt/yr Figure 4.1) thus potentially leading a reduction in ozone formation for S2 and S3 compared to S1.

Our findings show that the conversion of diesel vehicles to CNG tends to bring more air quality benefits than electrification of 2W and 3W for both $PM_{2.5}$ and ozone. However, the small reduction in $PM_{2.5}$ obtained (within 5 % to baseline values) highlights the need to combine traffic emissions reduction with emissions reduction from other sectors regardless of the season to achieve substantial reduction in $PM_{2.5}$ concentrations. Vehicle electrification alone could bring an increase in ozone concentrations especially during post-monsoon, while conversion to GNG brings reduction in ozone in both seasons. Thus,

electrification of 2W and 3W should be accompanied by the diesel vehicles conversion to CNG to limit ozone increase brought by EVs introduction. These findings highlights the importance of coordinated control of $PM_{2.5}$ and O_3 when considering emission control from traffic over Delhi. Given the positive bias in the model in reproducing absolute ozone concentrations, uncertainties remain in establishing if the increase in ozone will bring certain districts above the WHO recommended limit of 100 $\mu g\ m^{-3}$ for MDA8 ozone. This remains an important matter for future studies to address. Moreover, the changes in ozone from reducing transport emissions may depend on the proportion of VOCs and NO_x emitted from the road transport relative to other anthropogenic sources (Nelson et al., 2021). We considered these other sources as constant in this study, but in reality they are going to be targeted in emissions reduction strategies, and thus potentially change the chemical environment for ozone formation in Delhi. Finally, electrification of vehicles has higher potential for reduction of GHG emissions, while conversion to CNG might increase GHG emissions, especially methane (Andress et al., 2011; Pan et al., 2019; Qiao et al., 2020). Thus air quality benefit should be considered along with climate benefit in an integrated assessment of cleaner mobility strategies for the city of Delhi.

Chapter 5

Conclusions

In this chapter, I review and summarise the main aims and key findings of my thesis, and I discuss its implications along with limitations and uncertainties. Finally, I present possible routes of future work stemming out of this thesis.

5.1 Summary of key findings

With this thesis, I aimed at deepening our understanding of outdoor air pollution in Delhi megacity, the capital of India, with a focus on the impact of on-road transport emissions on surface levels of $PM_{2.5}$ and its implications for air quality policymaking. This goal was addressed by integrating high resolution atmospheric chemistry transport model, WRF-Chem, with locally developed emission inventories for Delhi, and by applying different sensitivity analysis techniques.

In Chapter 2 I investigated and quantified the seasonal drivers and source contributions to $PM_{2.5}$ and its components across the Indo-Gangetic Plain (IGP), where Delhi is located. A perturbative approach was used to compare the importance of anthropogenic, biogenic, and pyrogenic on seasonal surface distribution of $PM_{2.5}$ and organic aerosols across the IGP. In Chapter 3 I dealt with quantifying the role of the on-road transport sector on surface $PM_{2.5}$ over Delhi during the post-monsoon season, during which Delhi experiences severe levels of air pollution. I applied the emission reduction impact method (ERI) to quantify the contribution of on-road transport sector and its subsectors to $PM_{2.5}$

over Delhi. The on-road transport contribution to $PM_{2.5}$ was compared to the contribution of other main anthropogenic sectors, both from local and regional sources.

Finally, in Chapter 4 I investigated how the large scale adoption of electric and clean-fuel vehicles could impact air quality over Delhi in the future. The WRF-Chem model has been driven by four possible future transport emissions scenarios, and the impact on surface $PM_{2.5}$ and O_3 have been quantified for each scenario and compared to the current baseline situation across Delhi.

Below I provide a summary of the main findings of my thesis which addressed the main three scientific questions outlined at the beginning of this work in Section 1.1.

1. **What are the seasonal drivers of $PM_{2.5}$ in the Indo-Gangetic Plain, where Delhi is located?**

   (i) The IGP experiences the highest seasonal mean levels of $PM_{2.5}$ during the post-monsoon (October—December, 166 $\mu g\ m^{-3}$) and winter (January—February, 145$\mu g\ m^{-3}$) seasons with an heterogeneous spatial distribution, while surface $PM_{2.5}$ concentrations are lower during pre-monsoon (March—May, 95 $\mu g\ m^{-3}$) and monsoon (June—September, 79 $\mu g\ m^{-3}$) because of the influence of the monsoon which brings favourable meteorological conditions for pollutant dispersion. However, all seasonal mean values of $PM_{2.5}$ still exceed the recommended levels, indicating that air pollution is a year-round problem.

   (ii) Anthropogenic emissions influence the magnitude and distribution of $PM_{2.5}$ and organic aerosols (OA) throughout the year, especially over urban sites, while pyrogenic emissions result in localized contributions over the central and upper parts of IGP in all non-monsoonal seasons, with the highest impact

during post-monsoon seasons corresponding to post-harvest reside burning season. Biogenic emissions contribute to the magnitude and distribution of $PM_{2.5}$ and OA mainly during the monsoon season, and show a substantial contribution to secondary organic aerosol (SOA) particularly over the lower IGP, where evergreen forest land is present near the coast of West Bengal and Bangladesh.

(iii) Organic aerosol represents a significant contribution to $PM_{2.5}$ throughout the year. On average, OA represents between 17–30% of $PM_{2.5}$ mass, with higher contribution during post-monsoon and winter seasons. Typically, POA contributes more to the OA loading than SOA in all seasons across the IGP. Anthropogenic and pyrogenic sources impact POA and SOA with similar patterns of $PM_{2.5}$ across the IGP during all seasons. Biogenic sources have a significant impact on SOA distribution across the IGP during the monsoon season and are limited to the lower IGP during the pre- and post-monsoon seasons because of the presence of evergreen forests in this region.

2. **What is the role of the on-road transport sector on $PM_{2.5}$ over Delhi during the post-monsoon season?**

(i) By using the WRF-Chem model and a series of sensitivity runs we find that the response between changes in emissions from different emissions sectors and $PM_{2.5}$ concentrations is linear at the city level scale during post-monsoon. We defined the range of validity of the linear response, which holds for reduction in emissions within 75%.

(ii) Local on-road transport sector contributes typically less than 10% to daily mean $PM_{2.5}$ over Delhi, rising to 17% if regional on-road transport from broader regional National Capital Region (NCR) sources are included. The largest individual contributions to average 24-h surface $PM_{2.5}$ over Delhi are from regional power and industry (14%) and domestic (11%) sectors.

(iii) The industry and power sectors from NCR dominate nighttime and almost all daytime concentrations of $PM_{2.5}$ over Delhi (10-25% day-night), with significant contributions from the NCR domestic sector (7-15% day-night). The contribution from the local on-road transport sector to surface $PM_{2.5}$ is largest (18%) during the evening traffic peak, and if the contribution from the regional on-road transport sector is also included the total impact from the traffic sector reaches almost 30%.

(iv) Within the on-road transport sector, two- and three-wheelers dominate the on-road transport contribution to daily mean $PM_{2.5}$ values (50%), together with heavy duty vehicles (30%). Two- and three-wheelers and heavy duty vehicles account combined for 60-70% of the total on-road transport impact on $PM_{2.5}$ throughout the day, with local two- and three-wheelers accounting between 30-40% of the total on- road transport hourly impact on $PM_{2.5}$ during daytime hours. The combined contribution from passenger cars and light duty vehicles and from resuspended road dust is marginal. This is consistent with heavy duty vehicles and two- and three-wheelers subsectors accounting for 50% of PM and SO_2, for more than 80% of NO_x, and for more than 90% of NMVOCs emissions from total on-road transport sector.

(v) We find that reduction in emissions from the transport sector lead the increase in surface ozone concentrations, and this is consistent with Delhi being a VOC-limited urban environment. Decreasing emissions from other sectors led to similar (but smaller) increases in surface ozone. Through a simplified health impact model for coordinated control of $PM_{2.5}$ and ozone, we find that, during the post-monsoon season, emission reductions from domestic and industry and power sectors should be prioritised over reducing emissions from the on-road transport sectors, if all pollutants are to be reduced by the same amount.

3. **Which will be the impact of electric and clean-fuel vehicles on future air quality over Delhi?**

The impact of four possible transport emissions scenarios for year 2030 is investigated: business as usual scenario (BAU), total electrification of two- and three-wheelers (S1), conversion to compressed natural gas (CNG) of all three- and four-wheelers and heavy duty vehicles (S2), and the combination of these two interventions (S3).

(i) Conversion of diesel vehicles to CNG brings larger reduction in $PM_{2.5}$ across Delhi districts (up to 5 $\mu g\ m^{-3}$) than the full electrification of two- and three-wheelers (within $\pm$ 1 $\mu g\ m^{-3}$) compared to the 2019 baseline values. The S3 scenario leads to improvements similar to the CNG conversion only scenario. The S2 and S3 scenarios bring reductions of average hourly $PM_{2.5}$ especially

during the evening traffic peak. However, for both seasons the maximum reduction on average 24h $PM_{2.5}$ concentrations for all the scenarios is within 5%.

(ii) Electrification of two- and three-wheelers increases 8-hours daily maximum (MDA8) O_3 by 1-3 $\mu g\ m^{-3}$ (1.3-3.5%) in pre-monsoon and by 6-11 $\mu g\ m^{-3}$, (5-13%) for post-monsoon compared to 2019 baseline values. The S2 scenario will bring an overall reduction of MDA8 O_3 by 2-5 $\mu g\ m^{-3}$ (2.3-5.3%) for pre-monsoon and up to -1 $\mu g\ m^{-3}$ for post-monsoon compared to the baseline values. Reduction in O_3 concentrations during the central hours of the day is found for all scenarios in pre-monsoon (up to -10 $\mu g\ m^{-3}$) except for S1, while only the S2 scenario reduces O_3 in post-monsoon (up to -3.5 $\mu g\ m^{-3}$).

(iii) The greater reduction in $PM_{2.5}$ from conversion to GNG (S2) compared to 2W and 3W electrification (S1), is possibly driven by the greater reduction in primary emissions of $PM_{2.5}$ and EC for the S2 scenario than the S1 scenario. While for ozone, NOx emissions under the S2 and S3 scenario increase compared to the S1 scenario ($\sim$ +30 kt/yr) thus potentially leading a reduction in ozone formation for S2 and S3 compared to S1 under the VOC-limited environment in Delhi.

5.2 Implications

Collectively, the findings of my thesis highlight different factors that can be relevant for designing effective policies to meet $PM_{2.5}$ air quality standards over Delhi megacity, with a focus on mitigating the impact from the on-road transport sector.

First, targeting reduction emissions from the on-road transport sector within Delhi is necessary, but not sufficient to bring $PM_{2.5}$ levels over Delhi to meet air quality standard levels. Air quality over Delhi is strongly influenced by regional and seasonal pollution sources from the IGP. Thus, efficiently mitigating levels of $PM_{2.5}$ will require a range of regional and state-level policies that address the influences of intra- and inter- state anthropogenic, pyrogenic, and biogenic emissions. In particular, cooperation for mitigation strategies between the Delhi megacity and the broader NCR is needed during period of severe air pollution such as the post-monsoon season. Stringent emission reductions (between 50-75%) of on-road transport sector emissions within Delhi and the NCR need to be integrated with similar cuts in emissions from the industrial and energy and domestic sectors over the broader NCR.

Second, to mitigate the impact of the on-road transport sector on $PM_{2.5}$, the focus should be on two and three-wheelers and heavy-duty vehicles, since these are the two vehicle categories that have the biggest contribution on $PM_{2.5}$ impact. Reduction of emissions for these vehicle categories should be prioritised both within Delhi city and for the broader NCR. Although these results have been demonstrated for the post-monsoon season only, they are likely to hold in other seasons as well, given the almost constant rate of transport emissions throughout the year combined with the overall linearity of $PM_{2.5}$ response to change in transport emissions.

Third, looking at possible short to medium term traffic emissions interventions to mitigate air pollution, the conversion of diesel vehicles to compressed natural gas (CNG) has the potential to bring more air quality benefits than vehicles electrification, both for $PM_{2.5}$ and O_3. Since vehicle electrification alone could increase ozone concentrations, transition to electric mobility should be accompanied by the diesel vehicles conversion to CNG to limit ozone increase and further reduce $PM_{2.5}$ concentrations. This highlights the importance of coordinated control of $PM_{2.5}$ and O_3 when considering emission control from traffic over Delhi. If mitigation strategies focus exclusively on minimising $PM_{2.5}$

exposure, e.g. through massive vehicle electrification, elevated levels of surface ozone (O_3) could become more of a significant health concern. This is important in VOC-limited urban environments such as Delhi, where reduction of emissions, especially from transport sector, could increase the adverse health impact from rising of ozone levels.

5.3 Limitations and uncertainties

My thesis has illustrated the ability of the atmospheric chemistry modelling approach for reproducing and interpreting surface $PM_{2.5}$ concentration on a regional and city scale level over the IGP and Delhi. It also showed to be suitable and useful for investigating the impacts of different emissions sources on $PM_{2.5}$ and explore how $PM_{2.5}$ concentrations might change under future emission scenarios. However, there are uncertainties and limitations to the methods I used in this thesis, which I discussed below.

First, there are model limitations in simulating observations, as highlighted in each research chapter in the evaluation section. Accurately modelling $PM_{2.5}$ and its components is highly-complex because of the many processes and parameters involved, and their sensitivity to factors such as meteorological conditions and emissions, as well as the model set-up and its resolution. In particular, over South Asia, it is challenging for models to capture the monsoon driven meteorology, in particular rainfall (Kumar et al., 2012b), which has implication on aqueous phase aerosol chemistry, wet deposition of aerosols and soluble trace gases. There is also increase evidence of the importance of organic aerosols over the IGP and Delhi (Bhandari et al., 2020; Gani et al., 2019; Singh et al., 2018), but processes that lead to the formation of organic aerosols are still not completely explained and understood (Fuzzi et al., 2015), and there is still lack of extensive and systematic observations for OA over this region. Thus modeling SOA over South Asia

remains a main challenge. As highlighted in Chapter 2, it is also challenging to estimate emission fluxes in a rapidly changing region such as South Asia and its cities, and consequently building emissions inventories to be used in models which are up-to-date for all the different sectors.

Second, the computational cost of running such complex model on a high-resolution spatial and temporal scales remains high. The breadth and depth of atmospheric processes included in the model across different scales come at a cost of the temporal and spatial scales that can be covered in a given study. Indeed, in this thesis I managed to focus on four representative months at 20km resolution for the regional study of IGP, but the more detailed analysis presented in Chapter 3 and Chapter 4 for the city of Delhi at 4km resolution was constrained to a shorter periods of time.

Third, the constraint to use a spatial resolution of 4km for Delhi also makes the results obtained reliable for a city scale only. My results might not be representative of areas at a sub-urban scale, where the higher resolution source attribution and thus potential impact reduction can vary from location to location. Especially over city hotsposts and during specific times of the day, the transport sector might have a bigger impact than reported in this thesis. In addition, socio-economical factors also play an important role in determining high air pollution inequalities within the city (Fecht et al., 2015; Lane et al., 2022; Nguyen and Marshall, 2018), which require a higher resolution modeling to be captured. Finally, averaging over a broader area such as a whole city tends to drives the responsibility towards regional action that might be less effective in solving the pollution issue in different parts of the city (Thunis et al., 2021).

5.4 Future research directions

My thesis focused on three main questions on air quality and on-road transport over Delhi as discussed above. However, the results, uncertainties and limitations which emerged from my work provide scope for future research on this area. In this section, I first identify research directions that can be in continuity with my thesis work, and then I identify broader areas where further research could improve our understanding of the role of on-road transport on air quality over Delhi, in order also to better inform air pollution mitigation strategies for the city.

In terms of future work in continuity with this thesis, I propose three main line of research:

- First, Chapter 3 briefly touched on the health impacts and benefits of emission reduction strategies, but a more comprehensive and systematic assessment could be performed, also for the transport-emissions scenarios in Chapter 4. Using established health impacts estimate approaches, such as the Global Burden of Diseases (GBD) methodology (GBD MAPS Working Group, 2018) or the Global Exposure Mortality Model (GEMM) (Burnett et al., 2018), it would be possible to quantify health impacts benefits of the proposed emissions reduction strategies in this thesis. In particular, a multi-pollutants assessment (e.g. considering $PM_{2.5}$, O_3 and NO_x) and the health impact could be performed.
- Second, although we used an advanced scheme for SOA formation (1-D VBS model) in the WRF-Chem set-up, secondary organic aerosol modelling is still poorely constrained over the IGP and Delhi. Improvements of the VBS scheme for the SOA formation in the WRF-Chem model, including constraining OA:OC ratios and extend the 1D to the 2D version of the VBS could be implemented, as already done in other regional air quality models over regions other than India (Koo et al.,

2014; Zhao et al., 2016). The VBS improvements could take advantage of newly available extensive measurements campaigns for PM and OA in Delhi Arub et al. (2020); Bryant et al. (2023); Gani et al. (2019); Patel et al. (2021); Reyes-Villegas et al. (2020) both for implementation and for evaluation.

- Third, this thesis was looking at the air quality in Delhi in almost present years (2017-2019), but the relative influence of different emissions sources and the broader photochemical environment is expected to change in the context of climate change in India. The controlling regime in ozone production in northern India has already shifted substantially since the 1970s (Ivatt et al., 2022), and ozone production and secondary aerosols production are expected to further change in this century on a global scale (Lin et al., 2016; Liu et al., 2022). The WRF-Chem model could be driven with future climate projections, e.g. using datasets from the Climate Models Intercomparison Project (CMIP) (Meehl et al., 2000), to investigate how air pollution over Delhi will change under climate change scenarios, in particular during extreme heatwaves events, which already are affecting India (Rohini et al., 2016).

In terms of broader areas of research on the topic of air pollution in megacities and traffic emission control strategies, the following could be possible directions:

- First, higher resolution modelling of air pollution is needed to characterise $PM_{2.5}$ at suburban spatial and temporal scales over Delhi and to establish which local controls can be effective at reducing pollution levels, especially for traffic emissions. In addition, sensitivity studies within the city will need to consider the location-dependent photochemical environment that will also help determine how the balance of emission changes will influence surface ozone and secondary aerosols production, in order to inform effective and impactful emissions control strategies that maximise health benefits for Delhi residents. This could be achieved by using

models that integrates chemical transport model with urban scale air pollution models (Benavides et al., 2019; Khan et al., 2021; Kim et al., 2018; McHugh et al., 1997). Emissions inventories at the street level would also need to be developed to be used in these model in order to maximise precision and accuracy of results.

- Second, the air quality issue could be explored through the environmental justice perspective, with the integration of socio-economical factors. Which demographics groups in Delhi are affected the most from poor air pollution and where? Who will benefit (or be damaged), from air quality management interventions, in particular the ones regarding cleaner transportation and sustainable mobility? The health assessment will also benefit from the higher resolution modelling and the better characterisation of air pollution under future climate.
- Third, integrated assessment modeling and system analysis of air pollution over Delhi is necessary to more comprehensively assess the socio-economic impacts of air pollution in the city,in order to inform strategies to build sustainable, just and resilient cities in line with the Paris Agreement and the UN Sustainable Development Goals.

Appendix A

Appendix to Chapter 2

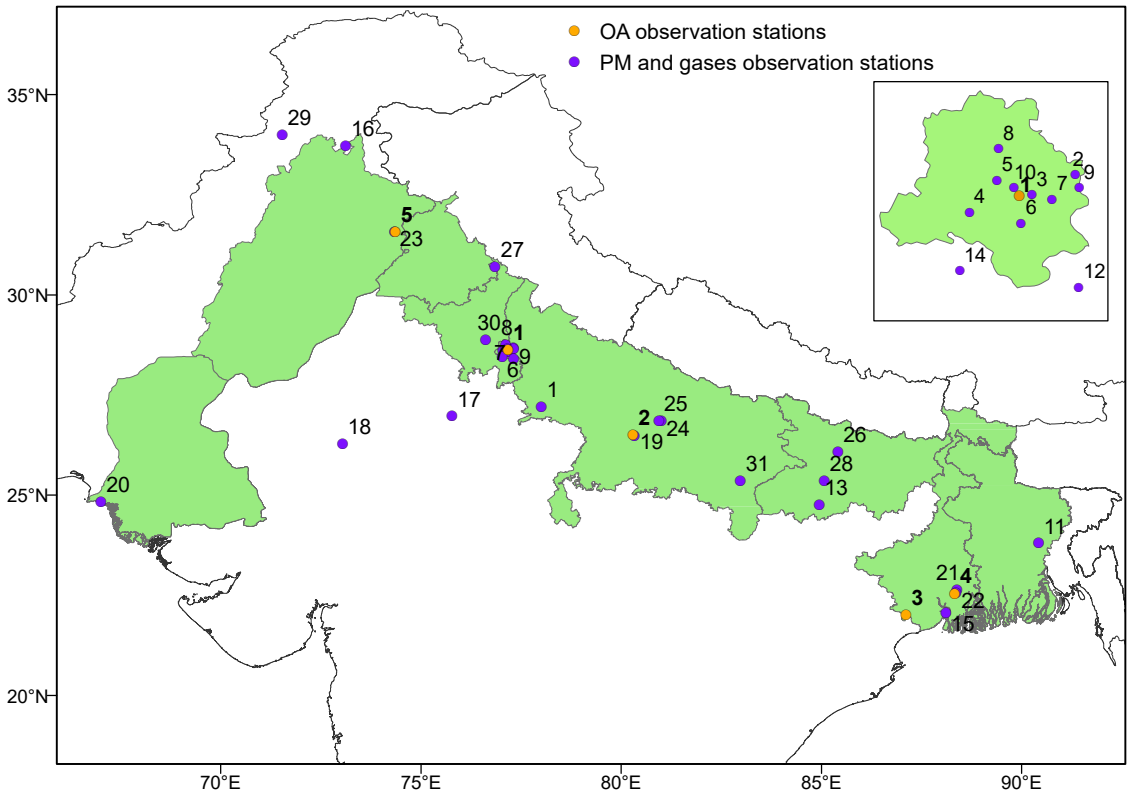

Figure A.1: Location of ground based observation for PM and gases (purple) and OA (orange). ID Number for each station correspond to ID number in table A2 and A4 respectively. The inset map shows in detail Delhi NCT.

number ID	city	station name	latitude	longitude
1	Agra	Sanjay Palace	27.20	78.01
2	Delhi	Income Tax Office	28.62	77.25
3	Delhi	Delhi Technological University	28.74	77.12
4	Delhi	Shadipur	28.65	77.16
5	Delhi	Anand Vihar	28.65	77.32
6	Delhi	Punjabi Bagh	28.67	77.12
7	Delhi	NSIT Dwarka	28.59	77.05
8	Delhi	IHBAS	28.68	77.31
9	Delhi	Mandir Marg	28.63	77.20
10	Delhi	R K Puram	28.56	77.17
11	Dhaka	US Diplomatic Post: Dhaka	23.80	90.42
12	Faridabad	Sector16A Faridabad	28.41	77.31
13	Gaya	Collectorate - Gaya - BSPCB	24.75	84.94
14	Gurgaon	Vikas Sadan Gurgaon - HSPCB	28.45	77.03
15	Haldia	Haldia - WBPCB	22.06	88.11
16	Islamabad	US Diplomatic Post: Islamabad	33.72	73.12
17	Jaipur	VK Industrial Area Jaipur - RSPCB	26.97	75.77
18	Jodhpur	Collectorate Jodhpur - RSPCB	26.29	73.04
19	Kanpur	Nehru Nagar	26.47	80.33
20	Karachi	US Diplomatic Post: Karachi	24.84	67.01
21	Kolkata	US Diplomatic Post: Kolkata	22.56	88.36
22	Kolkata	Rabindra Bharati University, Kolkata - WBSPCB	22.63	88.38
23	Lahore	US Diplomatic Post:Lahore	31.56	74.34
24	Lucknow	Central School	26.85	81.00
25	Lucknow	Lalbagh, DN Park	26.85	80.94
26	Muzaffarpur	Collectorate - Muzaffarpur - BSPCB	26.08	85.41
27	Panchkula	Sector 6 Panchkula - HSPCB	30.71	76.85
28	Patna	IGSC Planetarium Complex - Patna - BSPCB	25.36	85.08
29	Peshawar	US Diplomatic Post: Peshawar	34.01	71.54
30	Rohtak	MD University, Rohtak - HSPCB	28.88	76.62
31	Varanasi	Ardhali Bazar	25.35	82.98

Table A.1: List of selected ground-based stations and their measurements used for model evaluation.

Appendix B

Appendix to Chapter 3

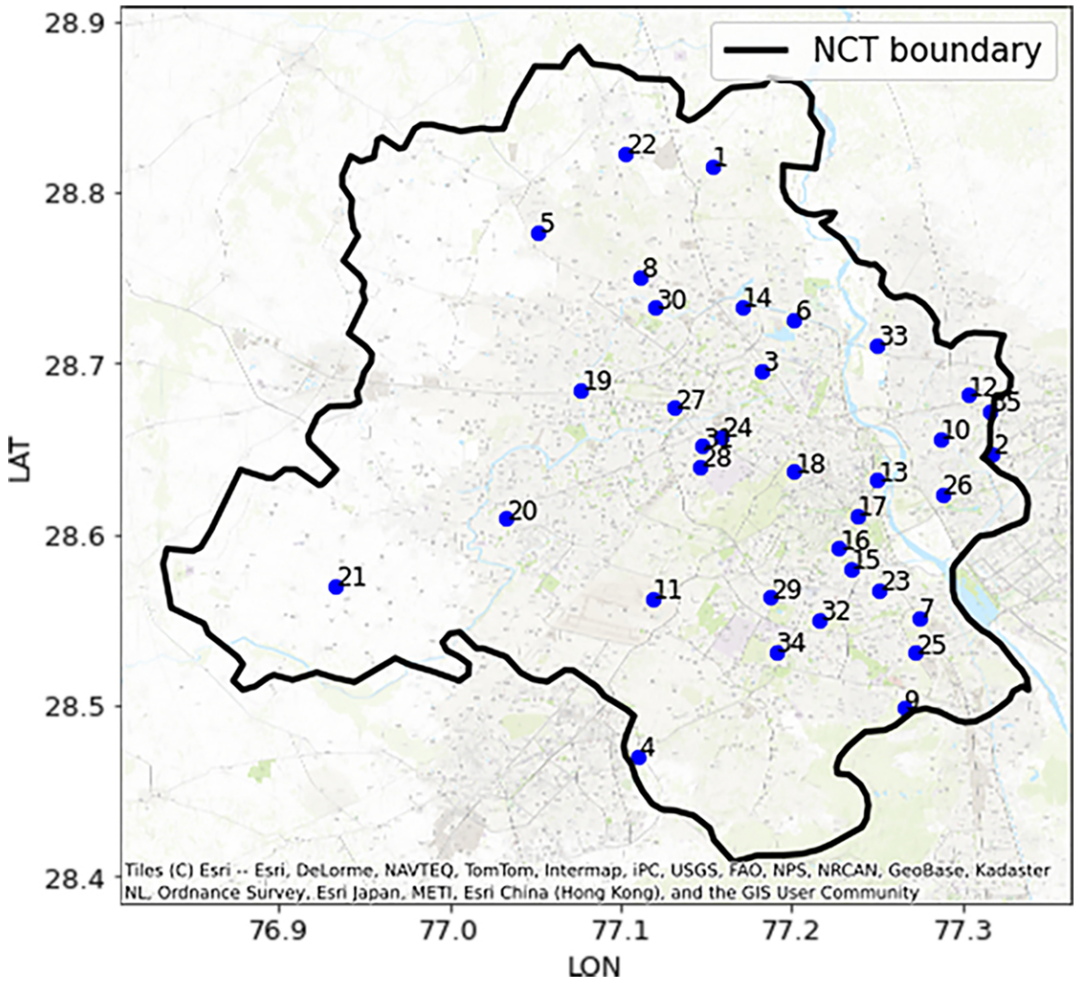

Figure B.1: Selected ground-based stations where $PM_{2.5}$ is measured for model evaluation for th post-monsoon season (data for 1-31 October 2019). Station numbers correspond to Table B.1.

ID	station	lat	lon
0	Alipur Delhi - DPCC	28.815	77.153
1	Anand Vihar Delhi - DPCC	28.647	77.316
2	Ashok Vihar Delhi - DPCC	28.695	77.182
3	Aya Nagar Delhi - IMD	28.471	77.110
4	Bawana Delhi - DPCC	28.776	77.051
5	Burari Crossing Delhi - IMD	28.726	77.201
6	CRRI Mathura Road Delhi - IMD	28.551	77.274
7	DTU Delhi - CPCB	28.750	77.111
8	Dr. Karni Singh Shooting Range Delhi - DPCC	28.499	77.265
9	IGI Airport (T3) Delhi - IMD	28.563	77.118
10	IHBAS Dilshad Garden Delhi - CPCB	28.681	77.303
11	ITO Delhi - CPCB	28.632	77.249
12	Jahangirpuri Delhi - DPCC	28.733	77.171
13	Jawaharlal Nehru Stadium Delhi - DPCC	28.580	77.234
14	Lodhi Road Delhi - IMD	28.592	77.227
15	Major Dhyan Chand National Stadium Delhi - DPCC	28.611	77.238
16	Mandir Marg Delhi - DPCC	28.636	77.201
17	Mundka Delhi - DPCC	28.685	77.077
18	NSIT Dwarka Delhi - CPCB	28.609	77.033
19	Najafgarh Delhi - DPCC	28.570	76.934
20	Narela Delhi - DPCC	28.823	77.102
21	Nehru Nagar Delhi - DPCC	28.568	77.251
22	North Campus DU Delhi - IMD	28.657	77.159
23	Okhla Phase-2 Delhi - DPCC	28.531	77.271
24	Patparganj Delhi - DPCC	28.624	77.287
25	Punjabi Bagh Delhi - DPCC	28.674	77.131
26	Pusa Delhi - DPCC	28.640	77.146
27	R K Puram Delhi - DPCC	28.563	77.187
28	Rohini Delhi - DPCC	28.733	77.120
29	Shadipur Delhi - CPCB	28.651	77.147
30	Sirifort Delhi - CPCB	28.550	77.216
31	Sonia Vihar Delhi - DPCC	28.711	77.249
32	Sri Aurobindo Marg Delhi - DPCC	28.531	77.190
33	Vivek Vihar Delhi - DPCC	28.672	77.315

Table B.1: Observation used for the model evaluation of $PM_{2.5}$ from control stations run by the Central Pollution Control Board (CPCB), the India Meteorological Department (IMD) and the Delhi Pollution Control Committee (DPCC). Data from these stations cover the period 6-16 October 2019.

MOZART	CB05
CH3CHO	ALD2+ALDX
C2H6	ETHA
C2H4	ETH
C2H5OH	ETOH
CH2O	FORM
ISOP	ISOP
CH3OH	MEOH
TOLUENE	TOL
XYLENE	XYL
C3H6	0.07165*OLE+0.07165*PAR
BIGENE	0.00653*OLE+0.0131*PAR
BIGALK	0.8371*PAR
PM2.5	PAL+PCA+PFE+PK+PMG+PMN+PMOTHR+PSI+PTI
NA	PNA
CL	PCL
EC	PEC
OC	POC
SO4	PSO4
NO3	PNO3
NH4	PNH4
PM10	PMC

Table B.2: The TERI/ARAI NMVOCs are speciated according to the CB05 chemical mechanism (Yarwood et al., 2005). This table shows the VOCs (molar) and PM (mass) mapping from the original CB05 mechanism to MOZART mechanism. The mapping is based on (Hodzic and Knote, 2014). The CBO5 is a carbon-bond mechanism (lumped structure) while MOZART uses surrogate species (lumped molecules). To get molar conversion for lumped species of BIGENE, BIGALK, C3H6: C3H6 + BIGENE + BIGALK = a(OLE + PAR)/2 + b(OLE + 2 PAR)/3 + c(IOLE + 2 PAR)/3 + d(5 PAR)/5 with a= 0.14,b+c = 0.02,d = 0.84.

Appendix C

Appendix to Chapter 4

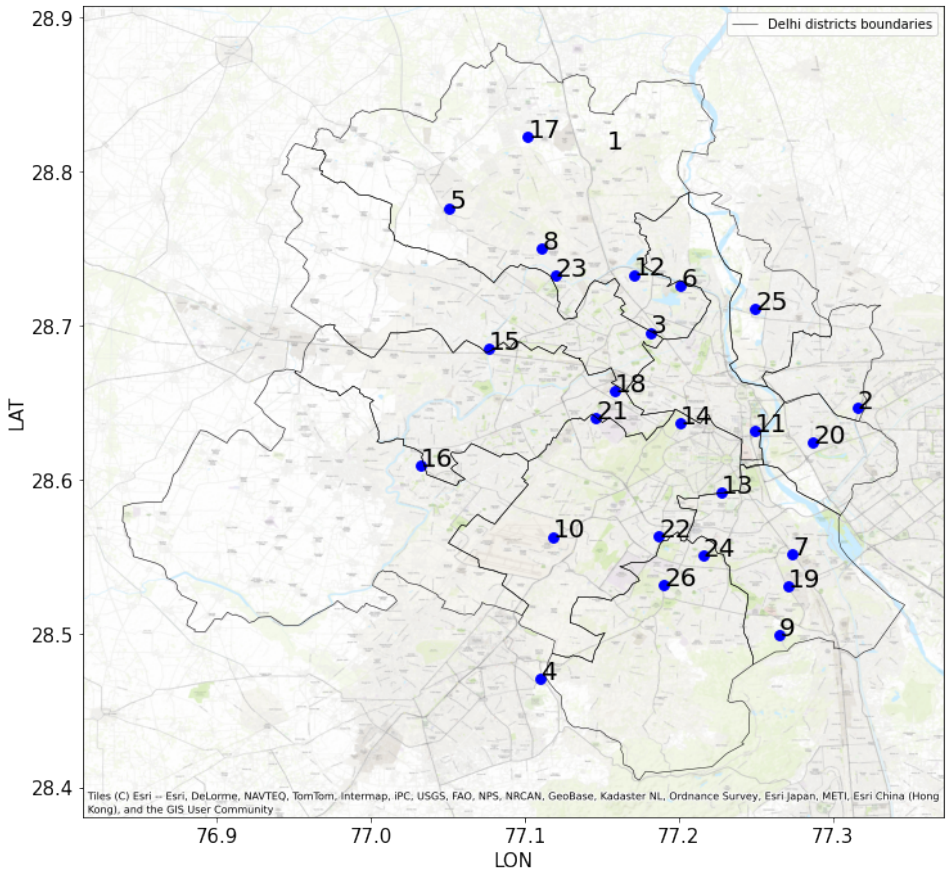

Figure C.1: Selected CPCB ground-based stations for $PM_{2.5}$ and O_3 observations for model evaluation for pre-monsoon (data for 1-30 April 2019) and post-monsoon season (data for 1-31 October 2019). Corresponded station to number is listed in Table C.1.

ID	station	lat	lon	season	$PM_{2.5}$	O_3
1	Alipur Delhi - DPCC	28.81533	77.15301	post	x	
				pre	x	x
2	Anand Vihar Delhi - DPCC	28.64684	77.31603	post	x	x
				pre	x	
3	Ashok Vihar Delhi - DPCC	28.69538	77.18167	post	x	x
				pre		x
4	Aya Nagar Delhi - IMD	28.47069	77.10994	post	x	x
				pre	x	
5	Bawana Delhi - DPCC	28.7762	77.05107	post	x	x
				pre		x
6	Burari Crossing Delhi - IMD	28.72565	77.20116	post	x	x
				pre		
7	CRRI Mathura Road Delhi - IMD	28.5512	77.27357	post	x	x
				pre	x	x
8	DTU Delhi - CPCB	28.75005	77.11126	post	x	x
				pre	x	
9	Dr. Karni Singh Shooting Range Delhi - DPCC	28.49857	77.26484	pre	x	x
				post	x	
10	East Arjun Nagar Delhi - CPCB	28.6556	77.28593	post		
				pre		x
11	IGI Airport (T3) Delhi - IMD	28.56278	77.11801	post	x	x
				pre	x	x
12	IHBAS Dilshad Garden Delhi - CPCB	28.68117	77.30252	post	x	
				pre	x	
13	ITO Delhi - CPCB	28.63169	77.24944	post	x	x
				pre	x	x
14	Jahangirpuri Delhi - DPCC	28.73282	77.17063	post	x	x
				pre	x	x
15	Jawaharlal Nehru Stadium Delhi - DPCC	28.58028	77.23383	pre		x
				post	x	x
16	Lodhi Road Delhi - IMD	28.59182	77.22731	pre	x	x
				post	x	x
17	Mandir Marg Delhi - DPCC	28.63643	77.20107	pre	x	x
				post	x	x
18	Mundka Delhi - DPCC	28.68468	77.07657	pre	x	x
				post	x	x
19	NSIT Dwarka Delhi - CPCB	28.60909	77.03254	pre	x	x
				post	x	x
20	Najafgarh Delhi - DPCC	28.57017	76.93376	pre		x
				post	x	x
21	Narela Delhi - DPCC	28.82284	77.10198	pre	x	x
				post	x	x
22	Nehru Nagar Delhi - DPCC	28.56789	77.25052	pre	x	
				post	x	x
23	North Campus DU Delhi - IMD	28.65738	77.15854	post	x	x
				pre	x	x
24	Okhla Phase-2 Delhi - DPCC	28.53079	77.27126	pre	x	x
				post	x	x
25	Patparganj Delhi - DPCC	28.62375	77.28721	pre	x	x
				post	x	x
26	Punjabi Bagh Delhi - DPCC	28.67405	77.13102	pre		x
				post	x	x
27	Pusa Delhi - DPCC	28.63965	77.14626	pre	x	x
				post	x	x
28	R K Puram Delhi - DPCC	28.56326	77.18694	pre	x	x
				post		x
29	Rohini Delhi - DPCC	28.73253	77.11992	pre	x	x
				post	x	x
30	Sirifort Delhi - CPCB	28.55042	77.21594	post	x	x
				pre		
31	Sonia Vihar Delhi - DPCC	28.71051	77.24949	pre	x	x
				post	x	x
32	Sri Aurobindo Marg Delhi - DPCC	28.53135	77.19016	post	x	x
				pre	x	

Table C.1: CPCB observation stations used for the model evaluation of $PM_{2.5}$ and O_3 for pre-monsoon (data for 1-30 April 2019) and post-monsoon season (data for 1-31 October 2019). pre = pre-monsoon , post = post-monsoon.

Bibliography

Abdel-Rahman, A. (1998). On the emissions from internal-combustion engines: a review. *International Journal of Energy Research*, 22(6):483–513.

ACOM-NCAR (2020). WRF-Chem Tools for the Community. `https://www2.acom.ucar.edu/wrf-chem/wrf-chem-tools-community`. last access: 30 November 2020.

Agarwala, M. and Chandel, A. (2020). Temporal role of crop residue burning (CRB) in Delhi's air pollution. *Environmental Research Letters*, 15(11):114020.

Agency, U. E. P. (2011). The benefits and costs of the Clean Air Act from 1990 to 2020.

Ahmadov, R., McKeen, S., Robinson, A., Bahreini, R., Middlebrook, A., De Gouw, J., Meagher, J., Hsie, E.-Y., Edgerton, E., Shaw, S., et al. (2012). A volatility basis set model for summertime secondary organic aerosols over the eastern United States in 2006. *Journal of Geophysical Research: Atmospheres*, 117(D6).

Ahmed, T., Ahmad, B., and Ahmad, W. (2015). Why do farmers burn rice residue? Examining farmers' choices in Punjab, Pakistan. *Land Use Policy*, 47:448–458.

Alam, K., Mukhtar, A., Shahid, I., Blaschke, T., Majid, H., Rahman, S., Khan, R., and Rahman, N. (2014). Source apportionment and characterization of particulate matter (PM_{10}) in urban environment of Lahore. *Aerosol Air Quality Research*, 14(7):1851–1861.

Amann, M., Purohit, P., Bhanarkar, A. D., Bertok, I., Borken-Kleefeld, J., Cofala, J., Heyes, C., Kiesewetter, G., Klimont, Z., Liu, J., et al. (2017). Managing future air quality in megacities: A case study for Delhi. *Atmospheric Environment*, 161:99–111.

Andress, D., Nguyen, T. D., and Das, S. (2011). Reducing GHG emissions in the United States' transportation sector. *Energy for Sustainable Development*, 15(2):117–136.

Apte, J. S., Kirchstetter, T. W., Reich, A. H., Deshpande, S. J., Kaushik, G., Chel, A., Marshall, J. D., and Nazaroff, W. W. (2011). Concentrations of fine, ultrafine, and black carbon particles in auto-rickshaws in New Delhi, India. *Atmospheric Environment*, 45(26):4470–4480.

Apte, J. S., Marshall, J. D., Cohen, A. J., and Brauer, M. (2015). Addressing global mortality from ambient $PM_{2.5}$. *Environmental Science & Technology*, 49(13):8057–8066.

Arub, Z., Bhandari, S., Gani, S., Apte, J. S., Hildebrandt Ruiz, L., and Habib, G. (2020). Air mass physiochemical characteristics over new delhi: impacts on aerosol hygroscopicity and cloud condensation nuclei (ccn) formation. *Atmospheric Chemistry and Physics*, 20(11):6953–6971.

Babaee, S., Nagpure, A. S., and DeCarolis, J. F. (2014). How much do electric drive vehicles matter to future US emissions? *Environmental science & technology*, 48(3):1382–1390.

Balakrishnan, K., Dey, S., Gupta, T., Dhaliwal, R., Brauer, M., Cohen, A. J., Stanaway, J. D., Beig, G., Joshi, T. K., Aggarwal, A. N., et al. (2019). The impact of air pollution on deaths, disease burden, and life expectancy across the states of India: the Global Burden of Disease Study 2017. *The Lancet Planetary Health*, 3(1):e26–e39.

Balasubramanian, S., McFarland, D. M., Koloutsou-Vakakis, S., Fu, K., Menon, R., Lehmann, C., and Rood, M. J. (2020). Effect of grid resolution and spatial representation of NH_3 emissions from fertilizer application on predictions of NH_3 and $PM_{2.5}$ concentrations in the United States Corn Belt. *Environmental Research Communications*, 2(2):025001.

Bangladesh Bureau of Statistics (2011). Population and housing census 2011. Technical report, Statistics Division Ministry of Planning Government of the People's Republic of Bangladesh.

Bansal, G. and Bandivadekar, A. (2013). Overview of India's vehicle emissions control program. *ICCT, Beijing, Berlin, Brussels, San Francisco, Washington*.

Barbar, M., Mallapragada, D. S., Alsup, M., and Stoner, R. (2021). Scenarios of future Indian electricity demand accounting for space cooling and electric vehicle adoption. *Scientific Data*, 8(1):1–11.

Bawase, M., Sathe, Y., Khandaskar, H., and Thipse, S. (2021). Chemical composition and source attribution of $PM_{2.5}$ and PM_{10} in Delhi-National Capital Region (NCR) of India: results from an extensive seasonal campaign. *Journal of Atmospheric Chemistry*, 78(1):35–58.

Begum, B. A., Hopke, P. K., and Markwitz, A. (2013). Air pollution by fine particulate matter in Bangladesh. *Atmospheric Pollution Research*, 4(1):75–86.

Behera, S. N. and Sharma, M. (2015). Spatial and seasonal variations of atmospheric particulate carbon fractions and identification of secondary sources at urban sites in North India. *Environmental Science and Pollution Research*, 22(17):13464–13476.

Beig, G., Chate, D. M., Ghude, S. D., Mahajan, A., Srinivas, R., Ali, K., Sahu, S., Parkhi, N., Surendran, D., and Trimbake, H. (2013). Quantifying the effect of air quality control measures during the 2010 Commonwealth Games at Delhi, India. *Atmospheric Environment*, 80:455–463.

Benavides, J., Snyder, M., Guevara, M., Soret, A., Pérez García-Pando, C., Amato, F., Querol, X., and Jorba, O. (2019). CALIOPE-Urban v1. 0: coupling R-LINE with a mesoscale air quality modelling system for urban air quality forecasts over Barcelona city (Spain). *Geoscientific Model Development*, 12(7):2811–2835.

Bergström, R., Denier Van Der Gon, H., Prévôt, A. S., Yttri, K. E., and Simpson, D. (2012). Modelling of organic aerosols over Europe (2002–2007) using a volatility basis set (VBS) framework: application of different assumptions regarding the formation of secondary organic aerosol. *Atmospheric Chemistry and Physics*, 12(18):8499–8527.

Bhandari, S., Gani, S., Patel, K., Wang, D. S., Soni, P., Arub, Z., Habib, G., Apte, J. S., and Hildebrandt Ruiz, L. (2020). Sources and atmospheric dynamics of organic aerosol in New Delhi, India: insights from receptor modeling. *Atmospheric Chemistry and Physics*, 20(2):735–752.

Bhowmik, H. S., Naresh, S., Bhattu, D., Rastogi, N., Prévôt, A. S., and Tripathi, S. N. (2020). Temporal and spatial variability of carbonaceous species (EC; OC; WSOC and SOA) in $PM_{2.5}$ aerosol over five sites of Indo-Gangetic Plain. *Atmospheric Pollution Research*, 12(1):375–390.

Bikkina, S., Andersson, A., Kirillova, E. N., Holmstrand, H., Tiwari, S., Srivastava, A., Bisht, D., and Gustafsson, Ö. (2019). Air quality in megacity of Delhi affected by countryside biomass burning. *Nature Sustainability*, page 1.

Bisht, D., Dumka, U., Kaskaoutis, D., Pipal, A., Srivastava, A., Soni, V., Attri, S., Sateesh, M., and Tiwari, S. (2015). Carbonaceous aerosols and pollutants over Delhi urban environment: temporal evolution, source apportionment and radiative forcing. *Science of the Total Environment*, 521:431–445.

Bran, S. H. and Srivastava, R. (2017). Investigation of $PM_{2.5}$ mass concentration over India using a regional climate model. *Environmental pollution*, 224:484–493.

Brasseur, G. P. and Jacob, D. J. (2017). *Modeling of Atmospheric Chemistry*. Cambridge University Press.

Bricker, O. P. and Rice, K. C. (1993). Acid rain. *Annual Review of Earth and Planetary Sciences*, 21:151–174.

Bryant, D. J., Nelson, B. S., Swift, S. J., Budisulistiorini, S. H., Drysdale, W. S., Vaughan, A. R., Newland, M. J., Hopkins, J. R., Cash, J. M., Langford, B., et al. (2023). Biogenic and anthropogenic sources of isoprene and monoterpenes and their secondary organic aerosol in delhi, india. *Atmospheric Chemistry and Physics*, 23(1):61–83.

Buchholz, R. R., Emmons, L. K., Tilmes, S., and The CESM2 Development Team, UCAR/NCAR - Atmospheric Chemistry Observations and Modeling Laboratory (2019). CESM2.1/CAM-chem Instantaneous Output for Boundary Conditions. https://doi.org/10.5065/NMP7-EP60. Subset: Lat: 0 to 50, Lon: 50 to 100, October 2017 - February 2018, Accessed 29 March 2020.

Burnett, R., Chen, H., Szyszkowicz, M., Fann, N., Hubbell, B., Pope Iii, C. A., Apte, J. S., Brauer, M., Cohen, A., Weichenthal, S., et al. (2018). Global estimates of mortality associated with long-term exposure to outdoor fine particulate matter. *Proceedings of the National Academy of Sciences*, 115(38):9592–9597.

CAQM (2022). Commission for Air Quality Management in National Capital Region and Adjoining Areas, Circulars & Orders. https://caqm.nic.in/. last access: 4 August 2022.

CEM (2017). Electric Vehicles Initiative (EVI). An initiative of the Clean Energy Ministerial," Clean Energy Ministerial (CEM). https://www.cleanenergyministerial.org/initiatives-campaigns/electric-vehicles-initiative/. last access: 06 June 2022.

Chameides, W., Lindsay, R., Richardson, J., and Kiang, C. (1988). The role of biogenic hydrocarbons in urban photochemical smog: Atlanta as a case study. *Science*, 241(4872):1473–1475.

Chatterjee, A., Dutta, C., Jana, T., and Sen, S. (2012). Fine mode aerosol chemistry over a tropical urban atmosphere: characterization of ionic and carbonaceous species. *Journal of Atmospheric Chemistry*, 69(2):83–100.

Chauhan, B. S., Mahajan, G., Sardana, V., Timsina, J., and Jat, M. L. (2012). Productivity and sustainability of the rice–wheat cropping system in the Indo-Gangetic Plains of the Indian subcontinent: problems, opportunities, and strategies. *Adv. Agron.*, 117:315–369.

Chen, Y., Beig, G., Archer-Nicholls, S., Drysdale, W., Acton, W. J. F., Lowe, D., Nelson, B., Lee, J., Ran, L., Wang, Y., et al. (2021). Avoiding high ozone pollution in Delhi, India. *Faraday Discussions*, 226:502–514.

Chen, Y., Wild, O., Ryan, E., Sahu, S. K., Lowe, D., Archer-Nicholls, S., Wang, Y., McFiggans, G., Ansari, T., Singh, V., et al. (2020). Mitigation of $PM_{2.5}$ and ozone pollution in Delhi: a sensitivity study during the pre-monsoon period. *Atmospheric Chemistry and Physics*, 20(1):499–514.

Chowdhury, S. and Dey, S. (2016). Cause-specific premature death from ambient $PM_{2.5}$ exposure in India: Estimate adjusted for baseline mortality. *Environment International*, 91:283–290.

Chowdhury, S., Dey, S., Di Girolamo, L., Smith, K. R., Pillarisetti, A., and Lyapustin, A. (2019). Tracking ambient $PM_{2.5}$ build-up in Delhi national capital region during the dry season over 15 years using a high-resolution (1 km) satellite aerosol dataset. *Atmospheric Environment*, 204:142–150.

Chowdhury, S., Dey, S., Tripathi, S. N., Beig, G., Mishra, A. K., and Sharma, S. (2017). "Traffic intervention" policy fails to mitigate air pollution in megacity Delhi. *Environmental Science & Policy*, 74:8–13.

Chowdhury, Z., Zheng, M., Schauer, J. J., Sheesley, R. J., Salmon, L. G., Cass, G. R., and Russell, A. G. (2007). Speciation of ambient fine organic carbon particles and source apportionment of $PM_{2.5}$ in Indian cities. *Journal of Geophysical Research: Atmospheres*, 112(D15).

Chuang, W. and Donahue, N. (2016). A two-dimensional volatility basis set–Part 3: Prognostic modeling and NOx dependence. *Atmospheric Chemistry and Physics*, 16(1):123–134.

Clappier, A., Belis, C. A., Pernigotti, D., and Thunis, P. (2017). Source apportionment and sensitivity analysis: two methodologies with two different purposes. *Geoscientific Model Development*, 10(11):4245–4256.

Cohen, A. J., Brauer, M., Burnett, R., Anderson, H. R., Frostad, J., Estep, K., Balakrishnan, K., Brunekreef, B., Dandona, L., Dandona, R., et al. (2017). Estimates and 25-year trends of the global burden of disease attributable to ambient air pollution: an analysis of data from the Global Burden of Diseases Study 2015. *The Lancet*, 389(10082):1907–1918.

Colvile, R., Hutchinson, E. J., Mindell, J., and Warren, R. (2001). The transport sector as a source of air pollution. *Atmospheric Environment*, 35(9):1537–1565.

Conibear, L., Butt, E. W., Knote, C., Arnold, S. R., and Spracklen, D. V. (2018). Residential energy use emissions dominate health impacts from exposure to ambient particulate matter in India. *Nature Communications*, 9(1):617.

Conibear, L., Reddington, C. L., Silver, B. J., Chen, Y., Knote, C., Arnold, S. R., and Spracklen, D. V. (2021). Statistical emulation of winter ambient fine particulate matter concentrations from emission changes in China. *GeoHealth*, 5(5).

Conibear, L. A., Butt, E. W., Knote, C., Lam, N. L., Arnold, S., Tibrewal, K., Venkataraman, C., Spracklen, D. V., and Bond, T. C. (2020). A complete transition to clean household energy can save one–quarter of the healthy life lost to particulate matter pollution exposure in India. *Environmental Research Letters*, 15(9):094096.

CPCB (2020). *National Ambient Air Quaility Status and Trends 2019*. Central Pollution Control Board, Ministry of Environment, Forest and Climate Change, Government of India.

CPCB (2021). Air Quality Automatic Monitoring Data. `https://app.cpcbccr.com/ccr/#/caaqm-dashboard-all/caaqm-landing`. last access: 30 June 2021.

Crippa, M., Guizzardi, D., Muntean, M., Schaaf, E., and Oreggioni, G. (2019a). EDGAR v5.0 Global Air Pollutant Emissions - Official Website. `https://edgar.jrc.ec.europa.eu/index.php/dataset_ap50`.

Crippa, M., Guizzardi, D., Muntean, M., Schaaf, E., and Oreggioni, G. (2019b). EDGAR v5.0 Global Air Pollutant Emissions. European Commission, Joint Research Centre (JRC) [Dataset].

Crippa, M., Oreggioni, G., Guizzardi, D., Muntean, M., Schaaf, E., Lo Vullo, E., Solazzo, E., Monforti-Ferrario, F., Olivier, J. G., and Vignati, E. (2019c). Fossil CO_2 and GHG emissions of all world countries. *Luxemburg: Publication Office of the European Union*.

Cunanan, C., Tran, M.-K., Lee, Y., Kwok, S., Leung, V., and Fowler, M. (2021). A review of heavy-duty vehicle powertrain technologies: Diesel engine vehicles, battery electric vehicles, and hydrogen fuel cell electric vehicles. *Clean Technologies*, 3(2):474–489.

Cusworth, D. H., Mickley, L. J., Sulprizio, M. P., Liu, T., Marlier, M. E., DeFries, R. S., Guttikunda, S. K., and Gupta, P. (2018). Quantifying the influence of agricultural fires in northwest India on urban air pollution in Delhi, India. *Environmental Research Letters*, 13(4):044018.

Dallmann, T. (2018). Use of remote-sensing technology for vehicle emissions monitoring and control. Technical report, International Council on Clean Transportation (ICCT).

Daly, A. and Zannetti, P. (2007). Air pollution modeling–An overview. *Ambient Air Pollution*, pages 15–28.

David, L. M., Ravishankara, A., Kodros, J. K., Pierce, J. R., Venkataraman, C., and Sadavarte, P. (2019). Premature mortality due to $PM_{2.5}$ over India: Effect of atmospheric transport and anthropogenic emissions. *GeoHealth*, 3(1):2–10.

Denier van der Gon, H. A., Gerlofs-Nijland, M. E., Gehrig, R., Gustafsson, M., Janssen, N., Harrison, R. M., Hulskotte, J., Johansson, C., Jozwicka, M., Keuken, M., et al. (2013). The policy relevance of wear emissions from road transport, now and in the future—an international workshop report and consensus statement. *Journal of the Air & Waste Management Association*, 63(2):136–149.

DESA, U. (2018). World urbanization prospects 2018.

Dobson, I. (1999). The VOC Solvent Emissions Directive an industry perspective. *Pigment & Resin Technology*, 28(2).

Donahue, N., Robinson, A., Stanier, C., and Pandis, S. (2006). Coupled partitioning, dilution, and chemical aging of semivolatile organics. *Environmental science & technology*, 40(8):2635–2643.

Donahue, N. M., Kroll, J., Pandis, S. N., and Robinson, A. L. (2012). A two-dimensional volatility basis set–Part 2: Diagnostics of organic-aerosol evolution. *Atmospheric Chemistry and Physics*, 12(2):615–634.

Du, Q., Zhao, C., Zhang, M., Dong, X., Chen, Y., Liu, Z., Hu, Z., Zhang, Q., Li, Y., Yuan, R., et al. (2020). Modeling diurnal variation of surface $PM_{2.5}$ concentrations over East China with WRF-Chem: Impacts from boundary-layer mixing and anthropogenic emission. *Atmospheric Chemistry and Physics*, 20(5):2839–2863.

Dumka, U., Tiwari, S., Kaskaoutis, D., Hopke, P., Singh, J., Srivastava, A., Bisht, D., Attri, S., Tyagi, S., Misra, A., et al. (2017). Assessment of $PM_{2.5}$ chemical compositions in Delhi: primary vs secondary emissions and contribution to light extinction coefficient and visibility degradation. *Journal of Atmospheric Chemistry*, 74(4):423–450.

EEA (2018). Progress of EU transport sector towards its environment and climate objectives. Technical report, European Environmental Agency.

Ek, M., Mitchell, K., Lin, Y., Rogers, E., Grunmann, P., Koren, V., Gayno, G., and Tarpley, J. (2003). Implementation of Noah land surface model advances in the National Centers for Environmental Prediction operational mesoscale Eta model. *J. Geophys. Res.-Atmos.*, 108(D22).

Emmons, L. K., Walters, S., Hess, P. G., Lamarque, J.-F., Pfister, G. G., Fillmore, D., Granier, C., Guenther, A., Kinnison, D., Laepple, T., et al. (2010). Description and evaluation of the Model for Ozone and Related chemical Tracers, version 4 (MOZART-4). *Geoscientific Model Development*, 3(1):43–67.

EPA (2018). Particulate Matter (PM) Pollution. Environmental protection Agency, `https://www.epa.gov/pm-pollution/particulate-matter-pm-basics#PM`.

EPRI (2007). Environmental assessment of plug-in hybrid electric vehicles. Technical report, Electric Power Research Institute (EPRI).

European Environmental Agency (2016). *Explaining Road Transport Emissions: A non-technical Guide*. Publications Office of the European Union.

Fecht, D., Fischer, P., Fortunato, L., Hoek, G., De Hoogh, K., Marra, M., Kruize, H., Vienneau, D., Beelen, R., and Hansell, A. (2015). Associations between air pollution and socioeconomic characteristics, ethnicity and age profile of neighbourhoods in England and the Netherlands. *Environmental Pollution*, 198:201–210.

Fountoukis, C., Koraj, D., Van Der Gon, H. D., Charalampidis, P., Pilinis, C., and Pandis, S. (2013). Impact of grid resolution on the predicted fine PM by a regional 3-D chemical transport model. *Atmospheric Environment*, 68:24–32.

Frey, H. C. (2018). Trends in onroad transportation energy and emissions. *Journal of the Air & Waste Management Association*, 68(6):514–563.

Friedl, M. A., Sulla-Menashe, D., Tan, B., Schneider, A., Ramankutty, N., Sibley, A., and Huang, X. (2010). MODIS Collection 5 global land cover: Algorithm refinements and characterization of new datasets. *Remote Sensing of the Environment*, 114(1):168–182.

Fuzzi, S., Baltensperger, U., Carslaw, K., Decesari, S., Denier van der Gon, H., Facchini, M. C., Fowler, D., Koren, I., Langford, B., Lohmann, U., et al. (2015). Particulate matter, air quality and climate: lessons learned and future needs. *Atmospheric Chemistry and Physics*, 15(14):8217–8299.

Gadgil, S. et al. (2003). The indian monsoon and its variability. *Annual Review of Earth and Planetary Sciences*, 31(1):429–467.

Gani, S., Bhandari, S., Seraj, S., Wang, D. S., Patel, K., Soni, P., Arub, Z., Habib, G., Hildebrandt Ruiz, L., and Apte, J. S. (2019). Submicron aerosol composition in the world's most polluted megacity: the Delhi Aerosol Supersite study. *Atmospheric Chemistry and Physics*, 19(10).

GBD MAPS Working Group (2018). Burden of disease attributable to major air pollution sources in india,special report 21. Technical report, Health Effects Institute.

Gelaro, R., McCarty, W., Suárez, M. J., Todling, R., Molod, A., Takacs, L., Randles, C. A., Darmenov, A., Bosilovich, M. G., Reichle, R., Wargan, K., Coy, L., Cullather, R., Draper, C., Akella, S., Buchard, V., Conaty, A., da Silva, A. M., Gu, W., Kim, G.-K., Koster, R., Lucchesi, R., Merkova, D., Nielsen, J. E., Partyka, G., Pawson, S., Putman, W., Rienecker, M., Schubert, S. D., Sienkiewicz, M., and Zhao, B. (2017). The modern-era retrospective analysis for research and applications, version 2 (MERRA-2). *Journal of Climate*, 30(14):5419–5454.

Gentner, D. R., Isaacman, G., Worton, D. R., Chan, A. W., Dallmann, T. R., Davis, L., Liu, S., Day, D. A., Russell, L. M., Wilson, K. R., et al. (2012). Elucidating secondary organic aerosol from diesel and gasoline vehicles through detailed characterization of organic carbon emissions. *Proceedings of the National Academy of Sciences*, 109(45):18318–18323.

Ghude, S. D., Chate, D., Jena, C., Beig, G., Kumar, R., Barth, M., Pfister, G., Fadnavis, S., and Pithani, P. (2016). Premature mortality in India due to $PM_{2.5}$ and ozone exposure. *Geophysical Research Letters*, 43(9):4650–4658.

Ghude, S. D., Pfister, G. G., Jena, C., Van Der A, R., Emmons, L. K., and Kumar, R. (2013). Satellite constraints of nitrogen oxide (NOx) emissions from India based on OMI observations and WRF-Chem simulations. *Geophysical Research Letters*, 40(2):423–428.

Gietl, J. K., Lawrence, R., Thorpe, A. J., and Harrison, R. M. (2010). Identification of brake wear particles and derivation of a quantitative tracer for brake dust at a major road. *Atmospheric Environment*, 44(2):141–146.

Goel, R. and Guttikunda, S. K. (2015). Evolution of on-road vehicle exhaust emissions in Delhi. *Atmospheric Environment*, 105:78–90.

Gómez Vilchez, J. J., Julea, A., Peduzzi, E., Pisoni, E., Krause, J., Siskos, P., and Thiel, C. (2019). Modelling the impacts of EU countries' electric car deployment plans on atmospheric emissions and concentrations. *European Transport Research Review*, 11(1):1–17.

Gordon, T., Presto, A., May, A., Nguyen, N., Lipsky, E., Donahue, N., Gutierrez, A., Zhang, M., Maddox, C., Rieger, P., et al. (2014). Secondary organic aerosol formation exceeds primary particulate matter emissions for light-duty gasoline vehicles. *Atmospheric Chemistry and Physics*, 14(9):4661–4678.

Govardhan, G., Nanjundiah, R. S., Satheesh, S., Krishnamoorthy, K., and Kotamarthi, V. (2015). Performance of WRF-Chem over Indian region: Comparison with measurements. *Journal of Earth System Science*, 124(4):875–896.

Government of Delhi NCT (2022). List of 11 districts in the Government of Delhi. http://revenue.delhi.gov.in/wps/wcm/connect/doit_revenue/Revenue/Home/Telephone+Directory/List+of+DC+in+Districts. last access: 06 June 2022.

Government of NCT of Delhi (2012). Statistical Abstract of Delhi 2012. Technical report, Government of NCT of Delhi, Directorate of Economics and Statistics.

Greenstone, M., , and Fan, C. (2020). Air Quality Life Index, Annual Update. Technical report, Energy Policy Institute at The University of Chicago (EPIC).

Grell, G. A. and Dévényi, D. (2002). A generalized approach to parameterizing convection combining ensemble and data assimilation techniques. *Geophysical Research Letters*, 29(14):38–1–38–4.

Grell, G. A., Peckham, S. E., Schmitz, R., McKeen, S. A., Frost, G., Skamarock, W. C., and Eder, B. (2005). Fully coupled "online" chemistry within the WRF model. *Atmospheric Environment*, 39(37):6957–6975.

Guenther, A., Karl, T., Harley, P., Wiedinmyer, C., Palmer, P., and Geron, C. (2006). Estimates of global terrestrial isoprene emissions using MEGAN (Model of Emissions of Gases and Aerosols from Nature). *Atmospheric Chemistry and Physics*, 6(11):3181–3210.

Gulia, S., Nagendra, S. S., Khare, M., and Khanna, I. (2015). Urban air quality management-A review. *Atmospheric Pollution Research*, 6(2):286–304.

Gumma, M. K., Thenkabail, P. S., Teluguntla, P., and Whitbread, A. M. (2019). Indo-Ganges River Basin Land Use/Land Cover (LULC) and Irrigated Area Mapping. In *Indus River Basin*, pages 203–228. Elsevier.

Gupta, M. and Mohan, M. (2013). Assessment of contribution to PM_{10} concentrations from long range transport of pollutants using WRF-Chem over a subtropical urban airshed. *Atmospheric Pollution Research*, 4(4):405–410.

Gupta, M. and Mohan, M. (2015). Validation of WRF-Chem model and sensitivity of chemical mechanisms to ozone simulation over megacity Delhi. *Atmospheric Environment*, 122:220–229.

Guttikunda, S. K., Goel, R., and Pant, P. (2014). Nature of air pollution, emission sources, and management in the Indian cities. *Atmospheric Environment*, 95:501–510.

Guttikunda, S. K. and Gurjar, B. R. (2012). Role of meteorology in seasonality of air pollution in megacity Delhi, India. *Environmental Monitoring and Assessment*, 184(5):3199–3211.

Guttikunda, S. K. and Jawahar, P. (2014). Atmospheric emissions and pollution from the coal-fired thermal power plants in India. *Atmospheric Environment*, 92:449–460.

Guttikunda, S. K. and Mohan, D. (2014). Re-fueling road transport for better air quality in India. *Energy Policy*, 68:556–561.

Hakkim, H., Kumar, A., Annadate, S., Sinha, B., and Sinha, V. (2021). RTEII: A new high-resolution (0.1 °$\times$ 0.1 °) road transport emission inventory for India of 74 speciated NMVOCs, CO, NOx, NH_3, CH_4, CO_2, $PM_{2.5}$ reveals massive overestimation of NOx and CO and missing nitromethane emissions by existing inventories. *Atmospheric Environment: X*, 11:100118.

Hakkim, H., Kumar, A., Sinha, B., and Sinha, V. (2022). Air pollution scenario analyses of fleet replacement strategies to accomplish reductions in criteria air pollutants and 74 VOCs over India. *Atmospheric Environment: X*, page 100150.

Hardacre, C. J., Palmer, P. I., Baumanns, K., Rounsevell, M., and Murray-Rust, D. (2013). Probabilistic estimation of future emissions of isoprene and surface oxidant chemistry associated with land-use change in response to growing food needs. *Atmospheric Chemistry and Physics*, 13(11):5451–5472.

He, X., Shen, W., Wallington, T. J., Zhang, S., Wu, X., Bao, Z., and Wu, Y. (2021). Asia Pacific road transportation emissions, 1900–2050. *Faraday Discussions*, 226:53–73.

Heard, D. E. and Pilling, M. J. (2003). Measurement of OH and HO2 in the troposphere. *Chemical Reviews*, 103(12):5163–5198.

Hodan, W. M. and Barnard, W. R. (2004). Evaluating the contribution of $PM_{2.5}$ precursor gases and re-entrained road emissions to mobile source $PM_{2.5}$ particulate matter emissions. *MACTEC Federal Programs, Research Triangle Park, NC*.

Hodzic, A., Jimenez, J. L., Madronich, S., Canagaratna, M., DeCarlo, P. F., Kleinman, L., and Fast, J. (2010). Modeling organic aerosols in a megacity: potential contribution of semi-volatile and intermediate volatility primary organic compounds to secondary organic aerosol formation. *Atmospheric Chemistry and Physics*, 10(12).

Hodzic, A. and Knote, C. (2014). WRF-Chem 3.6. 1: MOZART gas-phase chemistry with MOSAIC aerosols. *Atmospheric Chemistry Division (ACD), National Center for Atmospheric Research (NCAR)*, 7.

Hooftman, N., Messagie, M., Van Mierlo, J., and Coosemans, T. (2018). A review of the european passenger car regulations–real driving emissions vs local air quality. *Renewable and Sustainable Energy Reviews*, 86:1–21.

Hornbrook, R., Blake, D., Diskin, G., Fried, A., Fuelberg, H., Meinardi, S., Mikoviny, T., Richter, D., Sachse, G., Vay, S., et al. (2011). Observations of nonmethane organic compounds during ARCTAS- Part 1: Biomass burning emissions and plume enhancements. *Atmospheric Chemistry and Physics*, 11(21):11103–11130.

Horton, D. E., Schnell, J. L., Peters, D. R., Wong, D. C., Lu, X., Gao, H., Zhang, H., and Kinney, P. L. (2021). Effect of adoption of electric vehicles on public health and air pollution in China: a modelling study. *The Lancet Planetary Health*, 5:S8.

Huang, Y., Deng, T., Li, Z., Wang, N., Yin, C., Wang, S., and Fan, S. (2018). Numerical simulations for the sources apportionment and control strategies of $PM_{2.5}$ over Pearl River Delta, China, part I: Inventory and $PM_{2.5}$ sources apportionment. *Science of the Total Environment*, 634:1631–1644.

Huszar, P., Belda, M., and Halenka, T. (2016). On the long-term impact of emissions from central European cities on regional air quality. *Atmospheric Chemistry and Physics*, 16(3):1331–1352.

Iacono, M. J., Delamere, J. S., Mlawer, E. J., Shephard, M. W., Clough, S. A., and Collins, W. D. (2008). Radiative forcing by long-lived greenhouse gases: Calculations with the AER radiative transfer models. *J. Geophys. Res.-Atmos.*, 113(D13).

IEA (2021). Tracking Transport 2021. Technical report, International Energy Agency. last access: 16 June 2022.

Im, U. and Kanakidou, M. (2012). Impacts of East Mediterranean megacity emissions on air quality. *Atmospheric Chemistry and Physics*, 12(14):6335–6355.

India Meteorological Department (2020). Frequently asked questions (faq). `http://www.imdsikkim.gov.in/wxfaq.pdf`. last access: 30 November 2020.

Indian National Commission on Population (2020). Population projections for India and States 2011-2036. Technical report, Indian Ministry of Health Family welfare.

IPCC, Chapter 10 - Transport (2022). Climate Change 2022: Mitigation of Climate Change -Chapter 10: Transport. Technical report.

Ivatt, P. D., Evans, M. J., and Lewis, A. C. (2022). Suppression of surface ozone by an aerosol-inhibited photochemical ozone regime. *Nature Geoscience*, pages 1–5.

Jacob, D. J. (1999). *Introduction to atmospheric chemistry*. Princeton University Press.

Jacobson, M. Z. (2010). Short-term effects of controlling fossil-fuel soot, biofuel soot and gases, and methane on climate, Arctic ice, and air pollution health. *Journal of Geophysical Research: Atmospheres*, 115(D14).

Jain, S., Aggarwal, P., Sharma, P., and Kumar, P. (2016). Vehicular exhaust emissions under current and alternative future policy measures for megacity Delhi, India. *Journal of Transport & Health*, 3(3):404–412.

Jain, S., Sharma, S., Vijayan, N., and Mandal, T. (2020). Seasonal characteristics of aerosols ($PM_{2.5}$ and PM_{10}) and their source apportionment using PMF: A four year study over Delhi, India. *Environmental Pollution*, 262:114337.

Jalihal, S. A., Ravinder, K., and Reddy, T. (2005). Traffic characteristics of India. In *Proceedings of the Eastern Asia society for transportation studies*, volume 5, pages 1009–1024. Citeseer.

Janssens-Maenhout, G., Crippa, M., Guizzardi, D., Dentener, F., Muntean, M., Pouliot, G., Keating, T., Zhang, Q., Kurokawa, J., Wankmüller, R., et al. (2015). HTAP_v2. 2: a mosaic of regional and global emission grid maps for 2008 and 2010 to study hemispheric transport of air pollution. *Atmospheric Chemistry and Physics*, 15(19):11411–11432.

Jena, C., Ghude, S. D., Kumar, R., Debnath, S., Govardhan, G., Soni, V. K., Kulkarni, S. H., Beig, G., Nanjundiah, R. S., and Rajeevan, M. (2021). Performance of high resolution (400 m) $PM_{2.5}$ forecast over Delhi. *Scientific Reports*, 11(1):1–9.

Jerrett, M., Burnett, R. T., Pope III, C. A., Ito, K., Thurston, G., Krewski, D., Shi, Y., Calle, E., and Thun, M. (2009). Long-term ozone exposure and mortality. *New England Journal of Medicine*, 360(11):1085–1095.

Jethva, H., Chand, D., Torres, O., Gupta, P., Lyapustin, A., and Patadia, F. (2018). Agricultural burning and air quality over northern India: a synergistic analysis using NASA's A-train satellite data and ground measurements. *Aerosol Air Quality Research*, 18(7):1756–1773.

Jethva, H., Satheesh, S., and Srinivasan, J. (2005). Seasonal variability of aerosols over the Indo-Gangetic basin. *J. Geophys. Res.-Atmos.*, 110(D21).

Jethva, H., Torres, O., Field, R. D., Lyapustin, A., Gautam, R., and Kayetha, V. (2019). Connecting crop productivity, residue fires, and air quality over northern India. *Scientific Reports*, 9(1):1–11.

Jimenez, J. L., Canagaratna, M., Donahue, N., Prevot, A., Zhang, Q., Kroll, J. H., DeCarlo, P. F., Allan, J. D., Coe, H., Ng, N., et al. (2009). Evolution of organic aerosols in the atmosphere. *Science*, 326(5959):1525–1529.

Johns Hopkins University (2022). Coronavirus Resource Center. `https://coronavirus.jhu.edu/`.

Karambelas, A., Holloway, T., Kiesewetter, G., and Heyes, C. (2018). Constraining the uncertainty in emissions over India with a regional air quality model evaluation. *Atmospheric Environment*, 174:194–203.

Kathuria, V. (2004). Impact of CNG on vehicular pollution in Delhi: a note. *Transportation Research Part D: Transport and Environment*, 9(5):409–417.

Khan, B., Banzhaf, S., Chan, E. C., Forkel, R., Kanani-Sühring, F., Ketelsen, K., Kurppa, M., Maronga, B., Mauder, M., Raasch, S., et al. (2021). Development of an atmospheric chemistry model coupled to the PALM model system 6.0: implementation and first applications. *Geoscientific Model Development*, 14(2):1171–1193.

Kim, Y., Wu, Y., Seigneur, C., and Roustan, Y. (2018). Multi-scale modeling of urban air pollution: development and application of a Street-in-Grid model (v1. 0) by coupling MUNICH (v1. 0) and Polair3D (v1. 8.1). *Geoscientific Model Development*, 11(2):611–629.

Knote, C., Hodzic, A., and Jimenez, J. (2015). The effect of dry and wet deposition of condensable vapors on secondary organic aerosols concentrations over the continental US. *Atmospheric Chemistry and Physics*, 15(1):1–18.

Knote, C., Hodzic, A., Jimenez, J., Volkamer, R., Orlando, J., Baidar, S., Brioude, J., Fast, J., Gentner, D., Goldstein, A., et al. (2014). Simulation of semi-explicit mechanisms of SOA formation from glyoxal in aerosol in a 3-D model. *Atmospheric Chemistry and Physics*, 14(12):6213–6239.

Koo, B., Knipping, E., and Yarwood, G. (2014). 1.5-Dimensional volatility basis set approach for modeling organic aerosol in CAMx and CMAQ. *Atmospheric Environment*, 95:158–164.

Kota, S. H., Guo, H., Myllyvirta, L., Hu, J., Sahu, S. K., Garaga, R., Ying, Q., Gao, A., Dahiya, S., Wang, Y., et al. (2018). Year-long simulation of gaseous and particulate air pollutants in India. *Atmospheric Environment*, 180:244–255.

Kriegler, E., Bauer, N., Popp, A., Humpenöder, F., Leimbach, M., Strefler, J., Baumstark, L., Bodirsky, B. L., Hilaire, J., Klein, D., et al. (2017). Fossil-fueled development (SSP5): an energy and resource intensive scenario for the 21st century. *Global Environmental Change*, 42:297–315.

Krishna, R. K., Ghude, S. D., Kumar, R., Beig, G., Kulkarni, R., Nivdange, S., and Chate, D. (2019). Surface $PM_{2.5}$ estimate using satellite-derived aerosol optical depth over India. *Aerosol and Air Quality Research*, 19(1):25–37.

Kroll, J. H. and Seinfeld, J. H. (2008). Chemistry of secondary organic aerosol: Formation and evolution of low-volatility organics in the atmosphere. *Atmospheric Environment*, 42(16):3593–3624.

Kühlwein, J. and Friedrich, R. (2000). Uncertainties of modelling emissions from road transport. *Atmospheric Environment*, 34(27):4603–4610.

Kuik, F., Lauer, A., Churkina, G., van der Gon, D., Hugo, A., Fenner, D., Mar, K. A., and Butler, T. M. (2016). Air quality modelling in the Berlin–Brandenburg region using WRF-Chem v3. 7.1: sensitivity to resolution of model grid and input data. *Geoscientific Model Development*, 9(12):4339–4363.

Kulkarni, S. H., Ghude, S. D., Jena, C., Karumuri, R. K., Sinha, B., Sinha, V., Kumar, R., Soni, V., and Khare, M. (2020). How Much Does Large-Scale Crop Residue Burning Affect the Air Quality in Delhi? *Environmental Science and Technology*, 54(8):4790–4799.

Kumar, M., Parmar, K., Kumar, D., Mhawish, A., Broday, D., Mall, R., and Banerjee, T. (2018). Long-term aerosol climatology over Indo-Gangetic Plain: Trend, prediction and potential source fields. *Atmospheric Environment*, 180:37–50.

Kumar, M., Tiwari, S., Murari, V., Singh, A., and Banerjee, T. (2015a). Wintertime characteristics of aerosols at middle Indo-Gangetic Plain: Impacts of regional meteorology and long range transport. *Atmos. Environ.*, 104:162–175.

Kumar, M., Zhenying, S., Caleb, B., and Anup, B. (2022). Decarbonising India's road transport: a meta-analysis of road transport emissions models. *ICCT, Beijing, Berlin, Brussels, San Francisco, Washington*.

Kumar, P. and Chakrabarty, S. (2020). Total cost of ownership analysis of the impact of vehicle usage on the economic viability of electric vehicles in India. *Transportation Research Record*, 2674(11):563–572.

Kumar, P., Gulia, S., Harrison, R. M., and Khare, M. (2017). The influence of odd–even car trial on fine and coarse particles in Delhi. *Environmental Pollution*, 225:20–30.

Kumar, R., Barth, M., Pfister, G., Nair, V., Ghude, S. D., and Ojha, N. (2015b). What controls the seasonal cycle of black carbon aerosols in India? *J. Geophys. Res.-Atmos.*, 120(15):7788–7812.

Kumar, R., Barth, M., Pfister, G., Naja, M., and Brasseur, G. (2014). WRF-Chem simulations of a typical pre-monsoon dust storm in northern India: influences on aerosol optical properties and radiation budget. *Atmospheric Chemistry and Physics*, 14(5):2431–2446.

Kumar, R., Naja, M., Pfister, G., Barth, M., and Brasseur, G. (2012a). Simulations over South Asia using the Weather Research and Forecasting model with Chemistry (WRF-Chem): set-up and meteorological evaluation. *Geoscientific Model Development*, 5(2):321–343.

Kumar, R., Naja, M., Pfister, G., Barth, M., and Brasseur, G. (2013). Source attribution of carbon monoxide in India and surrounding regions during wintertime. *Journal of Geophysical Research: Atmospheres*, 118(4):1981–1995.

Kumar, R., Naja, M., Pfister, G., Barth, M., Wiedinmyer, C., and Brasseur, G. (2012b). Simulations over South Asia using the Weather Research and Forecasting model with Chemistry (WRF-Chem): chemistry evaluation and initial results. *Geoscientific Model Development*, 5(3):619.

Kunchala, R. K., Singh, B. B., Karumuri, R. K., Attada, R., Seelanki, V., and Kumar, K. N. (2022). Understanding the spatiotemporal variability and trends of surface ozone over India. *Environmental Science and Pollution Research*, 29(4):6219–6236.

Kusaka, H. and Kimura, F. (2004). Coupling a single-layer urban canopy model with a simple atmospheric model: Impact on urban heat island simulation for an idealized case. *J. Meteorol. Soc. Jpn.*, 82(1):67–80.

Kuttippurath, J., Singh, A., Dash, S., Mallick, N., Clerbaux, C., Van Damme, M., Clarisse, L., Coheur, P.-F., Raj, S., Abbhishek, K., and Varikodenf, H. (2020). Record high levels of atmospheric ammonia over India: Spatial and temporal analyses. *Science of the Total Environment*, 740:139986.

Lamb, W. F., Wiedmann, T., Pongratz, J., Andrew, R., Crippa, M., Olivier, J. G., Wiedenhofer, D., Mattioli, G., Al Khourdajie, A., House, J., et al. (2021). A review of trends and drivers of greenhouse gas emissions by sector from 1990 to 2018. *Environmental Research Letters*, 16(7):073005.

Lane, H. M., Morello-Frosch, R., Marshall, J. D., and Apte, J. S. (2022). Historical Redlining Is Associated with Present-Day Air Pollution Disparities in US Cities. *Environmental Science & Technology Letters*.

Lane, T. E., Donahue, N. M., and Pandis, S. N. (2008a). Effect of NOx on secondary organic aerosol concentrations. *Environmental Science and Technology*, 42(16):6022–6027.

Lane, T. E., Donahue, N. M., and Pandis, S. N. (2008b). Simulating secondary organic aerosol formation using the volatility basis-set approach in a chemical transport model. *Atmospheric Environment*, 42(32):7439–7451.

Lee, D., Köhler, I., Grobler, E., Rohrer, F., Sausen, R., Gallardo-Klenner, L., Olivier, J., Dentener, F., and Bouwman, A. (1997). Estimations of global no, emissions and their uncertainties. *Atmospheric Environment*, 31(12):1735–1749.

Lelieveld, J., Bourtsoukidis, E., Brühl, C., Fischer, H., Fuchs, H., Harder, H., Hofzumahaus, A., Holland, F., Marno, D., Neumaier, M., Pozzer, A., Schlager, H., Williams, J., Zahn, A., and H, Z. (2018). The South Asian monsoon—pollution pump and purifier. *Science*, 361(6399):270–273.

Levy, H. (1971). Normal atmosphere: Large radical and formaldehyde concentrations predicted. *Science*, 173(3992):141–143.

Levy, R., Mattoo, S., Munchak, L., Remer, L., Sayer, A., Patadia, F., and Hsu, N. (2013). The Collection 6 MODIS aerosol products over land and ocean. *Atmospheric Measurement Techniques*, 6(11):2989.

Li, F., Ou, R., Xiao, X., Zhou, K., Xie, W., Ma, D., Liu, K., and Song, Z. (2019). Regional comparison of electric vehicle adoption and emission reduction effects in China. *Resources, Conservation and Recycling*, 149:714–726.

Li, G., Zavala, M., Lei, W., Tsimpidi, A., Karydis, V., Pandis, S. N., Canagaratna, M., and Molina, L. (2011). Simulations of organic aerosol concentrations in Mexico City using the WRF-Chem model during the MCMA-2006/MILAGRO campaign. *Atmospheric Chemistry and Physics*, 11(8):3789–3809.

Li, J., Georgescu, M., Hyde, P., Mahalov, A., and Moustaoui, M. (2014). Achieving accurate simulations of urban impacts on ozone at high resolution. *Environmental Research Letters*, 9(11):114019.

Li, M., Karu, E., Brenninkmeijer, C., Fischer, H., Lelieveld, J., and Williams, J. (2018). Tropospheric OH and stratospheric OH and Cl concentrations determined from CH4, CH_3Cl, and SF_6 measurements. *NPJ Climate and Atmospheric Science*, 1(1):1–7.

Li, M., Zhang, Q., Kurokawa, J.-i., Woo, J.-H., He, K., Lu, Z., Ohara, T., Song, Y., Streets, D. G., Carmichael, G. R., et al. (2017). MIX: a mosaic Asian anthropogenic emission inventory under the international collaboration framework of the MICS-Asia and HTAP. *Atmospheric Chemistry and Physics*, 17(2):935–963.

Liang, X., Zhang, S., Wu, Y., Xing, J., He, X., Zhang, K. M., Wang, S., and Hao, J. (2019). Air quality and health benefits from fleet electrification in China. *Nature Sustainability*, 2(10):962–971.

Lin, G., Penner, J. E., and Zhou, C. (2016). How will SOA change in the future? *Geophysical Research Letters*, 43(4):1718–1726.

Liu, T., Marlier, M. E., DeFries, R. S., Westervelt, D. M., Xia, K. R., Fiore, A. M., Mickley, L. J., Cusworth, D. H., and Milly, G. (2018). Seasonal impact of regional outdoor biomass burning on air pollution in three Indian cities: Delhi, Bengaluru, and Pune. *Atmospheric environment*, 172:83–92.

Liu, Z., Doherty, R. M., Wild, O., O'connor, F. M., and Turnock, S. T. (2022). Tropospheric ozone changes and ozone sensitivity from the present day to the future under shared socio-economic pathways. *Atmospheric Chemistry and Physics*, 22(2):1209–1227.

Logan, J. A. (1983). Nitrogen oxides in the troposphere: Global and regional budgets. *Journal of Geophysical Research: Oceans*, 88(C15):10785–10807.

Lozej, C. and Bornstein, R. (1999). Comparison of nesting techniques within a meteorological model. preprints. In *Eighth Conference on Mesoscale Processes, Amer. Me-teor. Soc., Boulder, CO*, pages 372–375.

Malik, L., Tiwari, G., Thakur, S., and Kumar, A. (2019). Assessment of freight vehicle characteristics and impact of future policy interventions on their emissions in Delhi. *Transportation Research Part D: Transport and Environment*, 67:610–627.

Mallik, C. and Lal, S. (2014). Seasonal characteristics of SO_2, NO_2, and CO emissions in and around the Indo-Gangetic Plain. *Environmental Monitor Assessment*, 186(2):1295–1310.

Marlier, M. E., Jina, A. S., Kinney, P. L., and DeFries, R. S. (2016). Extreme air pollution in global megacities. *Current Climate Change Reports*, 2(1):15–27.

Masselot, P., Sera, F., Schneider, R., Kan, H., Lavigne, É., Stafoggia, M., Tobias, A., Chen, H., Burnett, R. T., Schwartz, J., et al. (2021). Differential mortality risks associated with $PM_{2.5}$ components: a multi-country, multi-city study. *Epidemiology*, 33(2):167–175.

McDonald, B. C., De Gouw, J. A., Gilman, J. B., Jathar, S. H., Akherati, A., Cappa, C. D., Jimenez, J. L., Lee-Taylor, J., Hayes, P. L., McKeen, S. A., et al. (2018). Volatile chemical products emerging as largest petrochemical source of urban organic emissions. *Science*, 359(6377):760–764.

McDuffie, E. E., Smith, S. J., O'Rourke, P., Tibrewal, K., Venkataraman, C., Marais, E. A., Zheng, B., Crippa, M., Brauer, M., and Martin, R. V. (2020). A global anthropogenic emission inventory of atmospheric pollutants from sector-and fuel-specific sources (1970–2017): an application of the Community Emissions Data System (CEDS). *Earth System Science Data*, 12(4):3413–3442.

McHugh, C., Carruthers, D., and Edmunds, H. (1997). Adms and adms–urban. *International Journal of Environment and Pollution*, 8(3-6):438–440.

McKee, D. (1993). *Tropospheric ozone: human health and agricultural impacts*. CRC Press.

Meehl, G. A., Boer, G. J., Covey, C., Latif, M., and Stouffer, R. J. (2000). The coupled model intercomparison project (cmip). *Bulletin of the American Meteorological Society*, 81(2):313–318.

Mhawish, A., Banerjee, T., Sorek-Hamer, M., Bilal, M., Lyapustin, A. I., Chatfield, R., and Broday, D. M. (2020). Estimation of High-Resolution $PM_{2.5}$ over the Indo-Gangetic Plain by Fusion of Satellite Data, Meteorology, and Land Use Variables. *Environmental Science and Technology*, 54(13):7891–7900.

MHI (2022). Faster Adoption and Manufacture of (Hybrid and) Electric Vehicles (FAME), Ministry of Heavy Industries and Public Enterprises. `https://dhi.nic.in/UserView/index?mid=2418`. last access: 18 June 2022.

Michael, M., Yadav, A., Tripathi, S., Kanawade, V., Gaur, A., Sadavarte, P., and Venkataraman, C. (2014). Simulation of trace gases and aerosols over the Indian domain: evaluation of the WRF-Chem model. *Geoscientific Model Development Discussions*, 7(1):431–482.

Ministry of Environment Government of Pakistan (2009). Land Use Atlas of Pakistan. Technical report, Government of Pakistan.

Ministry of Statistics, Government of India (2017). Statistical Year Book of India 2017. Technical report, Ministry of Statistics and Programme Implementation, Government of India. `https://www.usgs.gov/news/earthview-new-delhi-among-fastest-growing-urban-areas-world`.

Ministry of Urban Development, Government of India (2015). Annual Report 2014-2015. Technical report, National Capital Region Planning Board, Ministry of Urban Development, Government of India.

Mogno, C. and Marvin, M. R. (2022). EDGAR v5.0 emissions inventory speciated for the MOZART chemical mechanism (v1.0.0) [Dataset].

Mogno, C., Palmer, P. I., Knote, C., Yao, F., and Wallington, T. J. (2021). Seasonal distribution and drivers of surface fine particulate matter and organic aerosol over the Indo-Gangetic Plain. *Atmospheric Chemistry and Physics*, pages 1–39.

Mohan, M. and Bhati, S. (2011). Analysis of WRF model performance over subtropical region of Delhi, India. *Advances in Meteorology*, 2011.

Molina, L. T. (2021). Introductory lecture: Air Quality in Megacities. *Faraday Discussions*, 226:9–52.

Moran, M. D., Dastoor, A., and Morneau, G. (2014). Long-range transport of air pollutants and regional and global air quality modelling. In *Air Quality Management*, pages 69–98. Springer.

Morrison, H., Curry, J., and Khvorostyanov, V. (2005). A new double-moment microphysics parameterization for application in cloud and climate models. Part I: Description. *Journal of Atmospheric Science*, 62(6):1665–1677.

MoRTH (2021). *Road transport year book 2017-2018 and 2018 2019*. Ministry of Road Transport and Highways (MoRTH), Government of India.

Mukherjee, R., Rollend, D., Christie, G., Hadzic, A., Matson, S., Saksena, A., and Hughes, M. (2021). Towards Indirect Top-Down Road Transport Emissions Estimation. In *Proceedings of the IEEE/CVF Conference on Computer Vision and Pattern Recognition*, pages 1092–1101.

Murray, C. J., Aravkin, A. Y., Zheng, P., Abbafati, C., Abbas, K. M., Abbasi-Kangevari, M., Abd-Allah, F., Abdelalim, A., Abdollahi, M., Abdollahpour, I., et al. (2020). Global burden of 87 risk factors in 204 countries and territories, 1990–2019: a systematic analysis for the Global Burden of Disease Study 2019. *The Lancet*, 396(10258):1223–1249.

Nair, V. S., Moorthy, K. K., Alappattu, D. P., Kunhikrishnan, P., George, S., Nair, P. R., Babu, S. S., Abish, B., Satheesh, S., Tripathi, S. N., et al. (2007). Wintertime aerosol characteristics over the Indo-Gangetic Plain (IGP): Impacts of local boundary layer processes and long-range transport. *Journal of Geophysical Research: Atmospheres*, 112(D13).

Nakanishi, M. and Niino, H. (2006). An improved Mellor–Yamada level-3 model: Its numerical stability and application to a regional prediction of advection fog. *Boundary-Layer Meteorology*, 119(2):397–407.

NASA EO (2018). Urban Growth of New Delhi. Technical report, NASA Earth Observatory. `https://earthobservatory.nasa.gov/images/92813/urban-growth-of-new-delh`.

National Centers for Environmental Prediction, National Weather Service, NOAA, U.S. Department of Commerce (2015). Ncep gdas/fnl 0.25 degree global tropospheric analyses and forecast grids.

National Geographic (2021). Air pollution kills millions every year, like a 'pandemic in slow motion- National Geographic. `https://www.nationalgeographic.com/magazine/article/air-pollution-kills-millions-every-year-like-a-pandemic-in-slow-motion-feature?loggedin=true`.

Nault, B. A., Jo, D. S., McDonald, B. C., Campuzano-Jost, P., Day, D. A., Hu, W., Schroder, J. C., Allan, J., Blake, D. R., Canagaratna, M. R., et al. (2021). Secondary organic aerosols from anthropogenic volatile organic compounds contribute substantially to air pollution mortality. *Atmospheric Chemistry and Physics*, 21(14):11201–11224.

NCRPB, National Capital Region Planning Board (2022). Evolution of Concept of National Capital Region.

Nelson, B. S., Stewart, G. J., Drysdale, W. S., Newland, M. J., Vaughan, A. R., Dunmore, R. E., Edwards, P. M., Lewis, A. C., Hamilton, J. F., Acton, W. J., et al. (2021). In situ ozone production is highly sensitive to volatile organic compounds in Delhi, India. *Atmospheric Chemistry and Physics*, 21(17):13609–13630.

Ng, N., Chhabra, P., Chan, A., Surratt, J., Kroll, J., Kwan, A., McCabe, D., Wennberg, P., Sorooshian, A., Murphy, S., et al. (2007). Effect of NOx level on secondary organic aerosol (SOA) formation from the photooxidation of terpenes. *Atmospheric Chemistry and Physics*, 7(19):5159–5174.

Nguyen, N. P. and Marshall, J. D. (2018). Impact, efficiency, inequality, and injustice of urban air pollution: Variability by emission location. *Environmental Research Letters*, 13(2):024002.

NOAA (2020). Weather Research and Forecasting model coupled to Chemistry (WRF-Chem). `https://ruc.noaa.gov/wrf/wrf-chem/`.

Novelli, P. C., Steele, L. P., and Tans, P. P. (1992). Mixing ratios of carbon monoxide in the troposphere. *Journal of Geophysical Research: Atmospheres*, 97(D18):20731–20750.

Ojha, N., Sharma, A., Kumar, M., Girach, I., Ansari, T. U., Sharma, S. K., Singh, N., Pozzer, A., and Gunthe, S. S. (2020). On the widespread enhancement in fine particulate matter across the Indo-Gangetic Plain towards winter. *Scientific Reports*, 10(1):1–9.

Ojha, N., Soni, M., Kumar, M., Gunthe, S. S., Chen, Y., and Ansari, T. U. (2022). Mechanisms and pathways for coordinated control of fine particulate matter and ozone. *Current pollution reports*, pages 1–11.

OpenAQ (2020). Fighting air inequality through open data and community. `https://openaq.org/`.

Pakistan Bureau of Statistics (2017). Provisional Summary Results of 6th Population and Housing Census–2017. Technical report, Government of Pakistan Islamabad.

Palmer, P. I., Parrington, M., Lee, J. D., Lewis, A. C., Rickard, A., Bernath, P. F., Duck, T., Waugh, D., Tarasick, D., Andrews, S., et al. (2013). Quantifying the impact of BOReal forest fires on Tropospheric oxidants over the Atlantic using Aircraft and Satellites (BORTAS) experiment: design, execution and science overview. *Atmospheric Chemistry and Physics*, 13(13):6239–6261.

Pan, S., Roy, A., Choi, Y., Eslami, E., Thomas, S., Jiang, X., and Gao, H. O. (2019). Potential impacts of electric vehicles on air quality and health endpoints in the Greater Houston Area in 2040. *Atmospheric Environment*, 207:38–51.

Pandey, A., Brauer, M., Cropper, M. L., Balakrishnan, K., Mathur, P., Dey, S., Turkgulu, B., Kumar, G. A., Khare, M., Beig, G., et al. (2021). Health and economic impact of air pollution in the states of India: the Global Burden of Disease Study 2019. *The Lancet Planetary Health*, 5(1):e25–e38.

Pankow, J. F. (1994). An absorption model of gas/particle partitioning of organic compounds in the atmosphere. *Atmospheric Environment*, 28(2):185–188.

Pant, P., Shukla, A., Kohl, S. D., Chow, J. C., Watson, J. G., and Harrison, R. M. (2015). Characterization of ambient $PM_{2.5}$ at a pollution hotspot in New Delhi, India and inference of sources. *Atmospheric Environment*, 109:178–189.

Paolella, D. A., Tessum, C. W., Adams, P. J., Apte, J. S., Chambliss, S., Hill, J., Muller, N. Z., and Marshall, J. D. (2018). Effect of model spatial resolution on estimates of fine particulate matter exposure and exposure disparities in the United States. *Environmental Science and Technology Letters*, 5(7):436–441.

Patel, K., Campmier, M. J., Bhandari, S., Baig, N., Gani, S., Habib, G., Apte, J. S., and Hildebrandt Ruiz, L. (2021). Persistence of primary and secondary pollutants in delhi: concentrations and composition from 2017 through the covid pandemic. *Environmental Science & Technology Letters*, 8(7):492–497.

Peel, M. C., Finlayson, B. L., and McMahon, T. A. (2007). Updated world map of the Köppen-Geiger climate classification. *Hydrology and Earth System Sciences Discussions*, 4(2):439–473.

Pisoni, E., Guerreiro, C., Lopez-Aparicio, S., Guevara, M., Tarrason, L., Janssen, S., Thunis, P., Pfäfflin, F., Piersanti, A., Briganti, G., et al. (2019). Supporting the improvement of air quality management practices: The “FAIRMODE pilot” activity. *Journal of Environmental Management*, 245:122–130.

Powers, J. G., Klemp, J. B., Skamarock, W. C., Davis, C. A., Dudhia, J., Gill, D. O., Coen, J. L., Gochis, D. J., Ahmadov, R., Peckham, S. E., et al. (2017). The weather research and forecasting model: overview, system efforts, and future directions. *Bulletin of the American Meteorological Society*, 98(8):1717–1737.

Prather, M., Ehhalt, D., Dentener, F., Derwent, R., Dlugokencky, E., Holland, E., Isaksen, I., Katima, J., Kirchhoff, V., Matson, P., et al. (2001). Climate Change 2001: The Scientific Basis - Atmospheric chemistry and greenhouse gases. Contribution of Working Group I to the Third Assessment Report of the Intergovernmental Panel on Climate Change.

Presto, A. A., Huff Hartz, K. E., and Donahue, N. M. (2005). Secondary organic aerosol production from terpene ozonolysis. Effect of NOx concentration. *Environmental Science & Technology*, 39(18):7046–7054.

Public Heath England (2019). Indoor Air Quality Guidelines for selected Volatile Organic Compounds (VOCs) in the UK. *Public Heath England: London, GOV.UK*.

Qiao, Q., Zhao, F., Liu, Z., Hao, H., He, X., Przesmitzki, S. V., and Amer, A. A. (2020). Life cycle cost and GHG emission benefits of electric vehicles in China. *Transportation Research Part D: Transport and Environment*, 86:102418.

Rajput, P., Sarin, M., Sharma, D., and Singh, D. (2014). Organic aerosols and inorganic species from post-harvest agricultural-waste burning emissions over northern India: impact on mass absorption efficiency of elemental carbon. *Environ. Sci-Proc. Imp.*, 16(10):2371–2379.

Rakesh, V., Singh, R., and Joshi, P. C. (2009). Intercomparison of the performance of MM5/WRF with and without satellite data assimilation in short-range forecast applications over the Indian region. *Meteorol. Atmos. Phys.*, 105(3):133–155.

Ram, K., Sarin, M., and Hegde, P. (2008). Atmospheric abundances of primary and secondary carbonaceous species at two high-altitude sites in India: sources and temporal variability. *Atmospheric Environment*, 42(28):6785–6796.

Ram, K., Sarin, M., and Tripathi, S. (2012). Temporal trends in atmospheric $PM_{2.5}$, $PM_{2.5}$, elemental carbon, organic carbon, water-soluble organic carbon, and optical properties: impact of biomass burning emissions in the Indo-Gangetic Plain. *Environmental Science Technology*, 46(2):686–695.

Ramachandra, T. et al. (2009). Emissions from India's transport sector: statewise synthesis. *Atmospheric Environment*, 43(34):5510–5517.

Randerson, J., Chen, Y., Van Der Werf, G., Rogers, B., and Morton, D. (2012). Global burned area and biomass burning emissions from small fires. *Journal of Geophysical Research: Biogeosciences*, 117(G4).

Ratnam, J. V. and Kumar, K. K. (2005). Sensitivity of the simulated monsoons of 1987 and 1988 to convective parameterization schemes in MM5. *Journal of Climate*, 18(14):2724–2743.

Reátegui-Romero, W., Sánchez-Ccoyllo, O. R., de Fatima Andrade, M., and Moya-Alvarez, A. (2018). $PM_{2.5}$ estimation with the WRF–Chem model, produced by vehicular flow in the Lima metropolitan area. *Open Journal of Air Pollution*, 7(03):215.

Reddy, C. S., Pasha, S. V., Jha, C., Diwakar, P., and Dadhwal, V. (2016). Development of national database on long-term deforestation (1930–2014) in Bangladesh. *Global Planet. Change*, 139:173–182.

Requia, W. J., Mohamed, M., Higgins, C. D., Arain, A., and Ferguson, M. (2018). How clean are electric vehicles? Evidence-based review of the effects of electric mobility on air pollutants, greenhouse gas emissions and human health. *Atmospheric Environment*, 185:64–77.

Reyes-Villegas, E., Panda, U., Darbyshire, E., Cash, J. M., Joshi, R., Langford, B., Di Marco, C. F., Mullinger, N., Acton, W. J. F., Drysdale, W., et al. (2020). Pm1 composition and source apportionment at two sites in delhi, india across multiple seasons. *Atmospheric Chemistry and Physics Discussions*, (acp-2020-894):1–19.

Riedel, K. and Lassey, K. (2008). Detergent of the atmosphere. *Water Atmos*, 16(2).

Rigby, M., Montzka, S. A., Prinn, R. G., White, J. W., Young, D., O'doherty, S., Lunt, M. F., Ganesan, A. L., Manning, A. J., Simmonds, P. G., et al. (2017). Role of atmospheric oxidation in recent methane growth. *Proceedings of the National Academy of Sciences*, 114(21):5373–5377.

Riipinen, I., Pierce, J., Yli-Juuti, T., Nieminen, T., Häkkinen, S., Ehn, M., Junninen, H., Lehtipalo, K., Petäjä, T., Slowik, J., et al. (2011). Organic condensation: a vital link connecting aerosol formation to cloud condensation nuclei (CCN) concentrations. *Atmospheric Chemistry and Physics*, 11(8):3865–3878.

Ritchie, H. and Roser, M. (2021). Air Pollution. *Our World in Data*. https://ourworldindata.org/air-pollution.

Robinson, A. L., Donahue, N. M., Shrivastava, M. K., Weitkamp, E. A., Sage, A. M., Grieshop, A. P., Lane, T. E., Pierce, J. R., and Pandis, S. N. (2007). Rethinking organic aerosols: Semivolatile emissions and photochemical aging. *Science*, 315(5816):1259–1262.

Rohini, P., Rajeevan, M., and Srivastava, A. (2016). On the variability and increasing trends of heat waves over India. *Scientific reports*, 6(1):1–9.

Rösch, C., Kohajda, T., Röder, S., von Bergen, M., and Schlink, U. (2014). Relationship between sources and patterns of VOCs in indoor air. *Atmospheric Pollution Research*, 5(1):129–137.

Sakhamuri, S. and Cummings, S. (2019). Increasing trans-Atlantic intrusion of Sahara dust: a cause of concern? *The Lancet Planetary Health*, 3(6):e242–e243.

Schnell, J. L., Naik, V., Horowitz, L. W., Paulot, F., Ginoux, P., Zhao, M., and Horton, D. E. (2019). Air quality impacts from the electrification of light-duty passenger vehicles in the United States. *Atmospheric Environment*, 208:95–102.

Schnell, J. L., Naik, V., Horowitz, L. W., Paulot, F., Mao, J., Ginoux, P., Zhao, M., and Ram, K. (2018). Exploring the relationship between surface $PM_{2.5}$ and meteorology in Northern India. *Atmospheric Chemistry and Physics*, 18(10):10157–10175.

Seinfeld, J. H. and Pandis, S. N. (2016). *Atmospheric chemistry and physics: from air pollution to climate change*. John Wiley & Sons.

Sembhi, H., Wooster, M., Zhang, T., Sharma, S., Singh, N., Agarwal, S., Boesch, H., Gupta, S., Misra, A., Tripathi, S. N., Mor, S., and Khaiwal, R. (2020). Post-monsoon air quality degradation across Northern India: assessing the impact of policy-related shifts in timing and amount of crop residue burnt. *Environmental Research Letters*, 15(10):104067.

Sen, A., Miller, J., Bandivadekar, A., Sharma, M., Nagar, P. K., Singh, D., and Callahan, J. (2021a). Understanding the air quality and health impacts of large-scale vehicle electrification in India.

Sen, A., Miller, J., Bandivadekar, A., Sharma, M., Nagar, P. K., Singh, D., and Callahan, J. (2021b). Understanding the emissions impacts of large-scale vehicle electrification in India.

Shahid, M. Z., Liao, H., Li, J., Shahid, I., Lodhi, A., and Mansha, M. (2015). Seasonal variations of aerosols in Pakistan: Contributions of domestic anthropogenic emissions and transboundary transport. *Aerosol Air Qual. Res.*, 15:1580–1600.

Sharma, A., Ojha, N., Pozzer, A., Mar, K. A., Beig, G., Lelieveld, J., and Gunthe, S. S. (2017a). WRF-Chem simulated surface ozone over south Asia during the pre-monsoon: effects of emission inventories and chemical mechanisms. *Atmospheric Chemistry and Physics*, 17(23):14393–14413.

Sharma, M. and Dikshit, O. (2016). Comprehensive study on air pollution and green house gases (GHGs) in Delhi. Final report: air pollution components. Technical report, Department of Environment, Government of National Capital Territory of Delhi and Delhi Pollution Control Committee.

Sharma, S., Agarwal, P., Mandal, T., Karapurkar, S., Shenoy, D., Peshin, S., Gupta, A., Saxena, M., Jain, S., Sharma, A., et al. (2017b). Study on ambient air quality of megacity Delhi, India during odd–even strategy. *Mapan Journal of Metrology Society of India*, 32(2):155–165.

Sharma, S. and Khare, M. (2017). Simulating ozone concentrations using precursor emission inventories in Delhi–National Capital Region of India. *Atmospheric Environment*, 151:117–132.

Sharma, S., Mandal, T., Srivastava, M., Chatterjee, A., Jain, S., Saxena, M., Singh, B., Sharma, A., Adak, A., and Ghosh, S. (2016). Spatio-temporal variation in chemical characteristics of PM_{10} over Indo Gangetic Plain of India. *Environmental Science and Pollution Research*, 23(18):18809–18822.

Shrivastava, M., Fast, J., Easter, R., Gustafson Jr, W., Zaveri, R. A., Jimenez, J. L., Saide, P., and Hodzic, A. (2011). Modeling organic aerosols in a megacity: comparison of simple and complex representations of the volatility basis set approach. *Atmospheric Chemistry and Physics*, 11(13):6639–6662.

Singh, A., Gangopadhyay, S., Nanda, P., Bhattacharya, S., Sharma, C., and Bhan, C. (2008). Trends of greenhouse gas emissions from the road transport sector in India. *Science of the Total Environment*, 390(1):124–131.

Singh, A. P., Singh, R., Mina, U., Singh, M. P., and Varshney, C. K. (2011). Emissions of monoterpene from tropical Indian plant species and assessment of VOC emission from the forest of Haryana state. *Atmospheric Pollution Research*, 2(1):72–79.

Singh, N., Banerjee, T., Raju, M. P., Deboudt, K., Sorek-Hamer, M., Singh, R. S., and Mall, R. K. (2018). Aerosol chemistry, transport, and climatic implications during extreme biomass burning emissions over the Indo-Gangetic Plain. *Atmospheric Chemistry and Physics*, 18(19):14197–14215.

Singh, R. P. and Kaskaoutis, D. G. (2014). Crop residue burning: a threat to South Asian air quality. *Eos, Transactions American Geophysical Union*, 95(37):333–334.

Sirithian, D. and Thepanondh, S. (2016). Influence of grid resolution in modeling of air pollution from open burning. *Atmosphere*, 7(7):93.

Skamarock, W. C., Klemp, J. B., Dudhia, J., Gill, D. O., Barker, D. M., Wang, W., and Powers, J. G. (2008). A description of the Advanced Research WRF version 3. NCAR Technical note-475+ STR.

Smith, S. J., Pitcher, H., and Wigley, T. M. (2001). Global and regional anthropogenic sulfur dioxide emissions. *Global and Planetary Change*, 29(1-2):99–119.

Soret, A., Guevara, M., and Baldasano, J. (2014). The potential impacts of electric vehicles on air quality in the urban areas of Barcelona and Madrid (Spain). *Atmospheric Environment*, 99:51–63.

Srinivas, B. and Sarin, M. (2014). $PM_{2.5}$, EC and OC in atmospheric outflow from the Indo-Gangetic Plain: Temporal variability and aerosol organic carbon-to-organic mass conversion factor. *Science of the Total Environment*, 487:196–205.

Stavrakou, T., Müller, J.-F., Bauwens, M., De Smedt, I., Van Roozendael, M., Guenther, A., Wild, M., and Xia, X. (2014). Isoprene emissions over Asia 1979-2012: impact of climate and land-use changes. *Atmospheric Chemistry and Physics*, 14(9):4587–4605.

Steinemann, A. (2015). Volatile emissions from common consumer products. *Air Quality, Atmosphere & Health*, 8(3):273–281.

Stibig, H.-J., Belward, A., Roy, P., Rosalina-Wasrin, U., Agrawal, S., Joshi, P., Hildanus, Beuchle, R., Fritz, S., Mubareka, S., and Giri, C. (2007). A land-cover map for South and Southeast Asia derived from SPOT-VEGETATION data. *JJ. Biogeogr.*, 34(4):625–637.

Stone, E., Schauer, J., Quraishi, T. A., and Mahmood, A. (2010). Chemical characterization and source apportionment of fine and coarse particulate matter in Lahore, Pakistan. *Atmospheric Environment*, 44(8):1062–1070.

Suarez, J., Makridis, M., Anesiadou, A., Komnos, D., Ciuffo, B., and Fontaras, G. (2022). Benchmarking the driver acceleration impact on vehicle energy consumption and CO_2 emissions. *Transportation Research Part D: Transport and Environment*, 107:103282.

Surl, L., Palmer, P. I., and González Abad, G. (2018). Which processes drive observed variations of HCHO columns over India? *Atmospheric Chemistry and Physics*, 18:4549–4566.

Tan, J., Zhang, Y., Ma, W., Yu, Q., Wang, J., and Chen, L. (2015). Impact of spatial resolution on air quality simulation: A case study in a highly industrialized area in Shanghai, China. *Atmospheric Pollution Research*, 6(2):322–333.

Tatem, A. J. (2017). WorldPop, open data for spatial demography. *Scientific Data*, 4(1):1–4.

TERI & ARAI (2018). Source apportionment of $PM_{2.5}$ and PM_{10} of Delhi NCR for identification of major sources. Technical report, The Energy Resources Institute (TERI), Delhi and Automative Research Association of India (ARAI).

Thunis, P., Clappier, A., de Meij, A., Pisoni, E., Bessagnet, B., and Tarrason, L. (2021). Why is the city's responsibility for its air pollution often underestimated? A focus on $PM_{2.5}$. *Atmospheric Chemistry and Physics*, 21(24):18195–18212.

Thunis, P., Clappier, A., Pisoni, E., and Degraeuwe, B. (2015). Quantification of non-linearities as a function of time averaging in regional air quality modeling applications. *Atmospheric Environment*, 103:263–275.

Thunis, P., Clappier, A., Tarrasón, L., Cuvelier, C., Monteiro, A., Pisoni, E., Wesseling, J., Belis, C., Pirovano, G., Janssen, S., et al. (2019). Source apportionment to support air quality planning: Strengths and weaknesses of existing approaches. *Environment International*, 130:104825.

Tie, X., Geng, F., Guenther, A., Cao, J., Greenberg, J., Zhang, R., Apel, E., Li, G., Weinheimer, A., Chen, J., et al. (2013). Megacity impacts on regional ozone formation: observations and WRF-Chem modeling for the MIRAGE-Shanghai field campaign. *Atmospheric Chemistry and Physics*, 13(11):5655–5669.

Tie, X., Madronich, S., Walters, S., Zhang, R., Rasch, P., and Collins, W. (2003). Effect of clouds on photolysis and oxidants in the troposphere. *J. Geophys. Res.-Atmos.*, 108(D20).

Tiwari, S., Srivastava, A., Bisht, D., Parmita, P., Srivastava, M. K., and Attri, S. (2013). Diurnal and seasonal variations of black carbon and $PM_{2.5}$ over New Delhi, India: influence of meteorology. *Atmospheric Research*, 125:50–62.

Tiwari, S., Thomas, A., Rao, P., Chate, D., Soni, V. K., Singh, S., Ghude, S., Singh, D., and Hopke, P. K. (2018). Pollution concentrations in Delhi India during winter 2015–16: A case study of an odd-even vehicle strategy. *Atmospheric Pollution Research*, 9(6):1137–1145.

UN, DESA (2018). 2018 Revision of World Urbanization Prospects. Technical report, UN, United Nations, Department of Economic and Social Affairs.

UN DESA (2019a). 2018 Revision of World Urbanization Prospects. Technical report, United Nation Department of Economic and Social Affairs.

UN DESA (2019b). The World's Cities in 2018. Technical report, United Nation Department of Economic and Social Affairs.

US Embassy (2020). U.S. Embassy and Consulates' air quality monitors measure $PM_{2.5}$ data. `https://in.usembassy.gov/embassy-consulates/new-delhi/air-quality-data/`. (last access: 30 November 2020).

USGS (2016). EarthView–New Delhi Among Fastest Growing Urban Areas in the World. Technical report, U.S. Geological Survey. `https://www.usgs.gov/news/earthview-new-delhi-among-fastest-growing-urban-areas-world`.

Vadrevu, K. P., Ellicott, E., Badarinath, K., and Vermote, E. (2011). MODIS derived fire characteristics and aerosol optical depth variations during the agricultural residue burning season, north India. *Environmental Pollution*, 159(6):1560–1569.

Vallero, D. (2014). *Fundamentals of air pollution*. Academic Press.

Venkataraman, C., Brauer, M., Tibrewal, K., Sadavarte, P., Ma, Q., Cohen, A., Chaliyakunnel, S., Frostad, J., Klimont, Z., Martin, R. V., et al. (2018). Source influence on emission pathways and ambient $PM_{2.5}$ pollution over India (2015–2050). *Atmospheric Chemistry and Physics*, 18:8017–8039.

Vohra, K., Vodonos, A., Schwartz, J., Marais, E. A., Sulprizio, M. P., and Mickley, L. J. (2021). Global mortality from outdoor fine particle pollution generated by fossil fuel combustion: Results from GEOS-Chem. *Environmental Research*, 195:110754.

Wallace, L. A., Pellizzari, E., Leaderer, B., Zelon, H., and Sheldon, L. (1987). Emissions of volatile organic compounds from building materials and consumer products. *Atmospheric Environment*, 21(2):385–393.

Wang, H., He, X., Liang, X., Choma, E. F., Liu, Y., Shan, L., Zheng, H., Zhang, S., Nielsen, C. P., Wang, S., et al. (2020a). Health benefits of on-road transportation pollution control programs in China. *Proceedings of the National Academy of Sciences*, 117(41):25370–25377.

Wang, Q., Gu, J., and Wang, X. (2020b). The impact of Sahara dust on air quality and public health in European countries. *Atmospheric Environment*, 241:117771.

Wang, T., Song, Y., Xu, Z., Liu, M., Xu, T., Liao, W., Yin, L., Cai, X., Kang, L., Zhang, H., et al. (2020c). Why is the Indo-Gangetic Plain the region with the largest NH_3 column in the globe during pre-monsoon and monsoon seasons? *Atmospheric Chemistry and Physics*, 20(14):8727–8736.

Weiss, D. and Scherer, P. (2023). Mapping the territorial adaptation of technological trajectories: The phase-out of the internal combustion engine. In *Technologies in Decline*, pages 145–166. Routledge.

WHO (2018). WHO's Global Ambient Air Quality Database (updated 2018). World Health Organisation, `http://www.who.int/airpollution/data/cities/en/`.

WHO (2021). Ambient (outdoor) air quality and health, factsheet. `https://www.who.int/news-room/fact-sheets/detail/ambient-(outdoor)-air-quality-and-health`.

WHO (2021). *WHO global air quality guidelines: particulate matter ($PM_{2.5}$ and PM_{10}), ozone, nitrogen dioxide, sulfur dioxide and carbon monoxide*. World Health Organization.

Wiedinmyer, C., Akagi, S., Yokelson, R. J., Emmons, L., Al-Saadi, J., Orlando, J., and Soja, A. (2011). The Fire INventory from NCAR (FINN): a high resolution global model to estimate the emissions from open burning. *Geoscientific Model Development*, 4(3):625.

World Bank (2022). Open data. last access= 18 June 2022.

Xu, L., Yilmaz, H. Ü., Wang, Z., Poganietz, W.-R., and Jochem, P. (2020). Greenhouse gas emissions of electric vehicles in Europe considering different charging strategies. *Transportation Research Part D: Transport and Environment*, 87:102534.

Xue, T., Zheng, Y., Li, X., Liu, J., Zhang, Q., and Zhu, T. (2021). A component-specific exposure–mortality model for ambient $PM_{2.5}$ in China: findings from nationwide epidemiology based on outputs from a chemical transport model. *Faraday Discussions*, 226:551–568.

Yarwood, G., Rao, S., Yocke, M., and Whitten, G. (2005). Updates to the carbon bond mechanism: CB05, Report to the US Environmental Protection Agency. *ENVIRON International Corporation, Novato.[Available at http://www. camx. com/publ/pdfs/CB05_Final_Report_120805. pdf.]*.

Yeh, S., Gil, J., Kyle, P., Kishimoto, P., Cazzola, P., Craglia, M., Edelenbosch, O., Fragkos, P., Fulton, L., Liao, Y., et al. (2022). Improving future travel demand projections: a pathway with an open science interdisciplinary approach. *Progress in Energy*.

Zaveri, R. A., Easter, R. C., Fast, J. D., and Peters, L. K. (2008). Model for simulating aerosol interactions and chemistry (MOSAIC). *Journal of Geophysical Research: Atmospheres*, 113(D13).

Zhang, J., Huff Hartz, K. E., Pandis, S. N., and Donahue, N. M. (2006a). Secondary organic aerosol formation from limonene ozonolysis: Homogeneous and heterogeneous influences as a function of NOx. *The Journal of Physical Chemistry A*, 110(38):11053–11063.

Zhang, M., Uno, I., Zhang, R., Han, Z., Wang, Z., and Pu, Y. (2006b). Evaluation of the Models-3 Community Multi-scale Air Quality (CMAQ) modeling system with observations obtained during the TRACE-P experiment: Comparison of ozone and its related species. *Atmospheric Environment*, 40(26):4874–4882.

Zhang, Q., Beekmann, M., Drewnick, F., Freutel, F., Schneider, J., Crippa, M., Prevot, A. S., Baltensperger, U., Poulain, L., Wiedensohler, A., et al. (2013). Formation of organic aerosol in the Paris region during the MEGAPOLI summer campaign: evaluation of the volatility-basis-set approach within the CHIMERE model. *Atmospheric Chemistry and Physics*, 13(11):5767–5790.

Zhang, R., Lei, W., Tie, X., and Hess, P. (2004). Industrial emissions cause extreme urban ozone diurnal variability. *P. Natl. Acad. Sci. USA*, 101(17):6346–6350.

Zhao, B., Wang, S., Donahue, N. M., Jathar, S. H., Huang, X., Wu, W., Hao, J., and Robinson, A. L. (2016). Quantifying the effect of organic aerosol aging and intermediate-volatility emissions on regional-scale aerosol pollution in China. *Scientific Reports*, 6:28815.